MSc thesis

A shallow shear velocity model for Groningen

L.J. Hofman

Supervisors:
Dr. B. Dost
Dr. J.A.M. Paulssen
Dr. E.N Ruigrok

July 2016

Universiteit Utrecht

Koninklijk Nederlands
Meteorologisch Instituut
Ministerie van Infrastructuur en Milieu

Abstract

Depletion of the Groningen gas field in the Netherlands causes induced earthquakes. To monitor the seismicity in the area, a large network of borehole seismometers was installed early 2015. Each borehole consists of an accelerometer at the surface and four equally spaced geophones up to a depth of 200 meters. To estimate the probabilistic seismic hazard, a Ground Motion Prediction Equation (GMPE) was developed in a previous study. GMPEs are empirical equations linking geophysical properties of the crust to surface ground motions. A very important element in the GMPE is the shallow shear velocity structure. For the current model, different methods are used to estimate the shear velocities at different depth intervals. In this study, vertical compressional and shear wave velocity profiles are calculated for each of the boreholes using passive seismic interferometry. This method makes use of data recordings of local seismicity. The results are seismic velocity profiles for each of the borehole stations in the network. For the four different depth levels, the station results are interpolated to make contour maps. These maps correlate well to results from previous work. An important part of this study was to develop a method to estimate the horizontal orientations of the borehole geophones, which are required to derive the shear wave velocities using seismic interferometry. This method is based on cross-correlations of the geophone and the co-located surface accelerometer. In addition, by analysing data from the new network on a level that had not previously been done, several installation errors could be found and resolved.

Contents

1 Introduction

The province of Groningen in the North of the Netherlands holds the largest onshore natural gas field in Europe. The production of gas from this field started in the early sixties, shortly after its discovery. About two decades later earthquakes started to occur in the area. Although most of the earthquakes have local magnitudes of less than three, damage has been reported and this gave rise to a big political discussion.

In 1995, a network of 8 borehole stations was deployed to monitor the seismicity in the area. Since 2015, this network has been expanded with 70 new stations. Each station in this new network consists of an accelerometer at the surface and an array of four downhole geophones with a vertical spacing of 50 m (figure 1). The horizontal distance between the boreholes is in the order of 5 km. Figure 2 shows the stations of the new network on a map with their corresponding station codes. The stations are numbered from 1 up to and including 70. Five of the stations (G12, G15, G25, G35, G48) are not shown on this map because of technical problems. Apart from being able to determine earthquake locations and magnitudes with much greater accuracy than before, borehole seismometers can be used to gain valuable information about the subsurface. Shearer and Orcutt (1987) show how various near surface effects (site response) can be studied using borehole seismometers.

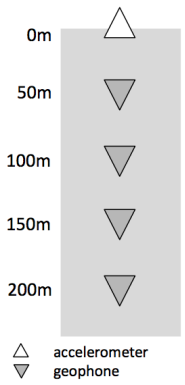

Figure 1: *Typical borehole setup in the Groningen network with one surface accelerometer and four downhole geophones.*

The risk and hazard of earthquakes can be assessed through ground-motion prediction equations (GMPEs). These are empirical models developed to link geophysical properties of the crust to the surface motion. For an earthquake of a given magnitude and location, the equation predicts the surface motion of the earth. GMPEs are mostly developed to predict ground motions for tectonic earthquakes as opposed to induced earthquakes. Induced earthquakes are usually lower in magnitude and occur in a very narrow depth range. Bommer et al. (2007) show that the GMPEs can not simply be extrapolated to predict ground motions for magnitudes outside of the range of magnitudes in the dataset used to derive the GMPEs. It is therefore important to derive GMPEs from the actual dataset of

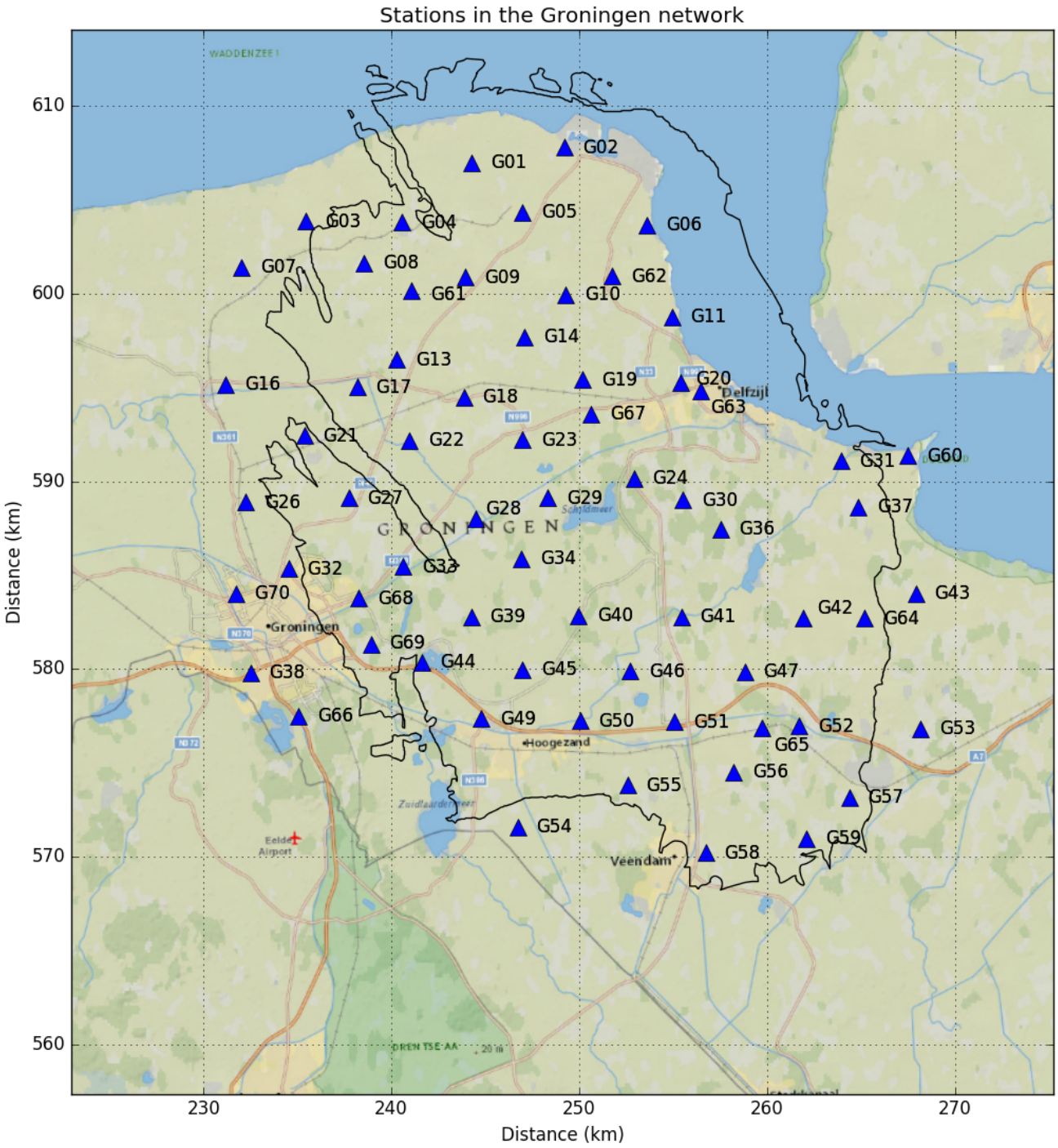

Figure 2: *Map showing the locations of the borehole stations in the Groningen network with their station codes. For reference, the outline of the Groningen gas field is drawn over the map. RD-system coordinates are shown along the axes in km.* *(Background map: National Geographic, Esri, DeLorme, HERE, INCREMENT P, NRCAN, METI)*

induced earthquakes in Groningen. Bommer et al. (2016) developed a GMPE specifically for the Groningen gas field and emphasised the different approach required to develop GMPEs for induced earthquakes rather than tectonic earthquakes. The small magnitudes and shallow depths of the induced earthquakes tend to be much more sensitive to local and regional structures. Therefore, GMPEs for induced earthquakes require a much more detailed model of the subsurface.

One of the key parameters in the GMPEs is the seismic shear wave (S-wave) velocity. Variations in seismic velocity, especially sharp contrasts, cause reflection and refraction of seismic waves. Especially the shallow seismic velocity structure has a large influence on the site response. The current GMPE (v1) (Bommer et al., 2016) assumes a constant S-wave velocity of 200 m/s in the upper 30 m (V_{S30}). This model does not include any lateral variation. The next version of the GMPE (v2) (Bommer et al., 2015) contains a more detailed shear velocity model. This model makes use of Cone Penetration Tests combined with lithological maps for the V_{S30}. An estimate of the V_{S65} is obtained by surface wave inversion from seismics. For the deeper structure the model relies on a time to depth (T2D) model where time domain seismic sections are converted to depth domain.

In this study, seismic P- and S-wave profiles are computed for each of the borehole stations in the new Groningen network using passive seismic interferometry (Wapenaar et al., 2010). With a single method, seismic velocities are calculated for four depth intervals from 0 to 200 m. This allows a solid comparison with the data from currently used approaches (Bommer et al., 2015). As an intermediate step, a method was developed to estimate the horizontal orientations of all of the borehole geophones in the network.

2 Methods

2.1 Interval velocities

This section describes how vertical P-wave and S-wave velocity profiles can be derived for the boreholes in the Groningen network using passive seismic interferometry. For local events, data from instruments at different levels within a borehole are cross-correlated and stacked to find the time delay in the intervals in the borehole. With the spacing between the instruments, this time delay can be converted to velocity. Vossen (2016) applied passive seismic interferometry to

the old (pre-2015) network in Groningen, and showed that stable results can be obtained for different subsets of earthquake data.

2.1.1 Seismic interferometry

A very brief introduction to seismic interferometry is given here. The theory described in this section mostly follows the principles described by Wapenaar et al. (2010). Further background theory can be found in Aki and Richards (2002).

To describe the propagation of seismic waves through the earth, we use a Green's function representation. This (unknown) function G describes how the seismic wave travels through a specific medium. If we consider a 1D example, equation 1 shows how the response u of the receiver at point x_a to a source at point x_s can be described as the convolution of the Green's function G and the source function s.

$$u(x_a, x_s, t) = G(x_a, x_s, t) * s(t) \tag{1}$$

If two receivers record a signal produced by one source at different locations, the cross-correlation of these recordings produces a signal that would be the response of one of the receivers if the other receiver was the source. Equation 2 shows that cross-correlation of the signals of a receiver at x_a and x_b produce the Green's function convolved with the auto-correlation of the source function.

$$u(x_a, x_s, t) * u(x_b, x_s, -t) = G(x_a, x_b, t) * (s(t) * s(-t)) \tag{2}$$

If we now compare the right hand side of equations 1 and 2, we see that the source location x_s has been replaced by x_b, and the source function by its auto-correlation. This means that the result of the cross-correlation produces a signal that would be measured at x_a, if the source was at x_b (with the source function being the auto-correlation of the original source function). In other words, we have now created a 'virtual source' at x_b. The cross-correlation reveals the time it takes for the wave to travel from point x_b to point x_a.

In multidimensional space, it gets a little more complex, because the ray paths of the seismic waves are unknown. Consider the setup shown in figure 3a. A cross-correlation of the receiver responses for one of the point sources gives the time delay from one receiver to the other, but we don't know from which direction the wave is coming. Each wave therefore takes a different amount of time to travel from x_b to x_a. For example, a source at $\phi_s = 90°$ will produce zero time delay.

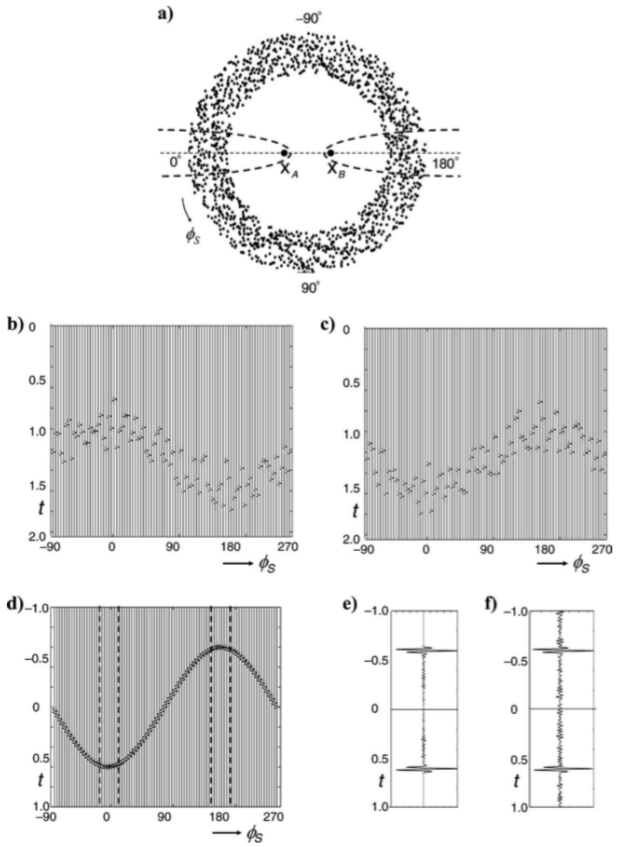

Figure 3: ***(a)*** *Distribution of sources around receivers x_a and x_b.* ***(b)*** *Responses of all signals at x_a.* ***(c)*** *Responses of all signals at x_b.* ***(d)*** *Cross-correlations of the responses of both receivers.* ***(e)*** *All cross-correlations stacked.* ***(f)*** *Same result but with using noise sources (not applied in this study). From Wapenaar et al. (2010)*

However, if we consider an isotropic distribution of sources, as in figure 3a and sum all the cross-correlations (3d) (often called 'stacking') we see that the resulting function (figure 3e) gives the maximum time delay between the receivers. The reason is that the time delay for sources around 0° and 180° approaches a stationary value and therefore the peaks in the cross-correlations interfere constructively while sources from all other directions interfere destructively. The main contributions to the result in figure 3e come from the regions indicated by the dashed lines in figures 3a and 3d. The peaks in figures 3e and 3f can therefore be interpreted as the maximum traveltime between x_a and x_b, or in other words, the time it would take for a wave to travel from a virtual source at x_b to the receiver at x_a.

In this study, passive seismic interferometry is used to determine the interval velocities in borehole seismometers. This means that the sources are local events (induced earthquakes) shown in figure 5, and the receivers are borehole seismometers (figures 1,2). Obviously, it would be impossible to obtain a perfect isotropic illumination as in figure 3a using real data in this setting. However, the assumption is made that enough of the seismic rays have inclinations within the Fresnel zone (figure 4). Like in the example illustrated in figure 3 the waves within the Fresnel zone will interfere constructively, while rays outside of the Fresnel zone will cancel out.

2.1.2 Data selection

Events Event meta-data is acquired through the KNMI event webservice using ObsPy (Beyreuther et al., 2010). Preferably, all events with $M_L > 1.5$ (local magnitude) are used (figure 5), but depending on the data availability for a specific station this criterion might be lowered to $M_L > 1.0$. For each of the events, 25 seconds of waveform data are used. The event origin time is always used as the starttime for the waveforms, regardless of the distance from the event to the station.

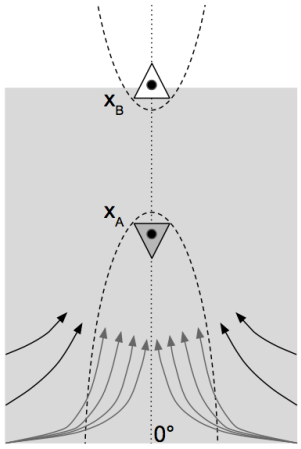

Figure 4: *Schematic representation of waves (arrows) entering the borehole to illustrate the assumption that enough of the waves come from within the Fresnel zone.*

Channels For the calculation of the P-wave velocities, only the vertical channels of the three component instruments are used. This is because the first P-wave is recorded mainly on the vertical component. It is important to notice that the accelerometers used in the Groningen network have a vertical component which is defined as positive in the upwards direction while the geophones record motion as positive in the downwards direction (more on the orientation of channels in Section 2.2.1).

For S-waves velocities, it is most convenient to use the transverse component of the instruments (i.e., the direction perpendicular to the propagation of the wave), since most of the SH-wave energy is recorded in this direction. The horizontal geophone channels are numbered 1 and 2, and have

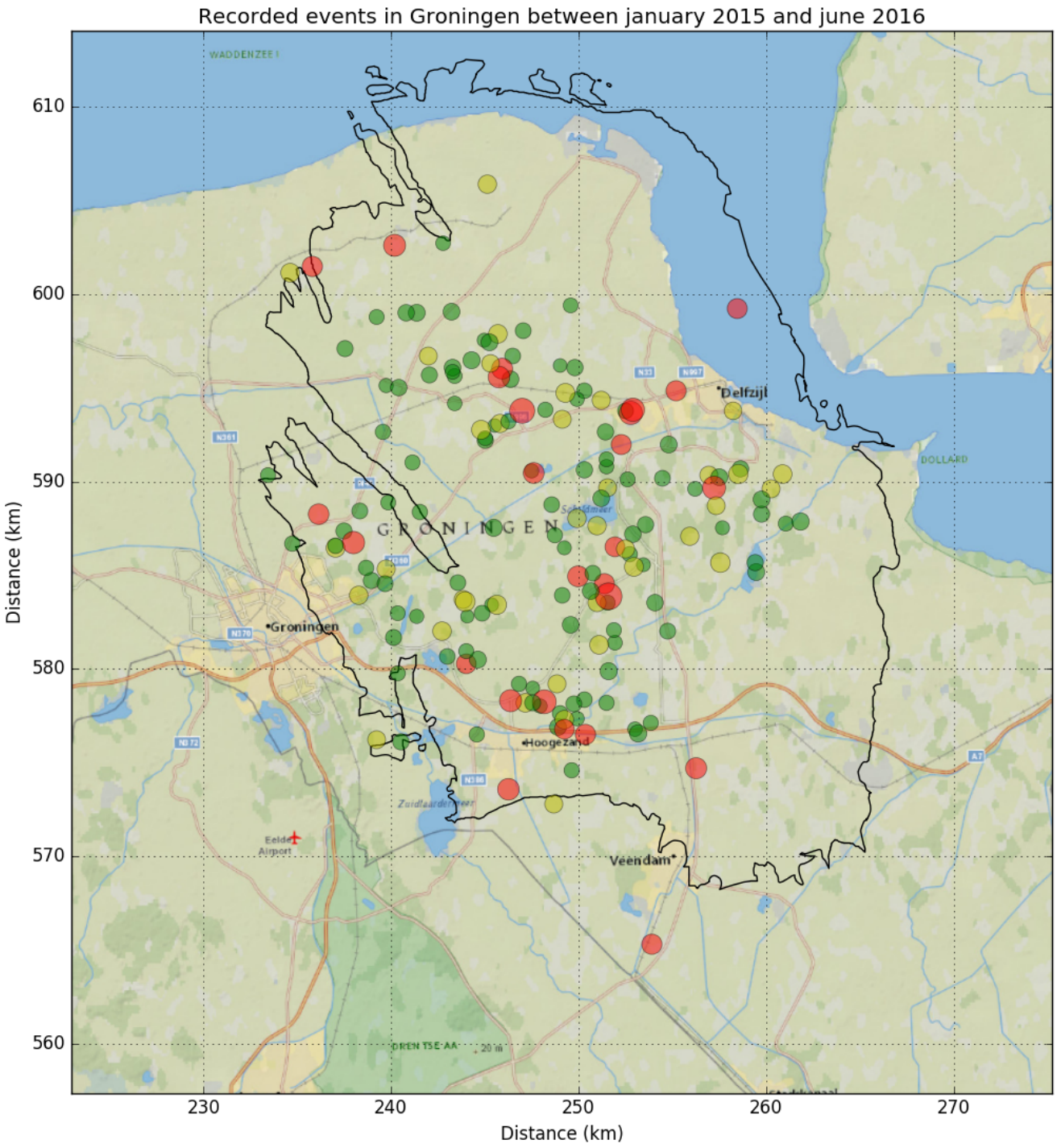

Figure 5: *Map showing the locations of recorded events in Groningen from January 2015 to June 2016. The green circles represent earthquakes with $M_L < 1.0$ (168), yellow circles indicate earthquakes with $M_L < 1.5$ (64) and red circles indicate earthquakes with $M_L > 1.5$ (26). The black line indicates the outline of the Groningen gas field. RD-system coordinates are shown along the axes in km.* (Background map: National Geographic, Esri, DeLorme, HERE, INCREMENT P, NRCAN, METI)

random orientations. To be able to rotate the instruments to radial and transverse components, the horizontal orientations of the geophone channels must be known. A method to estimate these orientations is provided in Section 2.2.

Pre-processing To be able to cross-correlate data from the accelerometer with the geophone data, it is important to correct for the instrument response. ObsPy provides a convenient tool to deconvolve the instrument response using the response information in the station meta-data provided by the station webservice (Beyreuther et al., 2010). In the same step the units of the accelerometers are converted from m/s^2 to m/s to match the units of the geophones. The waveforms are bandpass-filtered using a two-sided Butterworth filter (fourth order) between 3 and 25 Hz. Preliminary testing has shown that this band is appropriate for both P and S-waves (Vossen, 2016). In a few cases where the signals are too noisy, a more narrow bandpass filter is used. Using a two-sided filter is important to prevent phase shifts. When the horizontal components are used, an orientation correction is applied to the geophones in order to align the channels with the accelerometer. The conventions for positive directions of this coordinate frame (E,N,Z) are listed in table 2. Next, the components of both the accelerometer and the geophones are rotated to radial and transverse components using the event azimuth. The positive directions of this new coordinate frame (R,T,Z) are also listed in table 2.

2.1.3 Cross-correlations

For each of the selected events, the pre-processed waveforms are cross-correlated with the waveform from the surface accelerometer. This means that the surface level will be the autocorrelation of the accelerometer data, representing the virtual source. The cross-correlations are computed in the frequency domain. Following the convolution theorem, the Fourier transform of the cross-correlation of f and g is equal to the element-wise product of the complex conjugate of the Fourier transform of f and the Fourier transform of g (equation 3).

$$\mathcal{F}\{f \star g\} = (\mathcal{F}\{f\})^* \cdot \mathcal{F}\{g\} \tag{3}$$

Before the cross-correlation is transformed back to the temporal domain, spectral normalisation is applied to the cross-correlation to whiten the frequency spectrum. The main reason to use spectral normalisation (whitening) is to suppress monochromatic noise (Bensen et al., 2007). The amplitude of each frequency in the spectrum

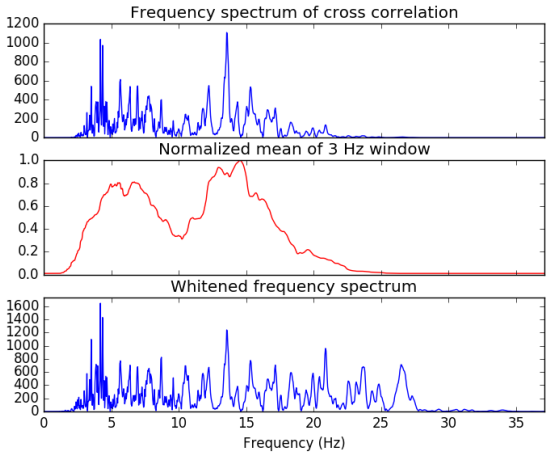

Figure 6: *Illustration of spectral normalisation. Top: Initial amplitude spectrum of the cross-correlation. Middle: Normalised average amplitude over a 3 Hz sliding window. Bottom: Normalised amplitude spectrum of the cross-correlation.*

is normalised by the average amplitude of a 3 Hz window around that frequency. An example of spectral normalisation can be seen in figure 6.

2.1.4 Stacking

For each depth level, the normalised cross-correlations of all events are stacked. An example of this process can be seen in figures 7a and 7b. The original cross-correlations contain a lot of noise with cross-correlation coefficients almost as high as (or even exceeding) the cross-correlation coefficients corresponding to the actual signal. Stacking greatly increases the signal to noise ratio. It can also be noted that the waves that interfere constructively are all very well aligned.

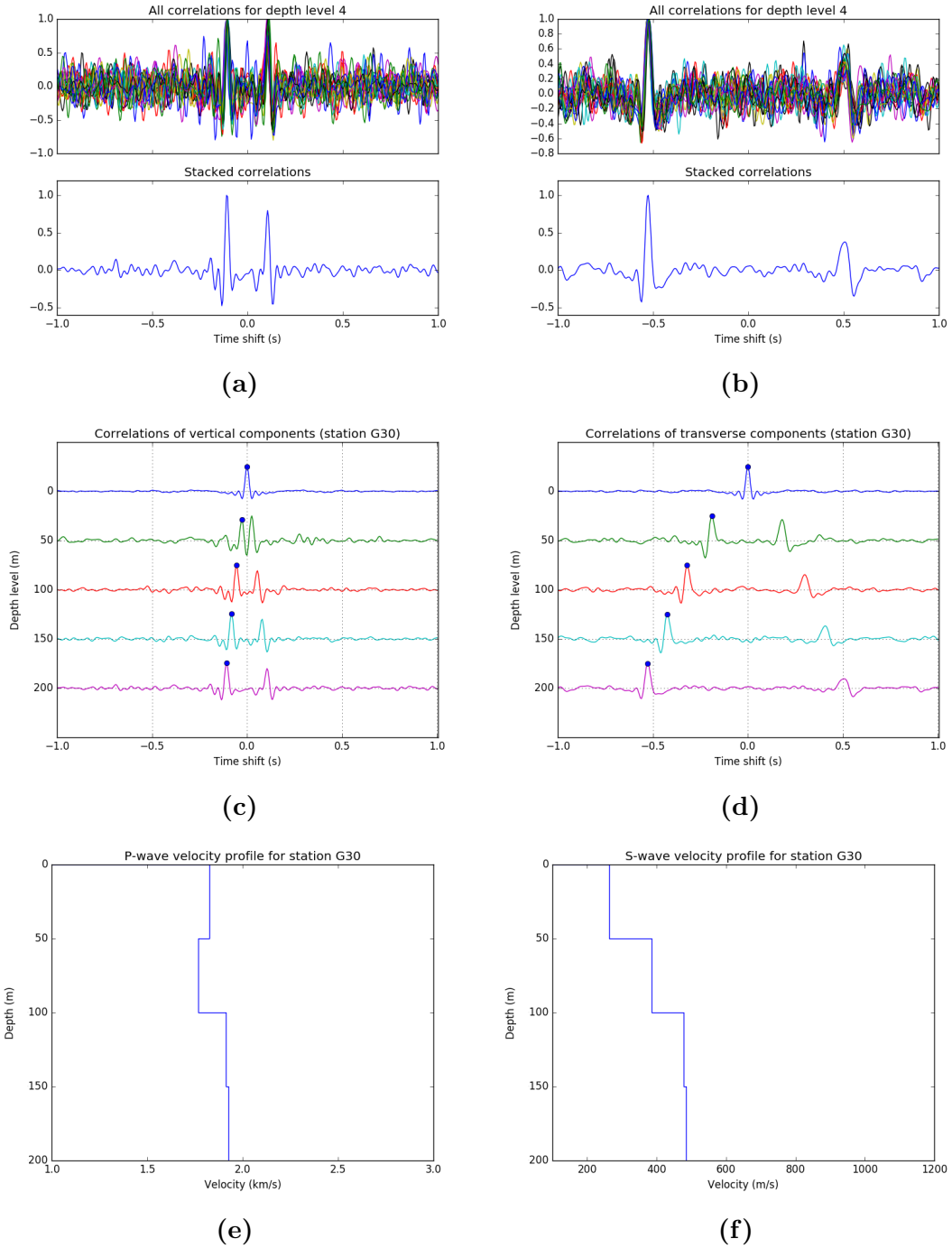

Figure 7: *The steps from cross-correlations to a velocity profile for station G30. Left for P-wave velocity, right for S-wave velocity.* ***(a)*** *Stacking of cross-correlations of the vertical components.* ***(b)*** *Stacking of cross-correlations of the transverse components.* ***(c)*** *Stacked cross-correlations of the vertical components on all depth levels.* ***(d)*** *Stacked cross-correlations of the transverse components on all depth levels.* ***(e)*** *P-wave velocity profile derived from figure 7c.* ***(f)*** *S-wave velocity profile derived from figure 7d.*

2.1.5 Velocities

In both figures 7c and 7d we can now clearly see a wave travelling upwards and being reflected downwards from the surface. The interval velocities of these waves can be determined from the time shift of the peaks at the different depth intervals. To measure the time differences accurately, the cross-correlations are interpolated using a cubic spline function. From the interpolated functions, the maximum values are determined. These are indicated by the blue dots on figures 7c and 7d. For each of the intervals between the seismometers, the time differences together with the vertical distance is used to calculate the interval velocities. The velocities are shown in figures 7e and 7f for the vertical and transverse components respectively. Here we can see that the cross-correlations of the vertical components result in velocities expected for the P-wave, while lower seismic velocities are derived from the cross-correlations of the transverse components. These correspond to velocities expected for the S-wave. Figures 7c and 7e are therefore associated with the first P-wave, and figures 7d and 7f are associated with the first S-wave. In Appendix A, the stacked cross-correlations and velocity profiles of all of the stations can be found.

2.2 Geophone orientations

To be able to calculate the interval S-wave velocities, as described in Section 2.1, the geophones must be rotated to radial and transverse components (directions parallel and perpendicular to the event azimuth). However, the horizontal orientations of the geophone channels are unknown. After drilling the 200 m deep borehole, the geophones are lowered into the hole hanging from a wire. During this process the geophones are free to spin around their vertical axis. Once the geophones are placed, the borehole is stuffed and there is no way to physically measure the orienations of the geophones. This section provides a method to estimate horizontal orientations of borehole geophones using local earthquake data. The method uses the co-located surface accelerometer as a reference, assuming that it is correctly oriented.

2.2.1 Coordinate frames

The first step of the method is to evaluate the coordinate frames of the accelerometers and geophones. The accelerometers used in the network are of the Episensor

ES-T type. The polarity convention used in these sensors is that East, North and upward directions are positive (Kinemetrics Episensor ES-T manual). This translates to the SEED volume as HG1=N. and HG2=E. For the downhole geophones, a different system is used in which the vertical component is positive in the downward direction, and the positive direction of HH1 is 90° clockwise of HH2 (table 1).

Orientation conventions for positive directions		
Channel code	Accelerometers	Geophones
HG1/HH1	North	HH2 + 90°
HG2/HH2	East	Any
HGZ/HHZ	Upwards	Downwards

Table 1: *Naming of the three channels of the accelerometers and geophones in the Groningen network and the directions of their positive axes.*

Using these assumptions, both the geophone and accelerometer data are transformed to a coordinate frame where East, North and upwards are the positive directions. Eventually the coordinate frames will be rotated to radial, transverse and vertical components. In that case, the radial component is defined as direction pointing from the source to the receiver, so the positive axis points away from the source. The transverse component is positive in the direction 90° clockwise of the positive radial direction. The vertical component is positive in the upwards direction (table 2).

Orientation conventions for positive directions			
Channel	Positive direction	Channel	Positive direction
N	North	R	Away from source
E	East	T	R + 90°
Z	Upwards	Z	Upwards

Table 2: *Conventions used in this study.*

2.2.2 Pre-processing

The pre-processing used for this method is mostly the same as described in Section 2.1.2. The waveforms are bandpass filtered between 3 Hz and 15 Hz. This is slightly different from the filter used in Section 2.1.2 because we are focusing purely on the S-wave here. Equation 4 shows how the accelerometer channels are rotated from (N,E) to (R,T), where α represents the event azimuth. For a positive azimuth, this corresponds to a clockwise rotation.

$$\begin{bmatrix} R \\ T \end{bmatrix} = \begin{bmatrix} \cos\alpha & \sin\alpha \\ -\sin\alpha & \cos\alpha \end{bmatrix} \begin{bmatrix} N \\ E \end{bmatrix} \tag{4}$$

The horizontal channels (1,2) of the geophones are rotated by the same amount (equation 5). Because the initial orientations of the geophone channels are unknown, the resulting orientations are not (R,T), but (R + θ,T + θ), where θ is the clockwise angle between north and channel 2, the angle we want to find.

$$\begin{bmatrix} \cos\alpha & \sin\alpha \\ -\sin\alpha & \cos\alpha \end{bmatrix} \begin{bmatrix} HH2 \\ HH1 \end{bmatrix} = \begin{bmatrix} \cos\alpha & \sin\alpha \\ -\sin\alpha & \cos\alpha \end{bmatrix} \begin{bmatrix} N+\theta \\ E+\theta \end{bmatrix} = \begin{bmatrix} R+\theta \\ T+\theta \end{bmatrix} \tag{5}$$

The event azimuth α is defined as the direction from a seismic source to the seismic station measured clockwise from north. This means that for each event, the radial and transverse directions will be different.

2.2.3 Cross-correlations and rotation

Cross-correlations are made between the accelerometer and geophone channels. The radial and transverse components are cross-correlated separately. The cross-correlations are performed in the frequency domain. Spectral whitening over a 3 Hz window is applied to each of the cross-correlations in order to get a more balanced frequency spectrum. Section 2.1.3 describes this step in more detail.

For each of the cross-correlations made, the maximum cross-correlation coefficient (CC) is stored. This value represents the similarity of geophone and accelerometer data. The geophone channels are then rotated counterclockwise with small increments, and for each step the maximum CC is again stored.

In case the signal to noise ratio would be very good, the maximum CC will increase until the geophone channels point in the same direction as the accelerometer channels. When the geophone channels point in the directions opposite of those of

the accelerometer, the maximum CC will be a negative value. If the channels point in perpendicular directions, the cross-correlation coefficient will be close to zero.

However, we are using real data here and the signal to noise ratios are generally poor. When the geophone channels are rotated perpendicular to the accelerometer channels, there will always be a peak in the cross-correlation caused by noise. This will cause jumps in the curve where its value should be zero. To solve this problem, the time shift of the signal needs to be determined first. In other words, we need to know which peak in the cross-correlation belongs to the actual S-wave signal. To achieve this, the geophone data is rotated by 360 degrees with larger (20°) steps, and for each step the time shift of the the maximum CC is stored. The mode of the time shift is then assumed to be the time shift of the signal.

When rotating the geophone for a second time, now with smaller increments (3°), only the CC belonging to the signal is stored. This will produce a smooth curve of the signal cross-correlation coefficient as a function of horizontal rotation of the geophone. The maximum value of this function represents the angle to which the geophone must be rotated to align its components with the surface accelerometer's (θ in equation 5). If we assume a correct accelerometer orientation, this angle corresponds to the horizontal orientation of the geophone with respect to north. In other words, the orientation of channel 2 will be equal to θ, and the orientation of channel 1 will be $\theta + 90°$.

2.2.4 Standard deviations

Because both channels of the geophones are used, two independent solutions can be calculated per event. The number of data available is therefore twice the number of available events. The standard deviation can be determined for each of the geophones by calculating the orientations individually from all available traces. Poor signal to noise ratios might result in an inaccurate orientation estimate. Therefore all traces that produce an orientation which differs from the mean by more than one standard deviation are dismissed.

The orientations of all geophones are included in Appendix B, along with the number of data used (number of traces after outlier removal), number of available traces, standard deviation, and a figure with the orientation curves.

3 Results

In this section, results are presented for all of the stations that were online and had data available at the time of this study (2016/07/12). Stations G12, G15, G25, G35, and G48 were not available due to technical issues. For stations G05 and G70 there were no event data available. Station G09 was left out of the results because the velocities derived from this station were unrealistically high, and stations G38 and G44 were left out due to the large amount of noise. This is discussed in Section 4.1.

3.1 Velocity profiles

Figure 8 shows the individual seismic velocity profiles for each of the 60 stations included in this study. The velocities are derived using the method described in Section 2.1. Figure 8a shows the P-wave velocity profiles and figure 8b shows the S-wave velocity profiles. On top of the individual profiles a mean profile is drawn together with the standard deviation from the mean.

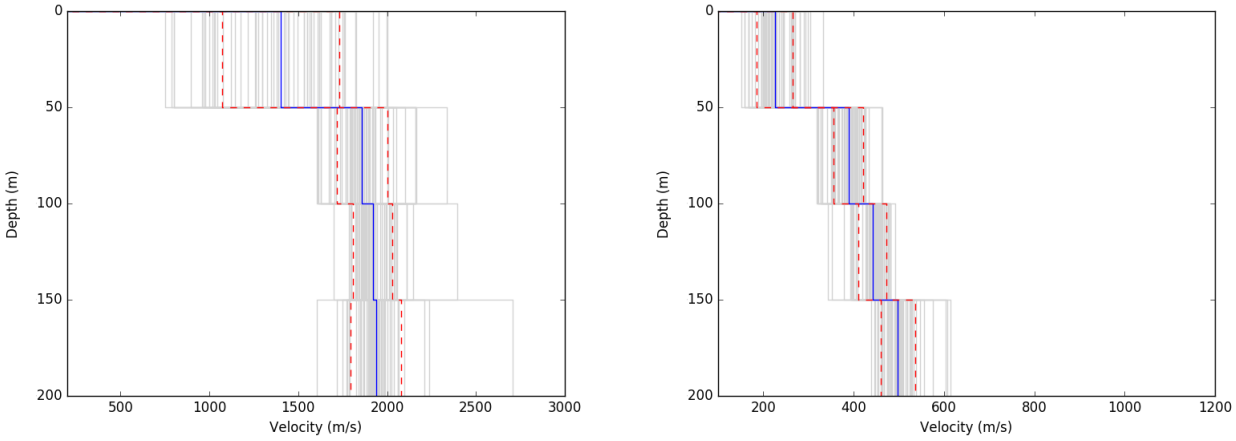

(a) **(b)**

Figure 8: *Velocity profiles for all 60 individual stations are drawn in light grey. The blue line indicates the mean velocity profile. The dashed red lines indicate the range covered by one standard deviation from the mean for each of the intervals.* ***(a)*** *P-wave velocity.* ***(b)*** *S-wave velocity.*

3.2 Interpolated velocity maps

Figures 9 and 10 show the interval velocities of all stations plotted on a map. Green colours represent low seismic velocities and red colours represent high seismic velocities. Colours inside the black triangles (stations) correspond with the values calculated with the method described in Section 2.1. The colours in between stations correspond with values interpolated with a nearest-neighbour method.

3.3 Geophone orientations

The orientations of the geophones have been estimated using the method explained in Section 2.2. Appendix B contains the results for all of the stations in the Groningen network. An example is given in figure 11 and table 3. The standard deviations for the orientations of all geophones are plotted in figure 12.

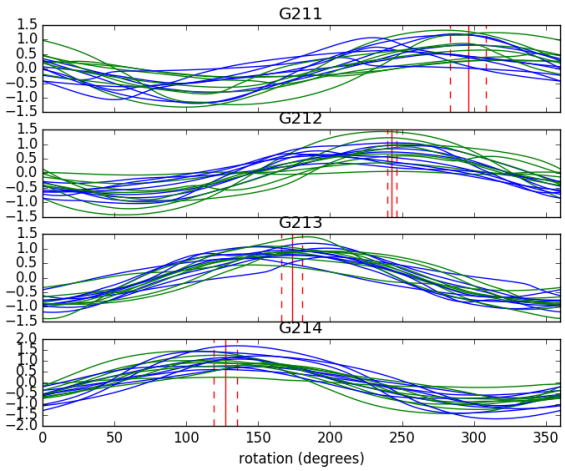

Figure 11: *Orientation curves for station G21. The lines indicate the maximum cross-correlation coefficient (with the surface accelerometer) as a function of counterclockwise rotation of the geophone. Blue lines are for the radial components, green lines for the transverse components. The vertical red lines indicate the average rotation +/- one standard deviation.*

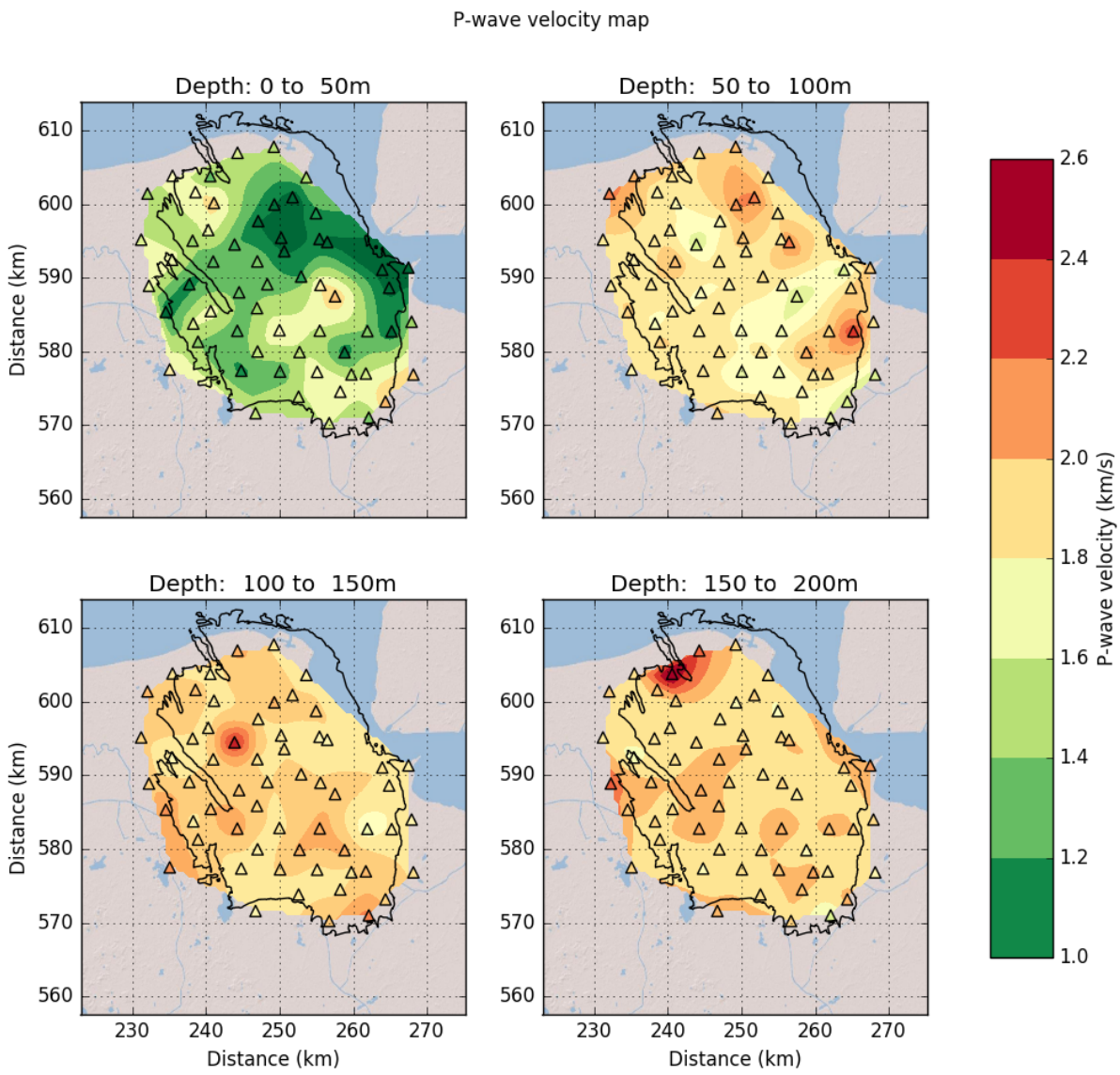

Figure 9: *Map showing the P-wave velocity for all stations in the Groningen network in four depth intervals. The triangles represent the values calculated from seismic interferometry, while the colours in between stations are calculated with a nearest-neighbour interpolation. The black line indicates the outline of the Groningen gas field. RD-system coordinates are shown along the axes in km.*

(Background map: Esri)

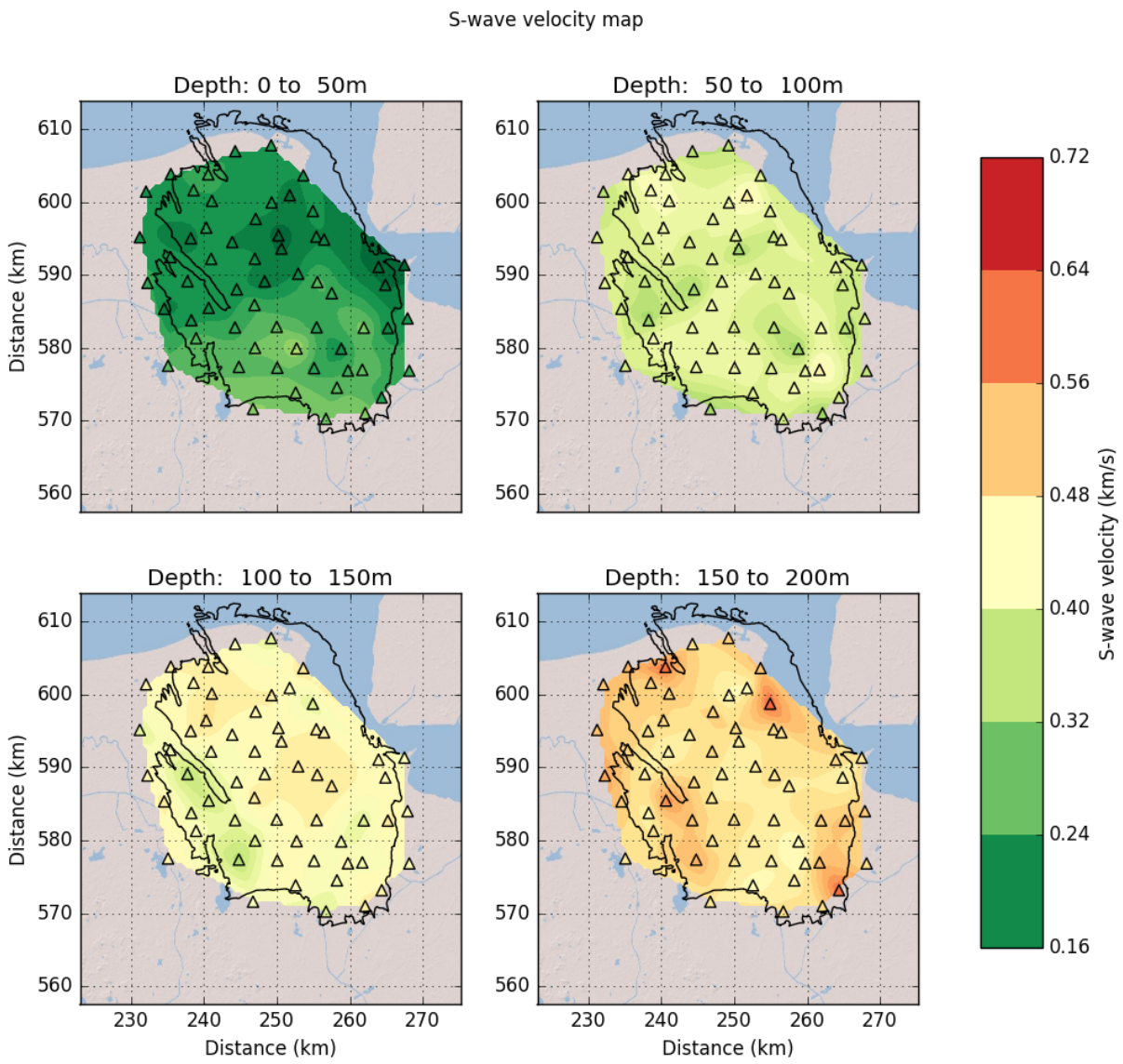

Figure 10: *Map showing the S-wave velocity for all stations in the Groningen network in four depth intervals. The triangles represent the values calculated from seismic interferometry, while the colours in between stations are calculated with a nearest neighbour interpolation. The black line indicates the outline of the Groningen gas field. RD-system coordinates are shown along the axes in km.*

(Background map: Esri)

Code	Channel 1	Channel 2	Data used	Standard deviation
G211	25.8°	295.8°	11/16	12.7°
G212	332.9°	242.9°	12/16	3.3°
G213	263.3°	173.3°	9/16	7.0°
G214	217.0°	127.0°	10/16	8.0°

Table 3: *This table shows the channel orientations of the geophones in station G21 in degrees clockwise from north. The standard deviations are based on orientations calculated from the individual events used. Data used shows how many traces were used for the final calculation and how many were initially found within the station lifetime.*

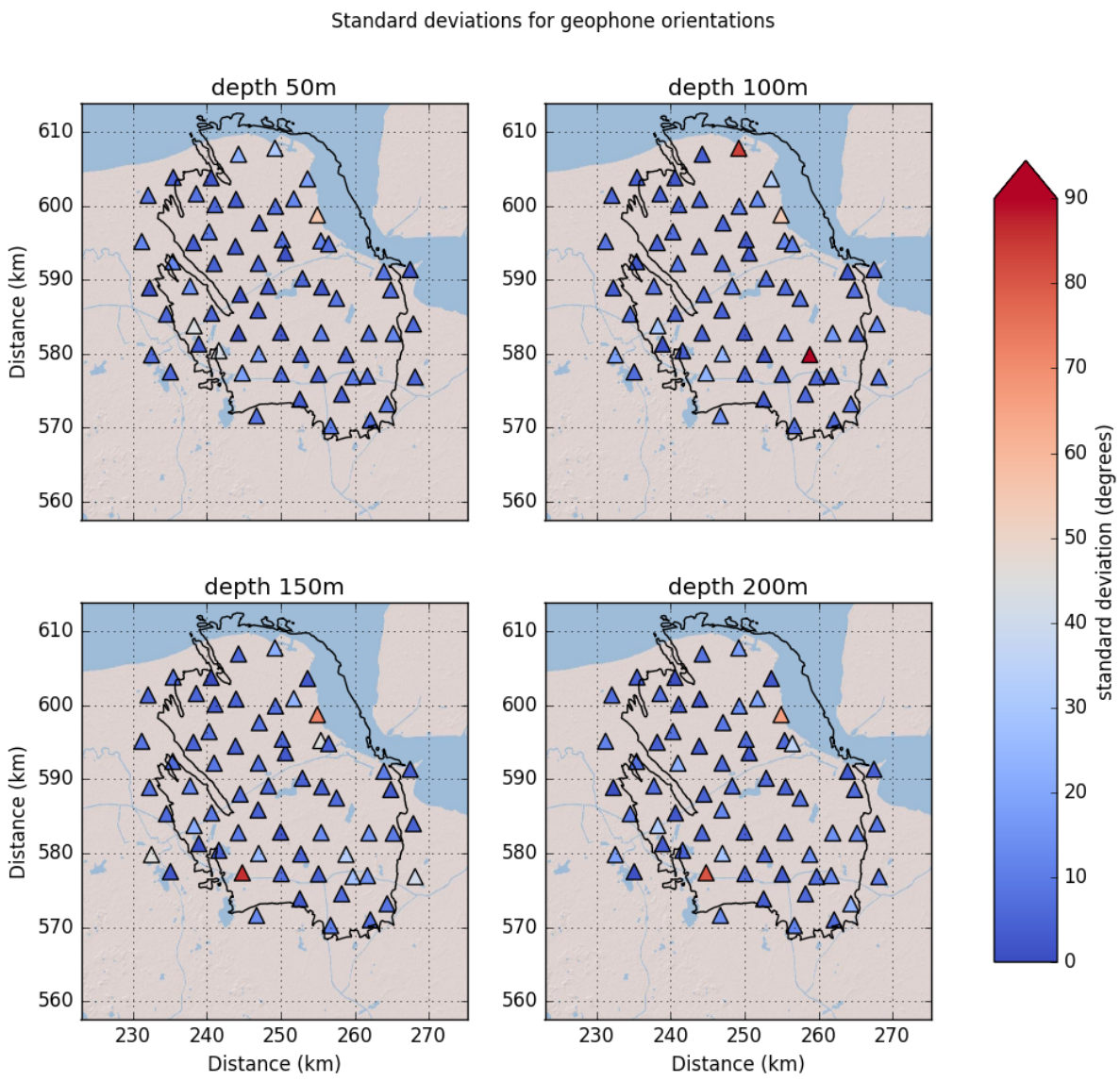

Figure 12: *Standard deviations for the orientations of the geophones. The black line indicates the outline of the Groningen gas field. RD-system coordinates are shown along the axes in km.* *(Background map: Esri)*

3.4 Detected errors in geophone metadata

During this study, a large amount of data was processed and evaluated. As a result, some errors were found in the naming of the geophones. For example in station G11 an upwards travelling wave would seem to arrive first at the 3rd geophone (G113), then at the 4th (G114), followed by G112 and G111. The errors were first detected in the stacked correlations and then checked by evaluating the traces from individual events. The event data for these stations is included in Appendix C. The original and corrected names of these geophones are shown in table 4. It should be noted that these errors are corrected retrospectively in the data headers. The examples included in Appendix C were made before these changes.

Assigned code	**Correct code**
G113	G114
G114	G113
G321	G322
G322	G323
G323	G324
G324	G321
G472	G474
G474	G472

Table 4: *Errors in the geophone name coding.*

When evaluating the seismic velocity maps, it was suspected that there were errors in the depth of some of the geophones. For example station G04 and G54 showed very high velocity anomalies on the lowest geophone intervals which could not be correlated to geological features. After requesting the documents from the drilling company, this presumption was confirmed. In table 5, all geophones that have deviating depths are listed.

Code	Intended depth	Actual depth
G044	200 m	185 m
G054	200 m	180 m
G071	50 m	30 m
G072	100 m	80 m
G073	150 m	130 m
G074	200 m	180 m
G104	200 m	197 m

Table 5: *Geophones in the Groningen network where the depth of placement is not as intended.*

4 Discussion

4.1 Seismic velocity profiles

Seismic interferometry relies on the assumption that the Fresnel zones are sufficiently illuminated, as explained in Section 2.1.1. It is not an unrealistic assumption because the fastest waves will travel through the deeper structures where the seismic velocity is higher than in the shallow crust. These will then refract steeply towards the surface and arrive with near vertical incidence. In the individual event cross-correlations in figures 7a and 7b, we can see that the traveltime is very stationary, since the peaks all line up exactly at the same time shift. This observation supports the assumption, because for waves from the Fresnel zone we would expect the traveltime to be stationary. If the waves are not from the Fresnel zone, such a result could only be achieved if all waves have exactly the same non vertical incidence angle. It would be interesting to study this problem by calculating the variety in incidence angles for each station.

Initially, a few anomalies existed in both the P-wave and S-wave maps where the seismic velocity was extremely high in the lowest interval. The question was whether this was a natural high velocity structure like a salt diapir, or an error on the lowest geophone. The fact that they occurred on both the P-wave and S-wave velocity maps could not rule out either of these possibilities. Reports from the installation of the borehole stations gave the answer. The lowest geophone was

placed at a depth of 185 m instead of 200 m. After studying the reports of all of the stations there seemed to be several boreholes where such errors existed. These are listed in table 5. The report of station G09 states no such thing. However, the seismic velocities on the lowest interval of this station are also extremely high (figure 23). Because no geological explanation could be found and the data quality seems to be very good, it is suspected that the lowest geophone of this station was also placed too shallow. Station G09 is not included in figures 9 and 10.

In Kruiver et al. (2015) a V_{S30} map was presented. This map is derived from a lithological map, where the lithologies are coloured according to their associated seismic S-wave velocities. The S-wave velocities are measured with Cone Penetration Tests (CPTs). The values are assumed to be an average S-wave velocity for the top 30 meters. It is therefore interesting to compare these results to the S-wave velocities for the interval between 0 and 50 m depth presented in this study. Both maps are plotted in figure 13, with the colours indicating approximately the same values.

The V_{S30} values in Kruiver et al. (2015) range from 156.1 m/s to 275 m/s. In figrue 8b, we can see that the values for the S-wave velocity in the upper interval plot mostly within the range from 150 m/s to 300 m/s. This is a very good overlap, considering the different approach. When comparing the maps in figure 13, it should be noted that the values from this study are interpolated in between the stations. It therefore has a very poor spatial resolution and will not be able to map the geological structures that can be seen in the map by Kruiver et al. (2015). However, the large scale lateral differences in S-wave velocity are definitely in agreement. A SW-NE line through the middle of the Groningen field separates a relatively low velocity zone in the northwest from a relatively high velocity zone in the southeast. The southeast part has a lower velocity zone in the northeast, around stations G31, G37, and G60. The similarity of the maps in figure 13 means that the lateral differences in shear wave velocity in this interval can be explained by lithological differences. High velocity Pleistocene sediments (mainly sands) occur more shallow in the southern part, and are overlain by lower velocity Holocene deposits (clay, peat) in the north.

In Bommer et al. (2015), a V_{S65} model is presented based on the reinterpretation of ground roll (i.e., surface wave) measurements from seismic surveys. They state that the values represent average S-wave velocities for a depth range from 50 to 120 m. In figure 14, the map is compared to the S-wave velocities for the interval

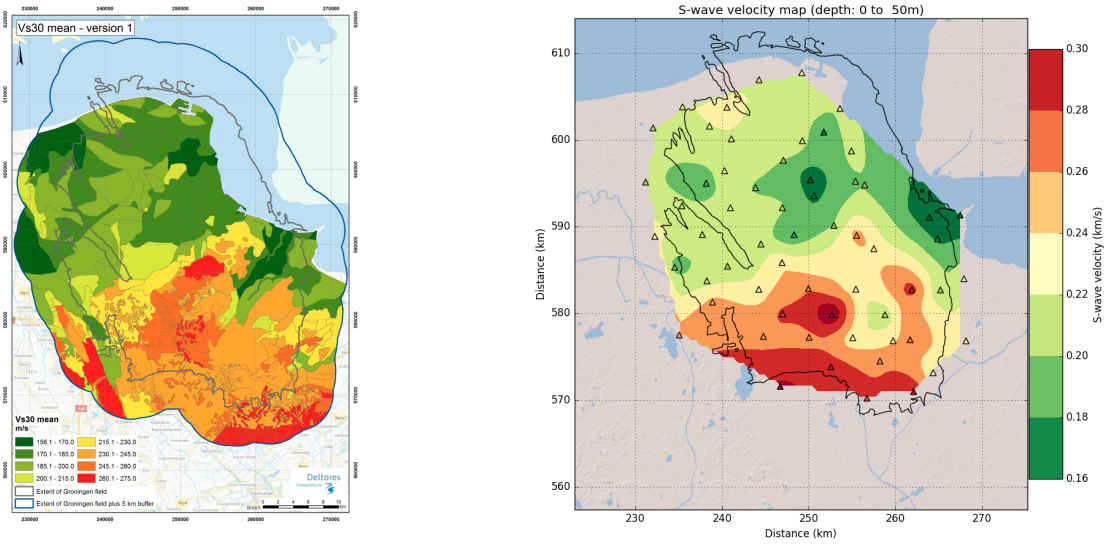

Figure 13: *Comparison of the V_{S30} map from Kruiver et al. (2015) (left), and the S-wave velocities between 0 and 50 m depth from this study (right). The black line indicates the outline of the Groningen gas field. RD-system coordinates are shown in m on the left image, and in km on the right image.*

between 50 and 100 m depth presented in this study. The values for V_{S65} in Bommer et al. (2015) range from 297.77 m/s to 452.62 m/s. In figure 8b, we can see that the values for the second depth interval (50 to 100 m) fall in the same range. Due to the extreme amount of receiver data from seismic surveys used to construct the V_{S65} map in Bommer et al. (2015), the spatial resolution is enough to recognise buried channel infills. This features can not be retrieved with passive seismic interferometry (figure 14). The high velocity areas in the northwest and southeast do overlap quite well.

The deeper V_S structure in Bommer et al. (2015) is assumed to vary linearly from 65 m to 350 m depth, where it reaches a stationary value of 639 m/s. The linear function is based on an empirical relationship between V_P and V_S. The average V_S values found in this study do seem to increase linearly between 50 m and 200 m depth, but more work needs to be done to compare the deeper V_S structures.

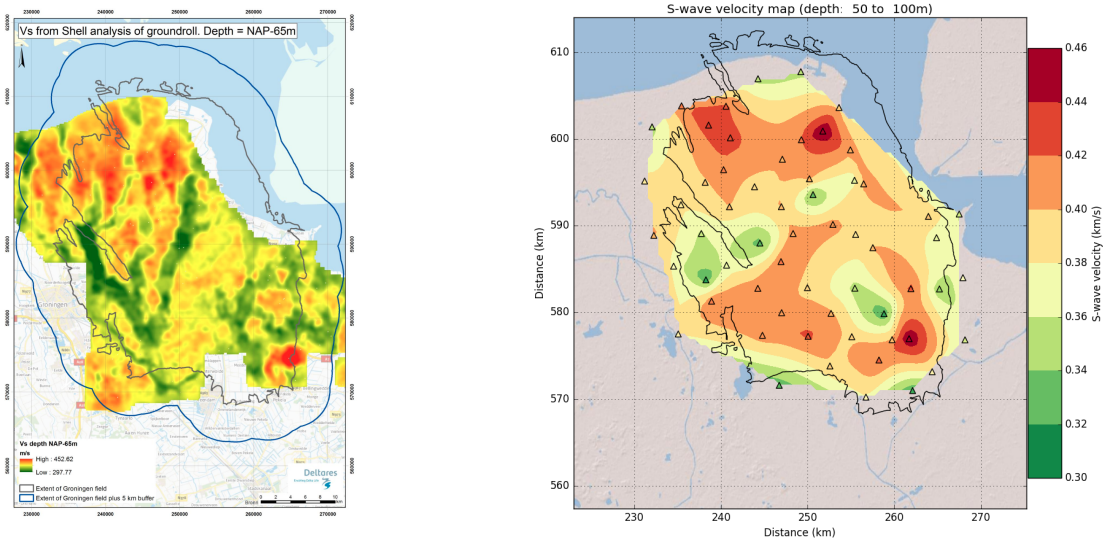

Figure 14: *Comparison of the V_{S65} map from Bommer et al. (2015) (left), and the S-wave velocities between 50 and 100 m depth from this study (right). The black line indicates the outline of the Groningen gas field. RD-system coordinates are shown in m on the left image, and in km on the right image.*

4.2 Geophone orientations

To determine the geophone orientations, it is assumed that the surface accelerometers are aligned to the north and east directions. Although this was the instruction when the network was installed, it is hard to tell with what precision this has been done. As a result, the orientations for a particular station may seem very accurate from the small standard deviations, but this only means that the orientation relative to the accelerometer is very well constrained. If the accelerometer is not precisely oriented, this error will affect the geophone orientations as well. If the orientations are slightly off, the transverse channel will still contain enough S-wave energy to be cross-correlated. Therefore it will still be possible to determine the S-wave velocity. However, if the orientation results were to be used for other applications that require more accuracy, it might be necessary to physically measure the accelerometer orientations.

Initially, a different method was developed to measure the geophone orientations based on deep, teleseismic events. It involved calculating the signal to noise ratio

for the first P-wave arrival. The horizontal channels were then rotated with small increments. The orientation at which the signal to noise ratio reaches a maximum should then be in the direction of the event azimuth, which would allow the declination from north to be determined. The advantage of this method is that the orientations of all instruments can be determined individually, independent of the orientation of the accelerometer.

The method seemed to work well for traditional stations of the NL network, for example station HGN. For stations in the Groningen network, the signal to noise ratios seemed to be generally too low for these remote events. A lot of effort was done to increase the signal to noise ratios by optimising the event selection, signal and noise window lengths, bandpass filter frequencies, and whitening filters. Finally it was concluded that signal to noise ratios of teleseismic recordings were insufficient on the stations in the Groningen network.

Traditionally, seismic stations are placed in solid basement rocks, like HGN is placed in metamorphic Carboniferous slate. This makes them excellent for monitoring global earthquakes with high signal to noise ratios. The Groningen network was deployed solely to monitor local seismicity, and stations are placed in loose Pleistocene and Holocene sediments making them very sensitive to noise from all kinds of local sources.

In some cases, the new orientation method also suffers from these low signal to noise ratios. In figure 12, the standard deviations for the orientations of all geophones are plotted on a map. Station G02 is the northernmost station on this map (see also figure 2). This station has very high standard deviations, especially on the second geophone (G022). Closer inspection reveals that this station is placed inside the Eemshaven harbour, surrounded by a lot of noise sources from traffic, windmills, ships and industry.

Other cases of large standard deviations can be caused by lack of data. Some of the stations had been running only for a few (quiet) months at the time of this study, and had data only for a few events. While for some stations this does not seem to be a problem (e.g., G69, see Appendix B), for other stations it can be problematic (e.g., G38, see Appendix B). Lowering the magnitude threshold from 1.5 to 1.0 can be a solution, as more events become available, but lower magnitude events generally produce lower signal to noise ratios.

To test the geophone orientations, we can take a look at event waveforms. In figure 15, three component waveforms are shown for an event close to the station

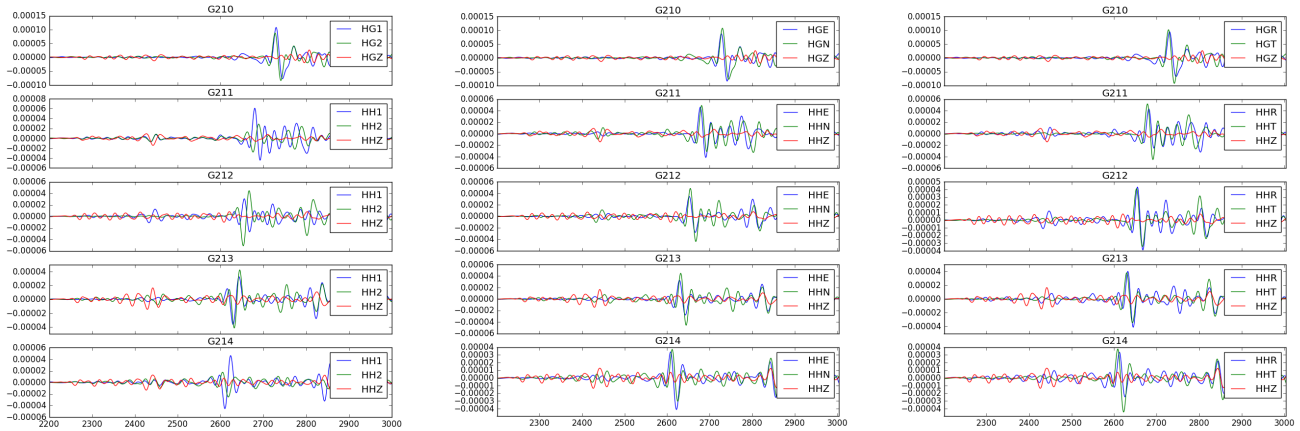

(a) **(b)** **(c)**

Figure 15: *Three componenet waveforms for station G21 for a magnitude 1.7 event on 2015-12-15(07:43:55). The event is almost pure south of the station, at a distance of approximately 4 km.* ***(a)*** *Waveforms with original (1,2,Z) channels.* ***(b)*** *Waveforms rotated to (E,N,Z) channels using the orientations in table 3.* ***(c)*** *Waveforms rotated to (R,T,Z) channels using the orientations in table 3 and the event azimuth.*

with a backazimuth of 180°. This means that the event is straight south of the station. The instrument responses have been removed here and the data is bandpass filtered from 2 Hz to 10 Hz. In figure 15a, the data is plotted in the original (1,2,Z) channels. The up and down going S-waves can easily be recognised but on each geophone they are recorded differently on the channels. This is because channels 1 and 2 have arbitrary orientations. In figure 15b, the channels are rotated to an (E,N,Z) system using the orientations derived with the method explained in Section 2.2. Here we can see that the channels are now aligned to one another, because the signal is recorded similarly on the horizontal channels of each of the geophones. The assumptions for the channel naming on the accelerometers and geophones are confirmed here, because we can see that the traces have the same polarity on the geophones and the accelerometer. Lastly, figure 15c can be used to check the R,T,Z system. Because the event is straight south from the station, the R channels should correspond to the N channels in figure 15b, and the T channels should correspond to the E channels.

5 Conclusions

Vertical seismic velocity profiles for both P and S-waves were derived for nearly all of the borehole stations in the Groningen network using passive seismic interferometry. In previous studies, the shear velocity structure used for the GMPE depends on different techniques for different depth intervals. This study provides a single method to derive the seismic velocities within four intervals from 0 m to 200 m depth. The resulting shear wave velocity map for the upper interval (0 to 50 m) correlates well with the seismic velocity structure derived from surface lithology, both in the range of velocities found and the spatial distribution of the velocities. For the second interval (50 to 100 m), the range of velocities found is well in agreement with results from surface wave inversion. The spatial distribution is harder to compare because of the difference in resolution, but the large scale structure is similar. For the intervals from 100 to 150 m and 150 to 200 m, previous studies did not include lateral variation in their shear velocity model but used a stationary value.

Horizontal orientations of the geophones in the Groningen network were derived using a new method based on cross-correlations with the accelerometers at the surface. This result is not only essential to derive the shear wave velocities using passive seismic interferometry, but can be used in the future for many other applications.

During this study, by processing and analysing a large amount of data from the new Groningen network, several errors in and inconsistencies were detected. In some cases the connections of the geophones were confused, and in some stations the depth of the geophones deviate from the intended depths.

References

Aki, K. and Richards, P. (2002). *Quantitative Seismology*. Geology (University Science Books).: Seismology. University Science Books.

Bensen, G., Ritzwoller, M., Barmin, M., Levshin, A., Lin, F., Moschetti, M., Shapiro, N., and Yang, Y. (2007). Processing seismic ambient noise data to obtain reliable broad-band surface wave dispersion measurements. *Geophysical Journal International*, 169(3):1239–1260.

Beyreuther, M., Barsch, R., Krischer, L., Megies, T., Behr, Y., and Wassermann, J. (2010). Obspy: A python toolbox for seismology. *Seismological Research Letters*, 81(3):530–533.

Bommer, J. J., Dost, B., Edwards, B., Rodriguez-Marek, A., Kruiver, P. P., Meijers, P., Ntinalexis, M., and Stafford, P. J. (2015). Development of version 2 GMPEs for response spectral accelerations and significant durations from induced earthquakes in the groningen field. *NAM*, Version 2, 29 October 2015.

Bommer, J. J., Dost, B., Edwards, B., Stafford, P. J., van Elk, J., Doornhof, D., and Ntinalexis, M. (2016). Developing an Application-Specific Ground-Motion Model for Induced Seismicity. *Bulletin of the Seismological Society of America*, 106(1):158–173.

Bommer, J. J., Stafford, P. J., Alarcón, J. E., and Akkar, S. (2007). The influence of magnitude range on empirical ground-motion prediction. *Bulletin of the Seismological Society of America*, 97(6):2152–2170.

Kruiver, P., de Lange, G., Wiersma, A., Meijers, P., Korff, M., Peeters, J., Stafleu, J., Harting, R., Dambrink, R., Busschers, F., and Gunnink, J. (2015). Geological schematisation of the shallow subsurface of Groningen. for site response to earthquakes for the Groningen gas field. *Deltares*, Report No. 1209862-005-GEO-0004-v5r, 16 March 2015.

Shearer, P. and Orcutt, J. (1987). Surface and near-surface effects on seismic waves-theory and borehole seismometer results. *Bulletin of the Seismological Society of America*, 77(4):1168–1196.

Vossen, C. (2016). *Near-surface Velocity Profiles of Groningen and surroundings extracted using Seismic Interferometry*. Universiteit Utrecht. MSc guided research report.

Wapenaar, K., Draganov, D., Snieder, R., Campman, X., and Verdel, A. (2010). Tutorial on seismic interferometry: Part 1 basic principles and applications. *Geophysics*, 75(5):75A195–75A209.

Appendices

A Velocity profiles

Station G01

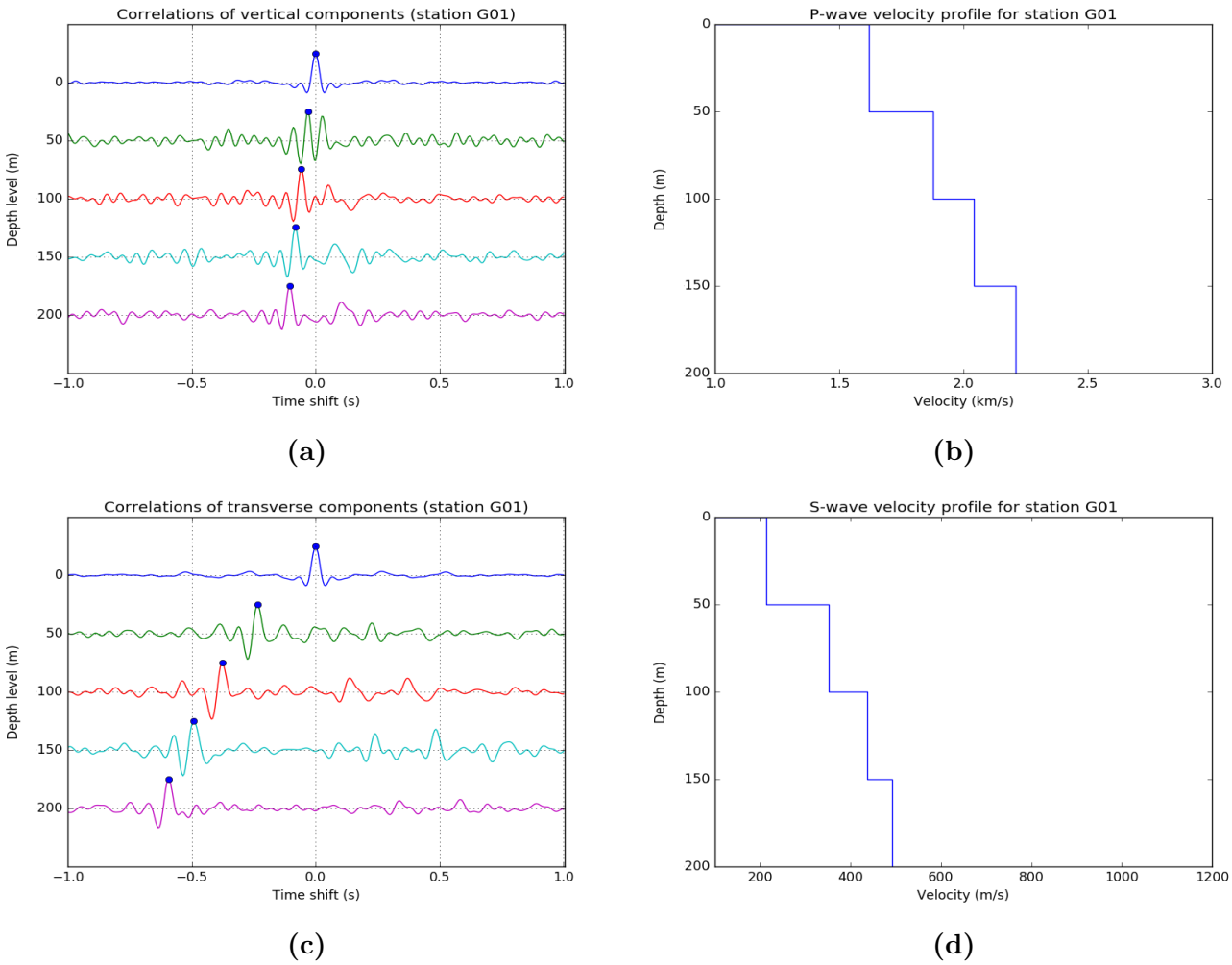

Figure 16: ***(a)*** *Stacked cross-correlations of the vertical components. Blue dot indicates the peak associated with the P-wave.* ***(b)*** *P-wave velocity profile calculated from the picks in figure 16a.* ***(c)*** *Stacked cross-correlations of the transverse components. Blue dot indicates the peak associated with the SH-wave.* ***(d)*** *S-wave velocity profiles calculated from the picks in figure 16c.*

Station G02

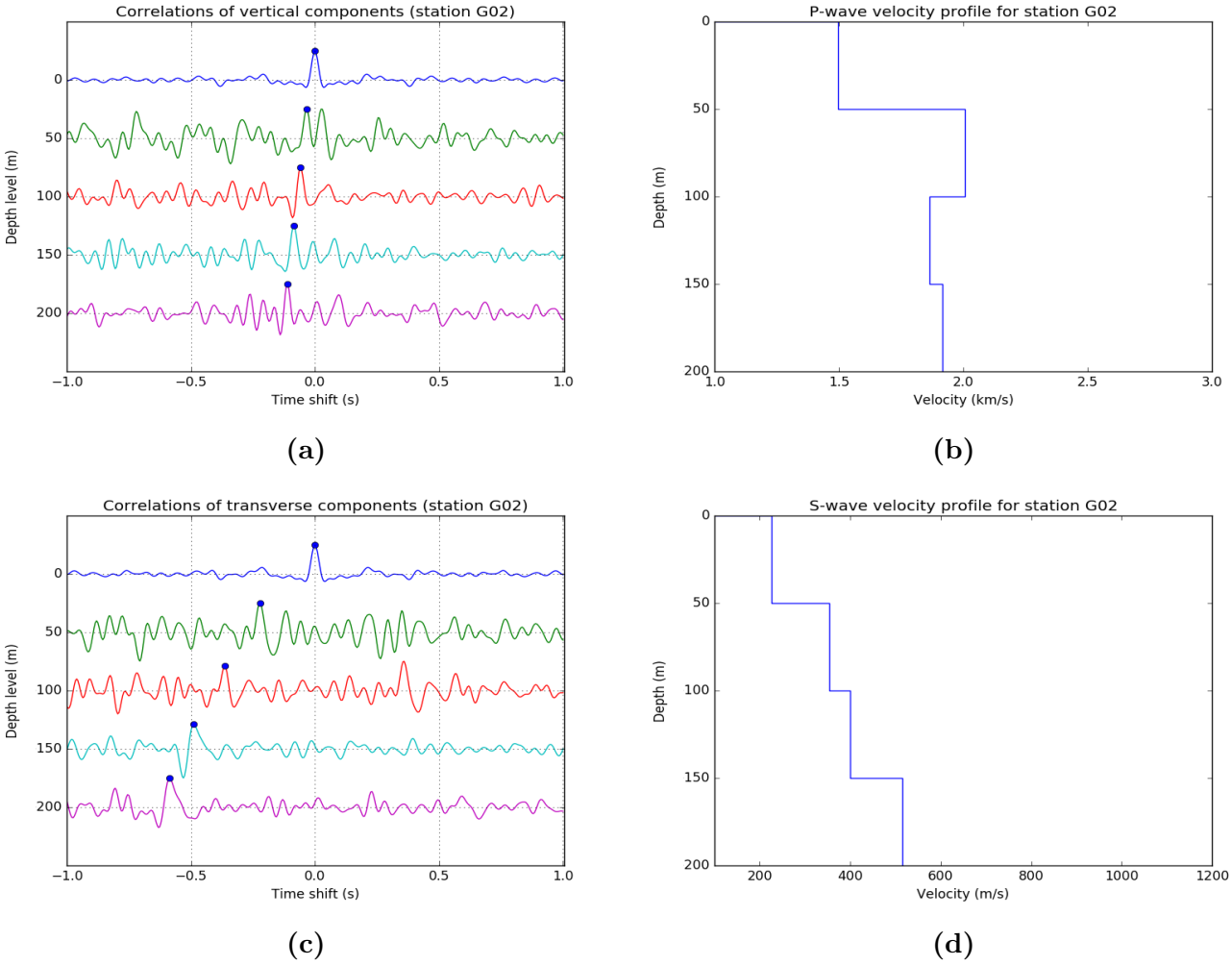

Figure 17: ***(a)*** *Stacked cross-correlations of the vertical components. Blue dot indicates the peak associated with the P-wave.* ***(b)*** *P-wave velocity profile calculated from the picks in figure 17a.* ***(c)*** *Stacked cross-correlations of the transverse components. Blue dot indicates the peak associated with the SH-wave.* ***(d)*** *S-wave velocity profiles calculated from the picks in figure 17c.*

Station G03

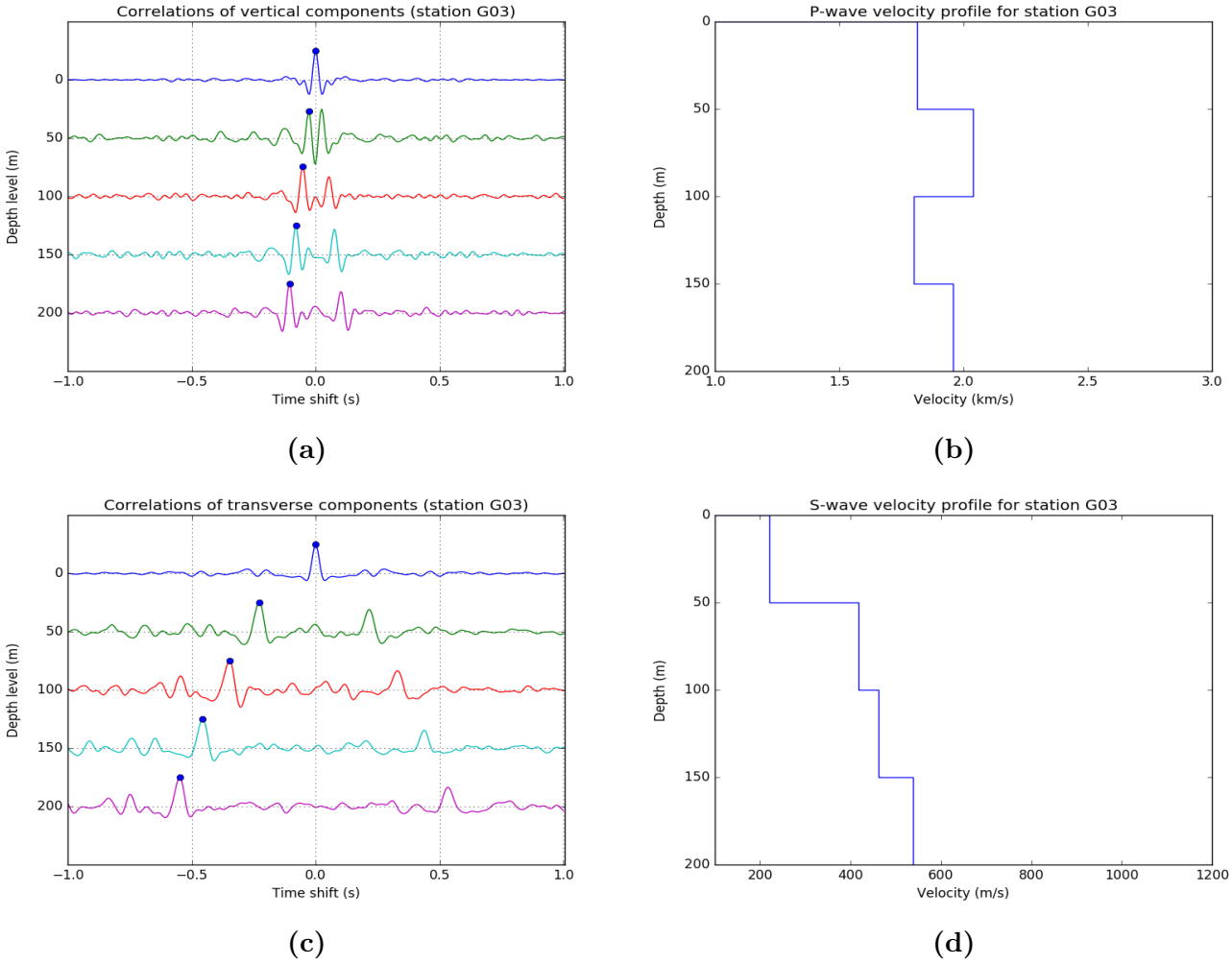

Figure 18: ***(a)*** *Stacked cross-correlations of the vertical components. Blue dot indicates the peak associated with the P-wave.* ***(b)*** *P-wave velocity profile calculated from the picks in figure 18a.* ***(c)*** *Stacked cross-correlations of the transverse components. Blue dot indicates the peak associated with the SH-wave.* ***(d)*** *S-wave velocity profiles calculated from the picks in figure 18c.*

Station G04

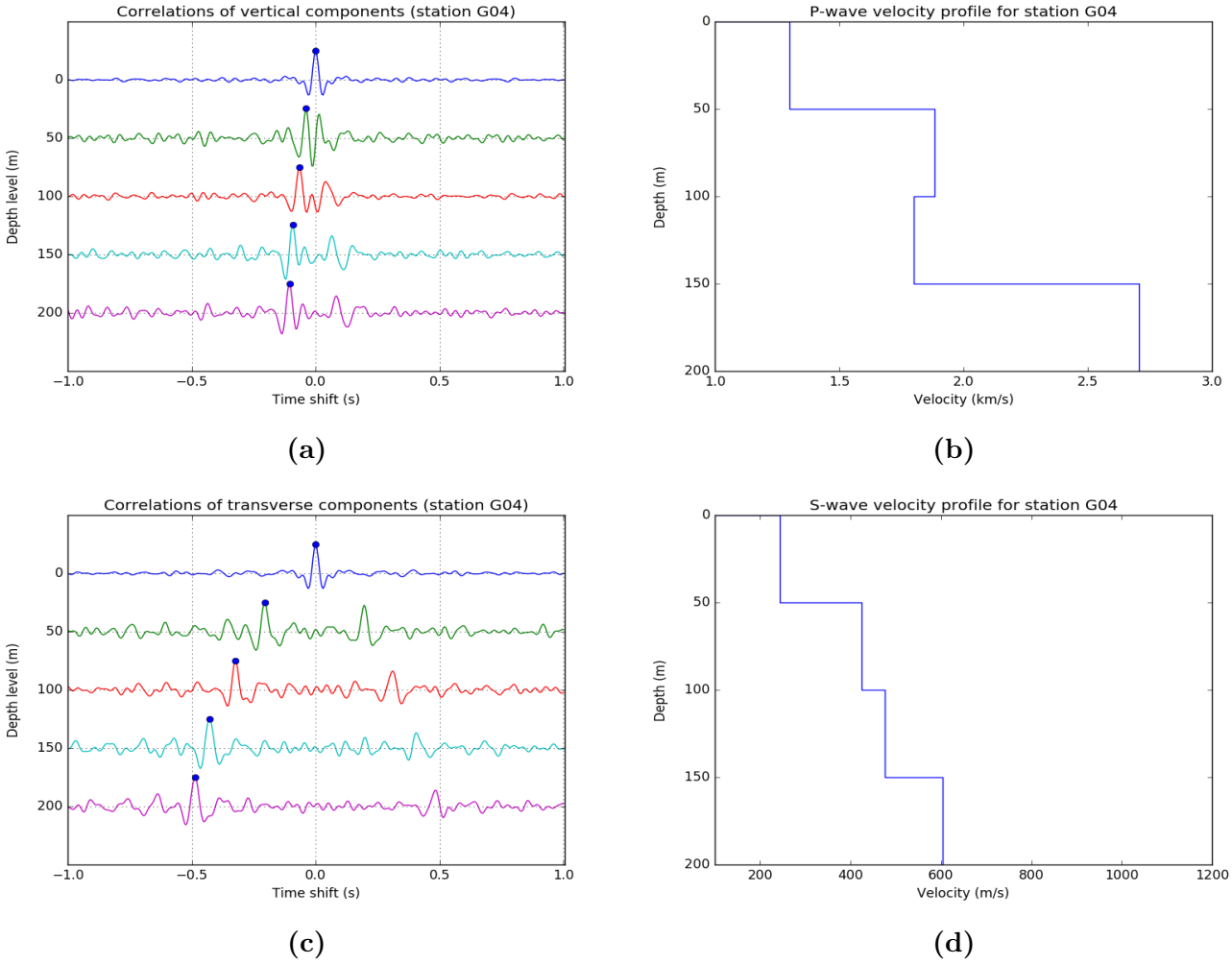

Figure 19: ***(a)*** *Stacked cross-correlations of the vertical components. Blue dot indicates the peak associated with the P-wave.* ***(b)*** *P-wave velocity profile calculated from the picks in figure 19a.* ***(c)*** *Stacked cross-correlations of the transverse components. Blue dot indicates the peak associated with the SH-wave.* ***(d)*** *S-wave velocity profiles calculated from the picks in figure 19c.*

NOTE: The lower geophone in this station (G044) has a depth of 185 m instead of 200 m. The velocities in the interval from 150 m to 185 m have been extrapolated to 200 m to match the rest of the data.

Station G06

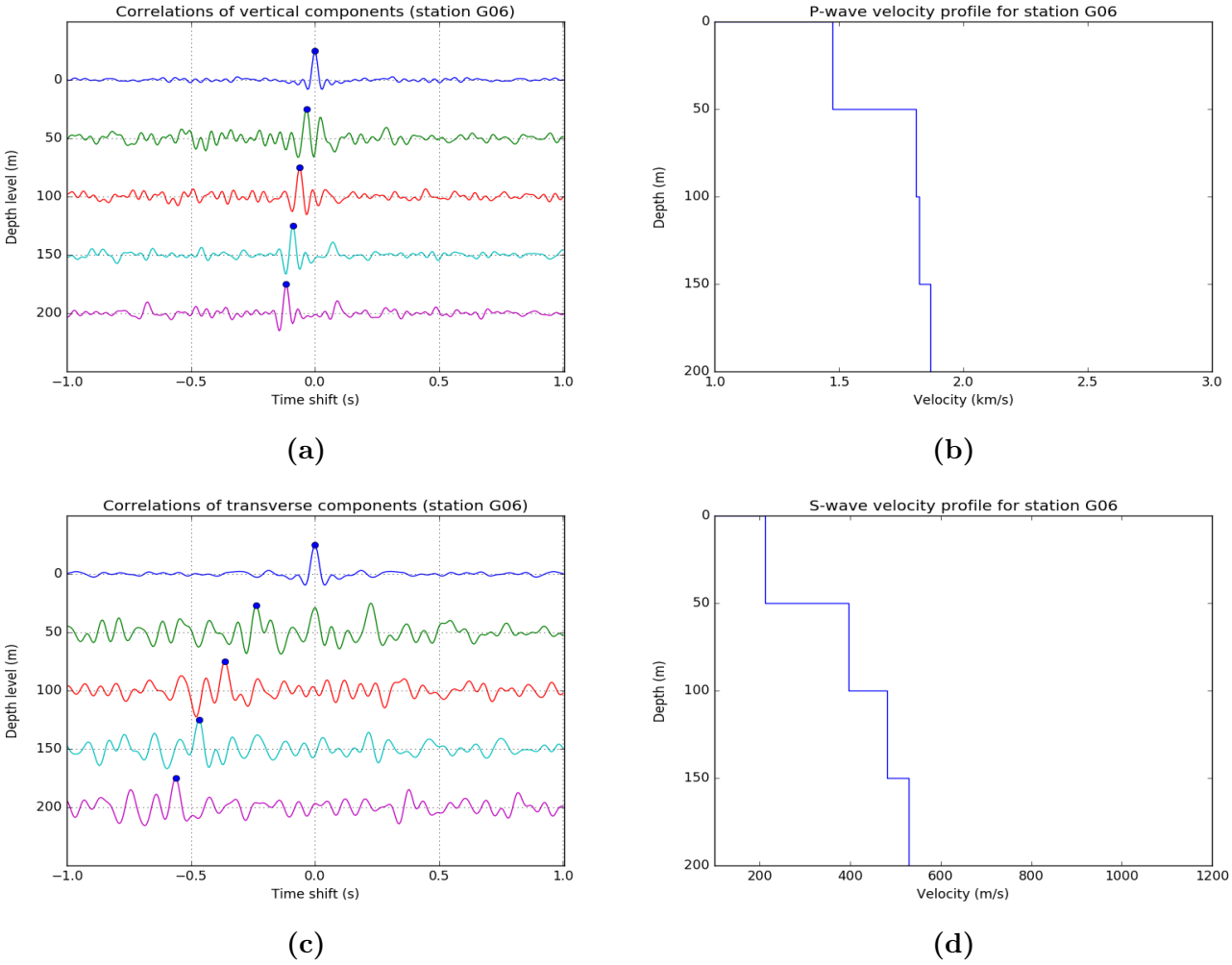

Figure 20: ***(a)*** *Stacked cross-correlations of the vertical components. Blue dot indicates the peak associated with the P-wave.* ***(b)*** *P-wave velocity profile calculated from the picks in figure 20a.* ***(c)*** *Stacked cross-correlations of the transverse components. Blue dot indicates the peak associated with the SH-wave.* ***(d)*** *S-wave velocity profiles calculated from the picks in figure 20c.*

Station G07

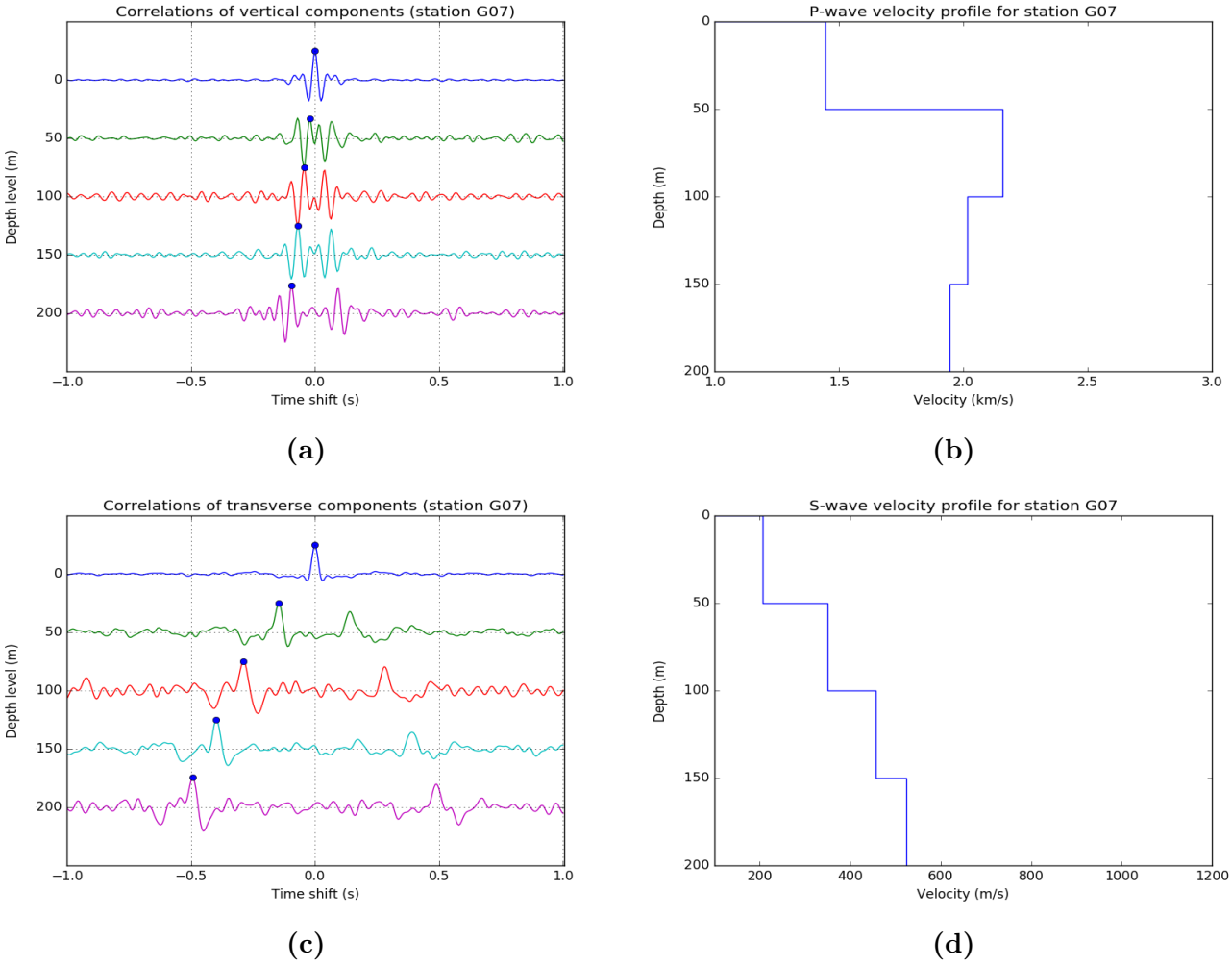

Figure 21: ***(a)*** *Stacked cross-correlations of the vertical components. Blue dot indicates the peak associated with the P-wave.* ***(b)*** *P-wave velocity profile calculated from the picks in figure 21a.* ***(c)*** *Stacked cross-correlations of the transverse components. Blue dot indicates the peak associated with the SH-wave.* ***(d)*** *S-wave velocity profiles calculated from the picks in figure 21c.*

NOTE: The geophones in this station are all placed 20 m shallower than they were supposed to. Velocities for the shallowest interval have been corrected, for the other intervals the depth error is ignored since the intervals overlap largely with the default intervals.

Station G08

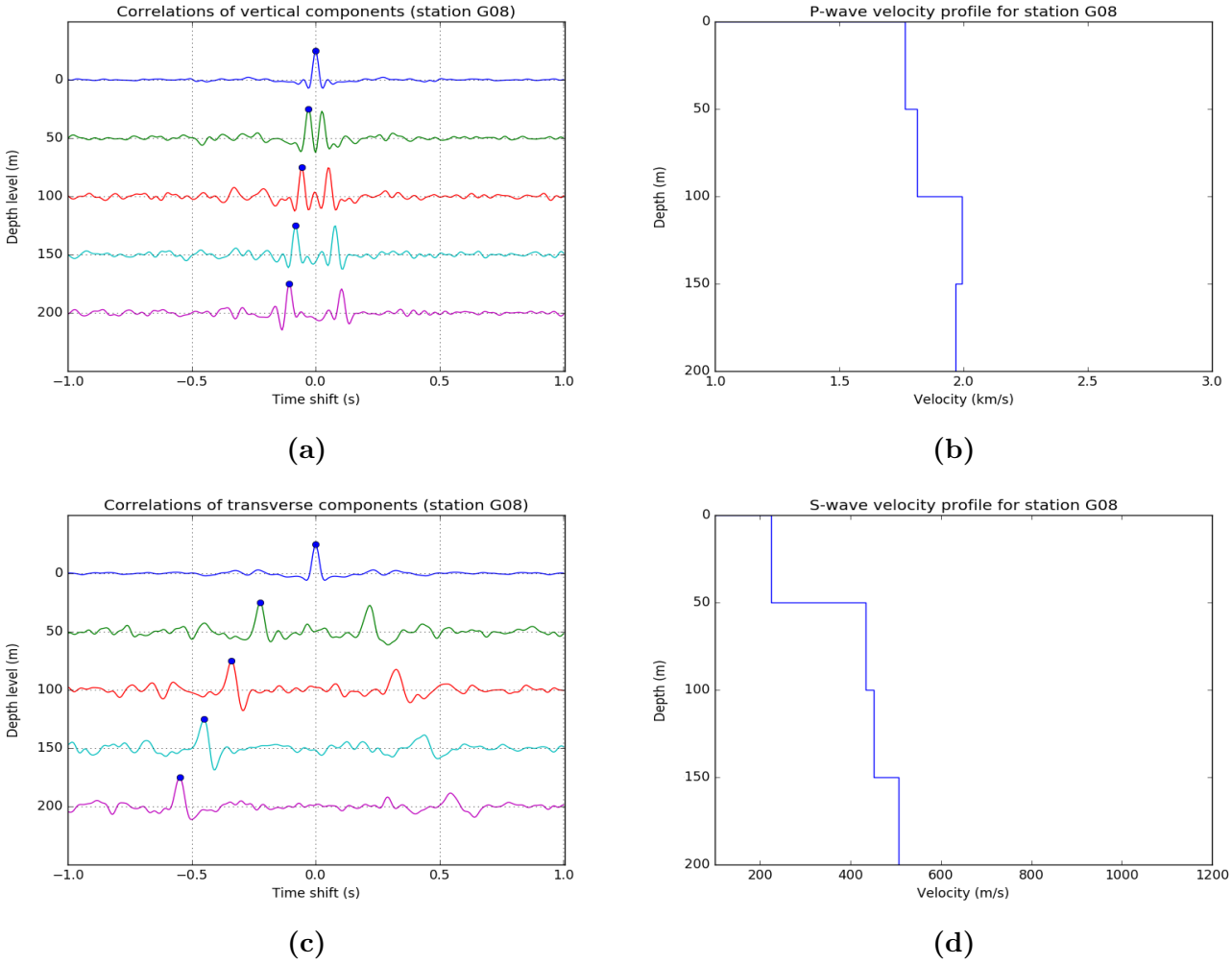

Figure 22: ***(a)*** *Stacked cross-correlations of the vertical components. Blue dot indicates the peak associated with the P-wave.* ***(b)*** *P-wave velocity profile calculated from the picks in figure 22a.* ***(c)*** *Stacked cross-correlations of the transverse components. Blue dot indicates the peak associated with the SH-wave.* ***(d)*** *S-wave velocity profiles calculated from the picks in figure 22c.*

Station G09

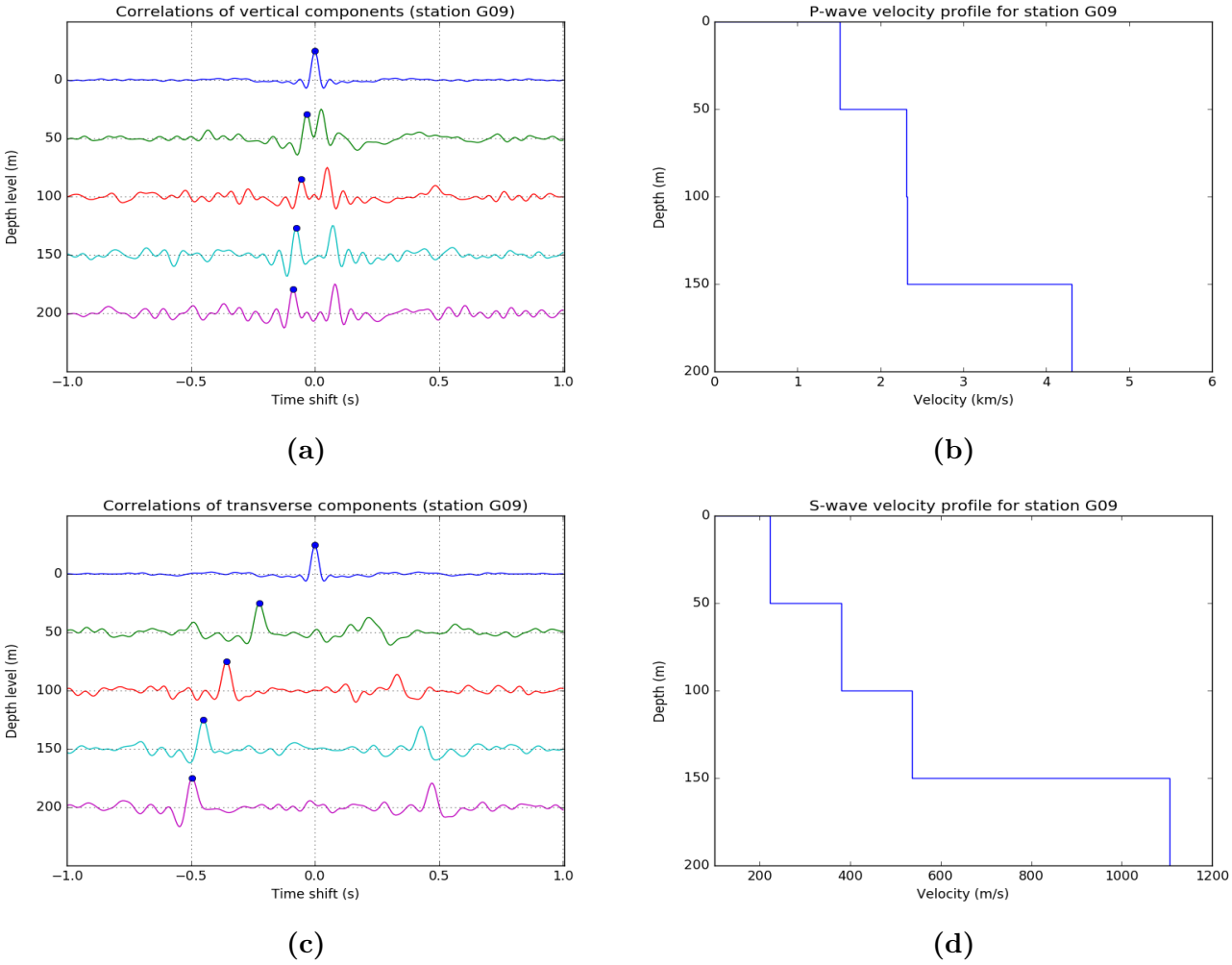

Figure 23: ***(a)*** *Stacked cross-correlations of the vertical components. Blue dot indicates the peak associated with the P-wave.* ***(b)*** *P-wave velocity profile calculated from the picks in figure 23a.* ***(c)*** *Stacked cross-correlations of the transverse components. Blue dot indicates the peak associated with the SH-wave.* ***(d)*** *S-wave velocity profiles calculated from the picks in figure 23c.*

NOTE: This result was not used because the velocities in the lowest interval are unrealistically high. It seems very likely that the depth of the lowest geophone is incorrect.

Station G10

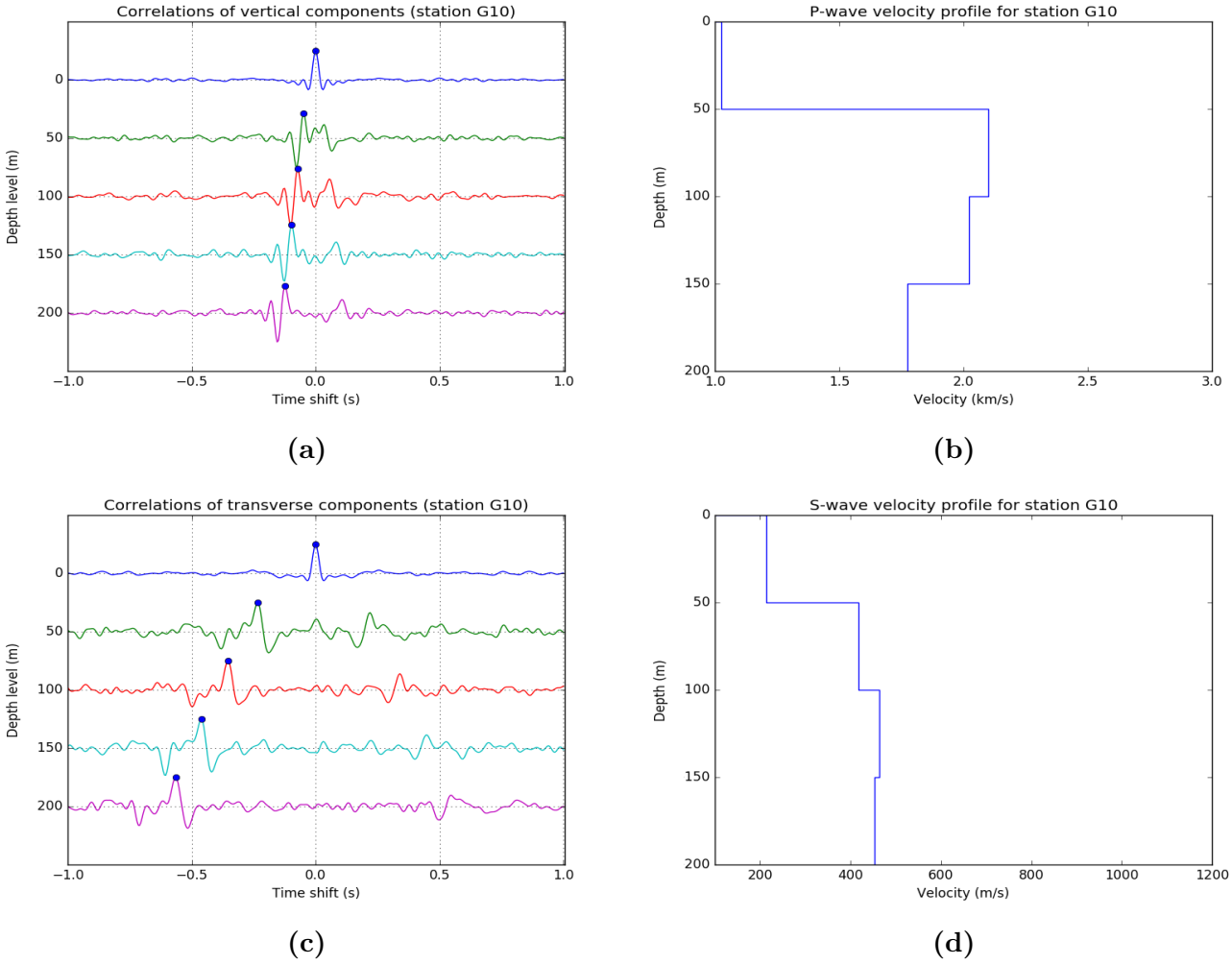

Figure 24: ***(a)*** *Stacked cross-correlations of the vertical components. Blue dot indicates the peak associated with the P-wave.* ***(b)*** *P-wave velocity profile calculated from the picks in figure 24a.* ***(c)*** *Stacked cross-correlations of the transverse components. Blue dot indicates the peak associated with the SH-wave.* ***(d)*** *S-wave velocity profiles calculated from the picks in figure 24c.*

NOTE: The lower geophone in this station (G104) has a depth of 197m instead of 200 m. Corrections have been made to the lower interval velocities.

Station G11

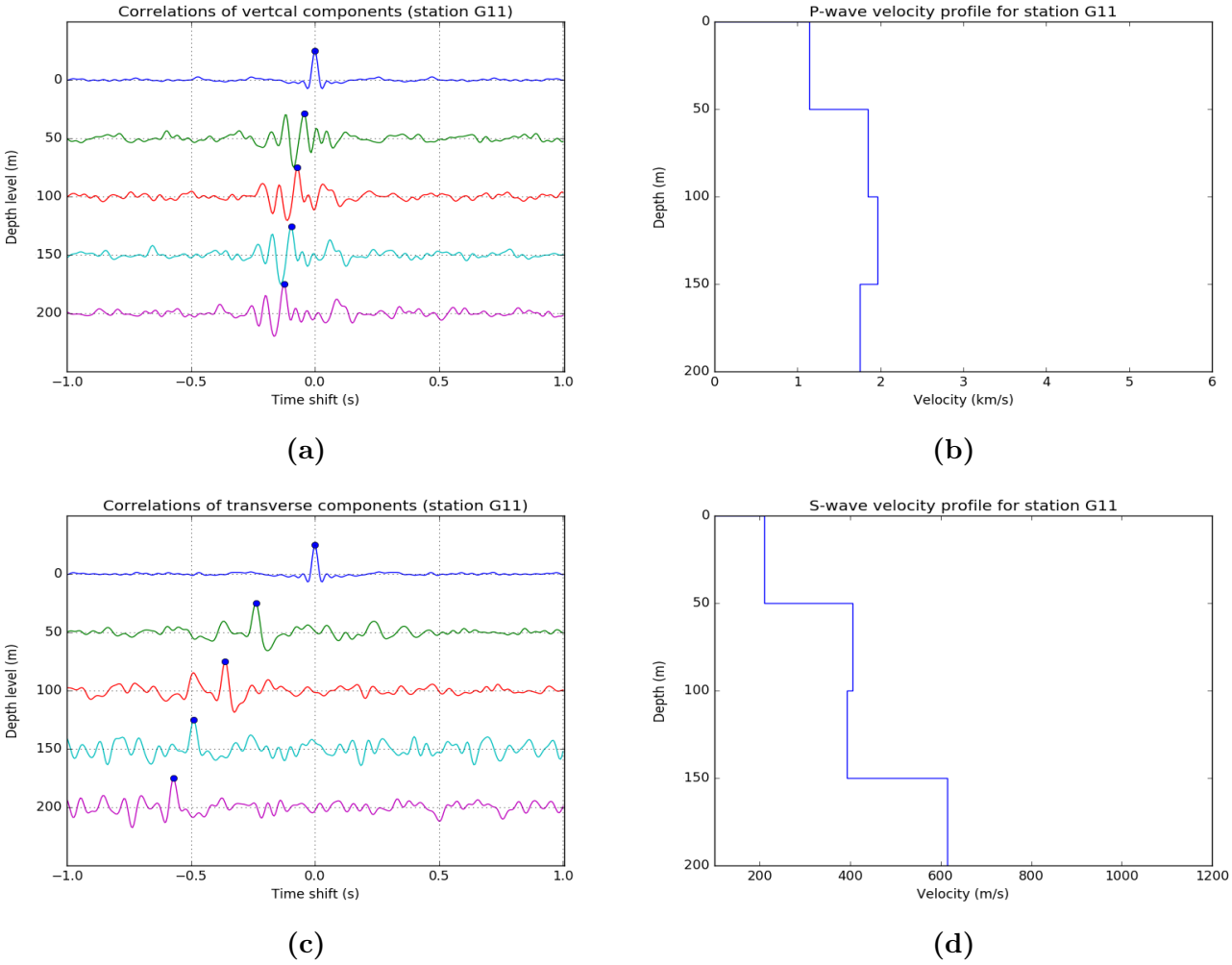

Figure 25: ***(a)*** *Stacked cross-correlations of the vertical components. Blue dot indicates the peak associated with the P-wave.* ***(b)*** *P-wave velocity profile calculated from the picks in figure 25a.* ***(c)*** *Stacked cross-correlations of the transverse components. Blue dot indicates the peak associated with the SH-wave.* ***(d)*** *S-wave velocity profiles calculated from the picks in figure 25c.*

NOTE: To obtain the above result, the geophone data from 150 m and 200 m (G113 and G114) were interchanged.

Station G13

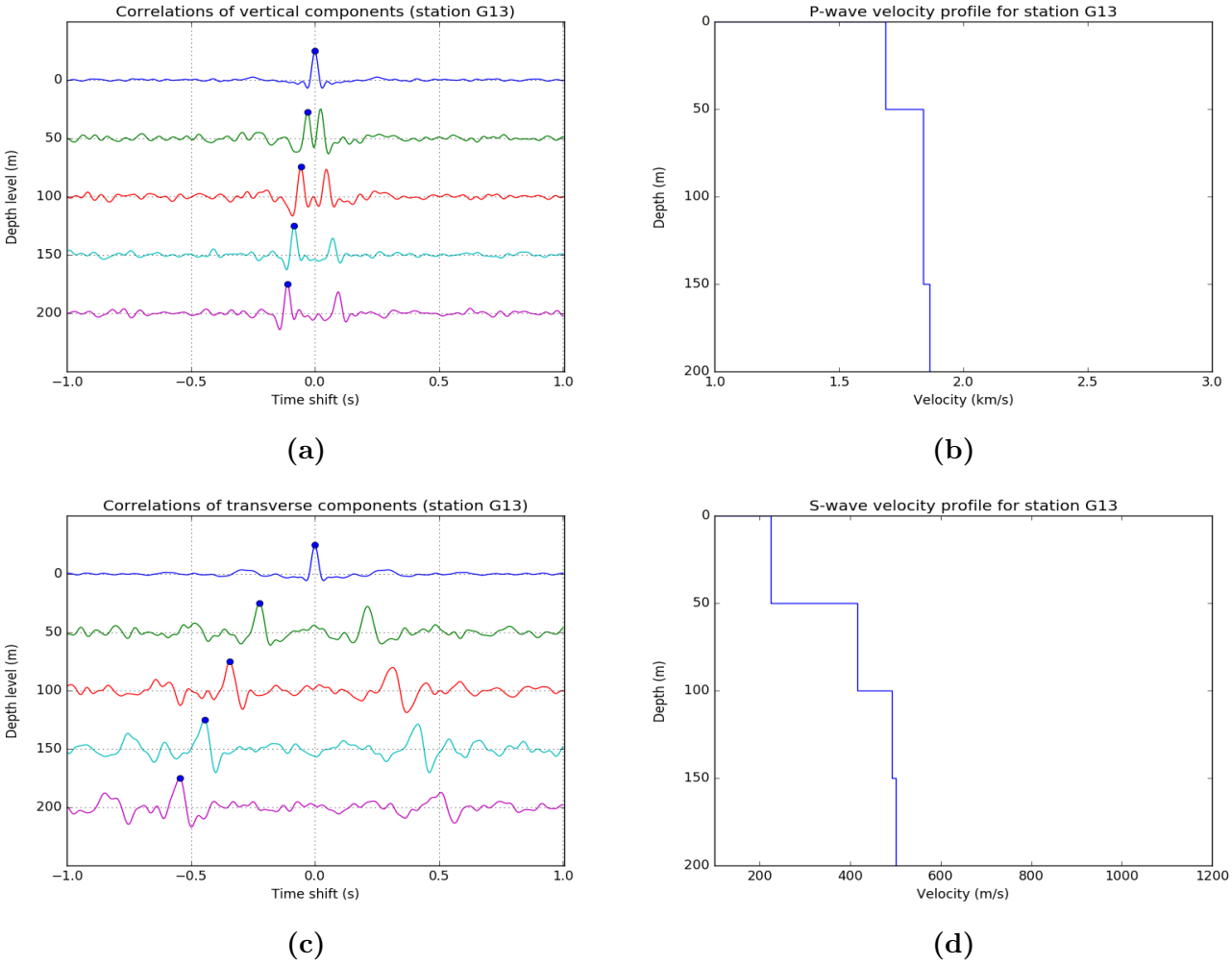

Figure 26: ***(a)*** *Stacked cross-correlations of the vertical components. Blue dot indicates the peak associated with the P-wave.* ***(b)*** *P-wave velocity profile calculated from the picks in figure 26a.* ***(c)*** *Stacked cross-correlations of the transverse components. Blue dot indicates the peak associated with the SH-wave.* ***(d)*** *S-wave velocity profiles calculated from the picks in figure 26c.*

Station G14

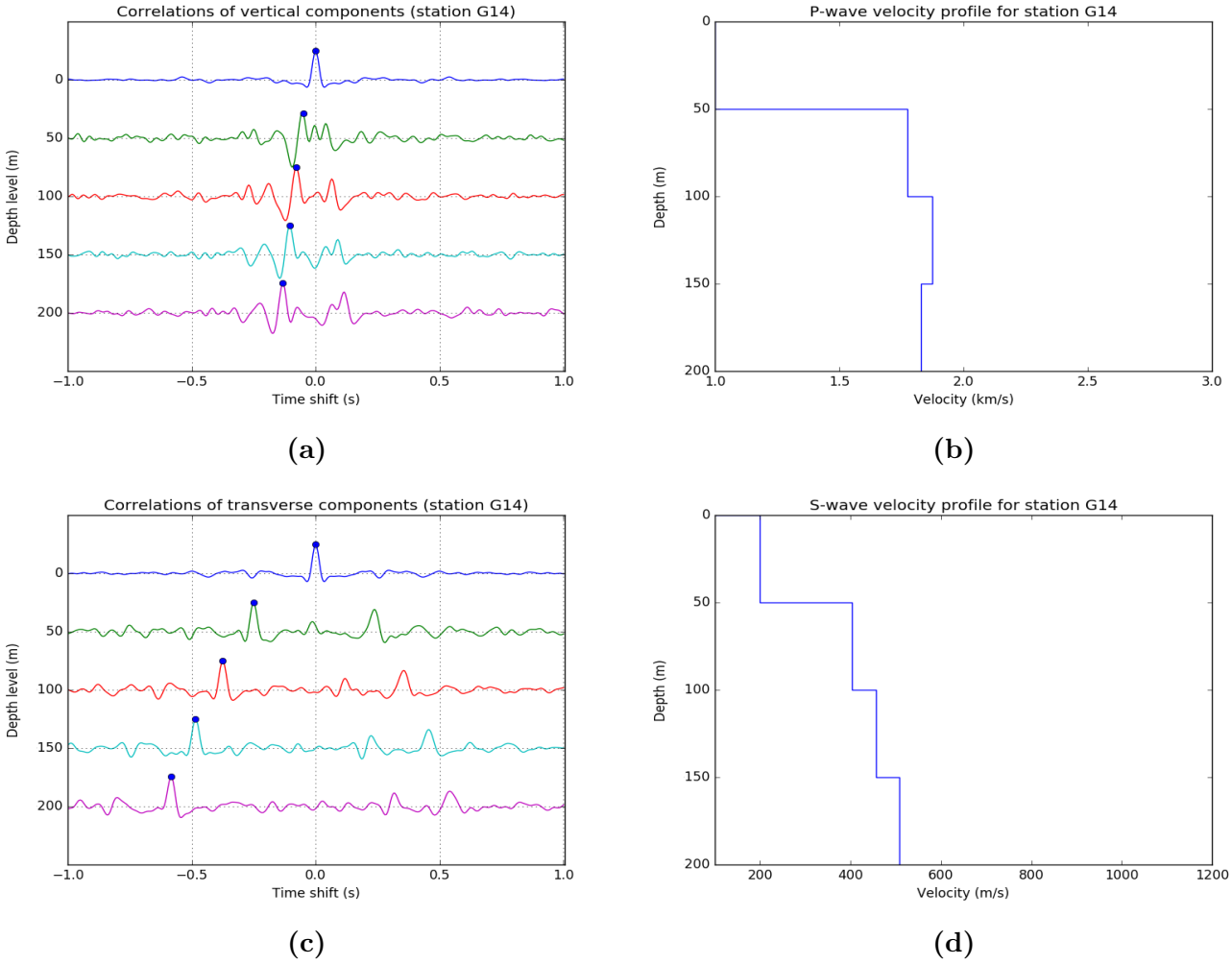

Figure 27: ***(a)*** *Stacked cross-correlations of the vertical components. Blue dot indicates the peak associated with the P-wave.* ***(b)*** *P-wave velocity profile calculated from the picks in figure 27a.* ***(c)*** *Stacked cross-correlations of the transverse components. Blue dot indicates the peak associated with the SH-wave.* ***(d)*** *S-wave velocity profiles calculated from the picks in figure 27c.*

Station G16

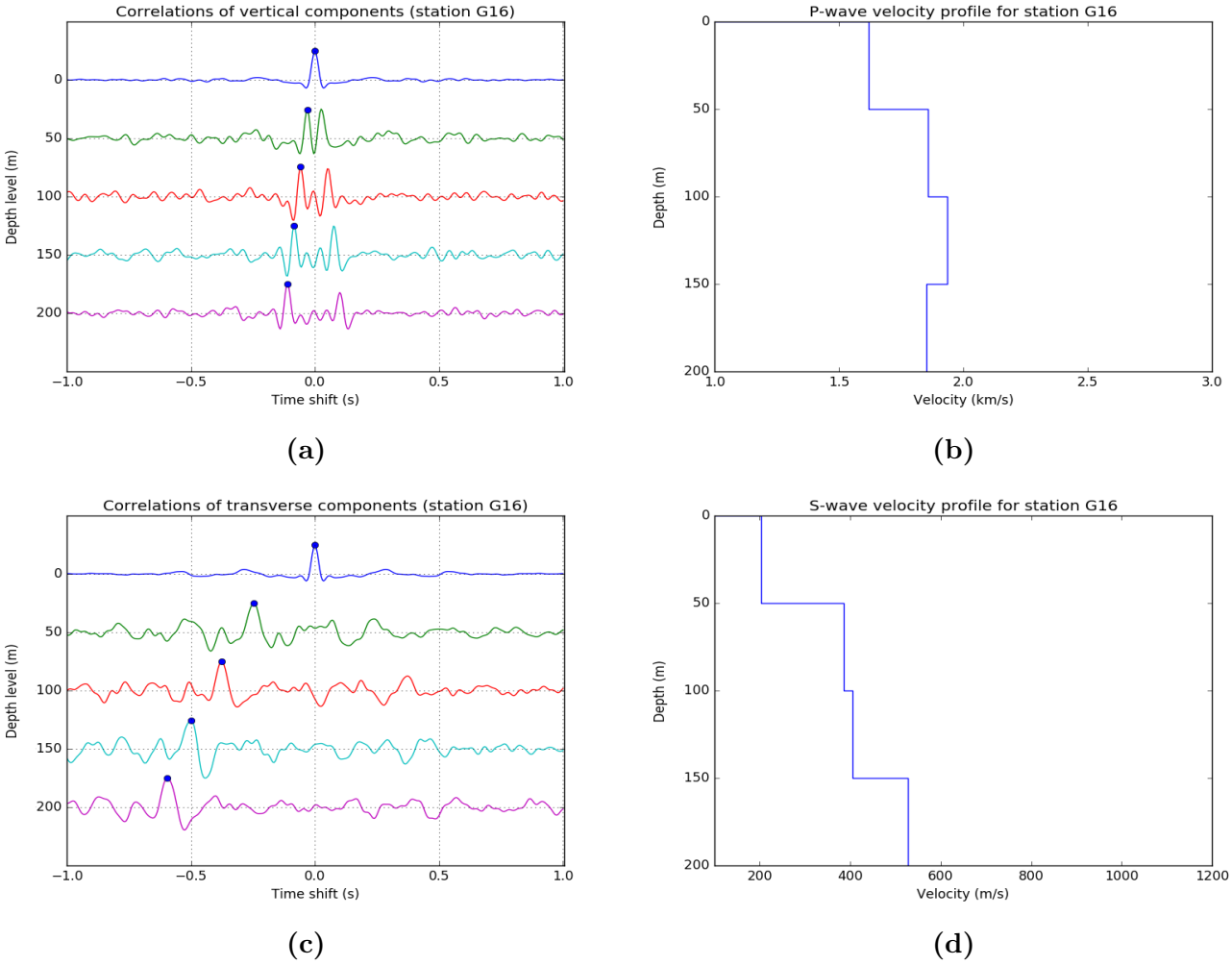

Figure 28: ***(a)*** *Stacked cross-correlations of the vertical components. Blue dot indicates the peak associated with the P-wave.* ***(b)*** *P-wave velocity profile calculated from the picks in figure 28a.* ***(c)*** *Stacked cross-correlations of the transverse components. Blue dot indicates the peak associated with the SH-wave.* ***(d)*** *S-wave velocity profiles calculated from the picks in figure 28c.*

Station G17

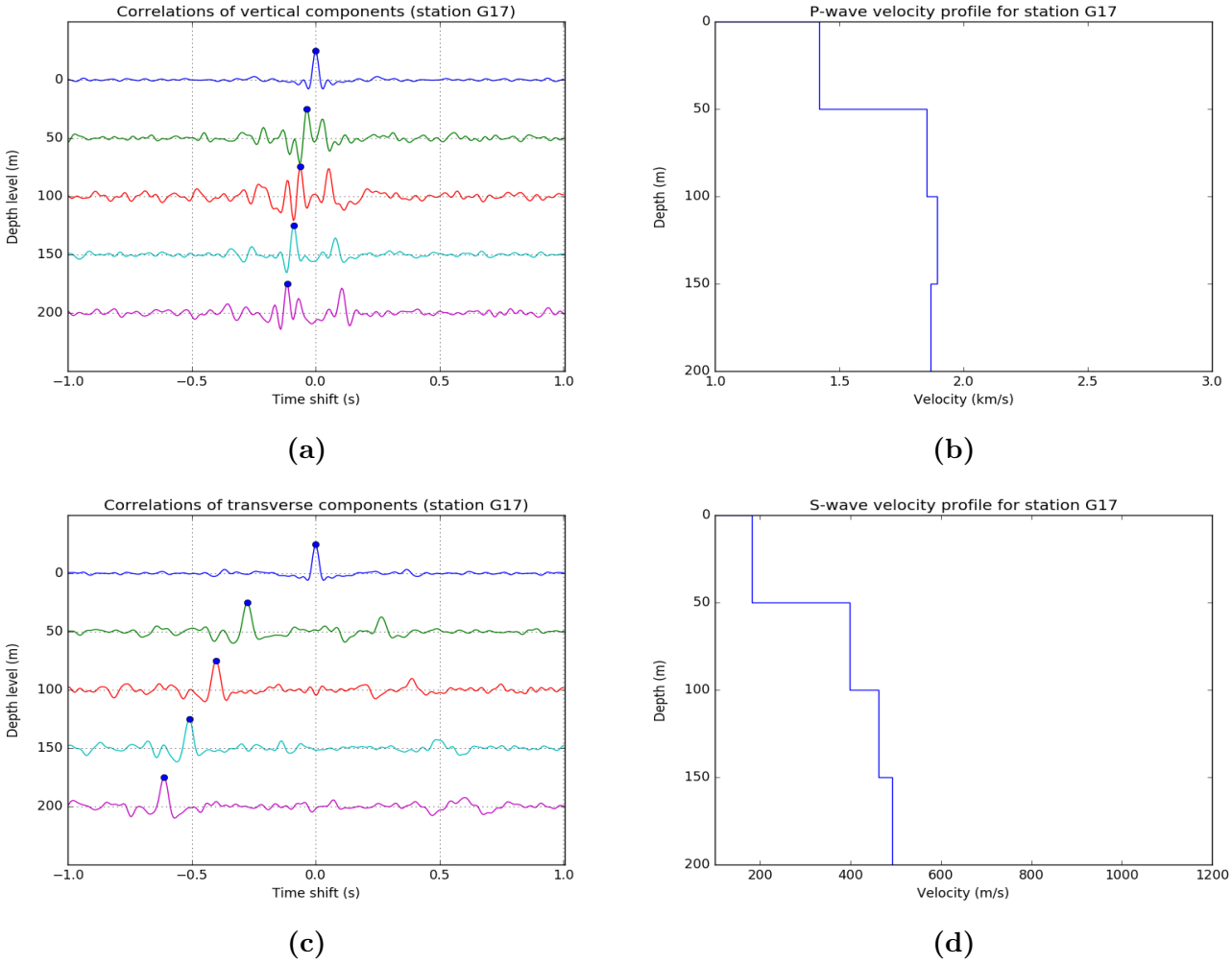

Figure 29: *(a) Stacked cross-correlations of the vertical components. Blue dot indicates the peak associated with the P-wave.* ***(b)*** *P-wave velocity profile calculated from the picks in figure 29a.* ***(c)*** *Stacked cross-correlations of the transverse components. Blue dot indicates the peak associated with the SH-wave.* ***(d)*** *S-wave velocity profiles calculated from the picks in figure 29c.*

Station G18

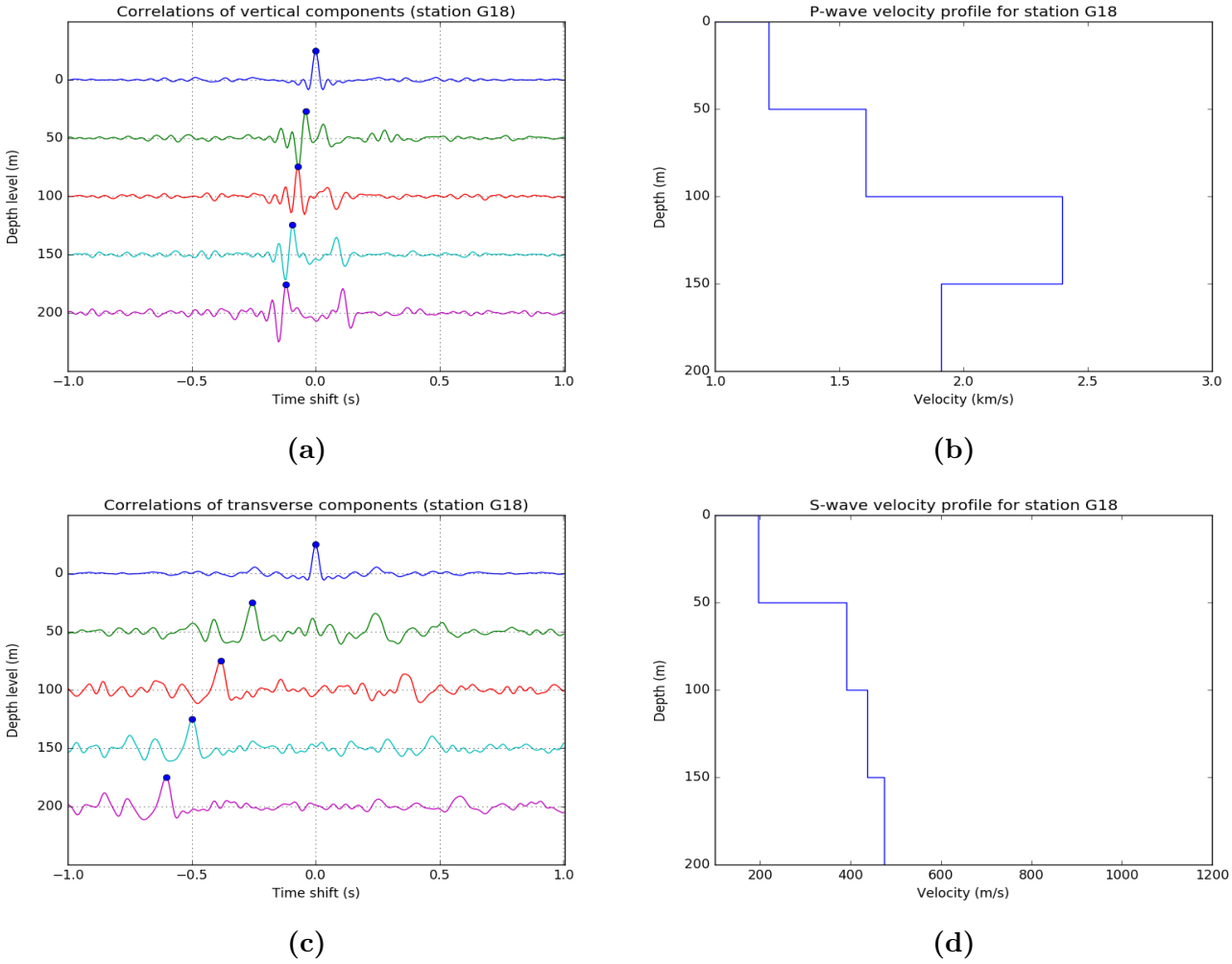

Figure 30: ***(a)*** *Stacked cross-correlations of the vertical components. Blue dot indicates the peak associated with the P-wave.* ***(b)*** *P-wave velocity profile calculated from the picks in figure 30a.* ***(c)*** *Stacked cross-correlations of the transverse components. Blue dot indicates the peak associated with the SH-wave.* ***(d)*** *S-wave velocity profiles calculated from the picks in figure 30c.*

Station G19

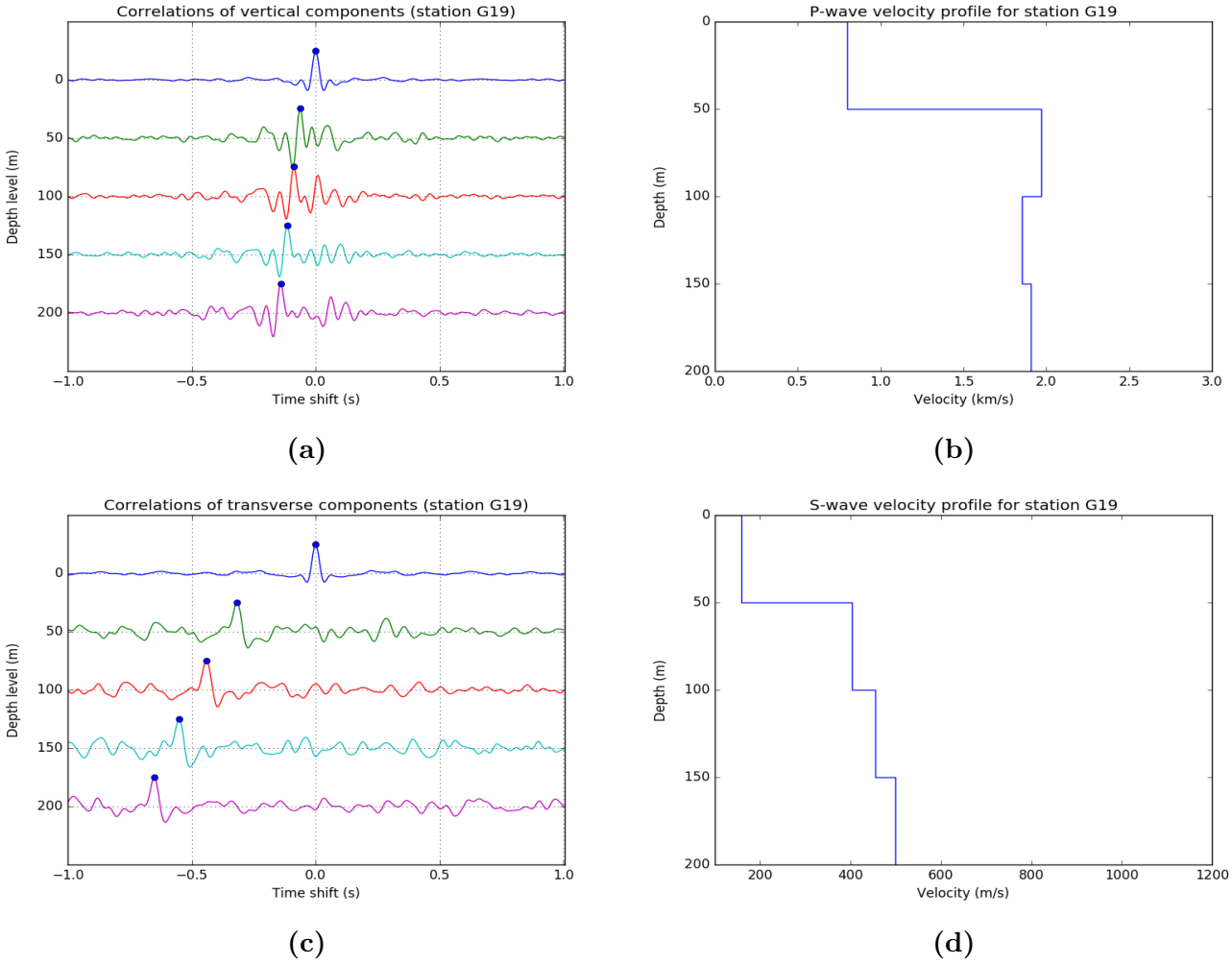

Figure 31: ***(a)*** *Stacked cross-correlations of the vertical components. Blue dot indicates the peak associated with the P-wave.* ***(b)*** *P-wave velocity profile calculated from the picks in figure 31a.* ***(c)*** *Stacked cross-correlations of the transverse components. Blue dot indicates the peak associated with the SH-wave.* ***(d)*** *S-wave velocity profiles calculated from the picks in figure 31c.*

Station G20

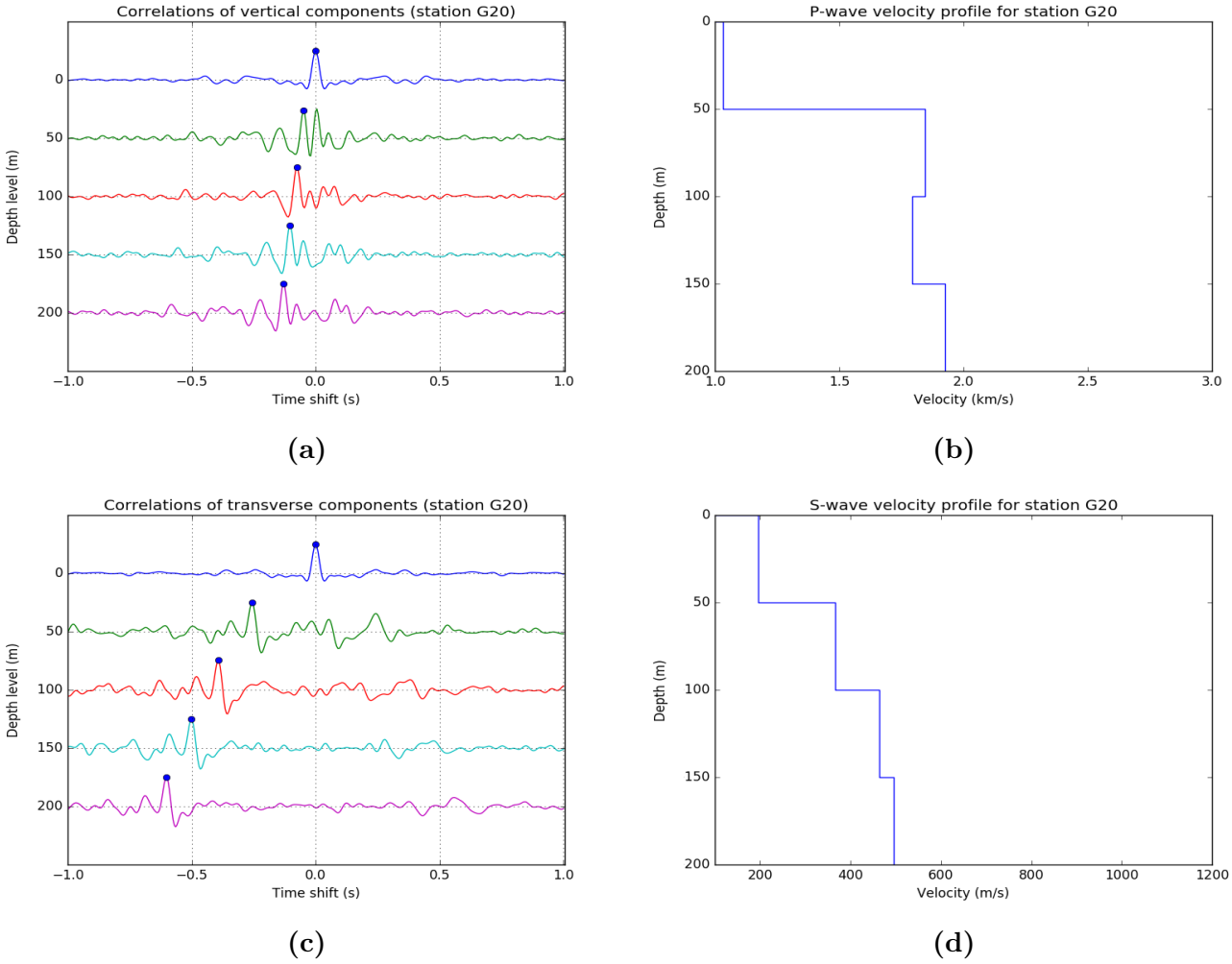

Figure 32: ***(a)*** *Stacked cross-correlations of the vertical components. Blue dot indicates the peak associated with the P-wave.* ***(b)*** *P-wave velocity profile calculated from the picks in figure 32a.* ***(c)*** *Stacked cross-correlations of the transverse components. Blue dot indicates the peak associated with the SH-wave.* ***(d)*** *S-wave velocity profiles calculated from the picks in figure 32c.*

Station G21

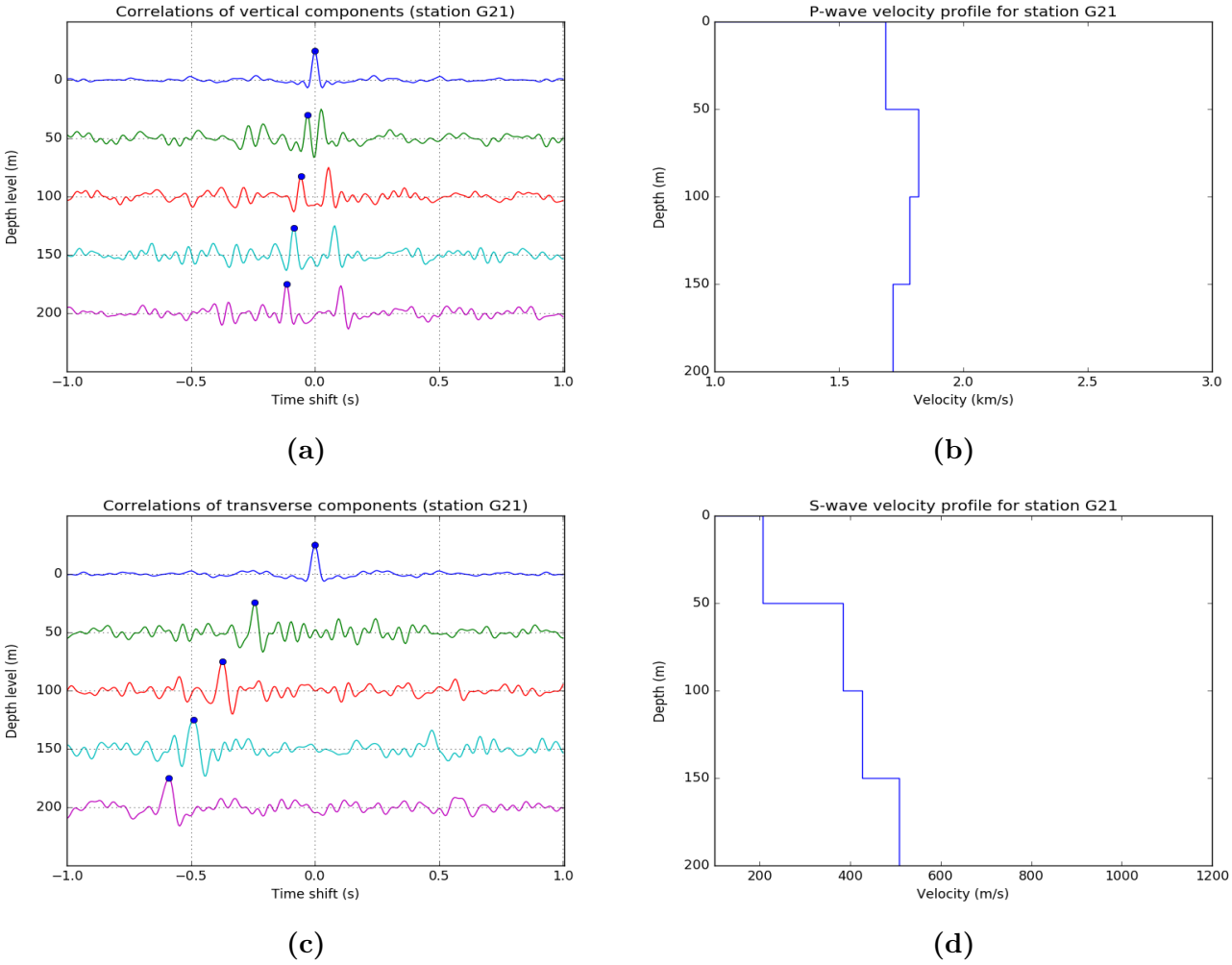

Figure 33: ***(a)*** *Stacked cross-correlations of the vertical components. Blue dot indicates the peak associated with the P-wave.* ***(b)*** *P-wave velocity profile calculated from the picks in figure 33a.* ***(c)*** *Stacked cross-correlations of the transverse components. Blue dot indicates the peak associated with the SH-wave.* ***(d)*** *S-wave velocity profiles calculated from the picks in figure 33c.*

Station G22

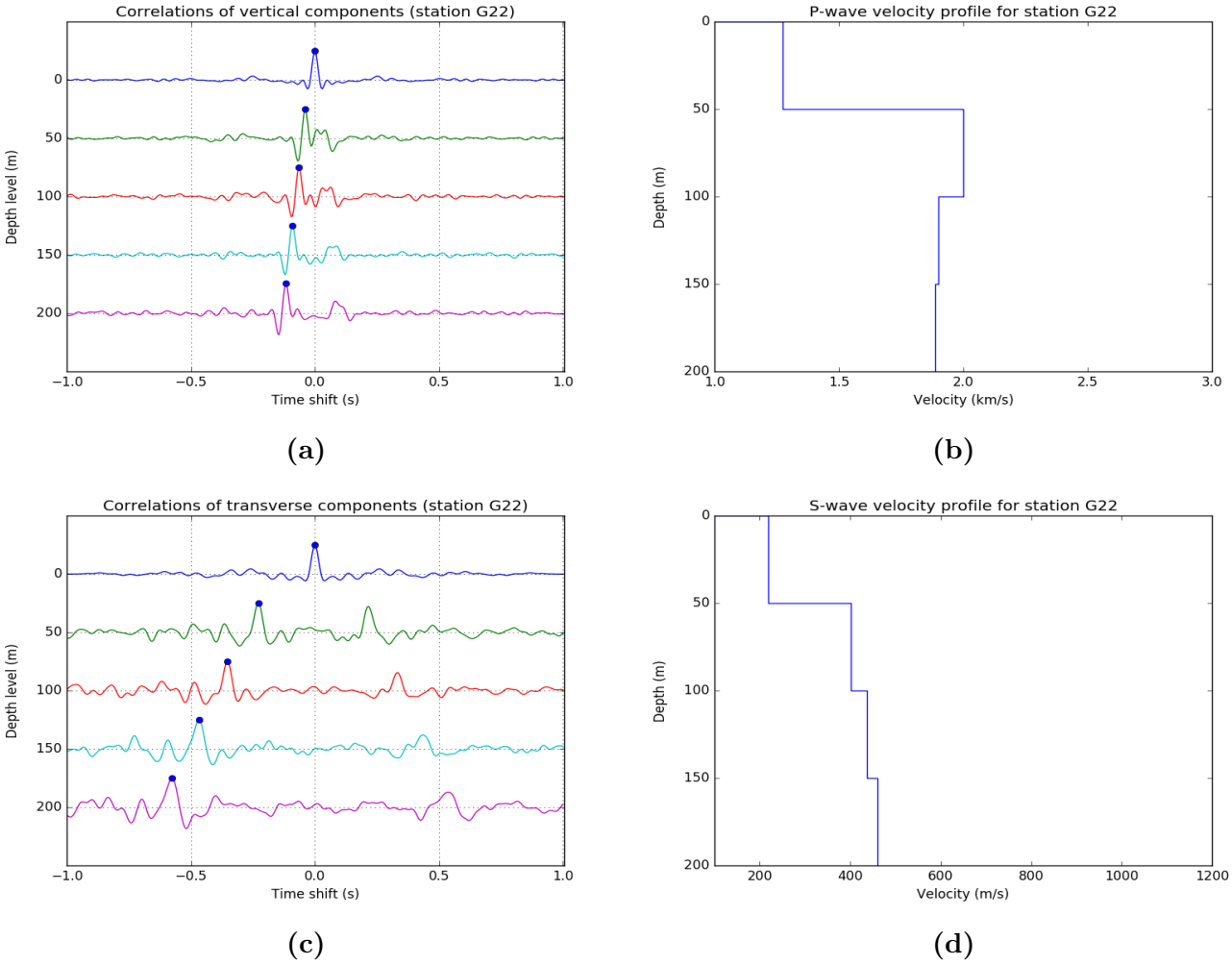

Figure 34: ***(a)*** *Stacked cross-correlations of the vertical components. Blue dot indicates the peak associated with the P-wave.* ***(b)*** *P-wave velocity profile calculated from the picks in figure 34a.* ***(c)*** *Stacked cross-correlations of the transverse components. Blue dot indicates the peak associated with the SH-wave.* ***(d)*** *S-wave velocity profiles calculated from the picks in figure 34c.*

Station G23

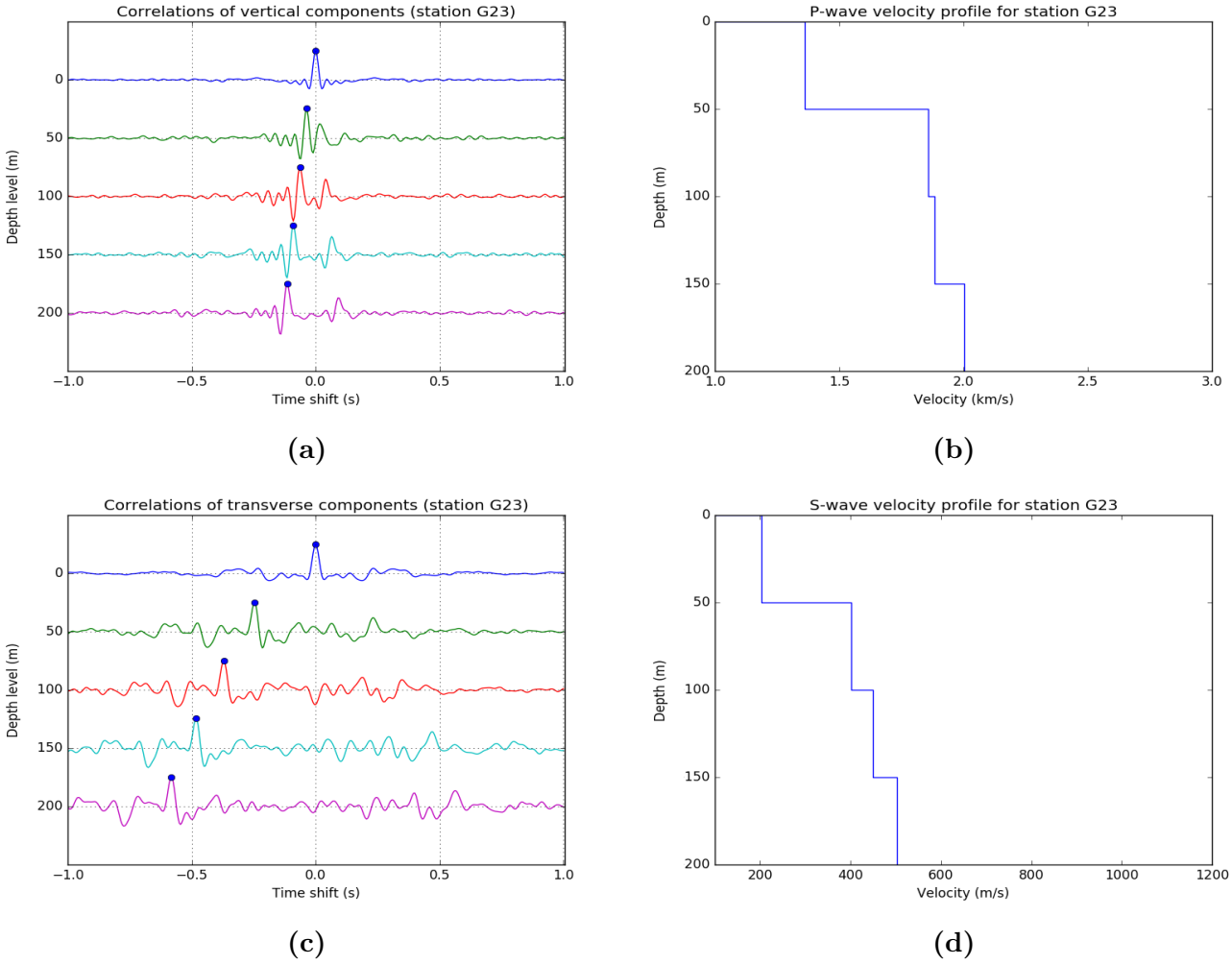

Figure 35: ***(a)*** *Stacked cross-correlations of the vertical components. Blue dot indicates the peak associated with the P-wave.* ***(b)*** *P-wave velocity profile calculated from the picks in figure 35a.* ***(c)*** *Stacked cross-correlations of the transverse components. Blue dot indicates the peak associated with the SH-wave.* ***(d)*** *S-wave velocity profiles calculated from the picks in figure 35c.*

Station G24

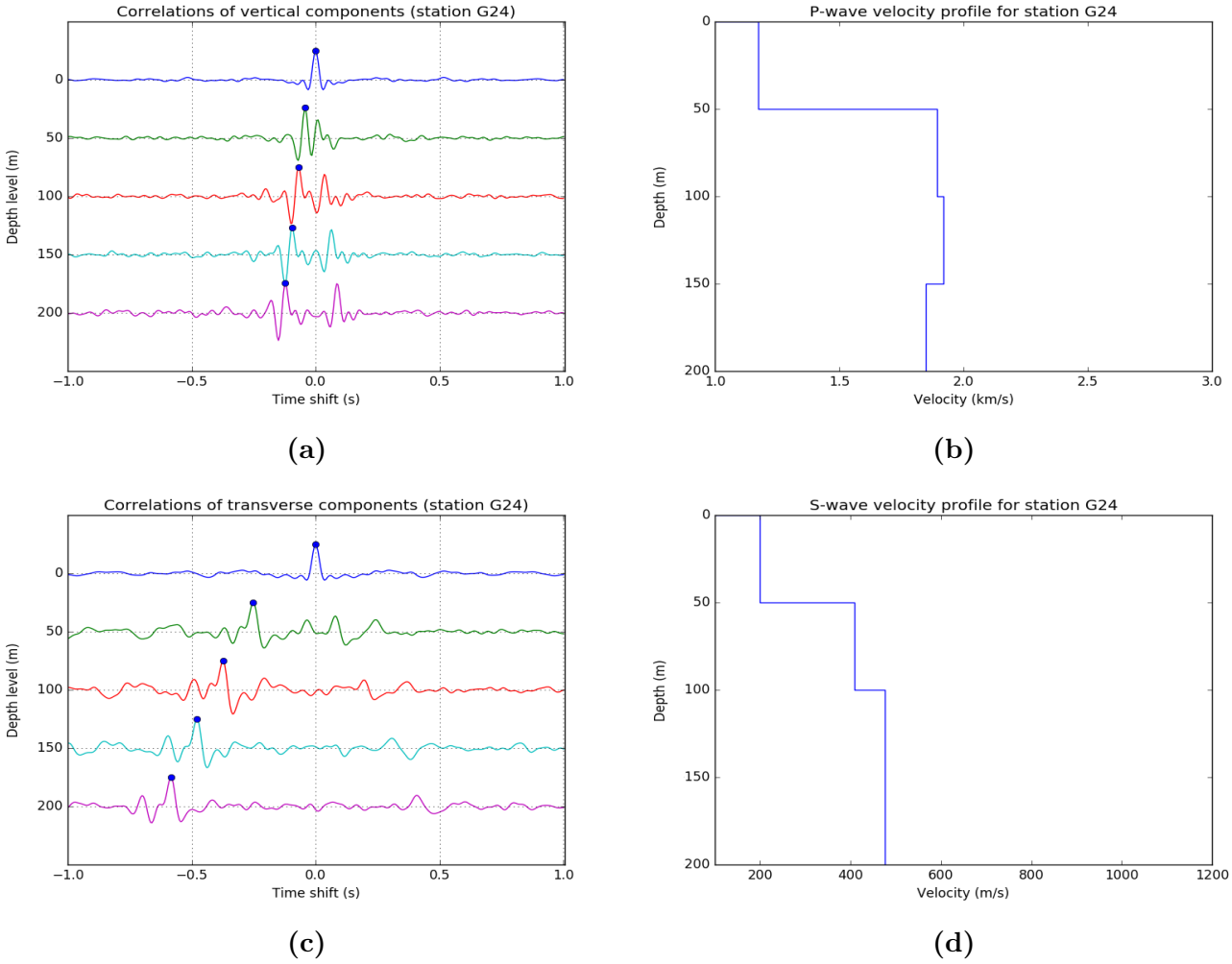

Figure 36: ***(a)*** *Stacked cross-correlations of the vertical components. Blue dot indicates the peak associated with the P-wave.* ***(b)*** *P-wave velocity profile calculated from the picks in figure 36a.* ***(c)*** *Stacked cross-correlations of the transverse components. Blue dot indicates the peak associated with the SH-wave.* ***(d)*** *S-wave velocity profiles calculated from the picks in figure 36c.*

Station G26

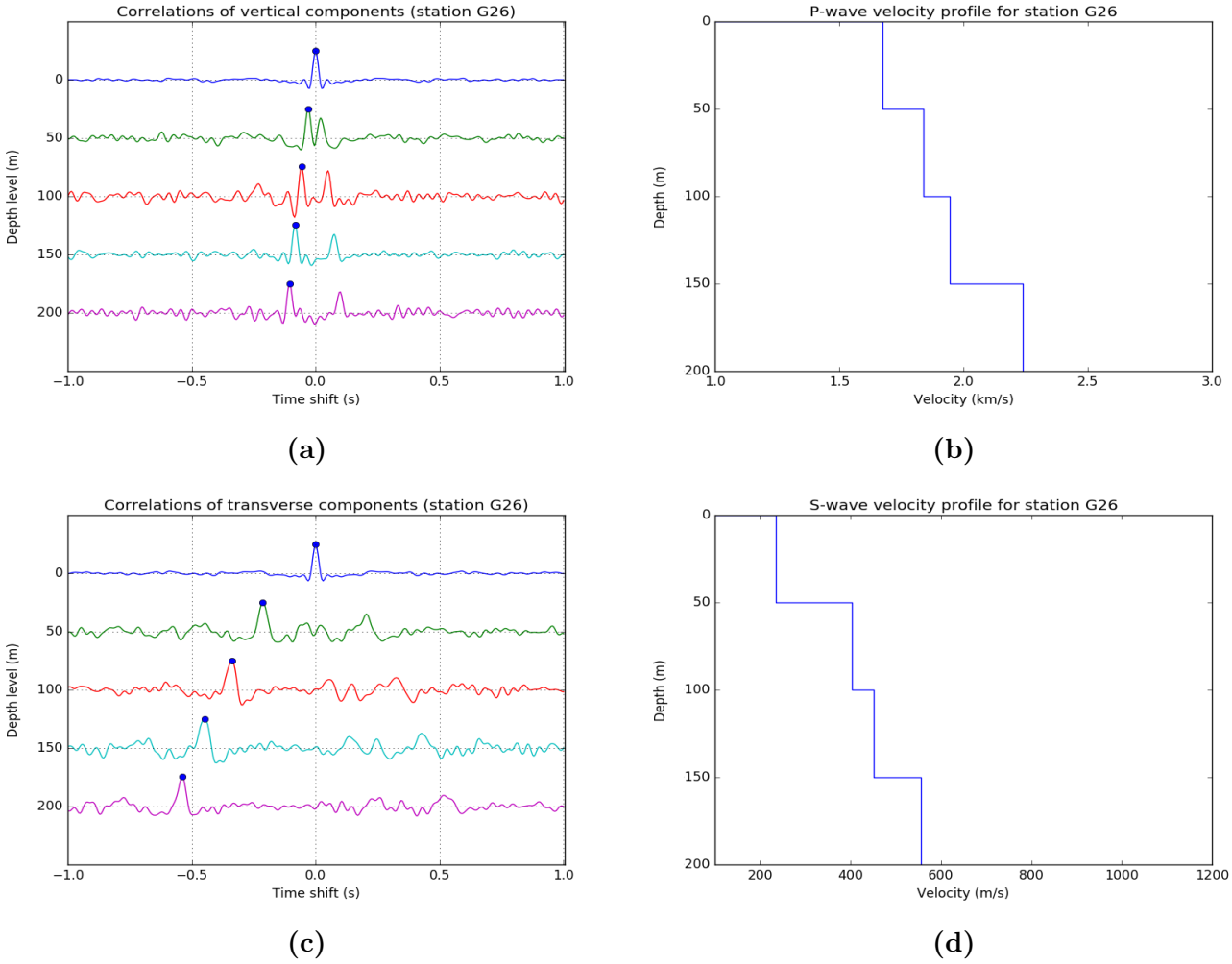

Figure 37: ***(a)*** *Stacked cross-correlations of the vertical components. Blue dot indicates the peak associated with the P-wave.* ***(b)*** *P-wave velocity profile calculated from the picks in figure 37a.* ***(c)*** *Stacked cross-correlations of the transverse components. Blue dot indicates the peak associated with the SH-wave.* ***(d)*** *S-wave velocity profiles calculated from the picks in figure 37c.*

Station G27

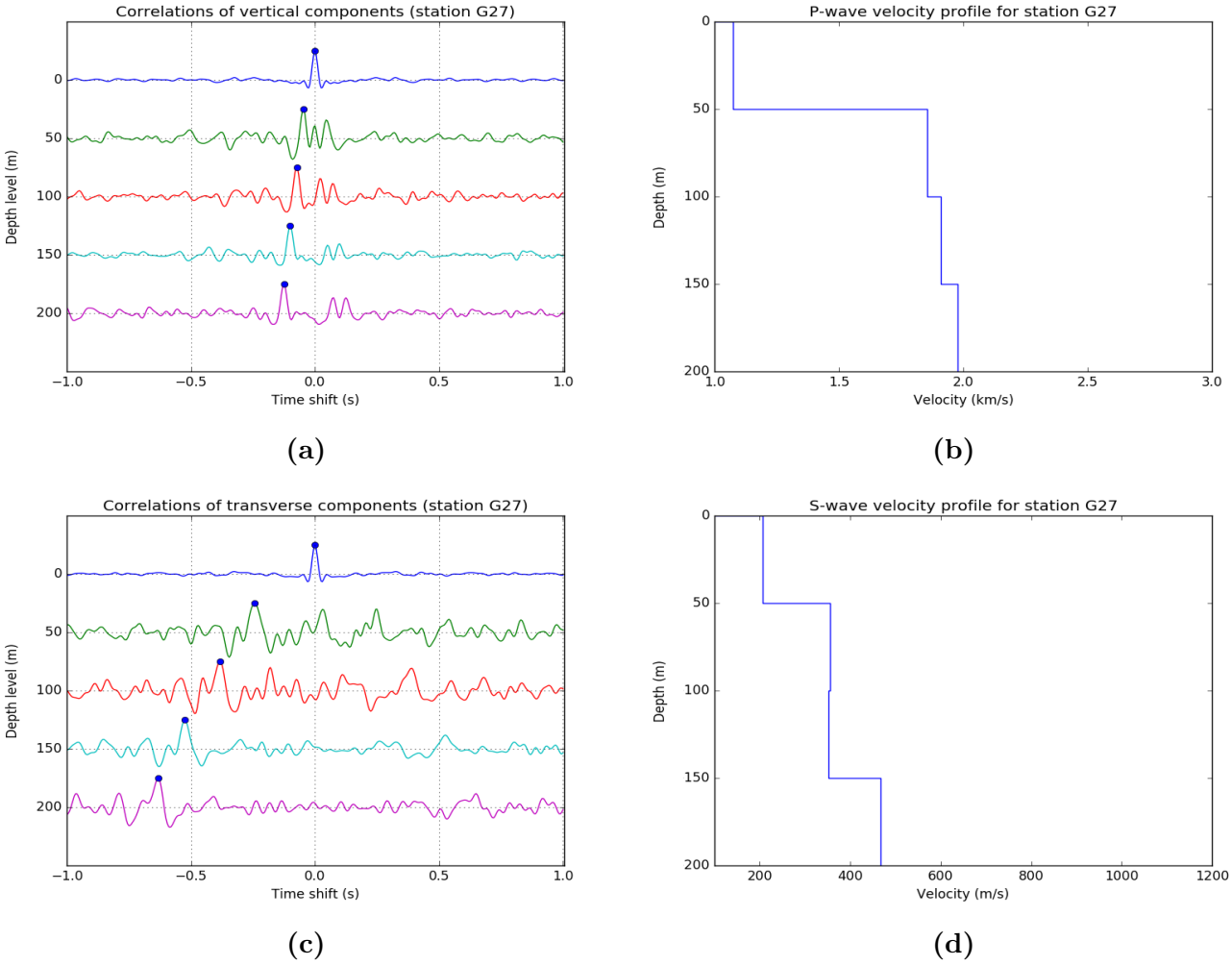

Figure 38: ***(a)*** *Stacked cross-correlations of the vertical components. Blue dot indicates the peak associated with the P-wave.* ***(b)*** *P-wave velocity profile calculated from the picks in figure 38a.* ***(c)*** *Stacked cross-correlations of the transverse components. Blue dot indicates the peak associated with the SH-wave.* ***(d)*** *S-wave velocity profiles calculated from the picks in figure 38c.*

Station G28

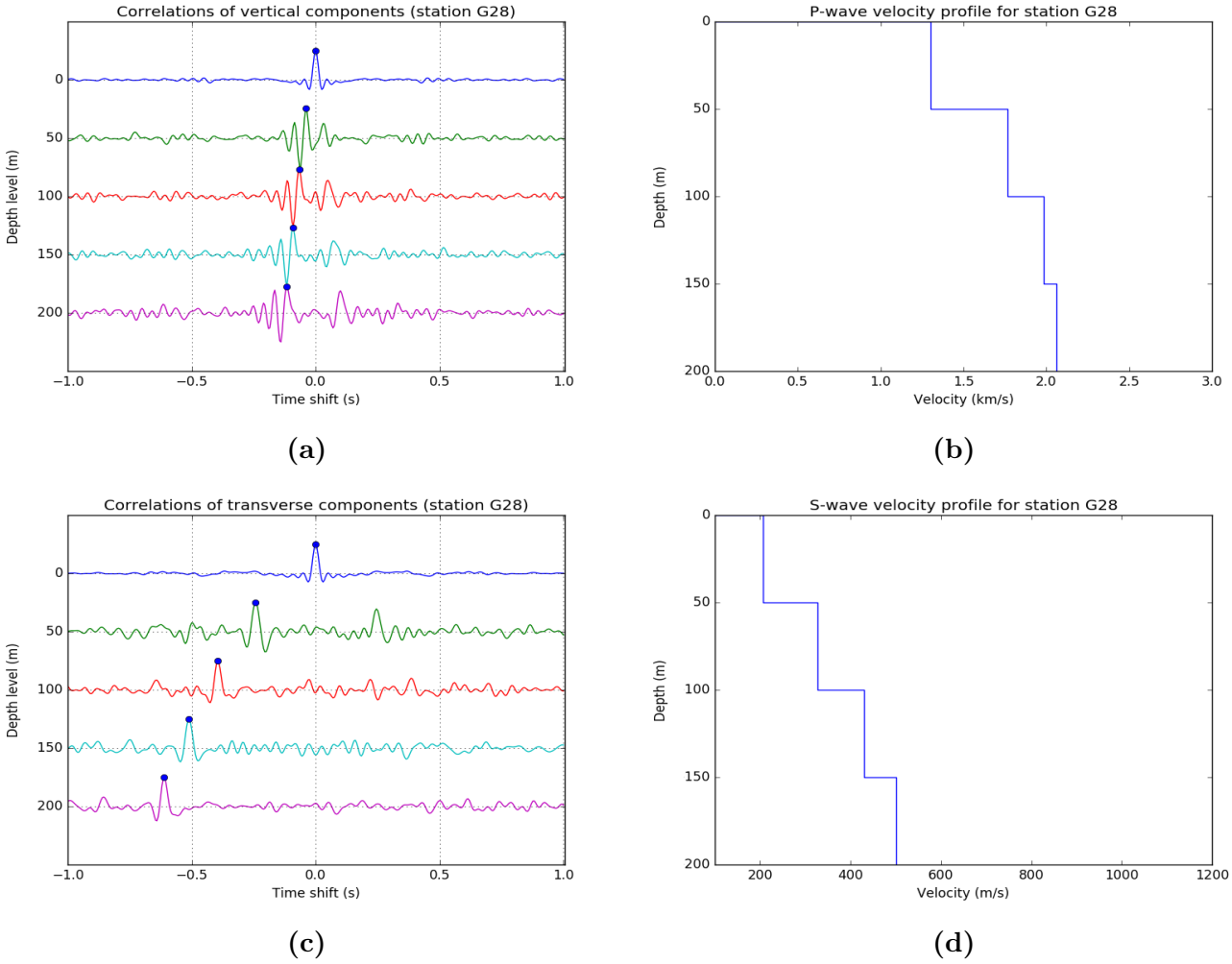

Figure 39: ***(a)*** *Stacked cross-correlations of the vertical components. Blue dot indicates the peak associated with the P-wave.* ***(b)*** *P-wave velocity profile calculated from the picks in figure 39a.* ***(c)*** *Stacked cross-correlations of the transverse components. Blue dot indicates the peak associated with the SH-wave.* ***(d)*** *S-wave velocity profiles calculated from the picks in figure 39c.*

Station G29

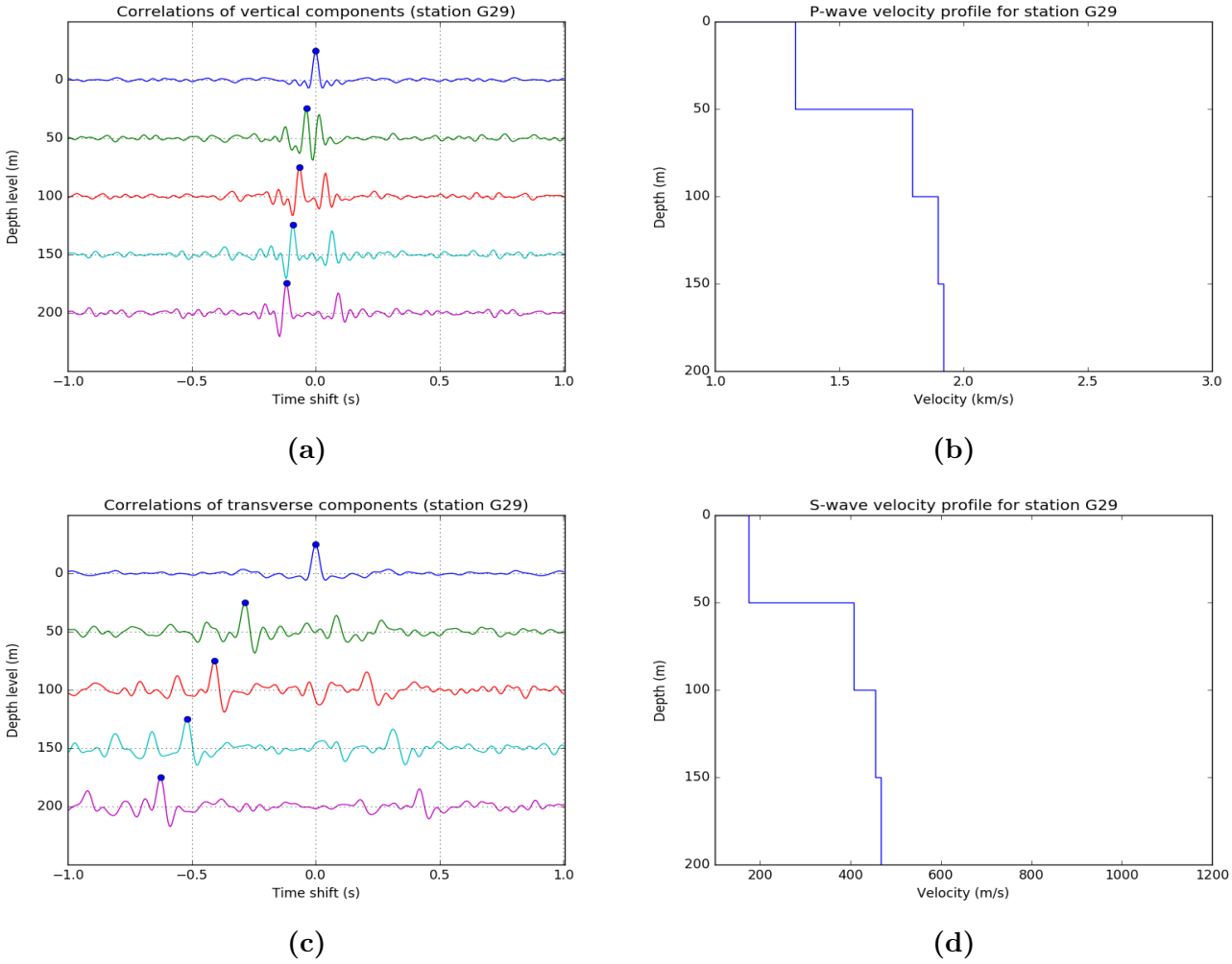

Figure 40: ***(a)*** *Stacked cross-correlations of the vertical components. Blue dot indicates the peak associated with the P-wave.* ***(b)*** *P-wave velocity profile calculated from the picks in figure 40a.* ***(c)*** *Stacked cross-correlations of the transverse components. Blue dot indicates the peak associated with the SH-wave.* ***(d)*** *S-wave velocity profiles calculated from the picks in figure 40c.*

Station G30

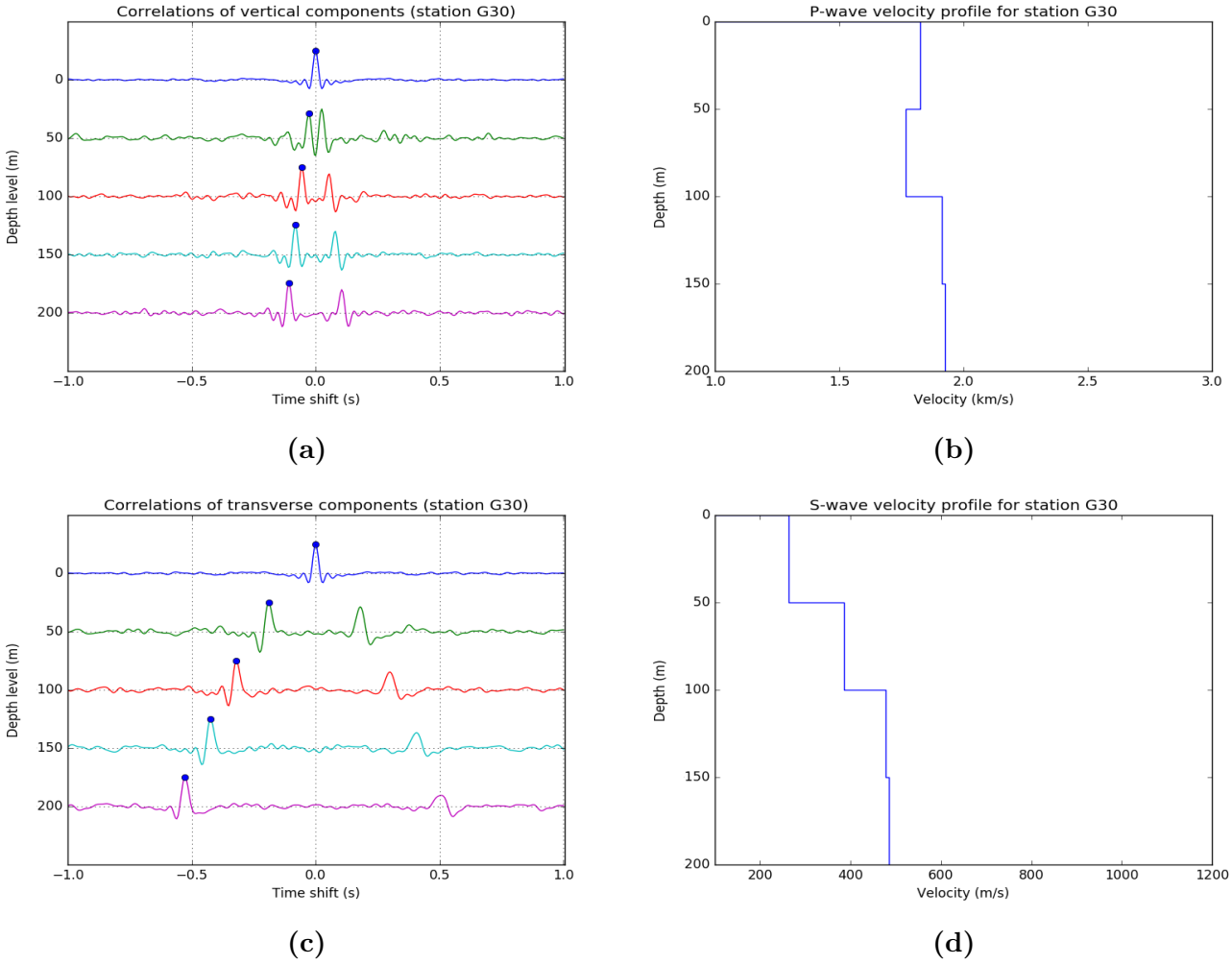

Figure 41: ***(a)*** *Stacked cross-correlations of the vertical components. Blue dot indicates the peak associated with the P-wave.* ***(b)*** *P-wave velocity profile calculated from the picks in figure 41a.* ***(c)*** *Stacked cross-correlations of the transverse components. Blue dot indicates the peak associated with the SH-wave.* ***(d)*** *S-wave velocity profiles calculated from the picks in figure 41c.*

Station G31

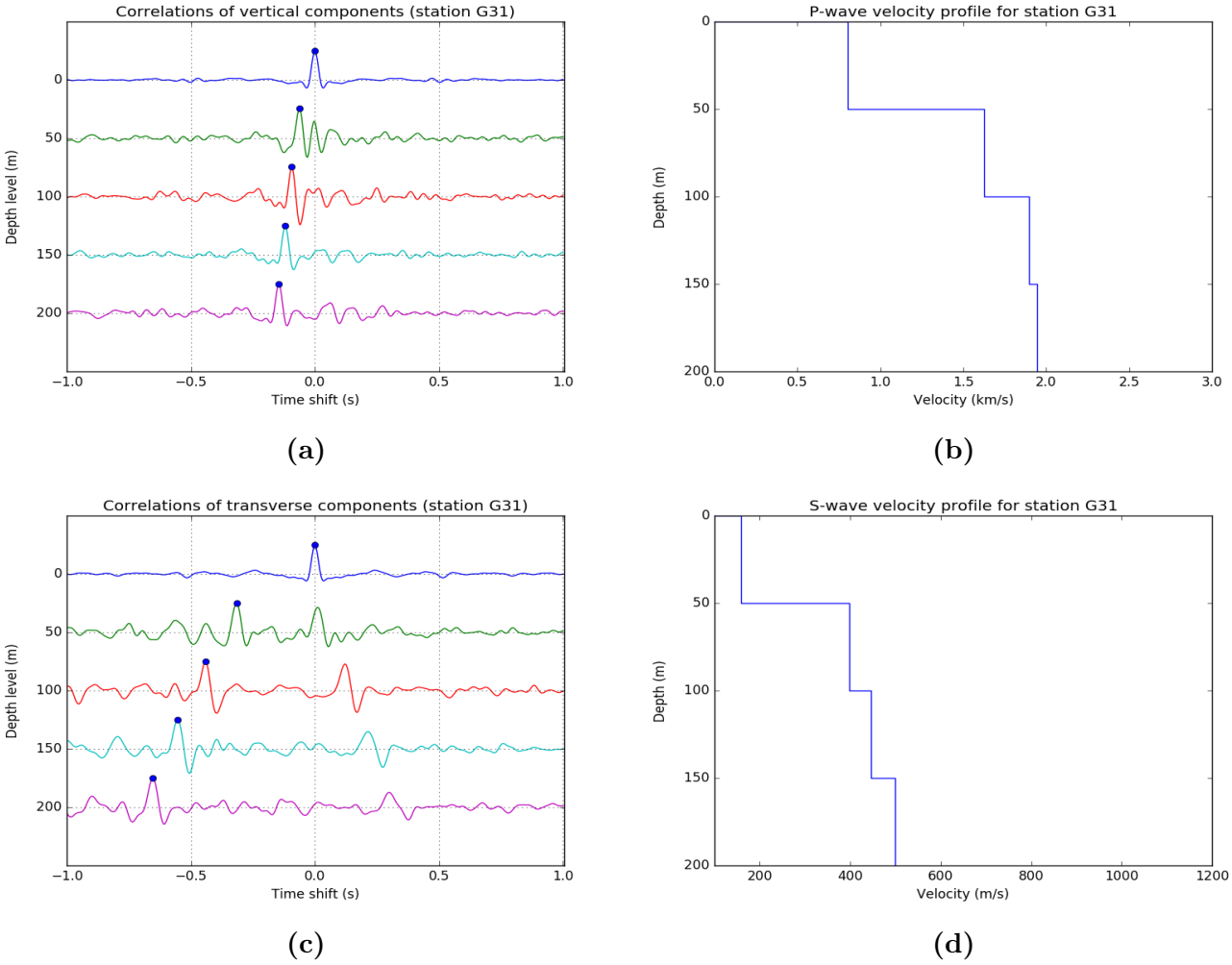

Figure 42: ***(a)*** *Stacked cross-correlations of the vertical components. Blue dot indicates the peak associated with the P-wave.* ***(b)*** *P-wave velocity profile calculated from the picks in figure 42a.* ***(c)*** *Stacked cross-correlations of the transverse components. Blue dot indicates the peak associated with the SH-wave.* ***(d)*** *S-wave velocity profiles calculated from the picks in figure 42c.*

Station G32

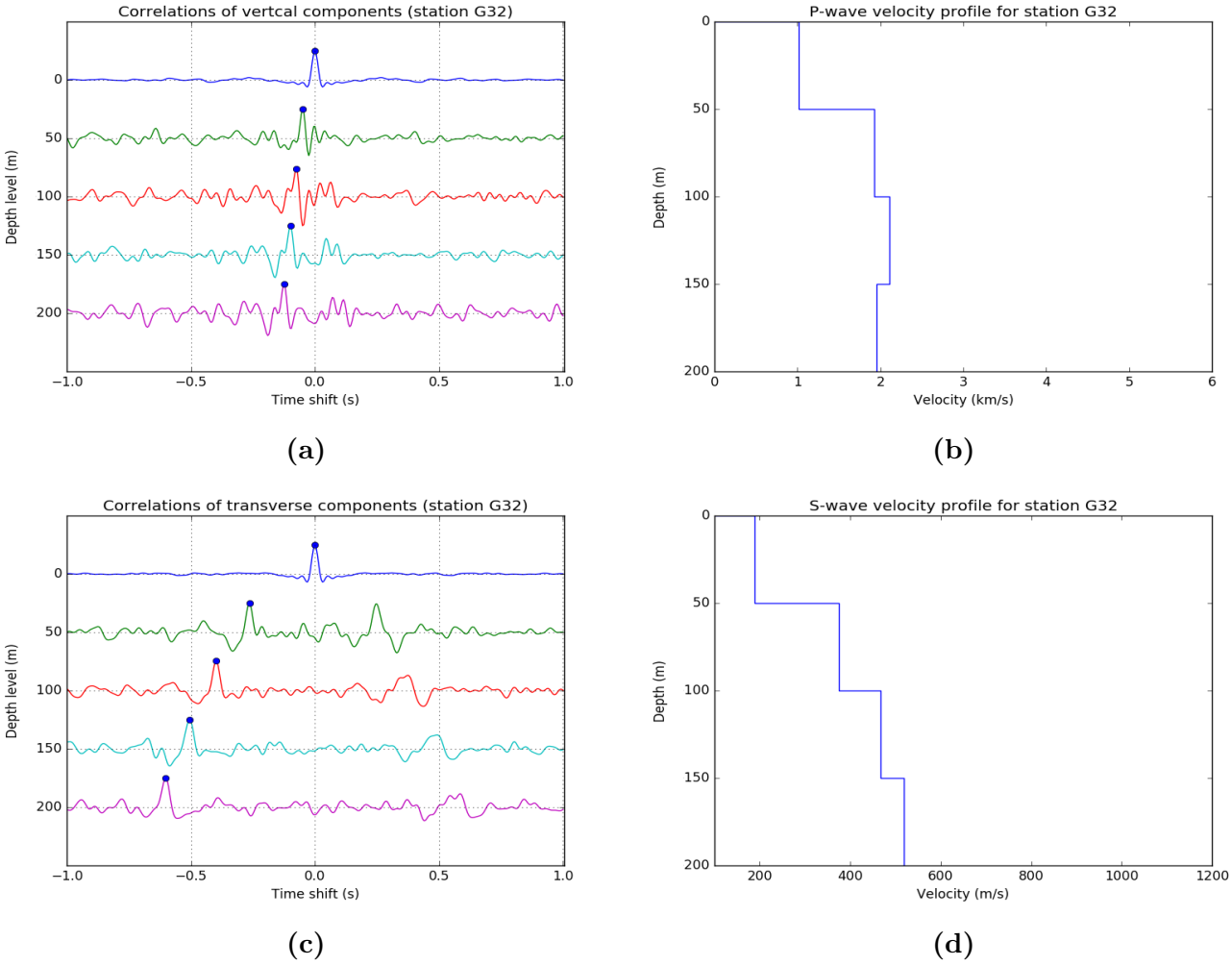

Figure 43: ***(a)*** *Stacked cross-correlations of the vertical components. Blue dot indicates the peak associated with the P-wave.* ***(b)*** *P-wave velocity profile calculated from the picks in figure 43a.* ***(c)*** *Stacked cross-correlations of the transverse components. Blue dot indicates the peak associated with the SH-wave.* ***(d)*** *S-wave velocity profiles calculated from the picks in figure 43c.*

NOTE: Geophone data were interchanged to obtain the above result. The shallowest level (50 m) shown here is G324, 100 m corresponds with G321, 150 m corresponds with G322, and 200 m corresponds with G323.

Station G33

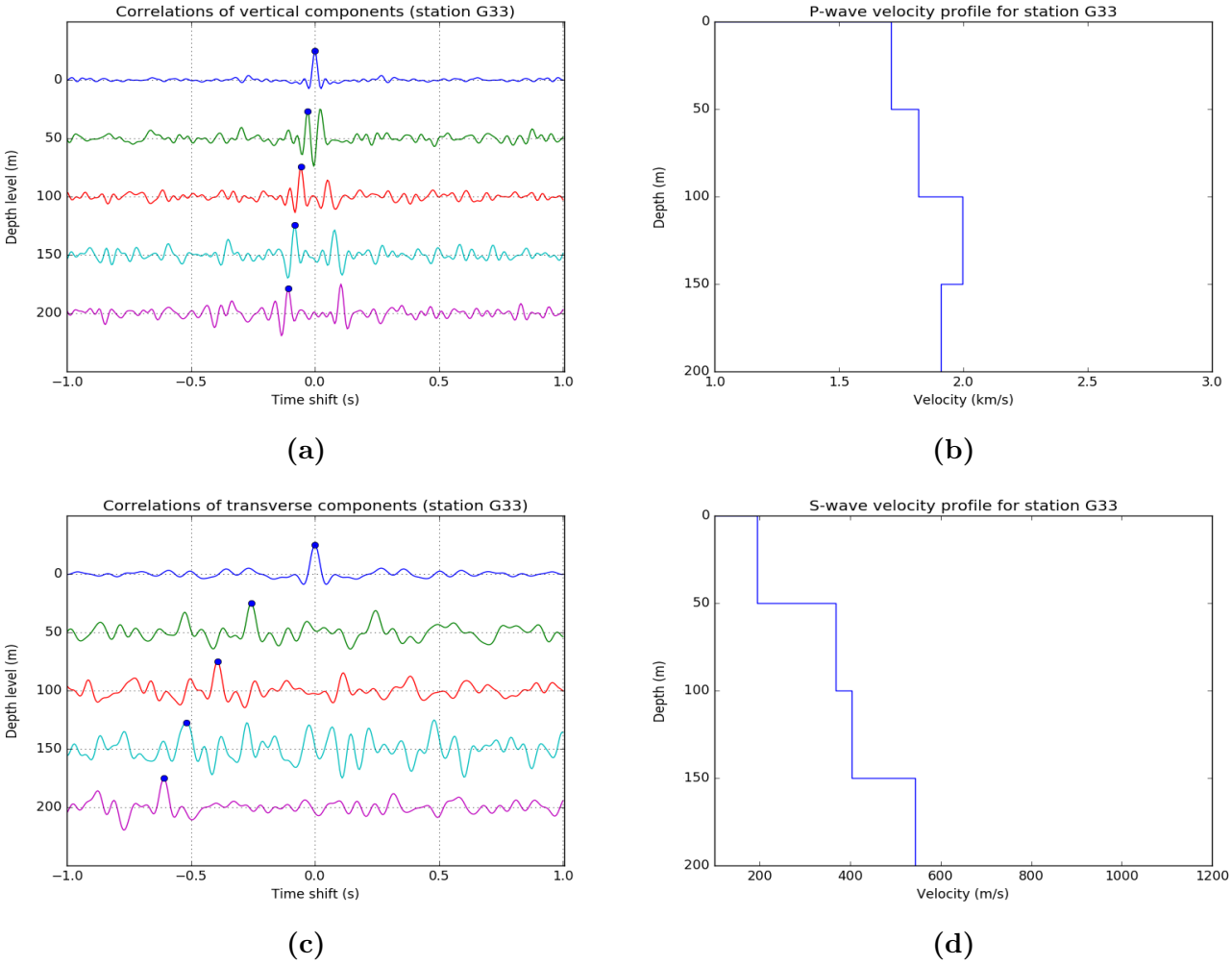

Figure 44: ***(a)*** *Stacked cross-correlations of the vertical components. Blue dot indicates the peak associated with the P-wave.* ***(b)*** *P-wave velocity profile calculated from the picks in figure 44a.* ***(c)*** *Stacked cross-correlations of the transverse components. Blue dot indicates the peak associated with the SH-wave.* ***(d)*** *S-wave velocity profiles calculated from the picks in figure 44c.*

Station G34

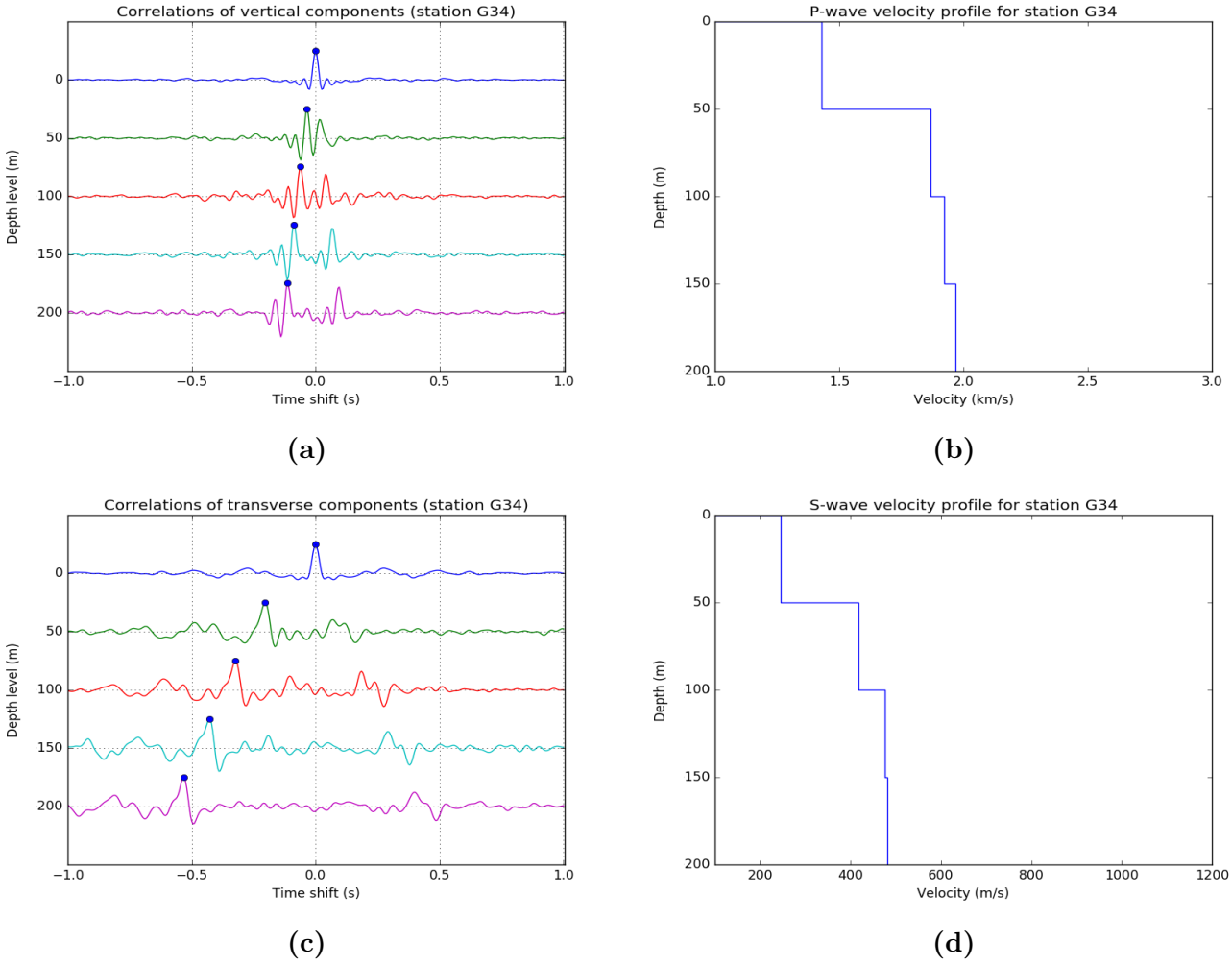

Figure 45: ***(a)*** *Stacked cross-correlations of the vertical components. Blue dot indicates the peak associated with the P-wave.* ***(b)*** *P-wave velocity profile calculated from the picks in figure 45a.* ***(c)*** *Stacked cross-correlations of the transverse components. Blue dot indicates the peak associated with the SH-wave.* ***(d)*** *S-wave velocity profiles calculated from the picks in figure 45c.*

Station G36

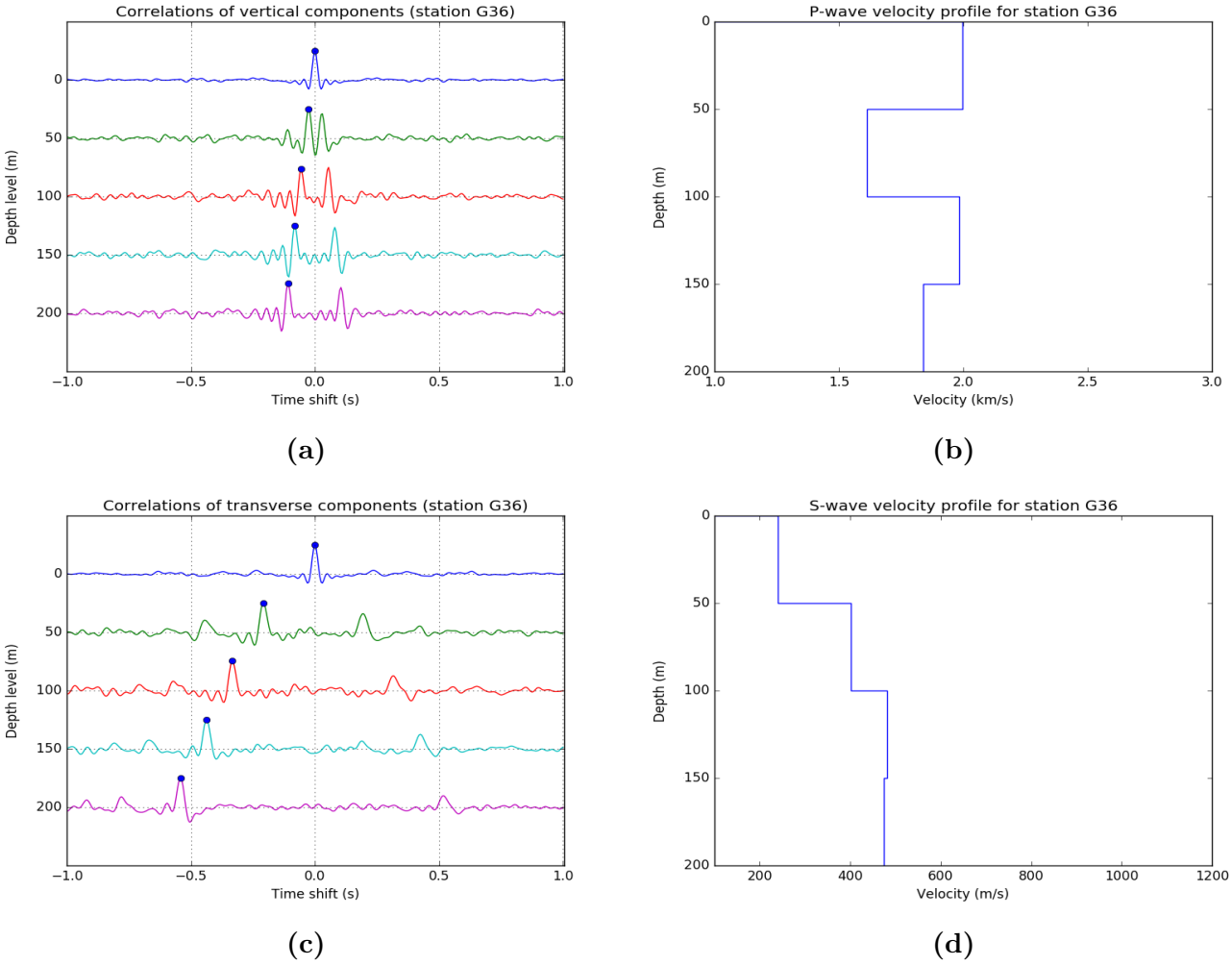

Figure 46: ***(a)*** *Stacked cross-correlations of the vertical components. Blue dot indicates the peak associated with the P-wave.* ***(b)*** *P-wave velocity profile calculated from the picks in figure 46a.* ***(c)*** *Stacked cross-correlations of the transverse components. Blue dot indicates the peak associated with the SH-wave.* ***(d)*** *S-wave velocity profiles calculated from the picks in figure 46c.*

Station G37

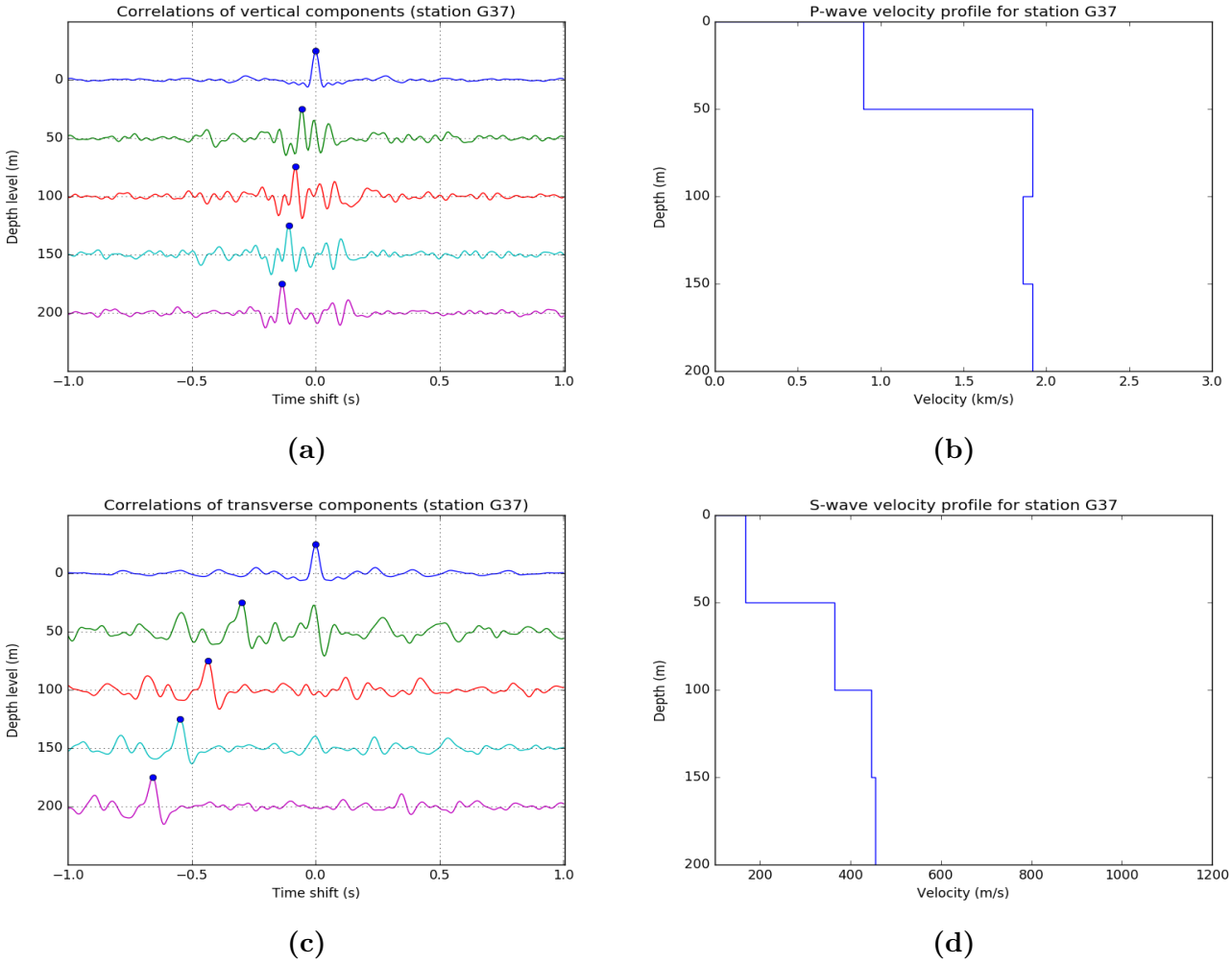

Figure 47: ***(a)*** *Stacked cross-correlations of the vertical components. Blue dot indicates the peak associated with the P-wave.* ***(b)*** *P-wave velocity profile calculated from the picks in figure 47a.* ***(c)*** *Stacked cross-correlations of the transverse components. Blue dot indicates the peak associated with the SH-wave.* ***(d)*** *S-wave velocity profiles calculated from the picks in figure 47c.*

Station G38

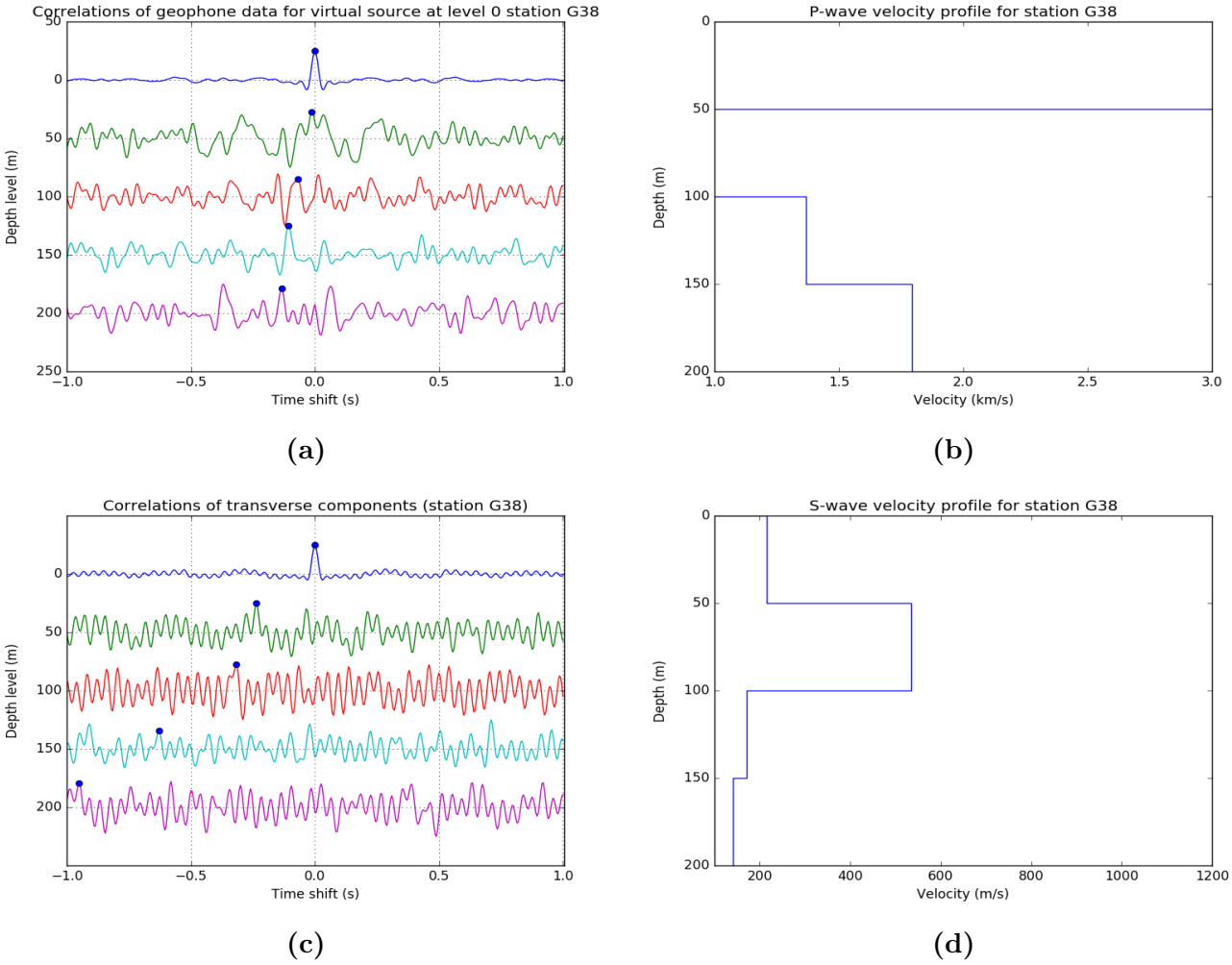

Figure 48: ***(a)*** *Stacked cross-correlations of the vertical components. Blue dot indicates the peak associated with the P-wave.* ***(b)*** *P-wave velocity profile calculated from the picks in figure 48a.* ***(c)*** *Stacked cross-correlations of the transverse components. Blue dot indicates the peak associated with the SH-wave.* ***(d)*** *S-wave velocity profiles calculated from the picks in figure 48c.*

NOTE: The result from this station was not used. The amount of noise was too high to be able to get a convincing result.

Station G39

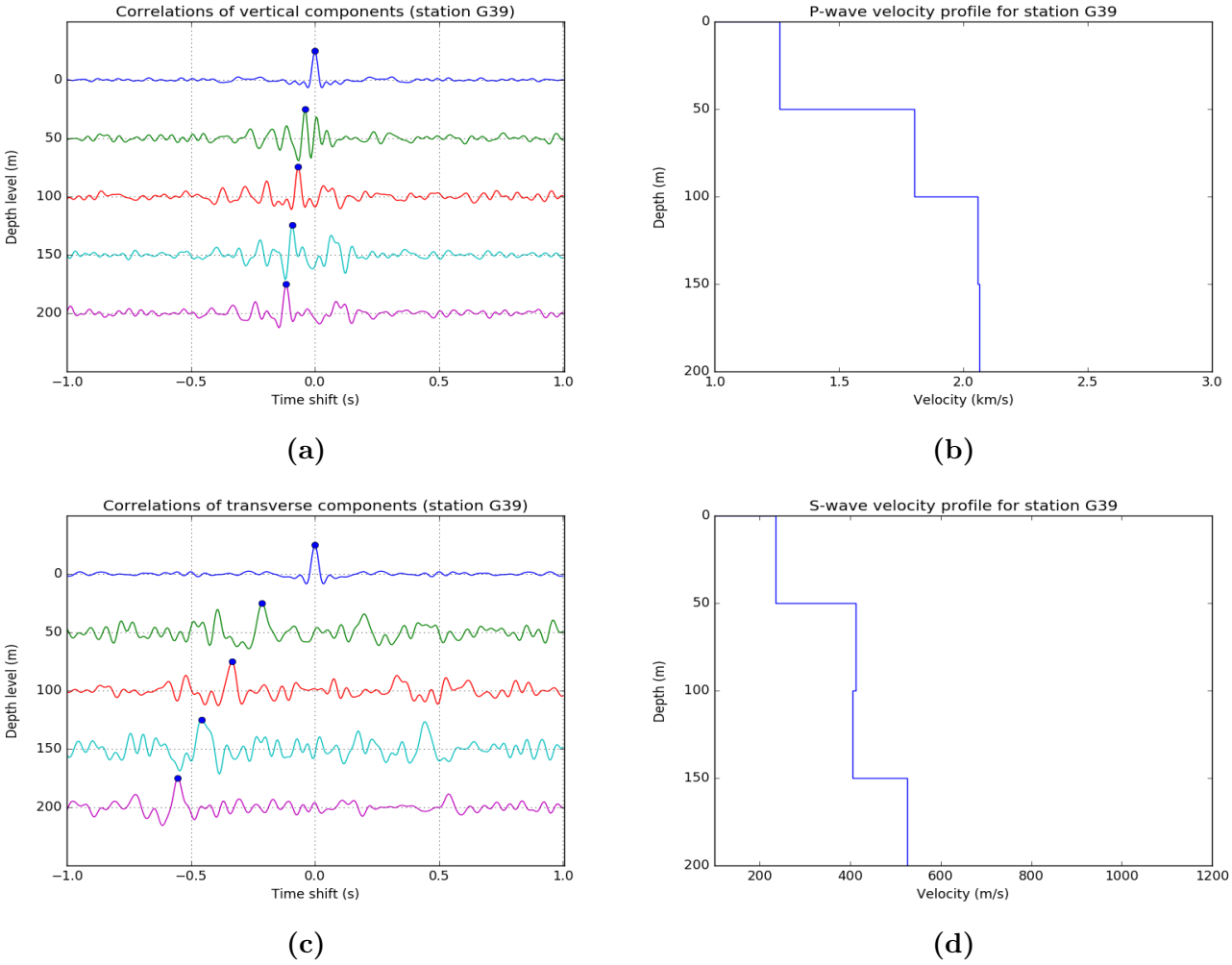

Figure 49: ***(a)*** *Stacked cross-correlations of the vertical components. Blue dot indicates the peak associated with the P-wave.* ***(b)*** *P-wave velocity profile calculated from the picks in figure 49a.* ***(c)*** *Stacked cross-correlations of the transverse components. Blue dot indicates the peak associated with the SH-wave.* ***(d)*** *S-wave velocity profiles calculated from the picks in figure 49c.*

Station G40

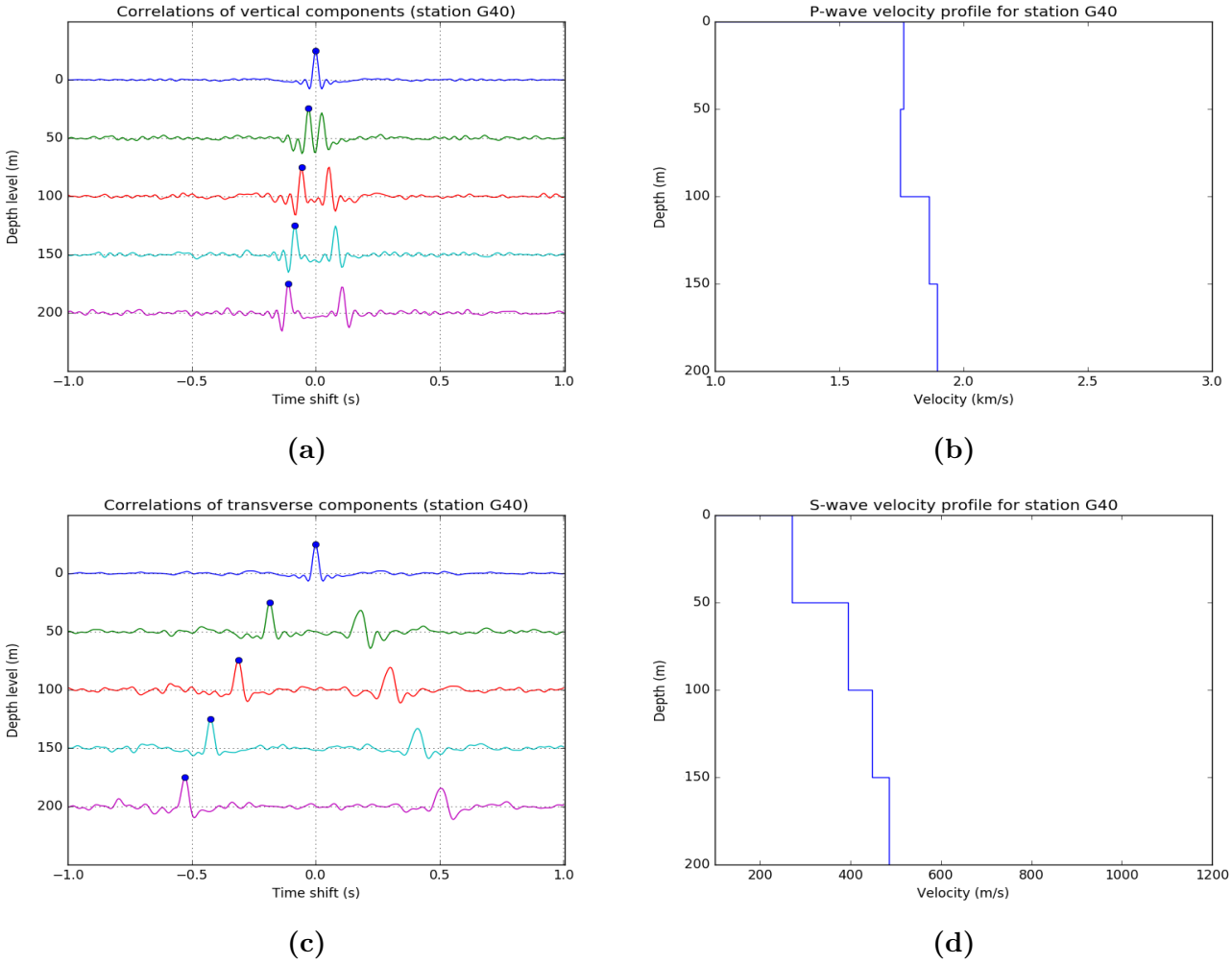

Figure 50: ***(a)*** *Stacked cross-correlations of the vertical components. Blue dot indicates the peak associated with the P-wave.* ***(b)*** *P-wave velocity profile calculated from the picks in figure 50a.* ***(c)*** *Stacked cross-correlations of the transverse components. Blue dot indicates the peak associated with the SH-wave.* ***(d)*** *S-wave velocity profiles calculated from the picks in figure 50c.*

Station G41

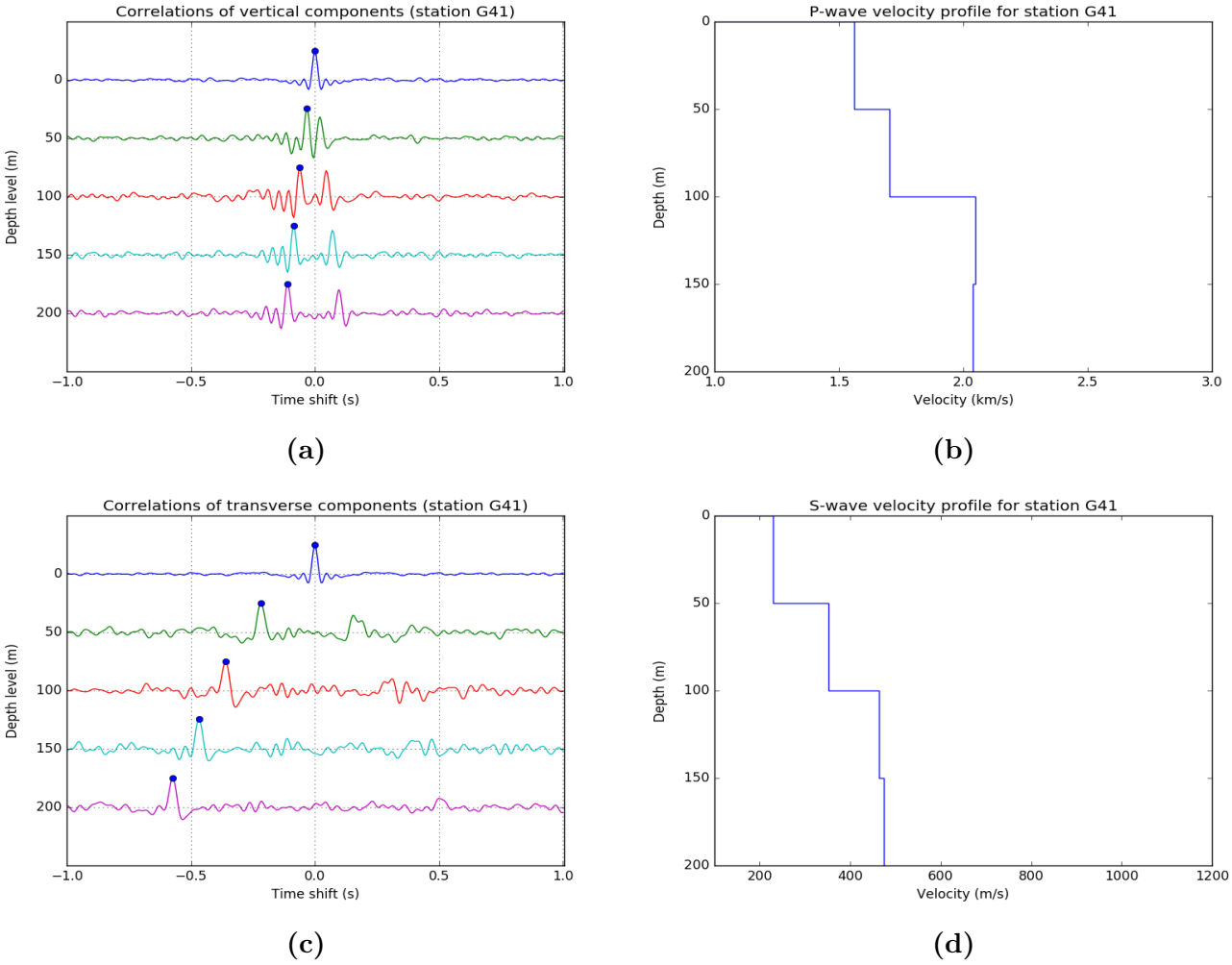

Figure 51: ***(a)*** *Stacked cross-correlations of the vertical components. Blue dot indicates the peak associated with the P-wave.* ***(b)*** *P-wave velocity profile calculated from the picks in figure 51a.* ***(c)*** *Stacked cross-correlations of the transverse components. Blue dot indicates the peak associated with the SH-wave.* ***(d)*** *S-wave velocity profiles calculated from the picks in figure 51c.*

Station G42

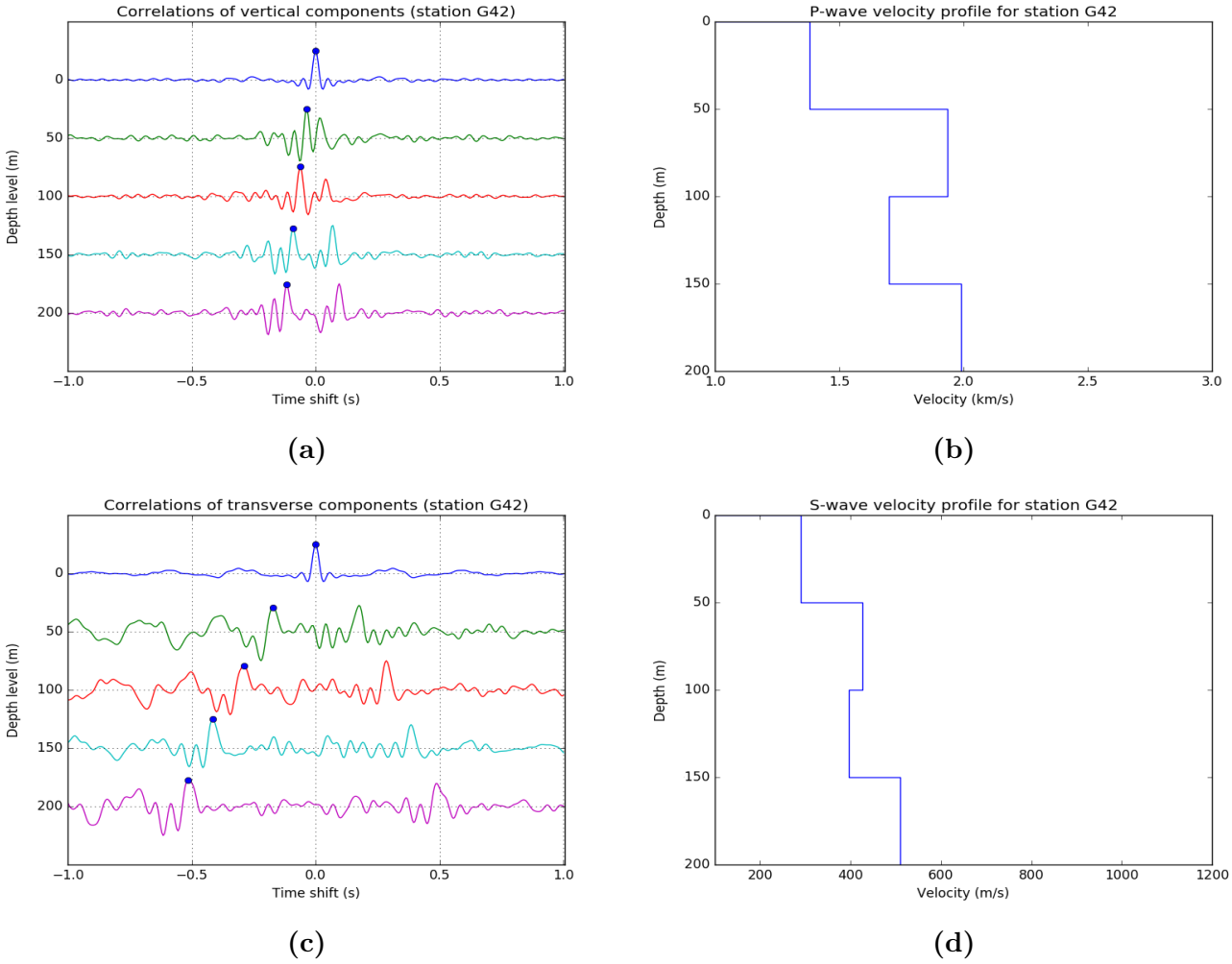

Figure 52: ***(a)*** *Stacked cross-correlations of the vertical components. Blue dot indicates the peak associated with the P-wave.* ***(b)*** *P-wave velocity profile calculated from the picks in figure 52a.* ***(c)*** *Stacked cross-correlations of the transverse components. Blue dot indicates the peak associated with the SH-wave.* ***(d)*** *S-wave velocity profiles calculated from the picks in figure 52c.*

Station G43

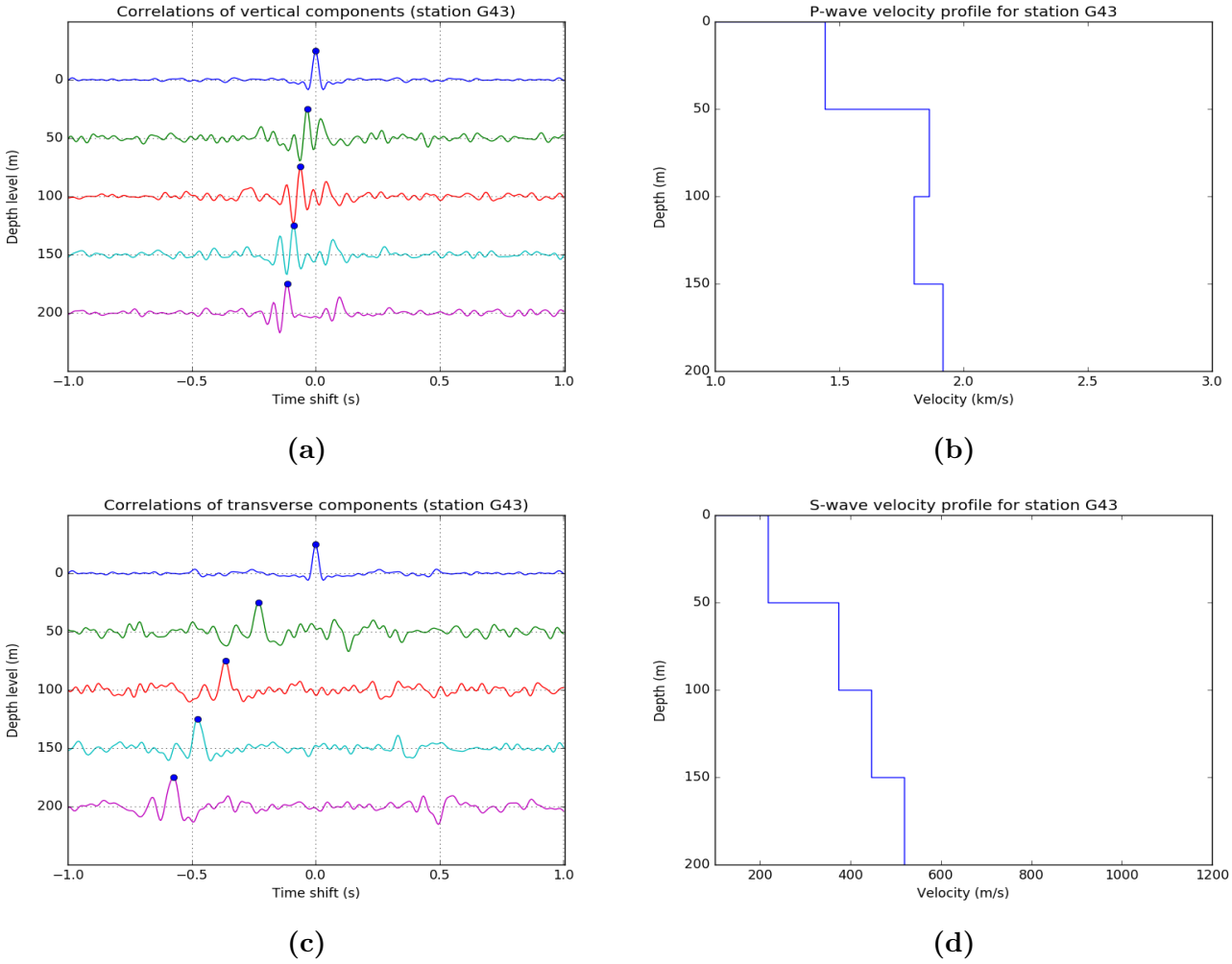

Figure 53: ***(a)*** *Stacked cross-correlations of the vertical components. Blue dot indicates the peak associated with the P-wave.* ***(b)*** *P-wave velocity profile calculated from the picks in figure 53a.* ***(c)*** *Stacked cross-correlations of the transverse components. Blue dot indicates the peak associated with the SH-wave.* ***(d)*** *S-wave velocity profiles calculated from the picks in figure 53c.*

Station G44

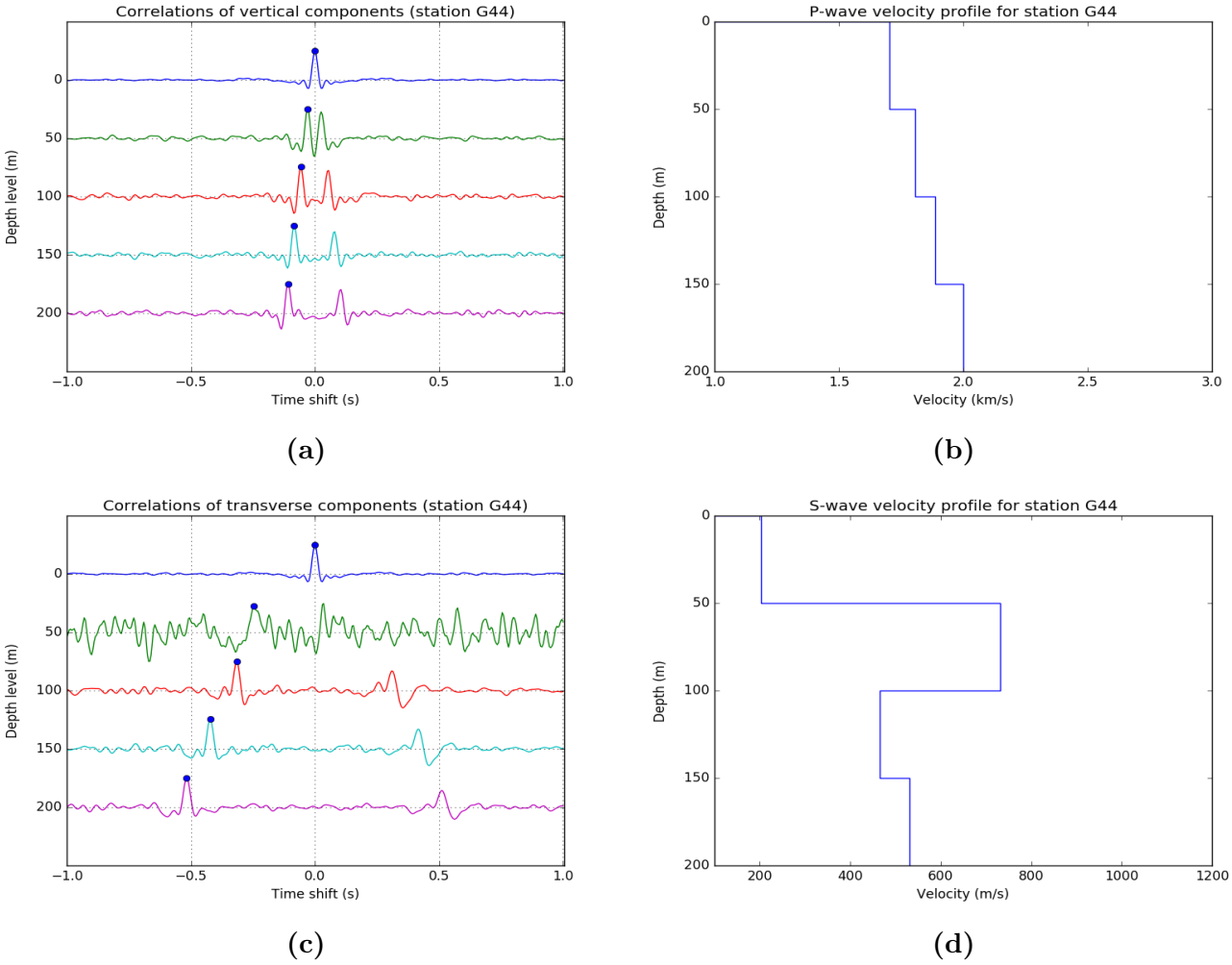

Figure 54: ***(a)*** *Stacked cross-correlations of the vertical components. Blue dot indicates the peak associated with the P-wave.* ***(b)*** *P-wave velocity profile calculated from the picks in figure 54a.* ***(c)*** *Stacked cross-correlations of the transverse components. Blue dot indicates the peak associated with the SH-wave.* ***(d)*** *S-wave velocity profiles calculated from the picks in figure 54c.*

NOTE: The result from this station was not used due to the amount of noise on the second geophone.

Station G45

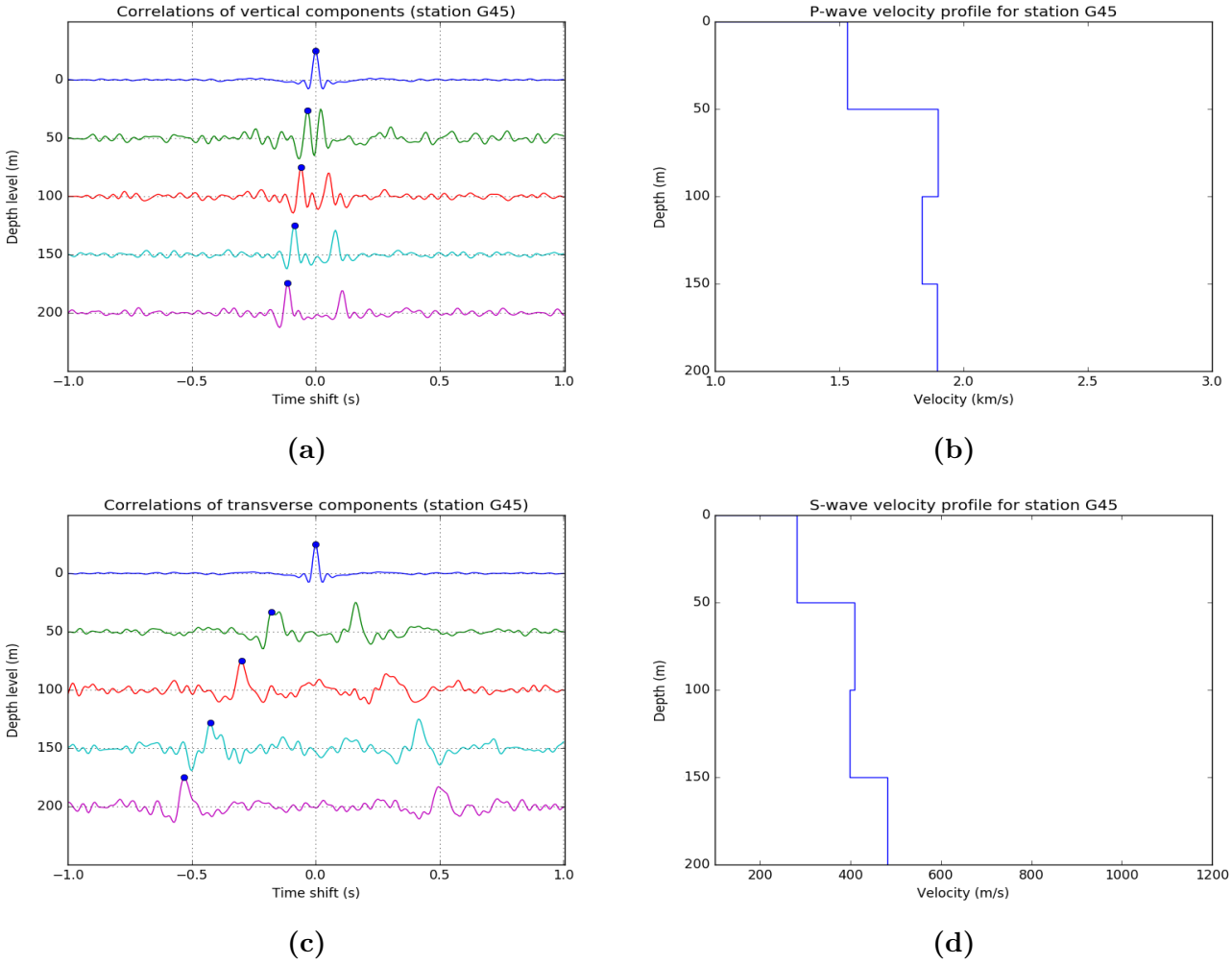

Figure 55: ***(a)*** *Stacked cross-correlations of the vertical components. Blue dot indicates the peak associated with the P-wave.* ***(b)*** *P-wave velocity profile calculated from the picks in figure 55a.* ***(c)*** *Stacked cross-correlations of the transverse components. Blue dot indicates the peak associated with the SH-wave.* ***(d)*** *S-wave velocity profiles calculated from the picks in figure 55c.*

Station G46

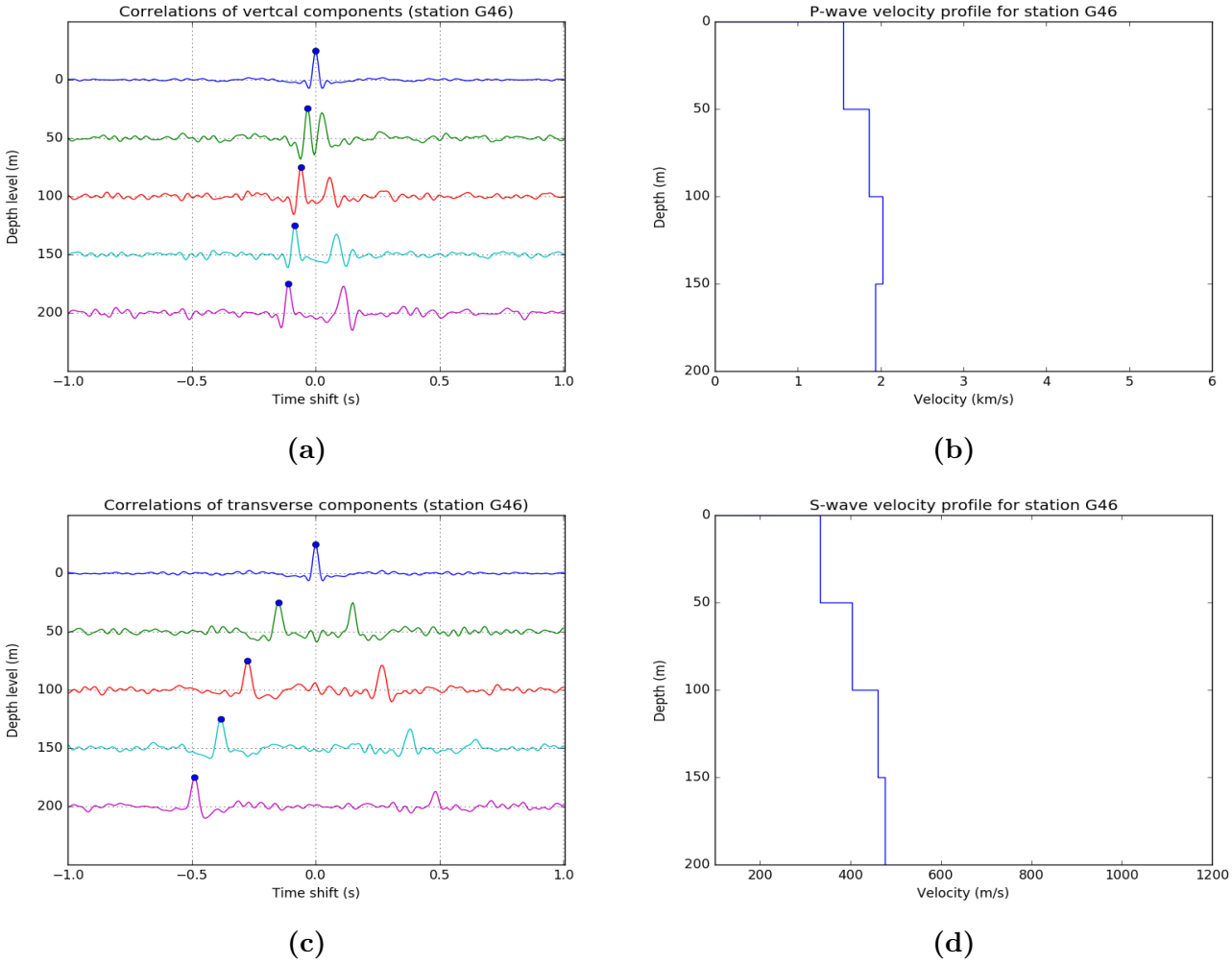

Figure 56: *(a) Stacked cross-correlations of the vertical components. Blue dot indicates the peak associated with the P-wave.* ***(b)*** *P-wave velocity profile calculated from the picks in figure 56a.* ***(c)*** *Stacked cross-correlations of the transverse components. Blue dot indicates the peak associated with the SH-wave.* ***(d)*** *S-wave velocity profiles calculated from the picks in figure 56c.*

Station G47

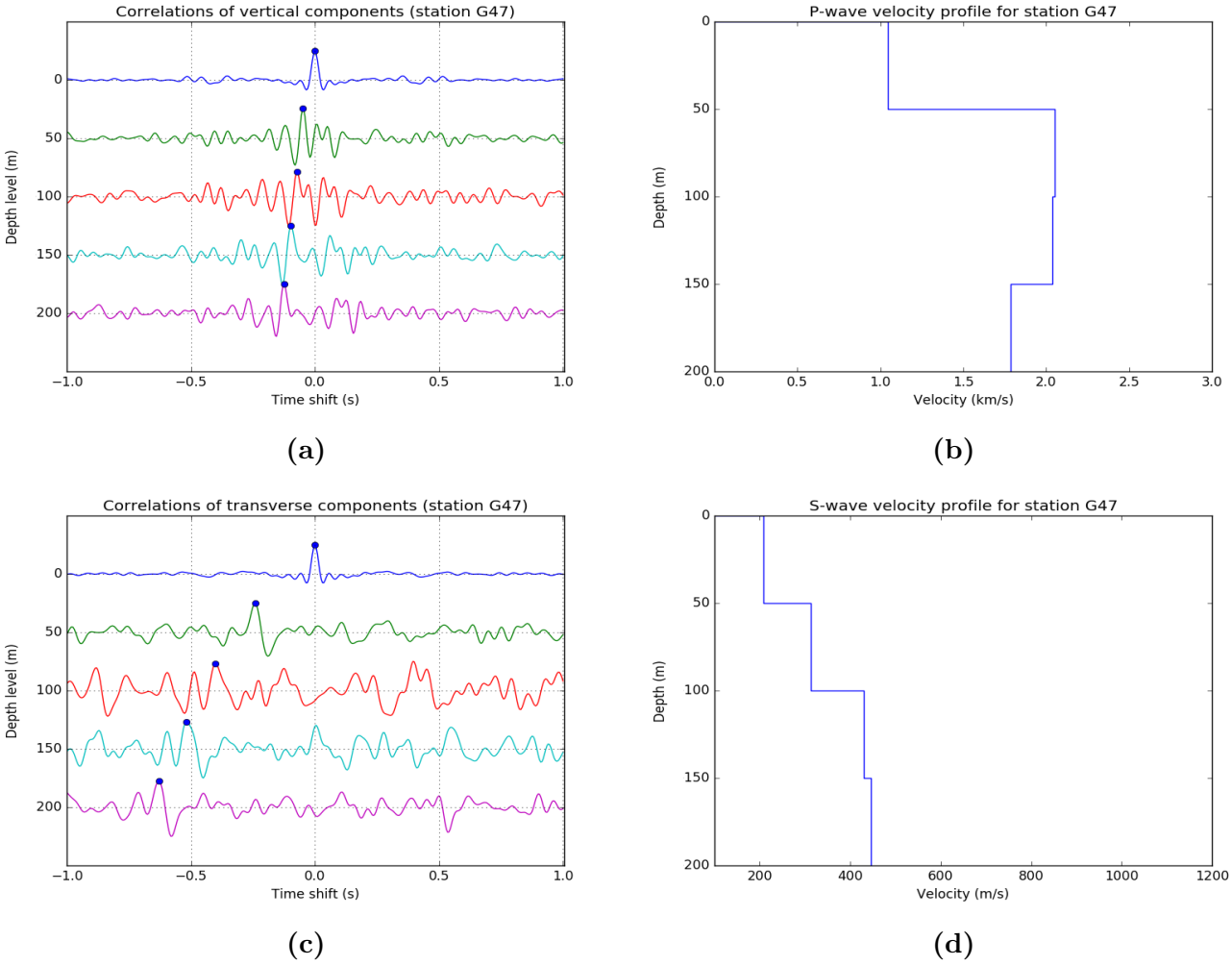

Figure 57: ***(a)*** *Stacked cross-correlations of the vertical components. Blue dot indicates the peak associated with the P-wave.* ***(b)*** *P-wave velocity profile calculated from the picks in figure 57a.* ***(c)*** *Stacked cross-correlations of the transverse components. Blue dot indicates the peak associated with the SH-wave.* ***(d)*** *S-wave velocity profiles calculated from the picks in figure 57c.*

NOTE: To obtain the above result, the geophone data from 100 m and 200 m (G472 and G474) were interchanged.

Station G49

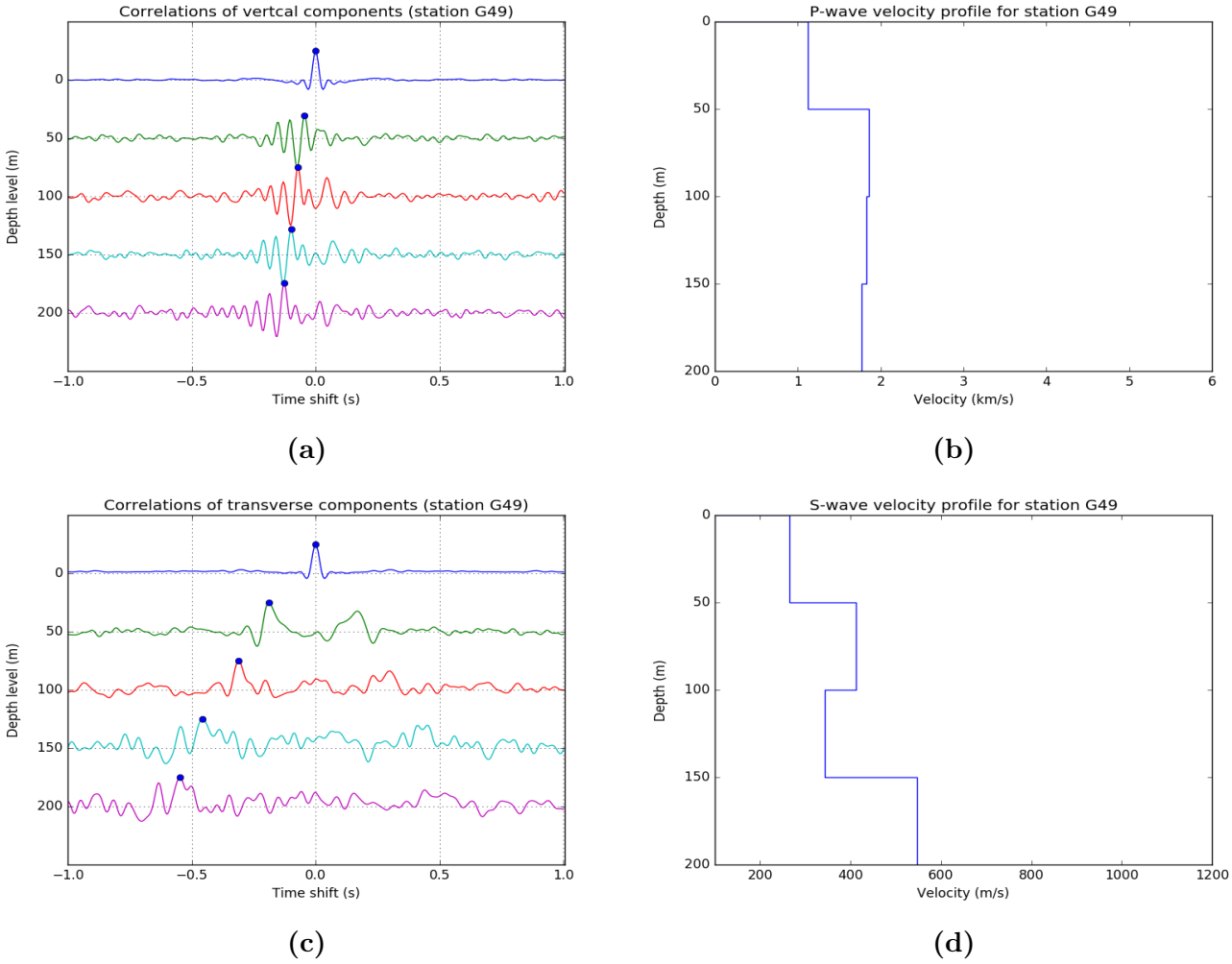

Figure 58: ***(a)*** *Stacked cross-correlations of the vertical components. Blue dot indicates the peak associated with the P-wave.* ***(b)*** *P-wave velocity profile calculated from the picks in figure 58a.* ***(c)*** *Stacked cross-correlations of the transverse components. Blue dot indicates the peak associated with the SH-wave.* ***(d)*** *S-wave velocity profiles calculated from the picks in figure 58c.*

Station G50

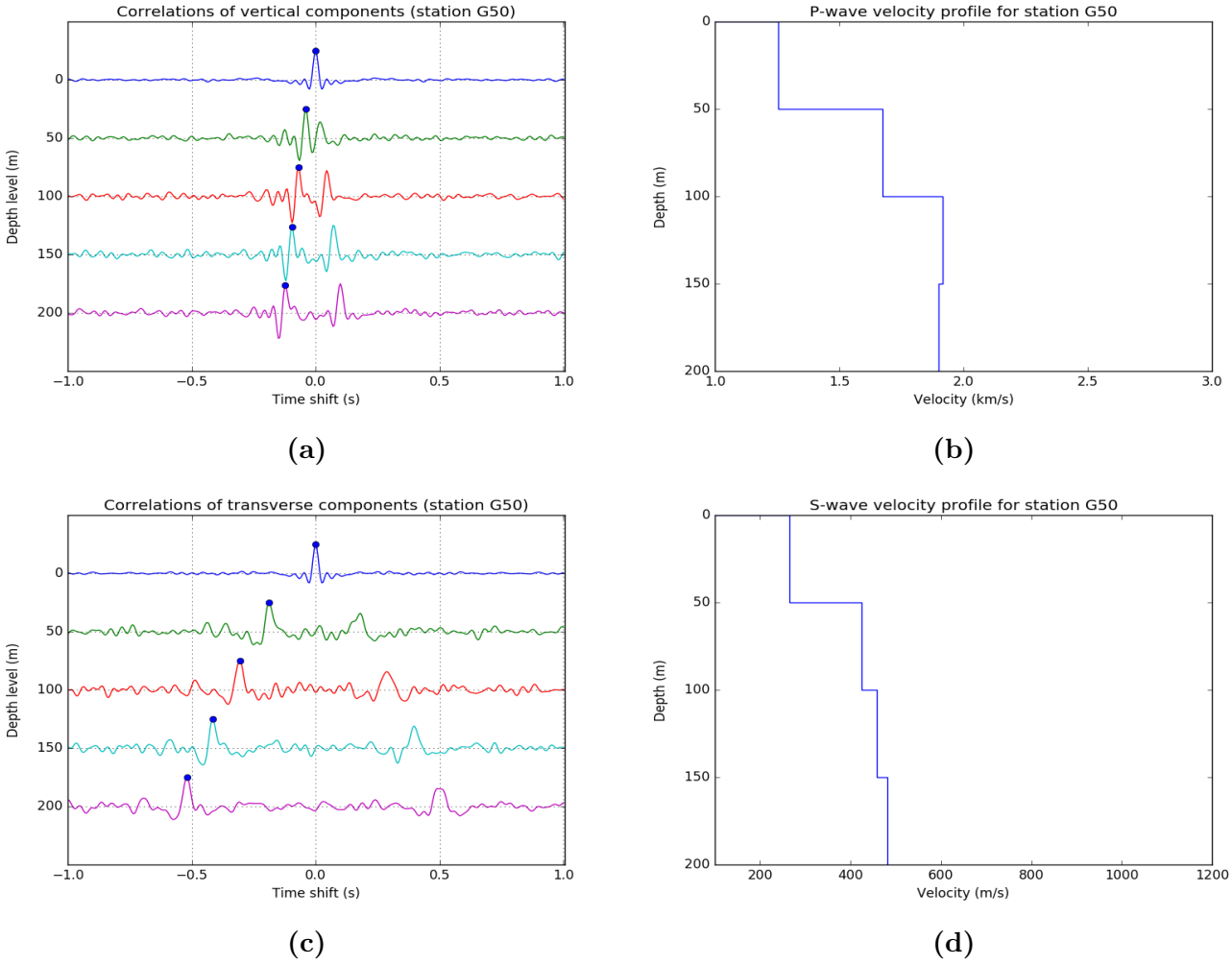

Figure 59: ***(a)*** *Stacked cross-correlations of the vertical components. Blue dot indicates the peak associated with the P-wave.* ***(b)*** *P-wave velocity profile calculated from the picks in figure 59a.* ***(c)*** *Stacked cross-correlations of the transverse components. Blue dot indicates the peak associated with the SH-wave.* ***(d)*** *S-wave velocity profiles calculated from the picks in figure 59c.*

Station G51

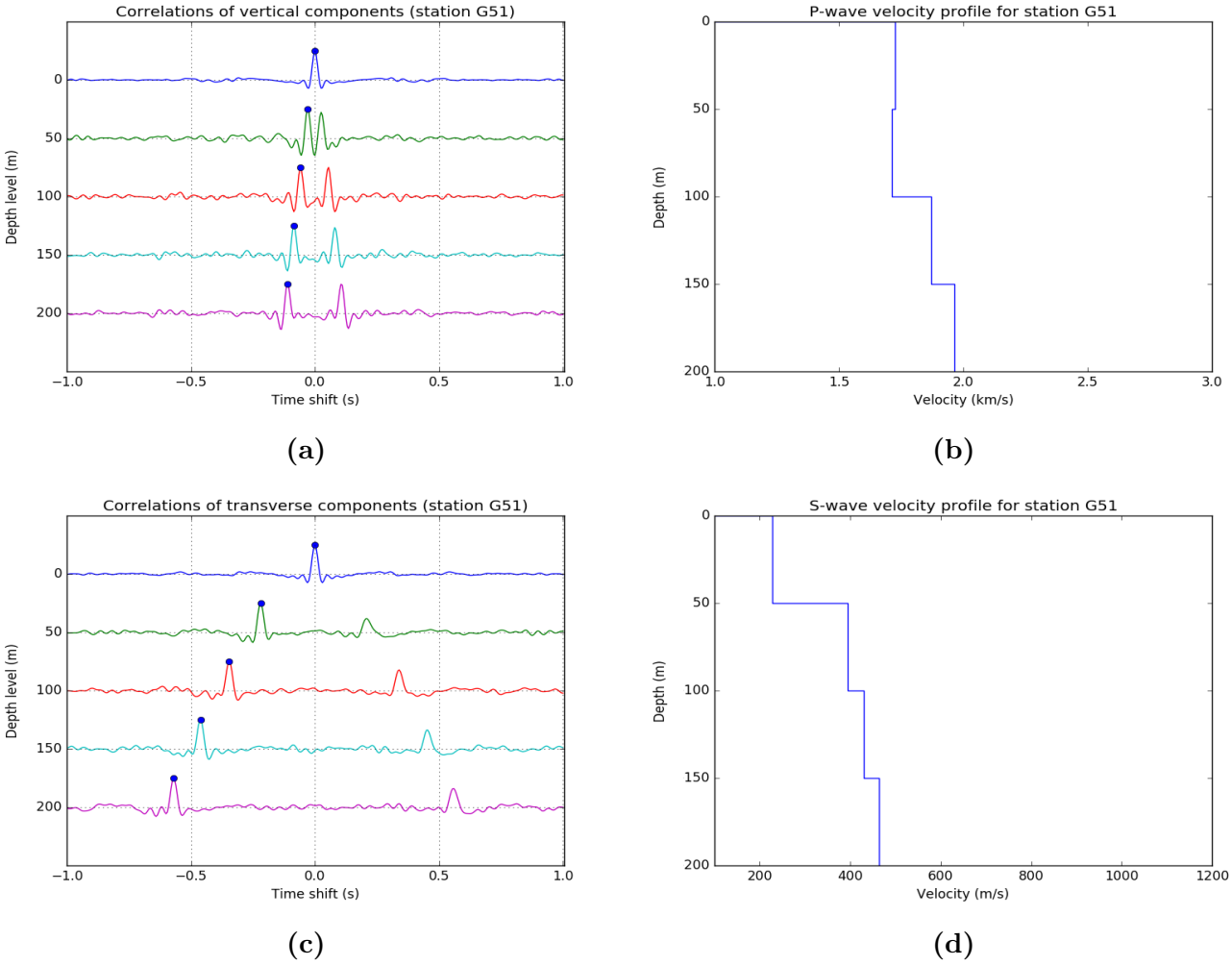

Figure 60: ***(a)*** *Stacked cross-correlations of the vertical components. Blue dot indicates the peak associated with the P-wave.* ***(b)*** *P-wave velocity profile calculated from the picks in figure 60a.* ***(c)*** *Stacked cross-correlations of the transverse components. Blue dot indicates the peak associated with the SH-wave.* ***(d)*** *S-wave velocity profiles calculated from the picks in figure 60c.*

Station G52

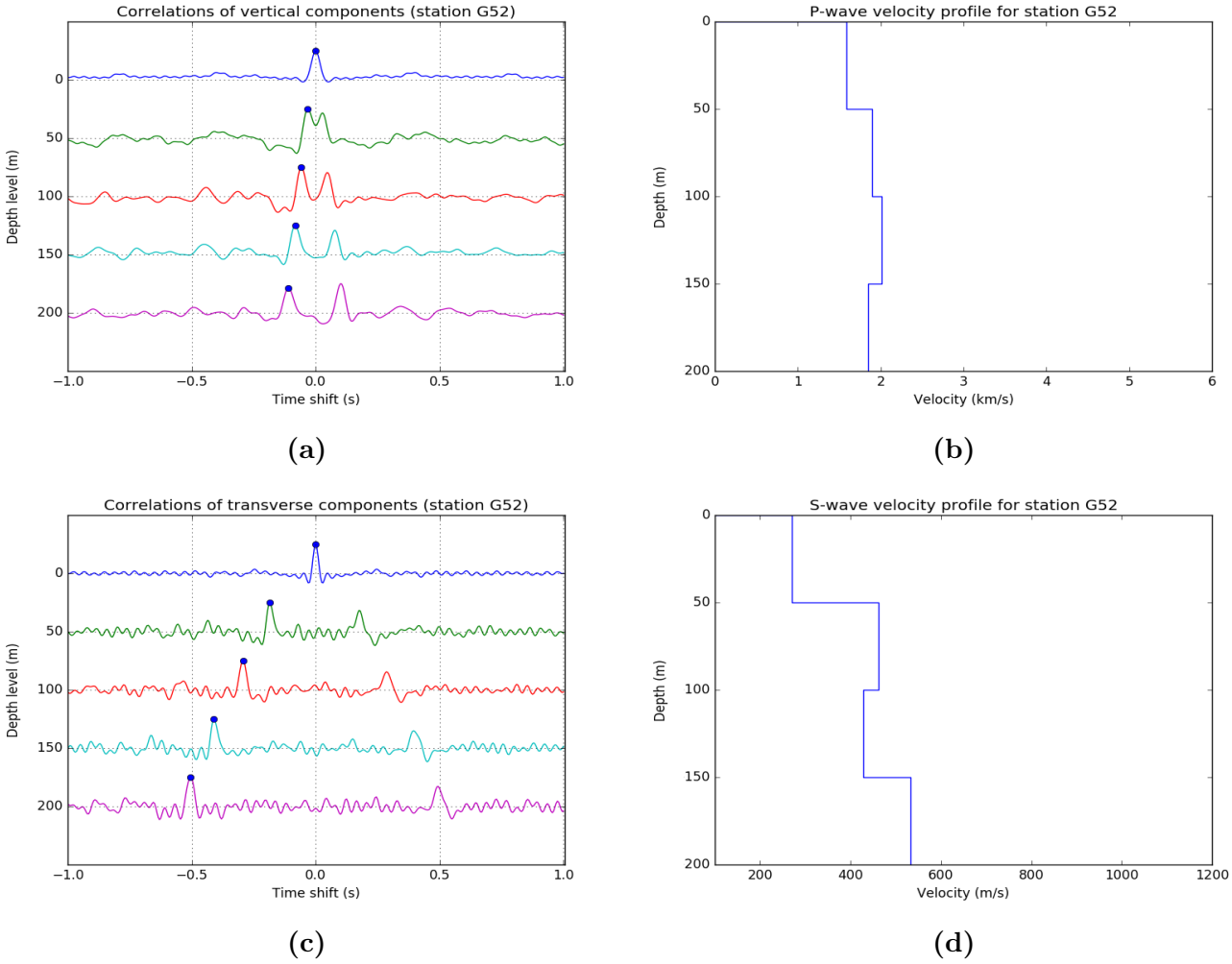

Figure 61: ***(a)*** *Stacked cross-correlations of the vertical components. Blue dot indicates the peak associated with the P-wave.* ***(b)*** *P-wave velocity profile calculated from the picks in figure 61a.* ***(c)*** *Stacked cross-correlations of the transverse components. Blue dot indicates the peak associated with the SH-wave.* ***(d)*** *S-wave velocity profiles calculated from the picks in figure 61c.*

Station G53

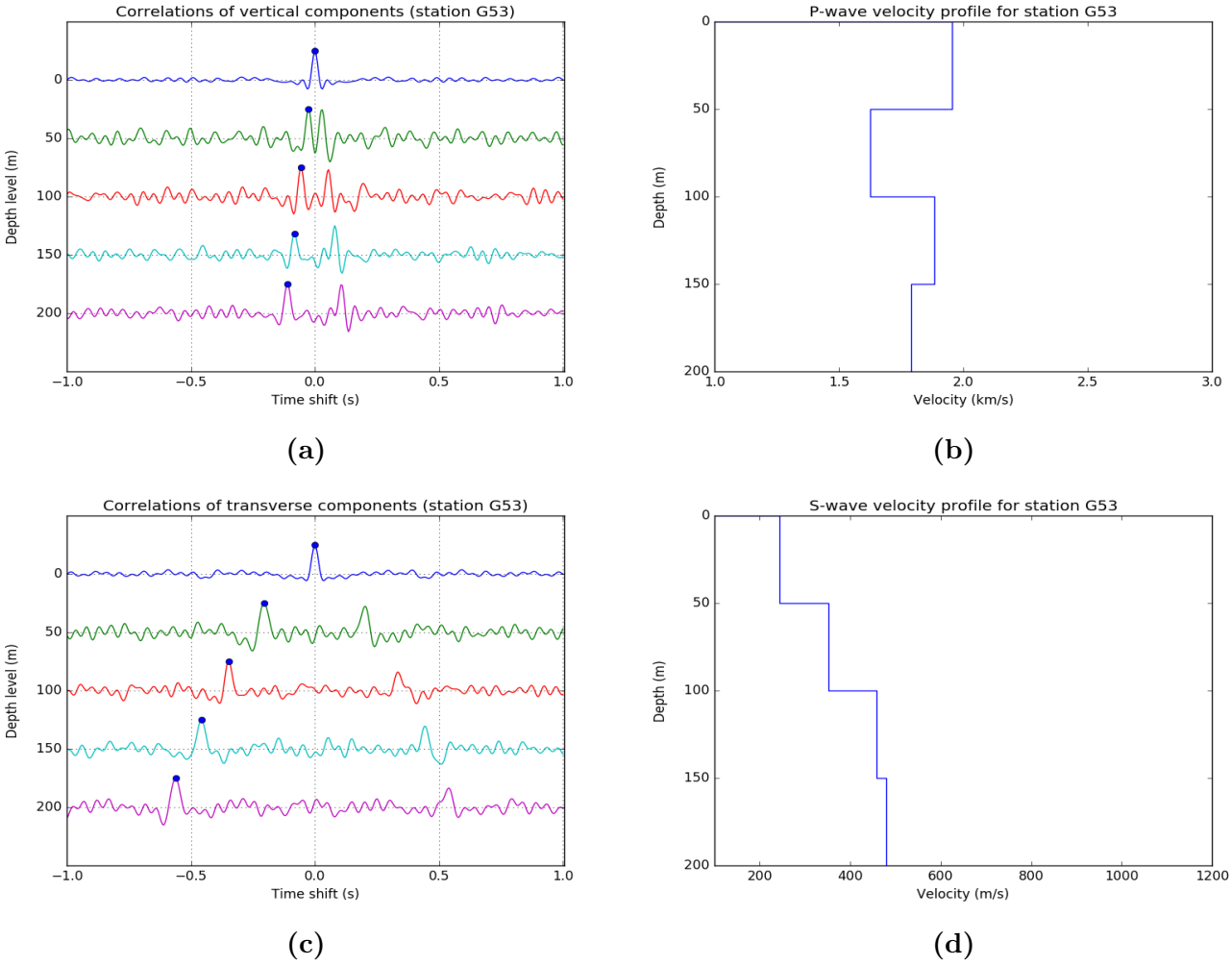

Figure 62: ***(a)*** *Stacked cross-correlations of the vertical components. Blue dot indicates the peak associated with the P-wave.* ***(b)*** *P-wave velocity profile calculated from the picks in figure 62a.* ***(c)*** *Stacked cross-correlations of the transverse components. Blue dot indicates the peak associated with the SH-wave.* ***(d)*** *S-wave velocity profiles calculated from the picks in figure 62c.*

Station G54

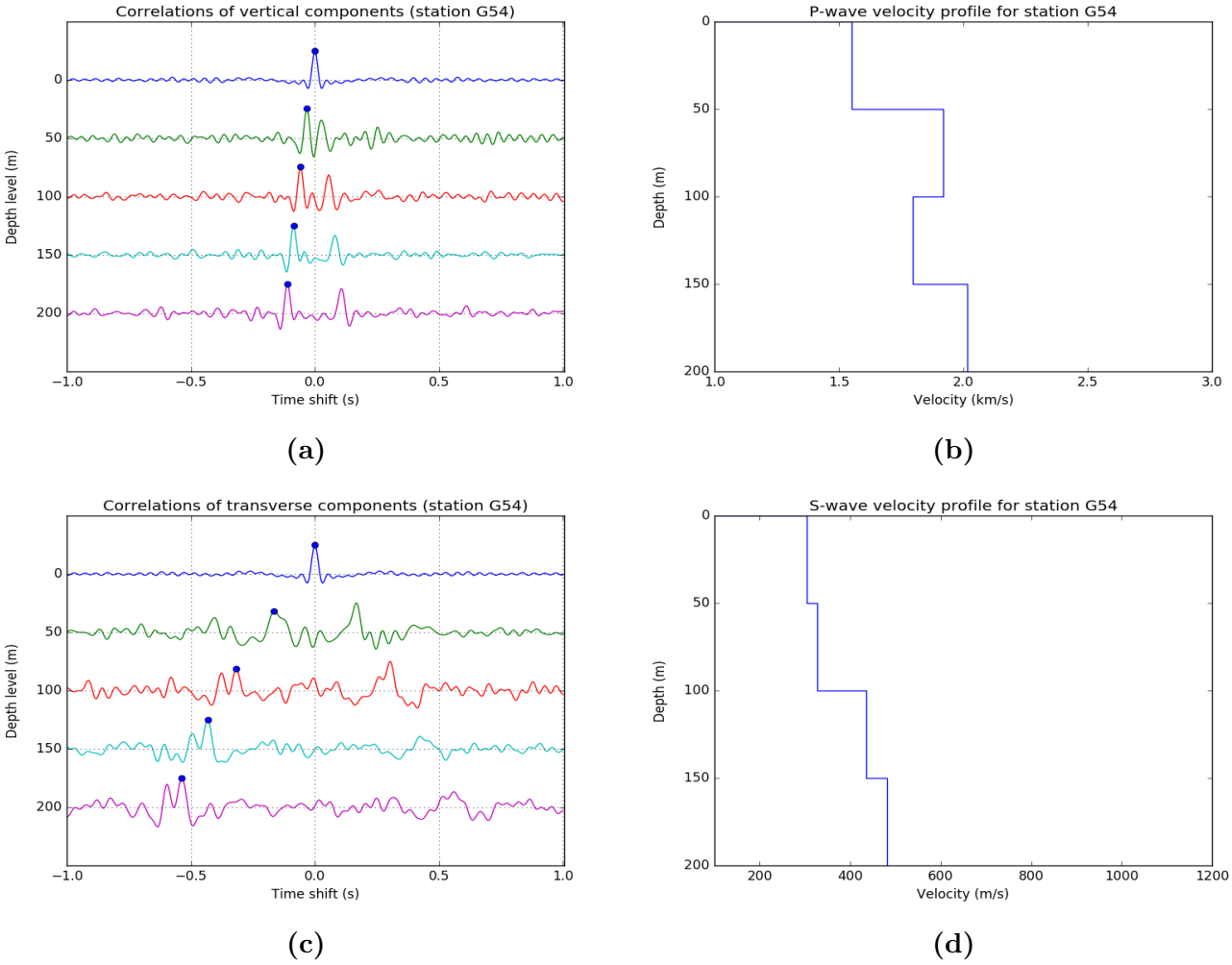

Figure 63: ***(a)*** *Stacked cross-correlations of the vertical components. Blue dot indicates the peak associated with the P-wave.* ***(b)*** *P-wave velocity profile calculated from the picks in figure 63a.* ***(c)*** *Stacked cross-correlations of the transverse components. Blue dot indicates the peak associated with the SH-wave.* ***(d)*** *S-wave velocity profiles calculated from the picks in figure 63c.*

Station G55

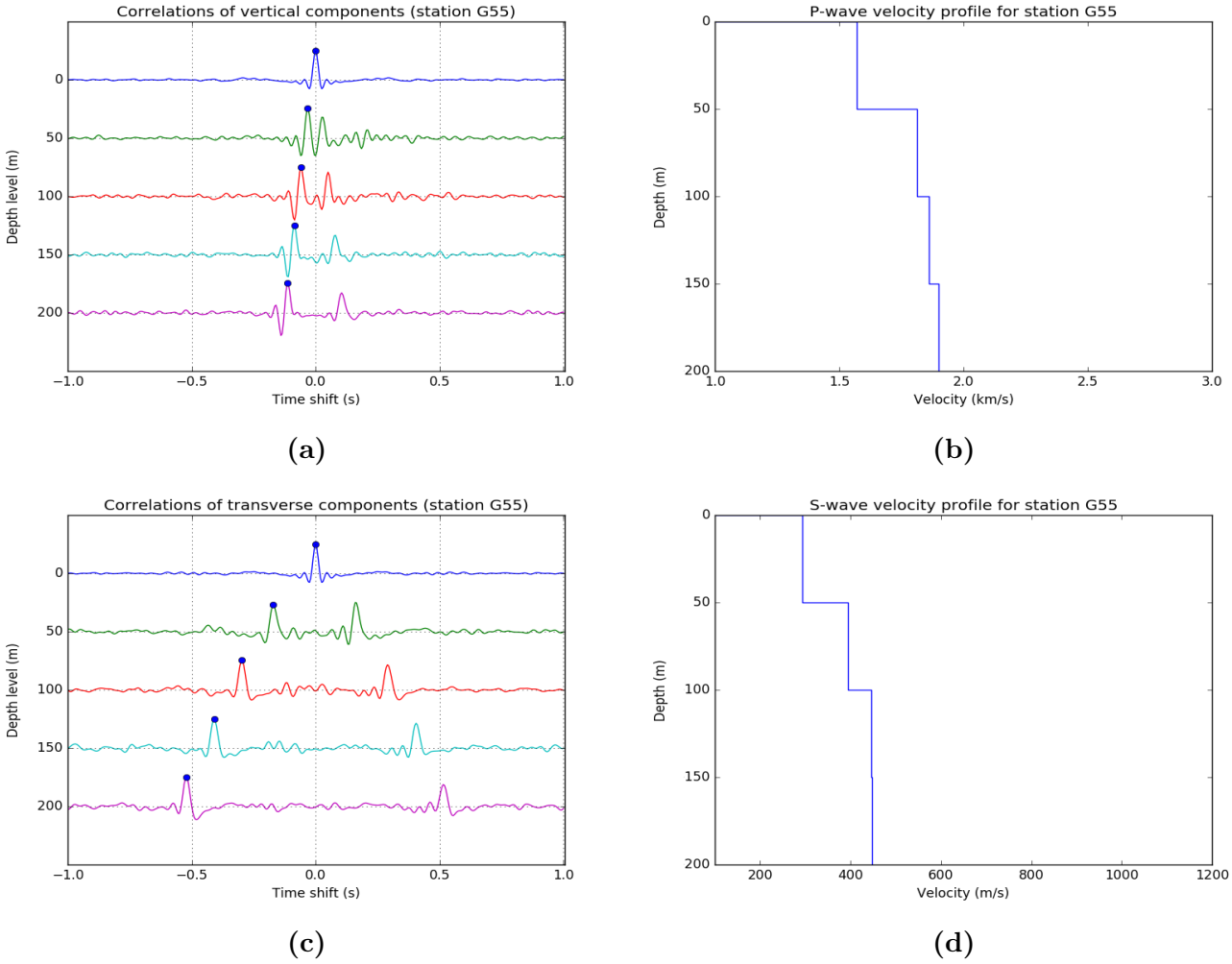

Figure 64: ***(a)*** *Stacked cross-correlations of the vertical components. Blue dot indicates the peak associated with the P-wave.* ***(b)*** *P-wave velocity profile calculated from the picks in figure 64a.* ***(c)*** *Stacked cross-correlations of the transverse components. Blue dot indicates the peak associated with the SH-wave.* ***(d)*** *S-wave velocity profiles calculated from the picks in figure 64c.*

Station G56

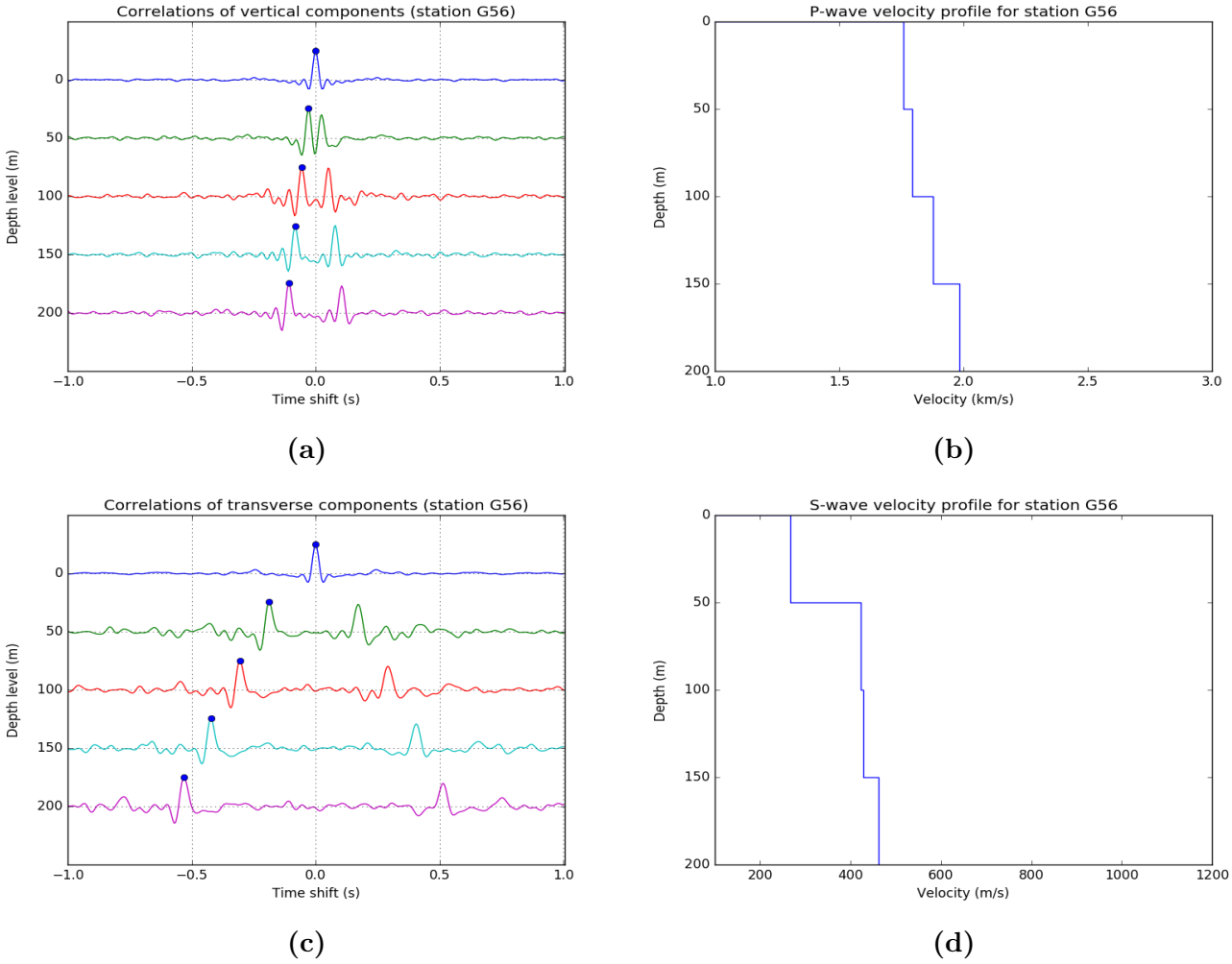

Figure 65: ***(a)*** *Stacked cross-correlations of the vertical components. Blue dot indicates the peak associated with the P-wave.* ***(b)*** *P-wave velocity profile calculated from the picks in figure 65a.* ***(c)*** *Stacked cross-correlations of the transverse components. Blue dot indicates the peak associated with the SH-wave.* ***(d)*** *S-wave velocity profiles calculated from the picks in figure 65c.*

Station G57

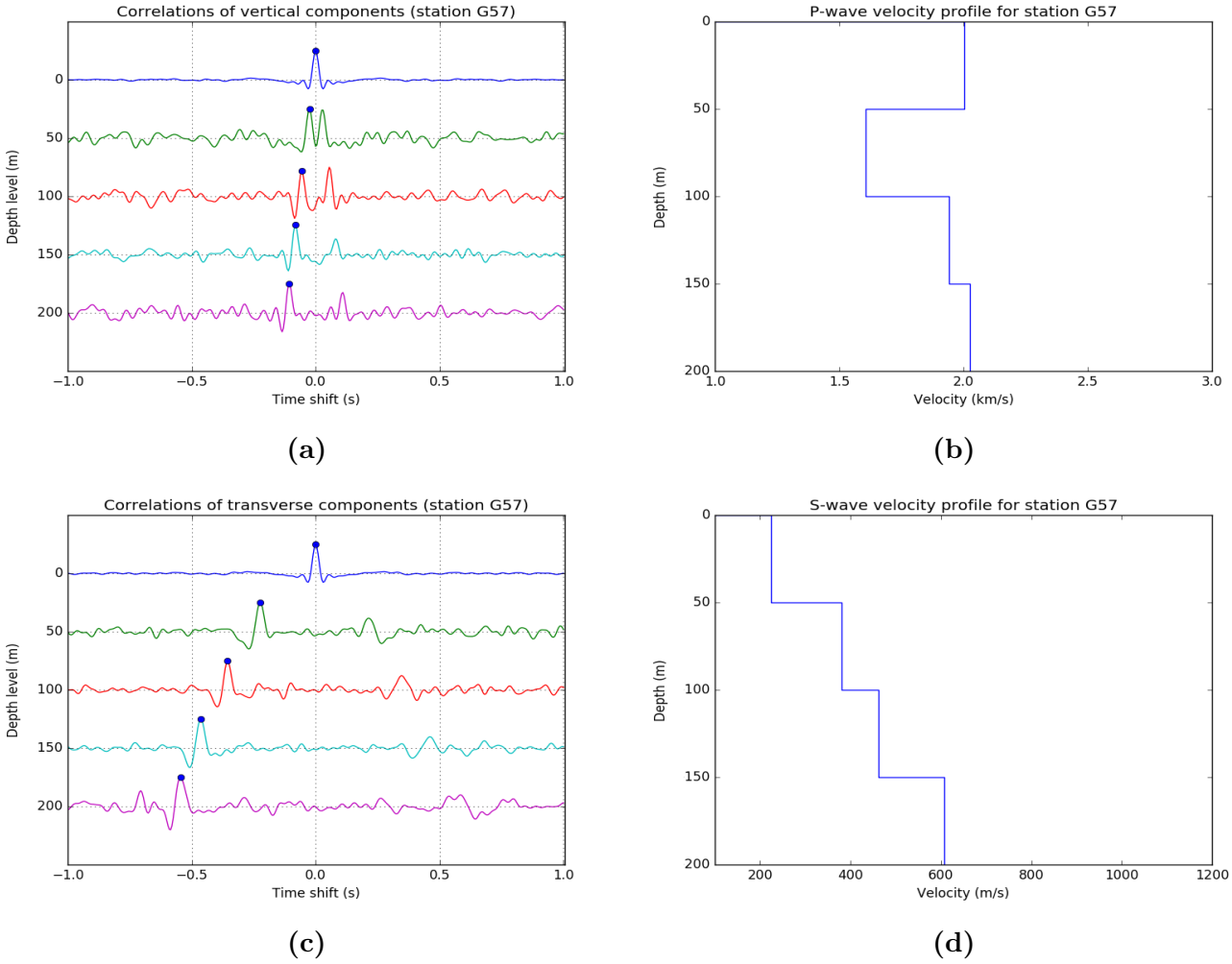

Figure 66: ***(a)*** *Stacked cross-correlations of the vertical components. Blue dot indicates the peak associated with the P-wave.* ***(b)*** *P-wave velocity profile calculated from the picks in figure 66a.* ***(c)*** *Stacked cross-correlations of the transverse components. Blue dot indicates the peak associated with the SH-wave.* ***(d)*** *S-wave velocity profiles calculated from the picks in figure 66c.*

Station G58

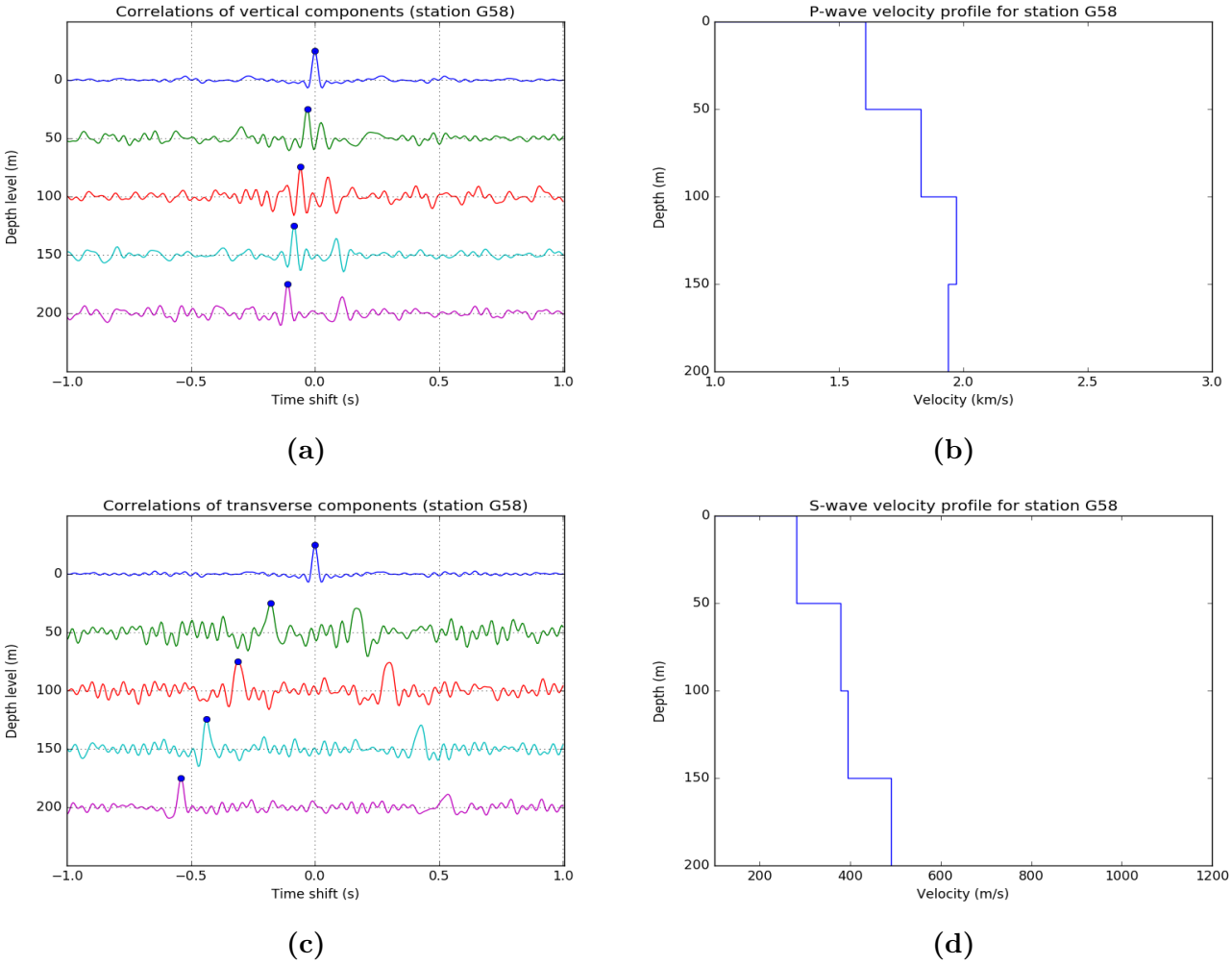

Figure 67: ***(a)*** *Stacked cross-correlations of the vertical components. Blue dot indicates the peak associated with the P-wave.* ***(b)*** *P-wave velocity profile calculated from the picks in figure 67a.* ***(c)*** *Stacked cross-correlations of the transverse components. Blue dot indicates the peak associated with the SH-wave.* ***(d)*** *S-wave velocity profiles calculated from the picks in figure 67c.*

Station G59

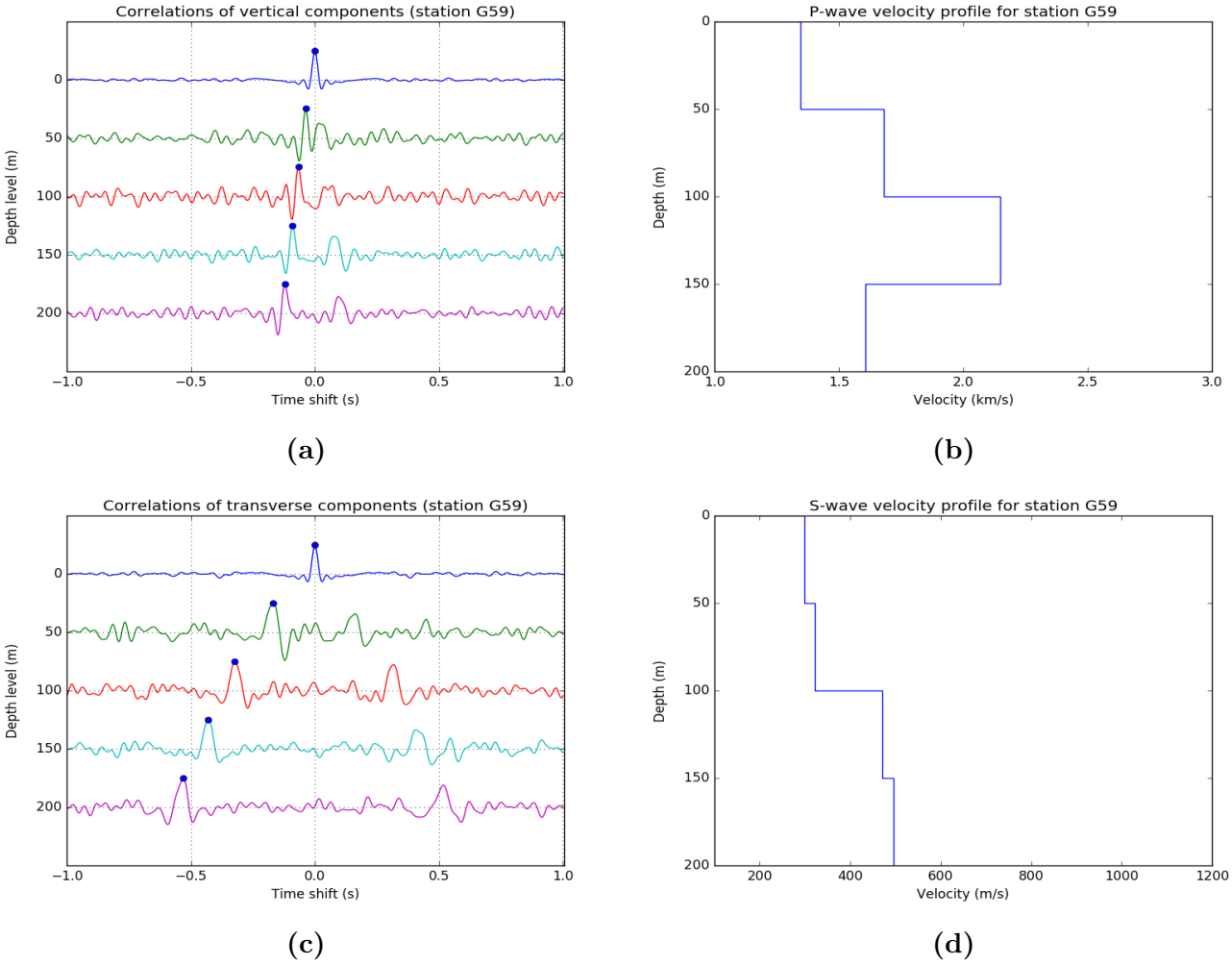

Figure 68: ***(a)*** *Stacked cross-correlations of the vertical components. Blue dot indicates the peak associated with the P-wave.* ***(b)*** *P-wave velocity profile calculated from the picks in figure 68a.* ***(c)*** *Stacked cross-correlations of the transverse components. Blue dot indicates the peak associated with the SH-wave.* ***(d)*** *S-wave velocity profiles calculated from the picks in figure 68c.*

Station G60

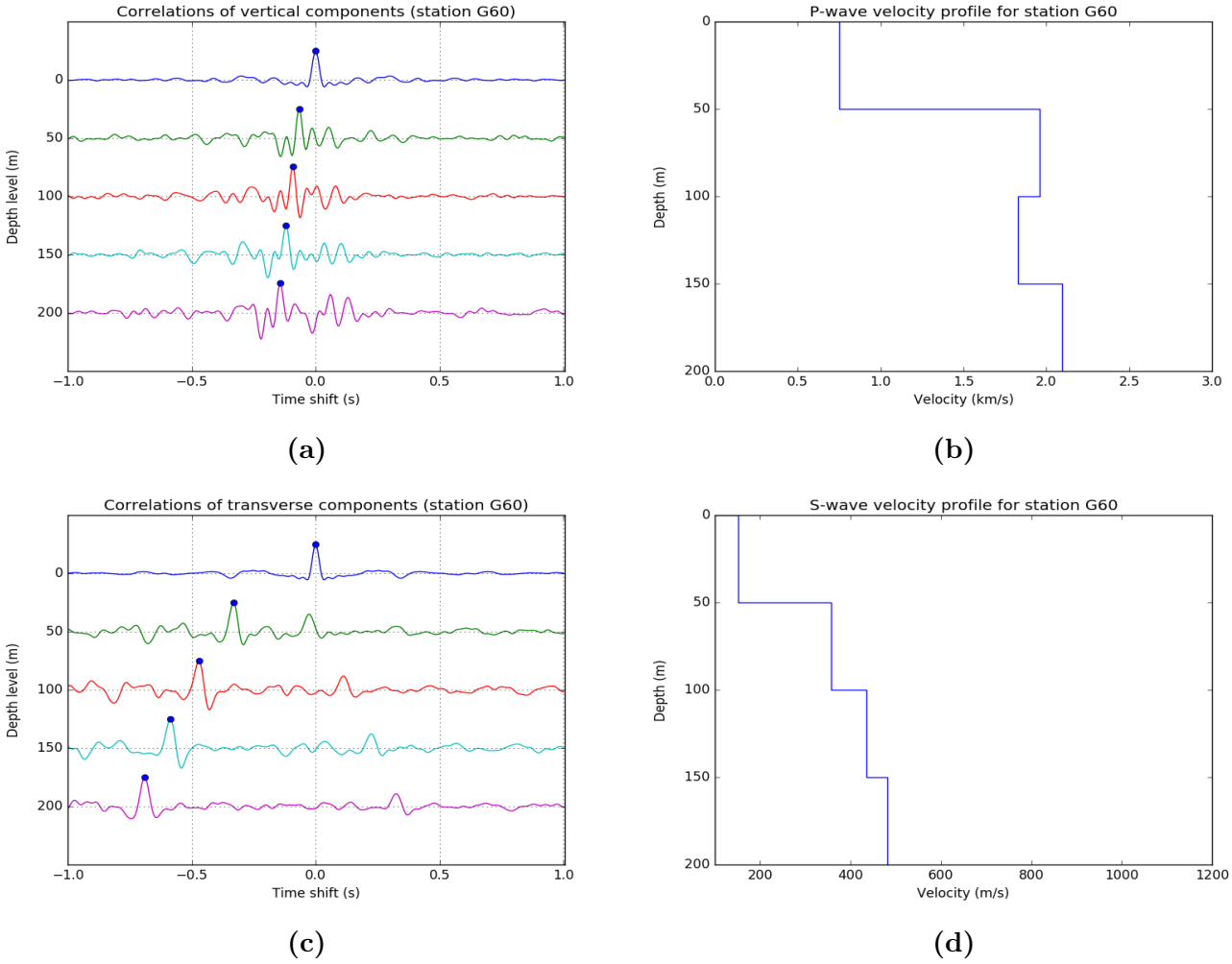

Figure 69: ***(a)*** *Stacked cross-correlations of the vertical components. Blue dot indicates the peak associated with the P-wave.* ***(b)*** *P-wave velocity profile calculated from the picks in figure 69a.* ***(c)*** *Stacked cross-correlations of the transverse components. Blue dot indicates the peak associated with the SH-wave.* ***(d)*** *S-wave velocity profiles calculated from the picks in figure 69c.*

Station G61

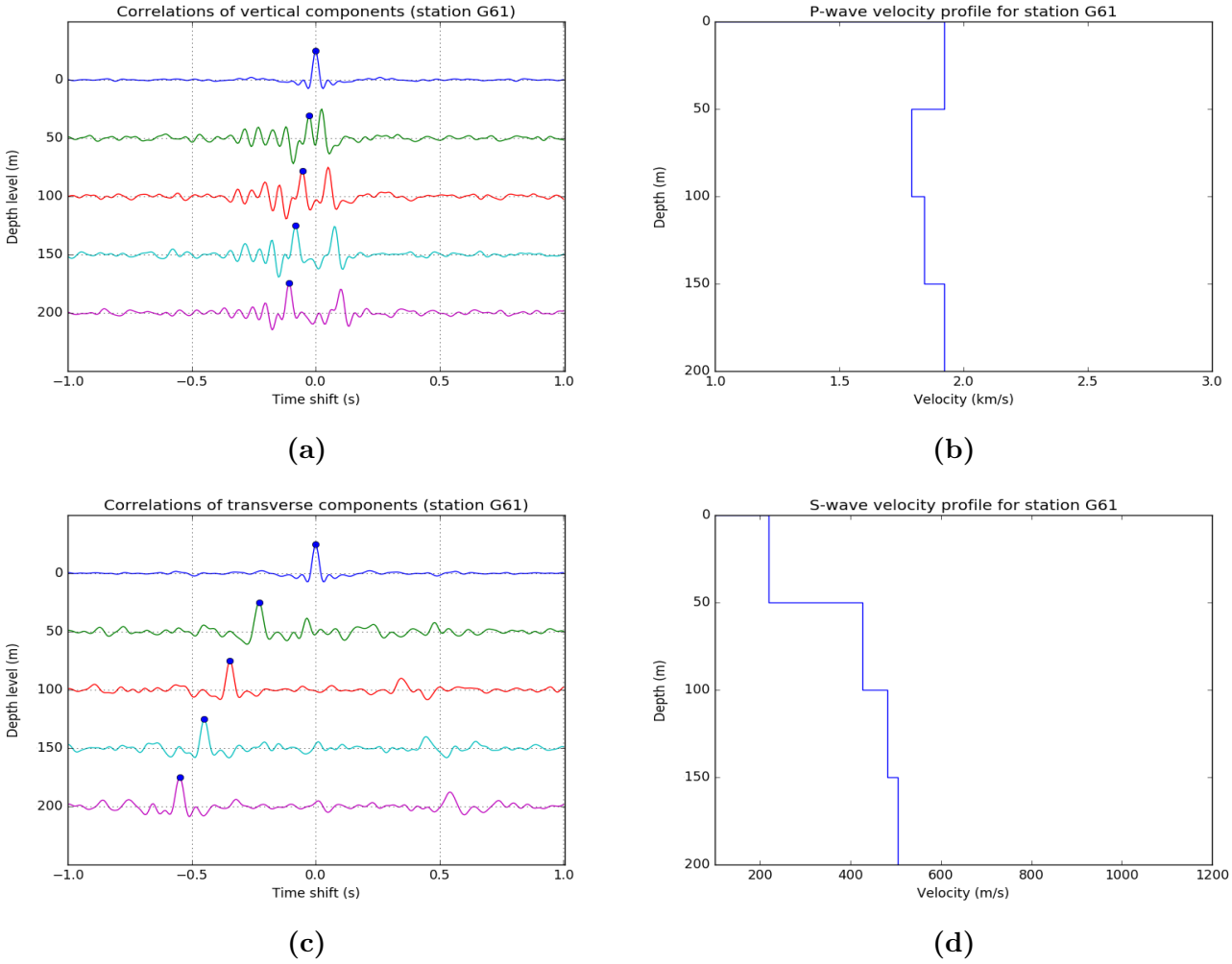

Figure 70: ***(a)*** *Stacked cross-correlations of the vertical components. Blue dot indicates the peak associated with the P-wave.* ***(b)*** *P-wave velocity profile calculated from the picks in figure 70a.* ***(c)*** *Stacked cross-correlations of the transverse components. Blue dot indicates the peak associated with the SH-wave.* ***(d)*** *S-wave velocity profiles calculated from the picks in figure 70c.*

Station G62

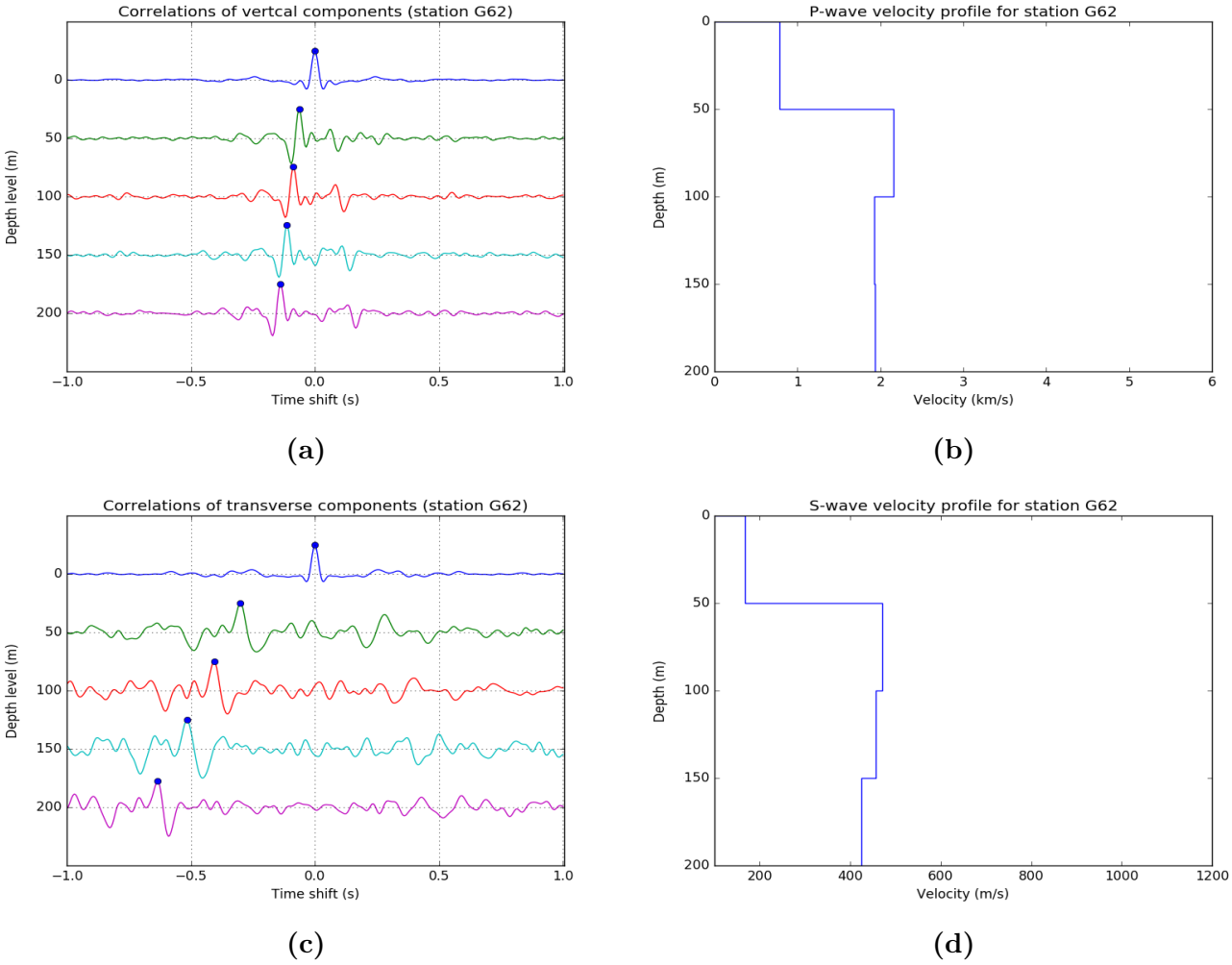

Figure 71: ***(a)*** *Stacked cross-correlations of the vertical components. Blue dot indicates the peak associated with the P-wave.* ***(b)*** *P-wave velocity profile calculated from the picks in figure 71a.* ***(c)*** *Stacked cross-correlations of the transverse components. Blue dot indicates the peak associated with the SH-wave.* ***(d)*** *S-wave velocity profiles calculated from the picks in figure 71c.*

Station G63

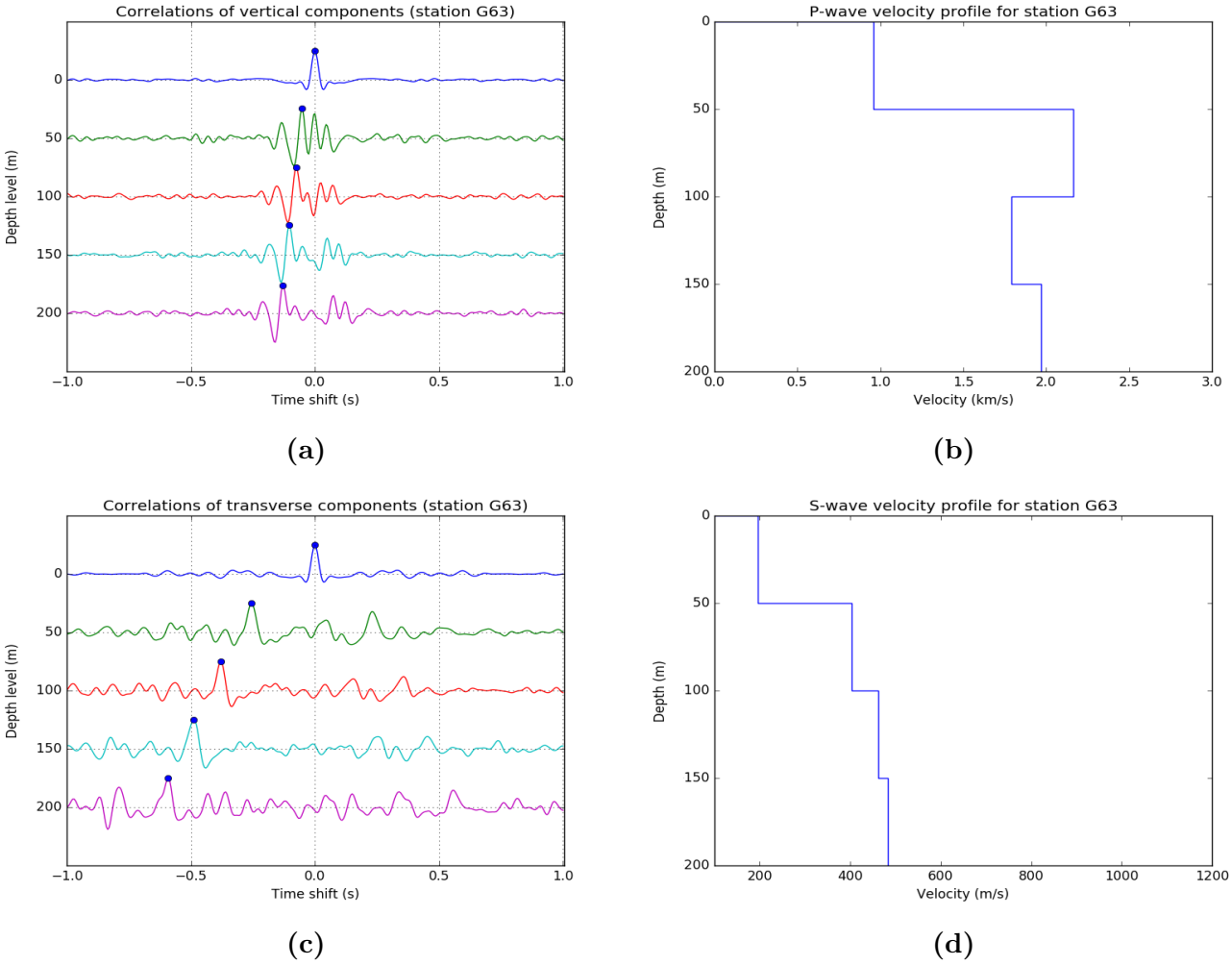

Figure 72: ***(a)*** *Stacked cross-correlations of the vertical components. Blue dot indicates the peak associated with the P-wave.* ***(b)*** *P-wave velocity profile calculated from the picks in figure 72a.* ***(c)*** *Stacked cross-correlations of the transverse components. Blue dot indicates the peak associated with the SH-wave.* ***(d)*** *S-wave velocity profiles calculated from the picks in figure 72c.*

Station G64

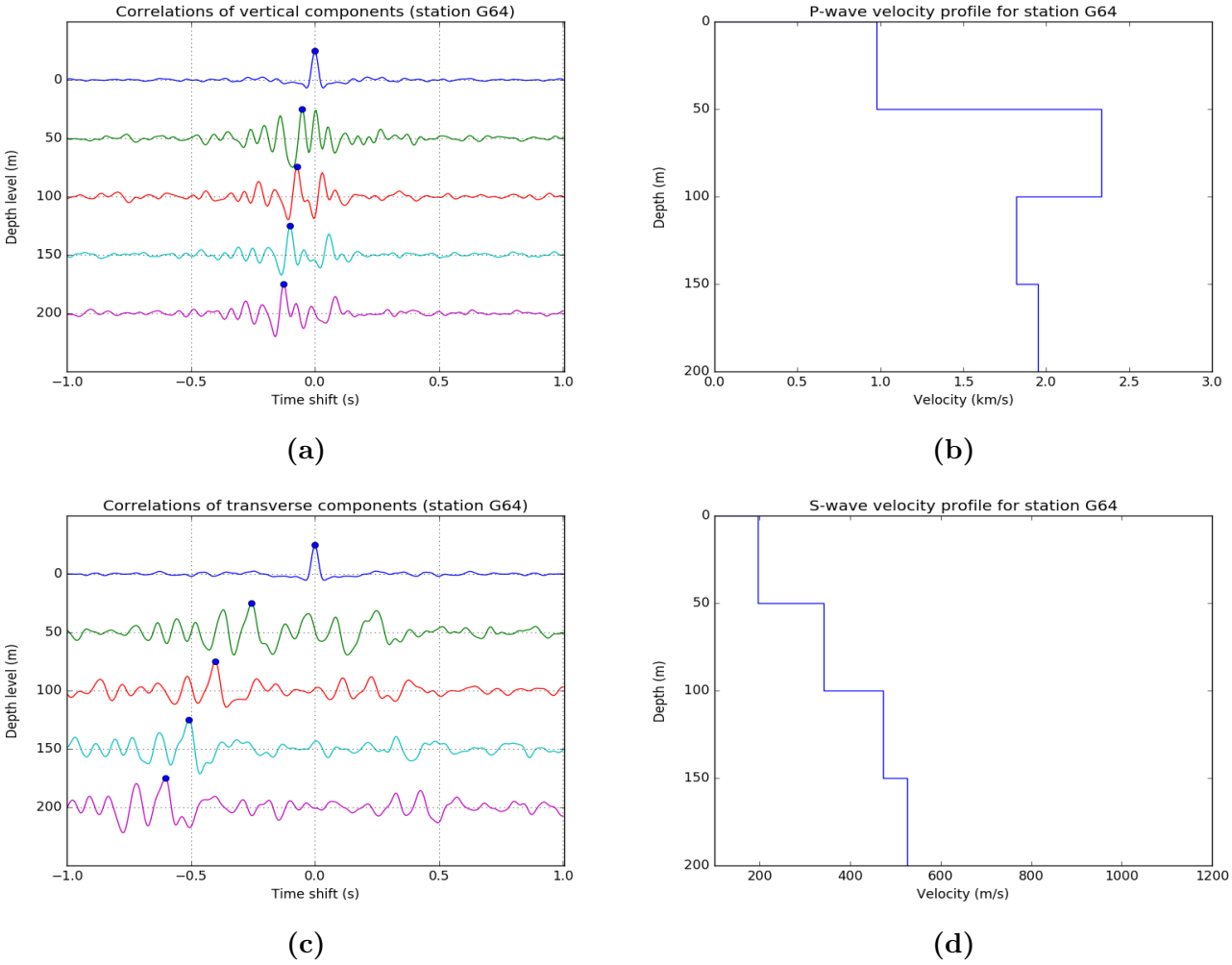

Figure 73: ***(a)*** *Stacked cross-correlations of the vertical components. Blue dot indicates the peak associated with the P-wave.* ***(b)*** *P-wave velocity profile calculated from the picks in figure 73a.* ***(c)*** *Stacked cross-correlations of the transverse components. Blue dot indicates the peak associated with the SH-wave.* ***(d)*** *S-wave velocity profiles calculated from the picks in figure 73c.*

Station G65

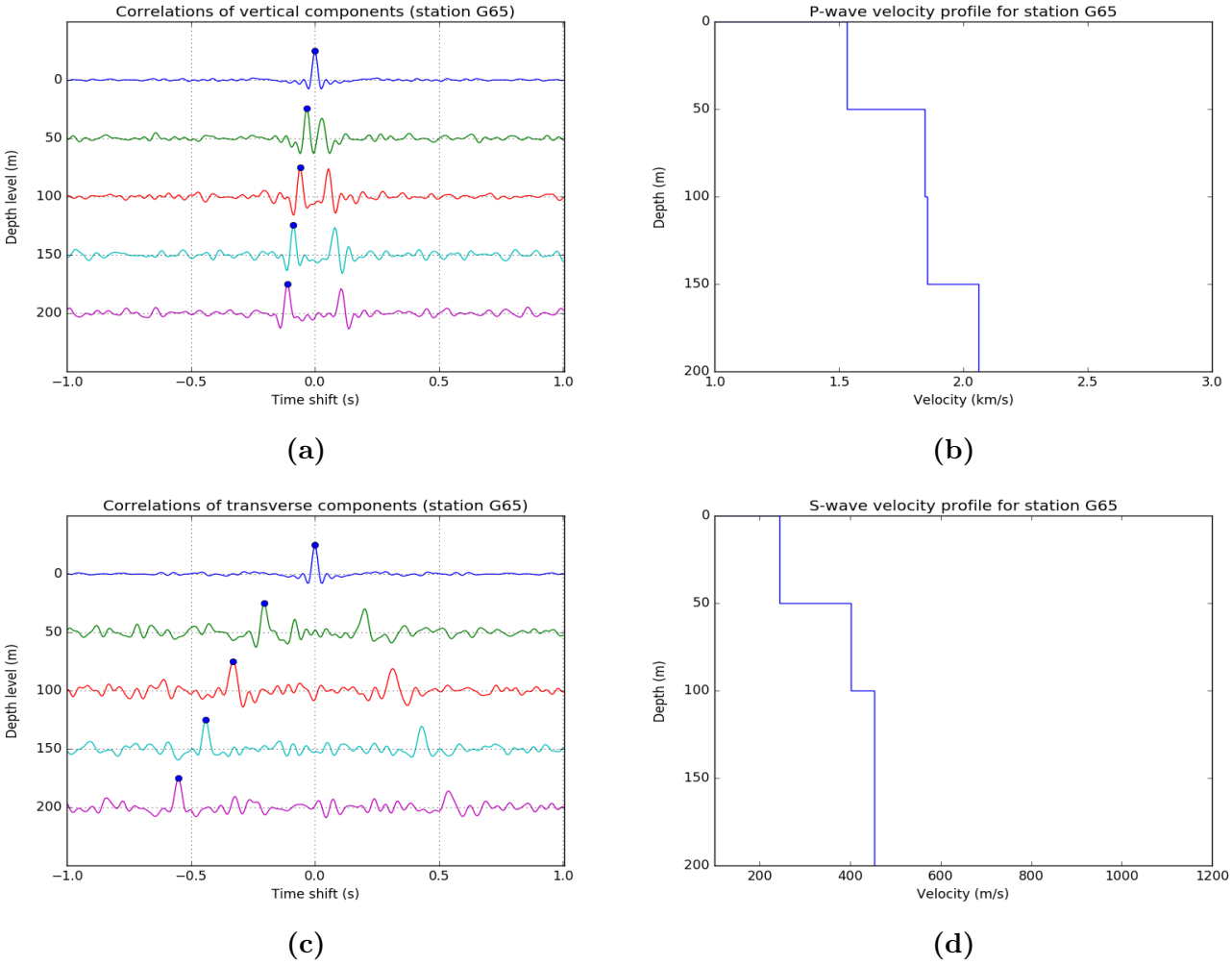

Figure 74: ***(a)*** *Stacked cross-correlations of the vertical components. Blue dot indicates the peak associated with the P-wave.* ***(b)*** *P-wave velocity profile calculated from the picks in figure 74a.* ***(c)*** *Stacked cross-correlations of the transverse components. Blue dot indicates the peak associated with the SH-wave.* ***(d)*** *S-wave velocity profiles calculated from the picks in figure 74c.*

Station G66

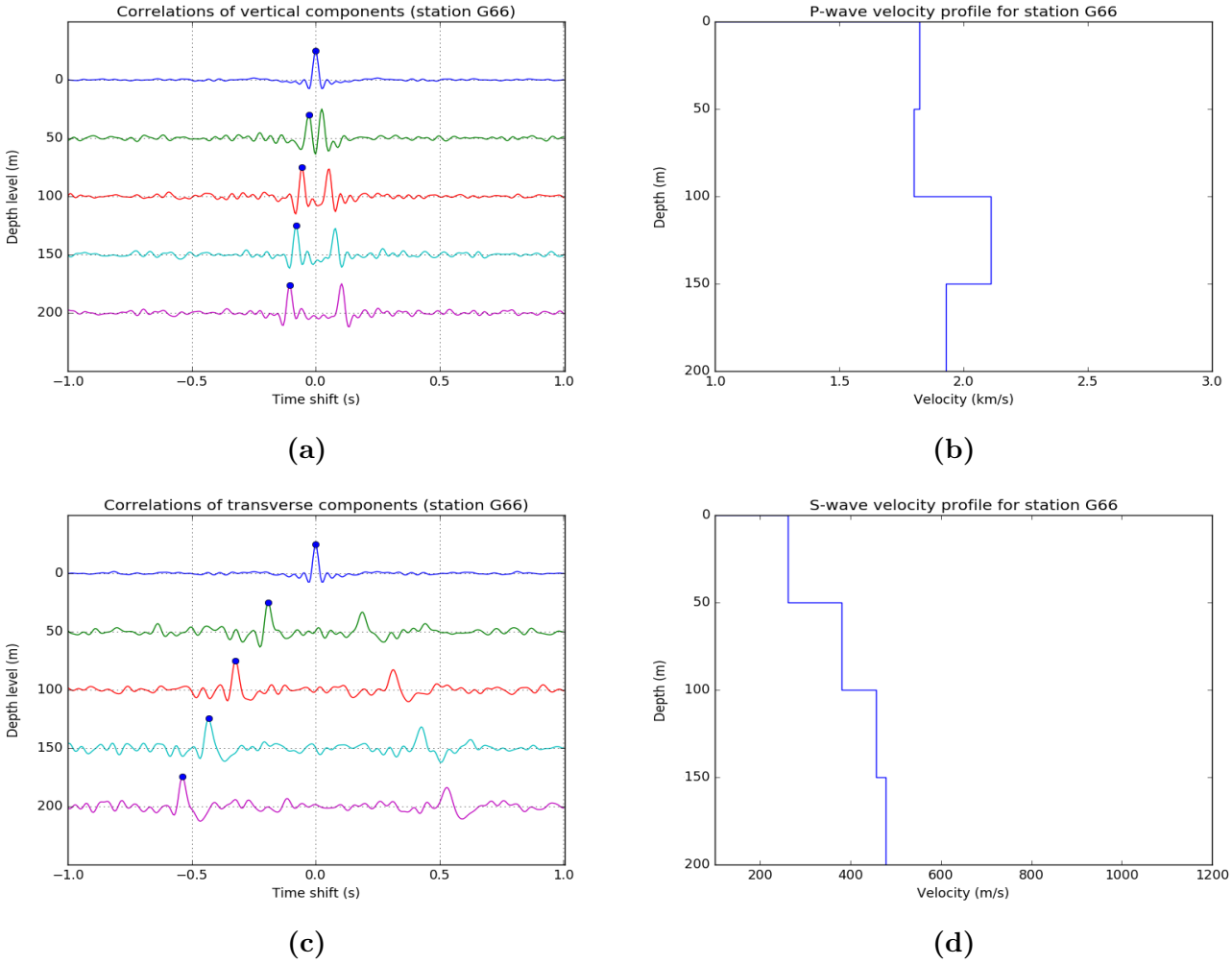

Figure 75: ***(a)*** *Stacked cross-correlations of the vertical components. Blue dot indicates the peak associated with the P-wave.* ***(b)*** *P-wave velocity profile calculated from the picks in figure 75a.* ***(c)*** *Stacked cross-correlations of the transverse components. Blue dot indicates the peak associated with the SH-wave.* ***(d)*** *S-wave velocity profiles calculated from the picks in figure 75c.*

Station G67

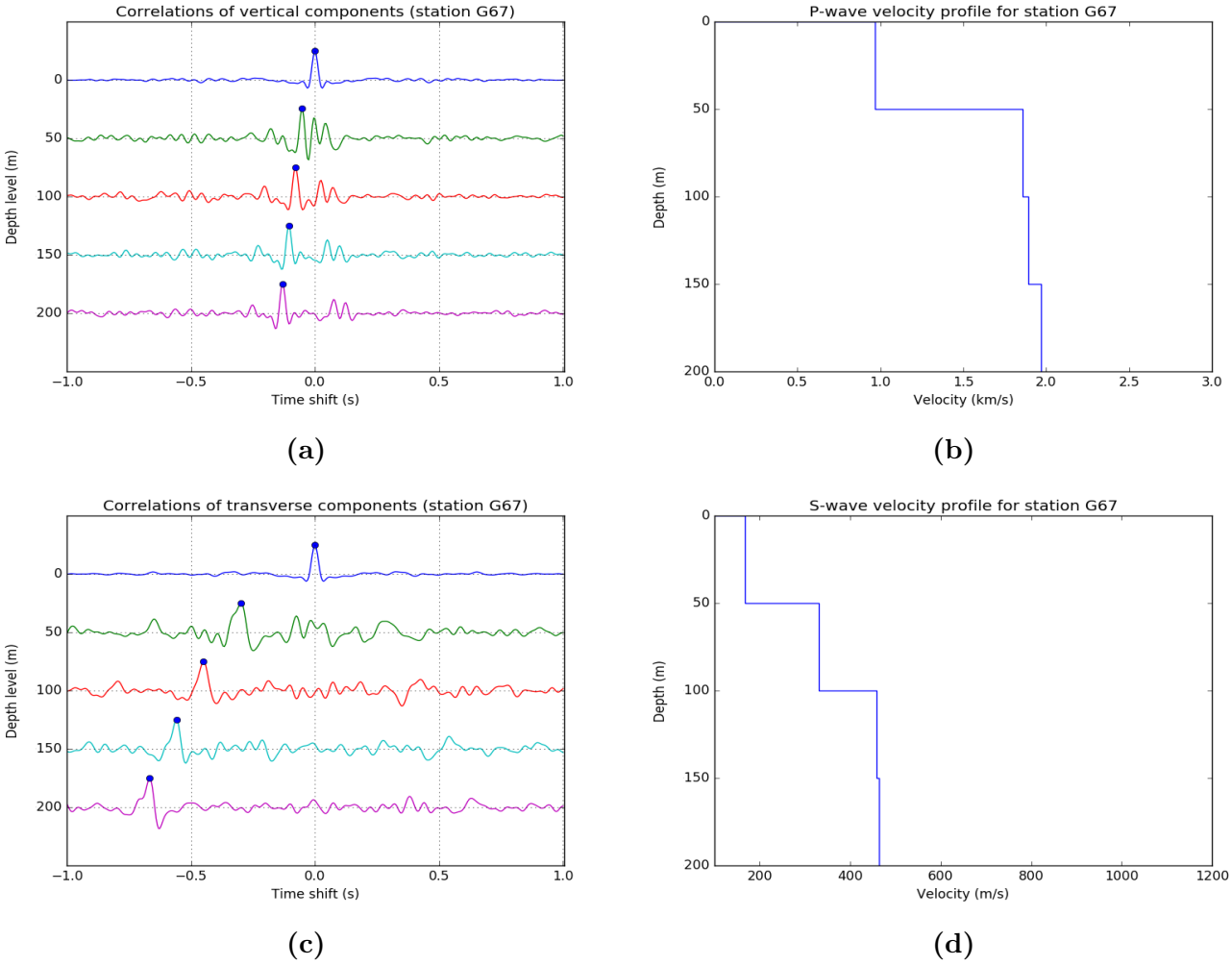

Figure 76: ***(a)*** *Stacked cross-correlations of the vertical components. Blue dot indicates the peak associated with the P-wave.* ***(b)*** *P-wave velocity profile calculated from the picks in figure 76a.* ***(c)*** *Stacked cross-correlations of the transverse components. Blue dot indicates the peak associated with the SH-wave.* ***(d)*** *S-wave velocity profiles calculated from the picks in figure 76c.*

Station G68

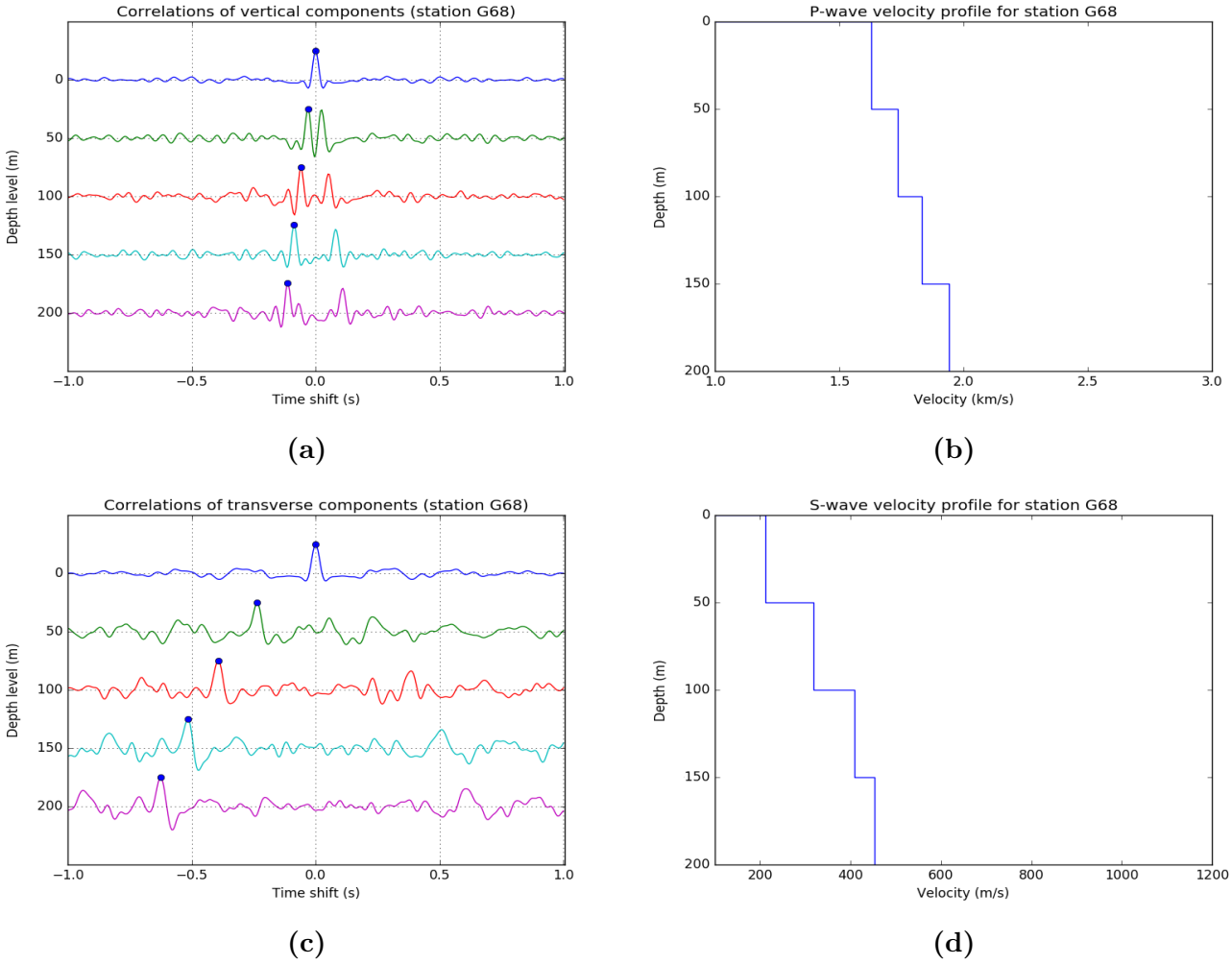

Figure 77: ***(a)*** *Stacked cross-correlations of the vertical components. Blue dot indicates the peak associated with the P-wave.* ***(b)*** *P-wave velocity profile calculated from the picks in figure 77a.* ***(c)*** *Stacked cross-correlations of the transverse components. Blue dot indicates the peak associated with the SH-wave.* ***(d)*** *S-wave velocity profiles calculated from the picks in figure 77c.*

Station G69

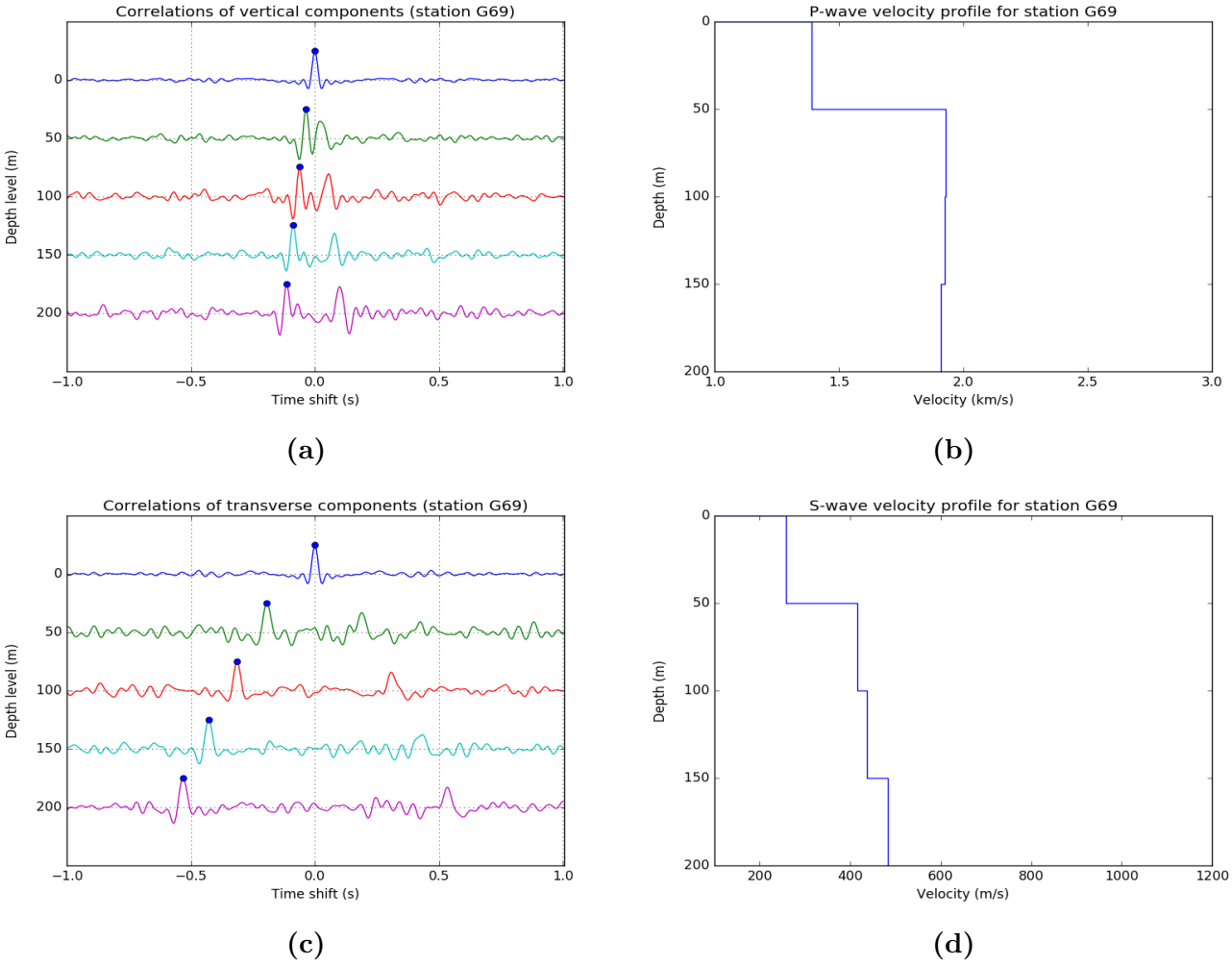

Figure 78: ***(a)*** *Stacked cross-correlations of the vertical components. Blue dot indicates the peak associated with the P-wave.* ***(b)*** *P-wave velocity profile calculated from the picks in figure 78a.* ***(c)*** *Stacked cross-correlations of the transverse components. Blue dot indicates the peak associated with the SH-wave.* ***(d)*** *S-wave velocity profiles calculated from the picks in figure 78c.*

B Geophone orientations

Station G01

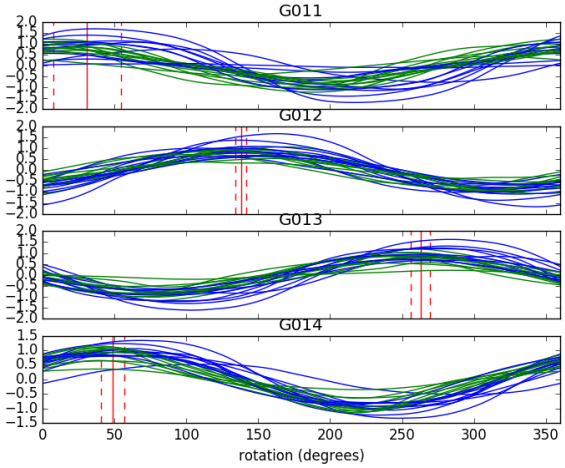

Figure 79: *Orientation curves for station G01. The lines indicate the maximum cross-correlation coefficient (with the surface accelerometer) as a function of counterclockwise rotation of the geophone. Blue lines are for the radial components, green lines for the transverse components. The vertical red lines indicate the average rotation +/- one standard deviation.*

Code	Channel 1	Channel 2	Data used	Standard deviation
G011	120.9°	30.9°	18/22	23.5°
G012	228.1°	138.1°	14/22	3.8°
G013	352.8°	262.8°	15/22	6.7°
G014	138.6°	48.6°	20/22	8.1°

Table 6: *This table shows the channel orientations of the geophones in station in degrees clockwise from north. The standard deviation refers to the orientations calculated from the individual events used. Data used shows how many traces were used for the final calculation and how many were initially found.*

Station G02

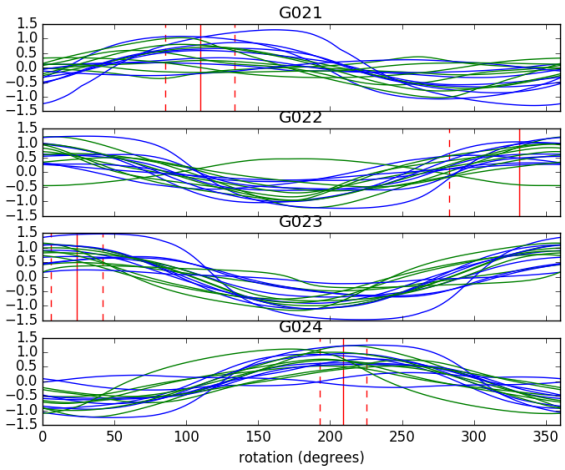

Figure 80: *Orientation curves for station G02. The lines indicate the maximum cross-correlation coefficient (with the surface accelerometer) as a function of counterclockwise rotation of the geophone. Blue lines are for the radial components, green lines for the transverse components. The vertical red lines indicate the average rotation +/- one standard deviation.*

Code	Channel 1	Channel 2	Data used	Standard deviation
G021	197.4°	107.4°	17/22	31.1°
G022	39.5°	309.5°	14/22	84.0°
G023	115.3°	25.3°	17/22	22.4°
G024	294.7°	204.7°	18/22	18.1°

Table 7: *This table shows the channel orientations of the geophones in station in degrees clockwise from north. The standard deviation refers to the orientations calculated from the individual events used. Data used shows how many traces were used for the final calculation and how many were initially found.*

NOTE: The standard deviations for this station are very large due to poor data quality. This station is placed in the Eemshaven harbour, where a lot of noise sources (traffic, ships, waves, windmills, industry) are located very close to the borehole (figure 2).

Station G03

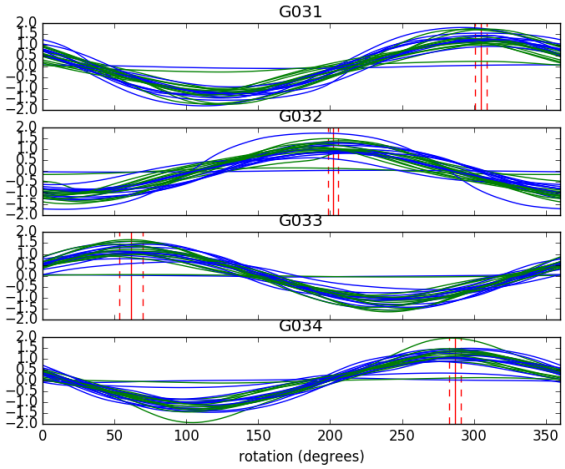

Figure 81: *Orientation curves for station G03. The lines indicate the maximum cross-correlation coefficient (with the surface accelerometer) as a function of counterclockwise rotation of the geophone. Blue lines are for the radial components, green lines for the transverse components. The vertical red lines indicate the average rotation +/- one standard deviation.*

Code	Channel 1	Channel 2	Data used	Standard deviation
G031	34.8°	304.8°	22/26	4.0°
G032	292.0°	202.0°	17/26	3.8°
G033	151.7°	61.7°	25/26	8.2°
G034	16.8°	286.8°	24/26	4.3°

Table 8: *This table shows the channel orientations of the geophones in station in degrees clockwise from north. The standard deviation refers to the orientations calculated from the individual events used. Data used shows how many traces were used for the final calculation and how many were initially found.*

Station G04

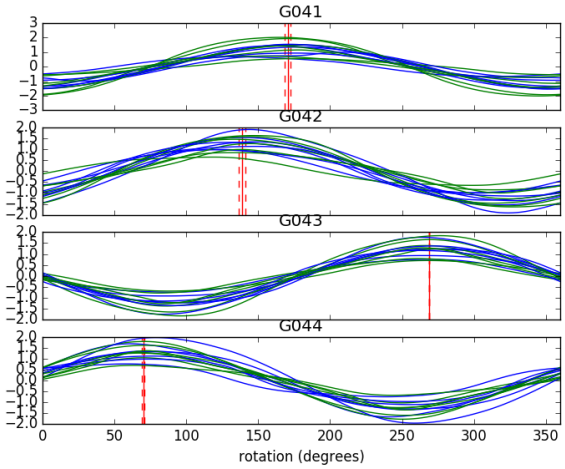

Figure 82: *Orientation curves for station G04. The lines indicate the maximum cross-correlation coefficient (with the surface accelerometer) as a function of counterclockwise rotation of the geophone. Blue lines are for the radial components, green lines for the transverse components. The vertical red lines indicate the average rotation +/- one standard deviation.*

Code	Channel 1	Channel 2	Data used	Standard deviation
G041	260.6°	170.6°	11/14	2.1°
G042	229.0°	139.0°	11/14	2.3°
G043	358.6°	268.6°	10/14	0.0°
G044	160.0°	70.0°	10/14	1.0°

Table 9: *This table shows the channel orientations of the geophones in station in degrees clockwise from north. The standard deviation refers to the orientations calculated from the individual events used. Data used shows how many traces were used for the final calculation and how many were initially found.*

Station G06

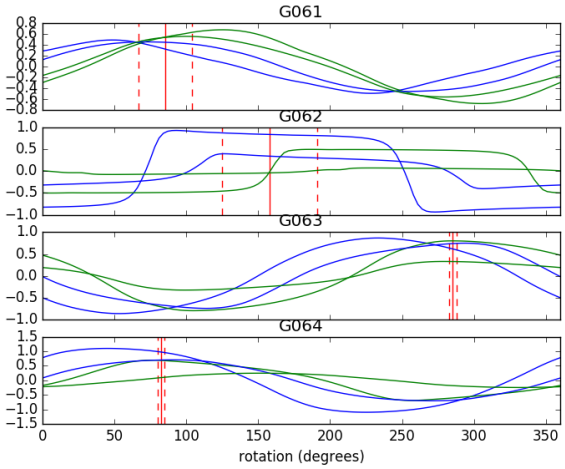

Figure 83: *Orientation curves for station G06. The lines indicate the maximum cross-correlation coefficient (with the surface accelerometer) as a function of counterclockwise rotation of the geophone. Blue lines are for the radial components, green lines for the transverse components. The vertical red lines indicate the average rotation +/- one standard deviation.*

Code	Channel 1	Channel 2	Data used	Standard deviation
G061	175.5°	85.5°	2/4	18.5°
G062	247.9°	157.9°	2/4	33.1°
G063	15.3°	285.3°	3/4	2.6°
G064	172.5°	82.5°	2/4	2.5°

Table 10: *This table shows the channel orientations of the geophones in station in degrees clockwise from north. The standard deviation refers to the orientations calculated from the individual events used. Data used shows how many traces were used for the final calculation and how many were initially found.*

Station G07

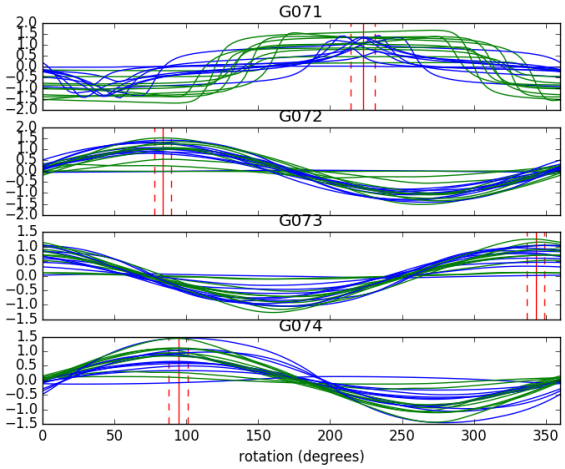

Figure 84: *Orientation curves for station G07. The lines indicate the maximum cross-correlation coefficient (with the surface accelerometer) as a function of counterclockwise rotation of the geophone. Blue lines are for the radial components, green lines for the transverse components. The vertical red lines indicate the average rotation +/- one standard deviation.*

Code	Channel 1	Channel 2	Data used	Standard deviation
G071	312.8°	222.8°	13/20	8.3°
G072	173.4°	83.4°	17/20	5.8°
G073	73.0°	343.0°	19/20	6.0°
G074	184.4°	94.4°	17/20	6.9°

Table 11: *This table shows the channel orientations of the geophones in station in degrees clockwise from north. The standard deviation refers to the orientations calculated from the individual events used. Data used shows how many traces were used for the final calculation and how many were initially found.*

Station G08

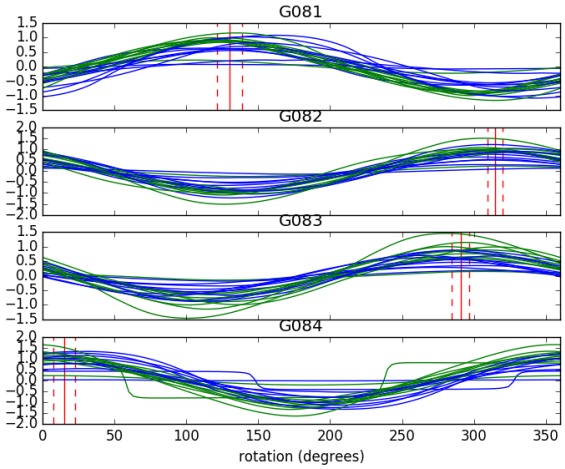

Figure 85: *Orientation curves for station G08. The lines indicate the maximum cross-correlation coefficient (with the surface accelerometer) as a function of counterclockwise rotation of the geophone. Blue lines are for the radial components, green lines for the transverse components. The vertical red lines indicate the average rotation +/- one standard deviation.*

Code	Channel 1	Channel 2	Data used	Standard deviation
G081	220.1°	130.1°	16/20	8.5°
G082	44.6°	314.6°	19/20	5.0°
G083	20.6°	290.6°	14/20	5.9°
G084	104.2°	14.2°	14/20	8.3°

Table 12: *This table shows the channel orientations of the geophones in station in degrees clockwise from north. The standard deviation refers to the orientations calculated from the individual events used. Data used shows how many traces were used for the final calculation and how many were initially found.*

Station G09

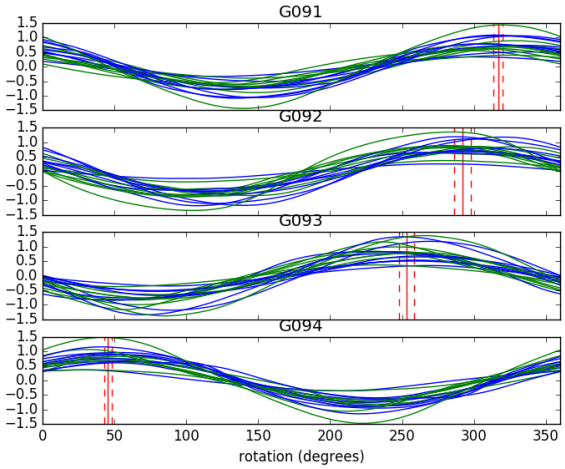

Figure 86: *Orientation curves for station G09. The lines indicate the maximum cross-correlation coefficient (with the surface accelerometer) as a function of counterclockwise rotation of the geophone. Blue lines are for the radial components, green lines for the transverse components. The vertical red lines indicate the average rotation +/- one standard deviation.*

Code	Channel 1	Channel 2	Data used	Standard deviation
G091	46.8°	316.8°	13/18	3.3°
G092	22.1°	292.1°	13/18	6.0°
G093	343.1°	253.1°	13/18	5.2°
G094	135.3°	45.3°	13/18	2.6°

Table 13: *This table shows the channel orientations of the geophones in station in degrees clockwise from north. The standard deviation refers to the orientations calculated from the individual events used. Data used shows how many traces were used for the final calculation and how many were initially found.*

Station G10

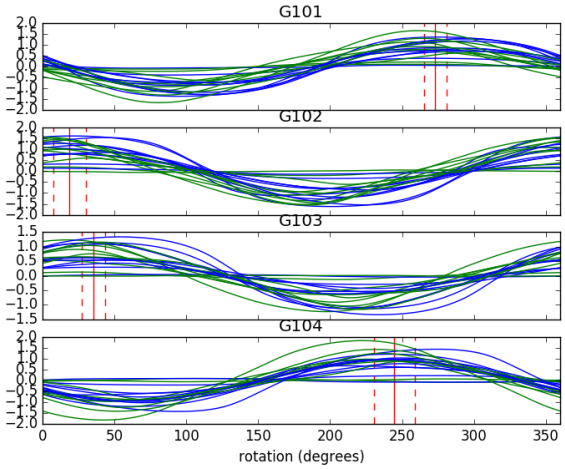

Figure 87: *Orientation curves for station G10. The lines indicate the maximum cross-correlation coefficient (with the surface accelerometer) as a function of counterclockwise rotation of the geophone. Blue lines are for the radial components, green lines for the transverse components. The vertical red lines indicate the average rotation +/- one standard deviation.*

Code	Channel 1	Channel 2	Data used	Standard deviation
G101	3.1°	273.1°	12/20	8.0°
G102	108.8°	18.8°	15/20	11.1°
G103	125.3°	35.3°	17/20	8.1°
G104	334.7°	244.7°	18/20	14.1°

Table 14: *This table shows the channel orientations of the geophones in station in degrees clockwise from north. The standard deviation refers to the orientations calculated from the individual events used. Data used shows how many traces were used for the final calculation and how many were initially found.*

Station G11

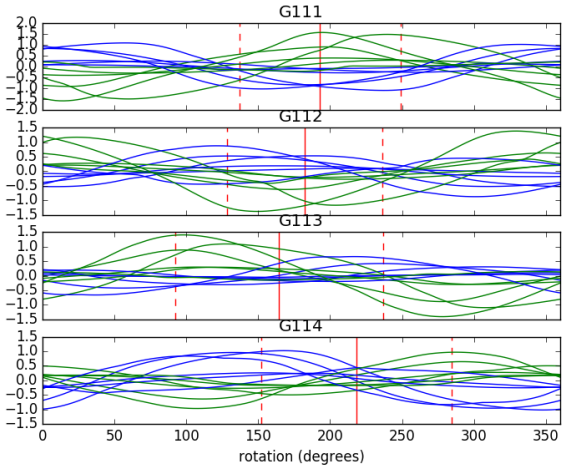

Figure 88: *Orientation curves for station G11. The lines indicate the maximum cross-correlation coefficient (with the surface accelerometer) as a function of counterclockwise rotation of the geophone. Blue lines are for the radial components, green lines for the transverse components. The vertical red lines indicate the average rotation +/- one standard deviation.*

Code	Channel 1	Channel 2	Data used	Standard deviation
G111	283.0°	193.0°	6/12	56.0°
G112	92.3°	2.3°	6/12	54.3°
G113	254.6°	164.6°	8/12	72.4°
G114	308.3°	218.3°	8/12	66.0°

Table 15: *This table shows the channel orientations of the geophones in station in degrees clockwise from north. The standard deviation refers to the orientations calculated from the individual events used. Data used shows how many traces were used for the final calculation and how many were initially found.*

NOTE: From the stacked cross-correlations of the transverse component in the seismic interferometry method, it appeared that the polarity of G112 was reversed. Therefore 180° were added manually to the orientation of this geophone.

Station G13

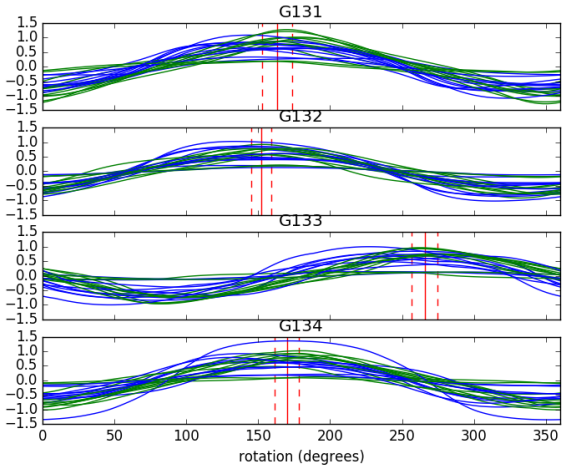

Figure 89: *Orientation curves for station G13. The lines indicate the maximum cross-correlation coefficient (with the surface accelerometer) as a function of counterclockwise rotation of the geophone. Blue lines are for the radial components, green lines for the transverse components. The vertical red lines indicate the average rotation +/- one standard deviation.*

Code	Channel 1	Channel 2	Data used	Standard deviation
G131	252.9°	162.9°	17/22	10.5°
G132	242.2°	152.2°	16/22	7.2°
G133	355.7°	265.7°	15/22	9.1°
G134	260.0°	170.0°	15/22	8.3°

Table 16: *This table shows the channel orientations of the geophones in station in degrees clockwise from north. The standard deviation refers to the orientations calculated from the individual events used. Data used shows how many traces were used for the final calculation and how many were initially found.*

Station G14

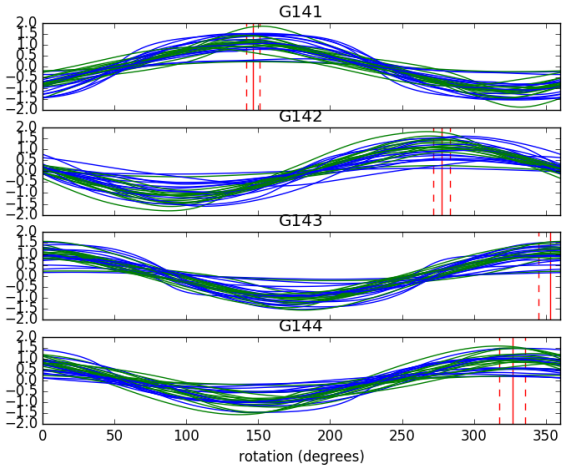

Figure 90: *Orientation curves for station G14. The lines indicate the maximum cross-correlation coefficient (with the surface accelerometer) as a function of counterclockwise rotation of the geophone. Blue lines are for the radial components, green lines for the transverse components. The vertical red lines indicate the average rotation +/- one standard deviation.*

Code	Channel 1	Channel 2	Data used	Standard deviation
G141	236.5°	146.5°	27/30	4.7°
G142	7.6°	277.6°	28/30	5.6°
G143	83.0°	353.0°	17/30	9.0°
G144	56.6°	326.6°	29/30	8.9°

Table 17: *This table shows the channel orientations of the geophones in station in degrees clockwise from north. The standard deviation refers to the orientations calculated from the individual events used. Data used shows how many traces were used for the final calculation and how many were initially found.*

Station G16

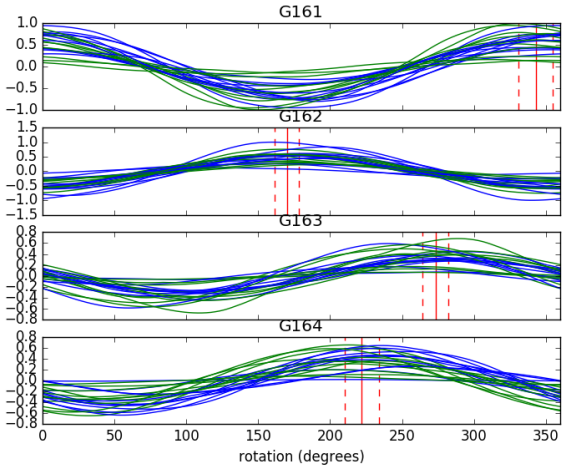

Figure 91: *Orientation curves for station G16. The lines indicate the maximum cross-correlation coefficient (with the surface accelerometer) as a function of counterclockwise rotation of the geophone. Blue lines are for the radial components, green lines for the transverse components. The vertical red lines indicate the average rotation +/- one standard deviation.*

Code	Channel 1	Channel 2	Data used	Standard deviation
G161	72.9°	342.9°	18/22	11.7°
G162	259.9°	169.9°	19/22	8.4°
G163	183.2°	93.2°	14/22	8.8°
G164	312.0°	222.0°	17/22	11.8°

Table 18: *This table shows the channel orientations of the geophones in station in degrees clockwise from north. The standard deviation refers to the orientations calculated from the individual events used. Data used shows how many traces were used for the final calculation and how many were initially found.*

NOTE: From the stacked cross-correlations of the transverse component in the seismic interferometry method, it appeared that the polarity of G163 was reversed. Therefore 180° were added manually to the orientation of this geophone.

Station G17

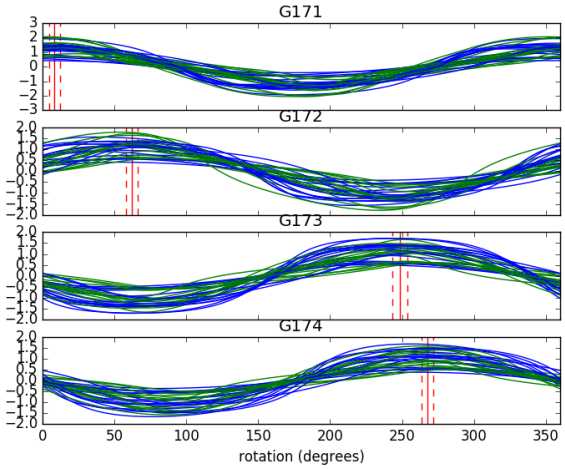

Figure 92: *Orientation curves for station G17. The lines indicate the maximum cross-correlation coefficient (with the surface accelerometer) as a function of counterclockwise rotation of the geophone. Blue lines are for the radial components, green lines for the transverse components. The vertical red lines indicate the average rotation +/- one standard deviation.*

Code	Channel 1	Channel 2	Data used	Standard deviation
G171	98.3°	8.3°	19/32	3.7°
G172	152.1°	62.1°	26/32	4.3°
G173	338.5°	248.5°	23/32	5.0°
G174	357.5°	267.5°	24/32	4.2°

Table 19: *This table shows the channel orientations of the geophones in station in degrees clockwise from north. The standard deviation refers to the orientations calculated from the individual events used. Data used shows how many traces were used for the final calculation and how many were initially found.*

Station G18

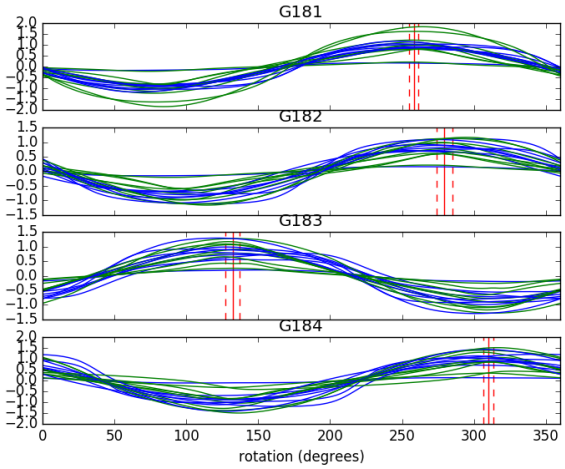

Figure 93: *Orientation curves for station G18. The lines indicate the maximum cross-correlation coefficient (with the surface accelerometer) as a function of counterclockwise rotation of the geophone. Blue lines are for the radial components, green lines for the transverse components. The vertical red lines indicate the average rotation +/- one standard deviation.*

Code	Channel 1	Channel 2	Data used	Standard deviation
G181	348.2°	258.2°	15/18	3.3°
G182	9.4°	279.4°	14/18	5.4°
G183	222.2°	132.2°	15/18	4.9°
G184	40.0°	310.0°	13/18	3.4°

Table 20: *This table shows the channel orientations of the geophones in station in degrees clockwise from north. The standard deviation refers to the orientations calculated from the individual events used. Data used shows how many traces were used for the final calculation and how many were initially found.*

Station G19

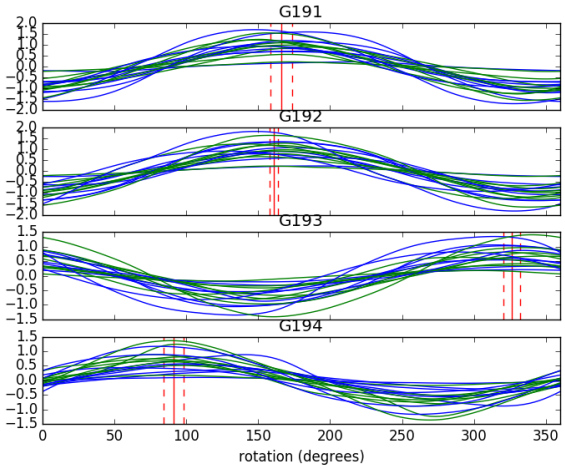

Figure 94: *Orientation curves for station G19. The lines indicate the maximum cross-correlation coefficient (with the surface accelerometer) as a function of counterclockwise rotation of the geophone. Blue lines are for the radial components, green lines for the transverse components. The vertical red lines indicate the average rotation +/- one standard deviation.*

Code	Channel 1	Channel 2	Data used	Standard deviation
G191	256.1°	166.1°	16/18	7.5°
G192	250.8°	160.8°	13/18	3.1°
G193	56.4°	326.4°	13/18	5.8°
G194	181.2°	91.2°	14/18	6.7°

Table 21: *This table shows the channel orientations of the geophones in station in degrees clockwise from north. The standard deviation refers to the orientations calculated from the individual events used. Data used shows how many traces were used for the final calculation and how many were initially found.*

Station G20

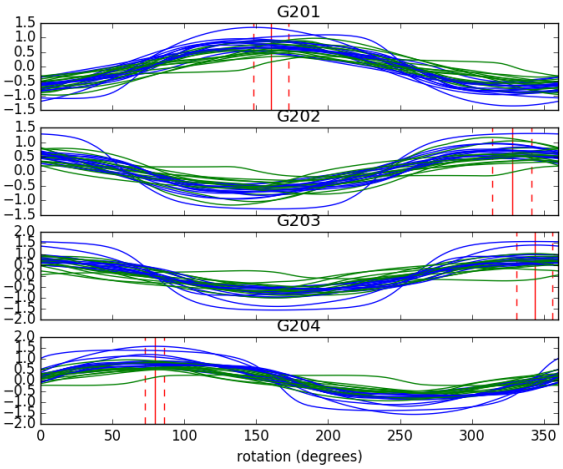

Figure 95: *Orientation curves for station G20. The lines indicate the maximum cross-correlation coefficient (with the surface accelerometer) as a function of counterclockwise rotation of the geophone. Blue lines are for the radial components, green lines for the transverse components. The vertical red lines indicate the average rotation +/- one standard deviation.*

Code	Channel 1	Channel 2	Data used	Standard deviation
G201	250.3°	160.3°	18/28	12.1°
G202	56.7°	326.7°	24/28	12.7°
G203	63.5°	333.5°	22/28	44.8°
G204	169.3°	79.3°	22/28	6.6°

Table 22: *This table shows the channel orientations of the geophones in station in degrees clockwise from north. The standard deviation refers to the orientations calculated from the individual events used. Data used shows how many traces were used for the final calculation and how many were initially found.*

Station G21

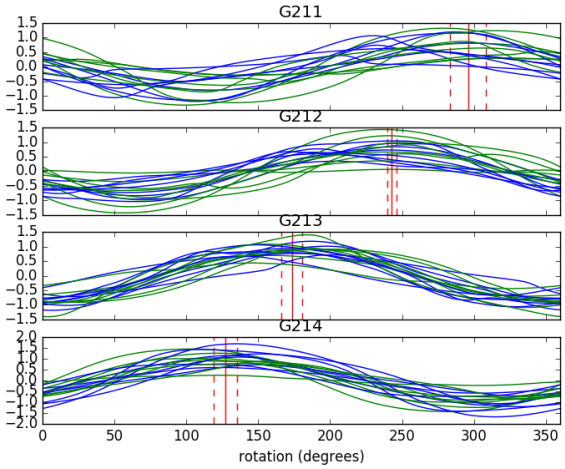

Figure 96: *Orientation curves for station G21. The lines indicate the maximum cross-correlation coefficient (with the surface accelerometer) as a function of counterclockwise rotation of the geophone. Blue lines are for the radial components, green lines for the transverse components. The vertical red lines indicate the average rotation +/- one standard deviation.*

Code	Channel 1	Channel 2	Data used	Standard deviation
G211	25.8°	295.8°	11/16	12.7°
G212	332.9°	242.9°	12/16	3.3°
G213	263.3°	173.3°	9/16	7.0°
G214	217.0°	127.0°	10/16	8.0°

Table 23: *This table shows the channel orientations of the geophones in station in degrees clockwise from north. The standard deviation refers to the orientations calculated from the individual events used. Data used shows how many traces were used for the final calculation and how many were initially found.*

Station G22

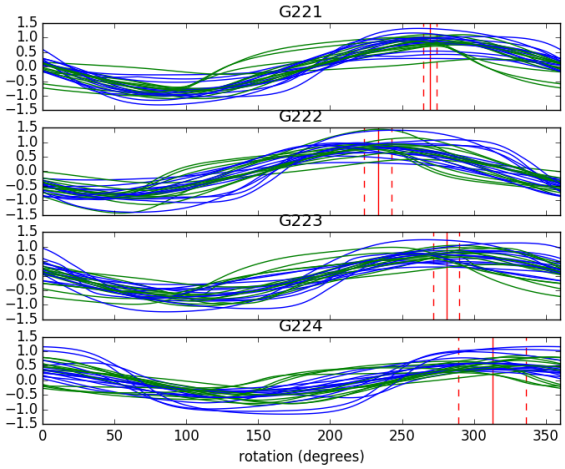

Figure 97: *Orientation curves for station G22. The lines indicate the maximum cross-correlation coefficient (with the surface accelerometer) as a function of counterclockwise rotation of the geophone. Blue lines are for the radial components, green lines for the transverse components. The vertical red lines indicate the average rotation +/- one standard deviation.*

Code	Channel 1	Channel 2	Data used	Standard deviation
G221	359.3°	269.3°	18/26	4.7°
G222	323.4°	233.4°	20/26	9.6°
G223	10.8°	280.8°	17/26	9.2°
G224	42.9°	312.9°	25/26	23.5°

Table 24: *This table shows the channel orientations of the geophones in station in degrees clockwise from north. The standard deviation refers to the orientations calculated from the individual events used. Data used shows how many traces were used for the final calculation and how many were initially found.*

Station G23

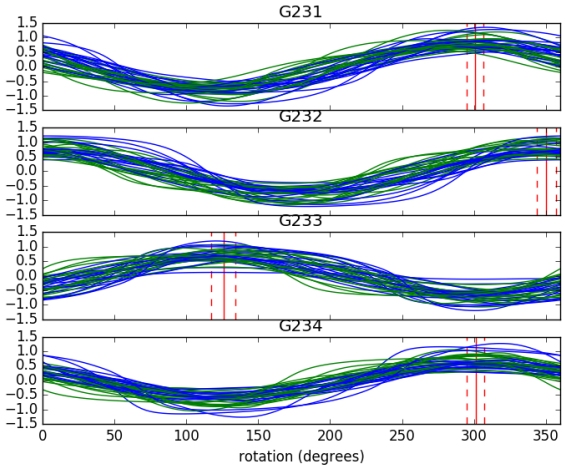

Figure 98: *Orientation curves for station G23. The lines indicate the maximum cross-correlation coefficient (with the surface accelerometer) as a function of counterclockwise rotation of the geophone. Blue lines are for the radial components, green lines for the transverse components. The vertical red lines indicate the average rotation +/- one standard deviation.*

Code	Channel 1	Channel 2	Data used	Standard deviation
G231	30.7°	300.7°	28/36	5.6°
G232	80.0°	350.0°	22/36	6.9°
G233	215.8°	125.8°	28/36	8.2°
G234	31.2°	301.2°	26/36	6.0°

Table 25: *This table shows the channel orientations of the geophones in station in degrees clockwise from north. The standard deviation refers to the orientations calculated from the individual events used. Data used shows how many traces were used for the final calculation and how many were initially found.*

Station G24

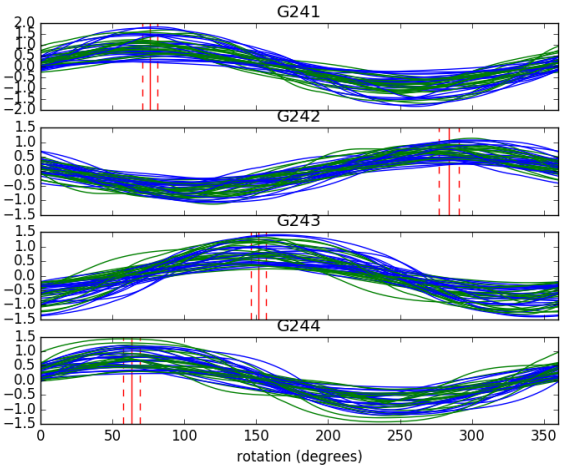

Figure 99: *Orientation curves for station G24. The lines indicate the maximum cross-correlation coefficient (with the surface accelerometer) as a function of counterclockwise rotation of the geophone. Blue lines are for the radial components, green lines for the transverse components. The vertical red lines indicate the average rotation +/- one standard deviation.*

Code	Channel 1	Channel 2	Data used	Standard deviation
G241	166.1°	76.1°	36/44	5.5°
G242	13.8°	283.8°	35/44	7.1°
G243	241.5°	151.5°	31/44	5.1°
G244	153.5°	63.5°	36/44	5.8°

Table 26: *This table shows the channel orientations of the geophones in station in degrees clockwise from north. The standard deviation refers to the orientations calculated from the individual events used. Data used shows how many traces were used for the final calculation and how many were initially found.*

Station G26

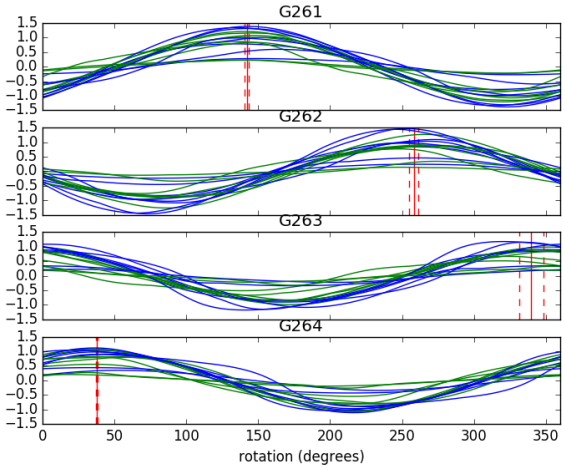

Figure 100: *Orientation curves for station G26. The lines indicate the maximum cross-correlation coefficient (with the surface accelerometer) as a function of counterclockwise rotation of the geophone. Blue lines are for the radial components, green lines for the transverse components. The vertical red lines indicate the average rotation +/- one standard deviation.*

Code	Channel 1	Channel 2	Data used	Standard deviation
G261	232.0°	142.0°	14/16	1.6°
G262	348.2°	258.2°	10/16	3.2°
G263	69.8°	339.8°	14/16	8.5°
G264	127.7°	37.7°	11/16	0.8°

Table 27: *This table shows the channel orientations of the geophones in station in degrees clockwise from north. The standard deviation refers to the orientations calculated from the individual events used. Data used shows how many traces were used for the final calculation and how many were initially found.*

Station G27

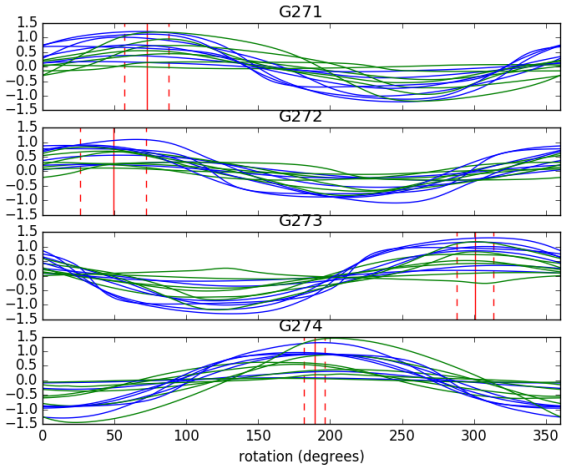

Figure 101: *Orientation curves for station G27. The lines indicate the maximum cross-correlation coefficient (with the surface accelerometer) as a function of counterclockwise rotation of the geophone. Blue lines are for the radial components, green lines for the transverse components. The vertical red lines indicate the average rotation +/- one standard deviation.*

Code	Channel 1	Channel 2	Data used	Standard deviation
G271	162.3°	72.3°	12/14	15.2°
G272	135.3°	45.3°	9/14	8.0°
G273	30.6°	300.6°	13/14	12.8°
G274	279.2°	189.2°	10/14	7.2°

Table 28: *This table shows the channel orientations of the geophones in station in degrees clockwise from north. The standard deviation refers to the orientations calculated from the individual events used. Data used shows how many traces were used for the final calculation and how many were initially found.*

Station G28

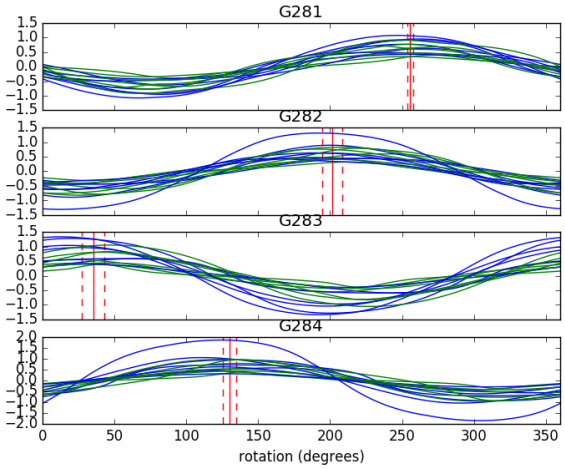

Figure 102: *Orientation curves for station G28. The lines indicate the maximum cross-correlation coefficient (with the surface accelerometer) as a function of counterclockwise rotation of the geophone. Blue lines are for the radial components, green lines for the transverse components. The vertical red lines indicate the average rotation +/- one standard deviation.*

Code	Channel 1	Channel 2	Data used	Standard deviation
G281	345.7°	255.7°	10/14	2.0°
G282	291.4°	201.4°	11/14	7.0°
G283	125.2°	35.2°	11/14	7.7°
G284	220.2°	130.2°	12/14	4.6°

Table 29: *This table shows the channel orientations of the geophones in station in degrees clockwise from north. The standard deviation refers to the orientations calculated from the individual events used. Data used shows how many traces were used for the final calculation and how many were initially found.*

NOTE: No data for events with $M_L > 1.5$ were available for this station, therefore the magnitude threshold was lowered to 1.0.

Station G29

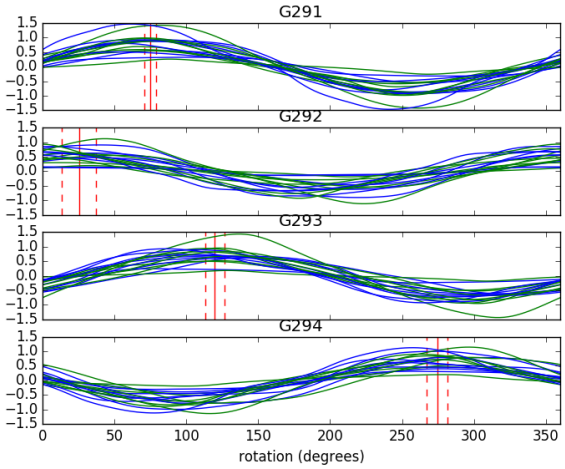

Figure 103: *Orientation curves for station G29. The lines indicate the maximum cross-correlation coefficient (with the surface accelerometer) as a function of counterclockwise rotation of the geophone. Blue lines are for the radial components, green lines for the transverse components. The vertical red lines indicate the average rotation +/- one standard deviation.*

Code	Channel 1	Channel 2	Data used	Standard deviation
G291	165.0°	75.0°	15/18	4.2°
G292	113.8°	23.8°	12/18	12.7°
G293	209.7°	119.7°	12/18	6.7°
G294	4.4°	274.4°	12/18	7.4°

Table 30: *This table shows the channel orientations of the geophones in station in degrees clockwise from north. The standard deviation refers to the orientations calculated from the individual events used. Data used shows how many traces were used for the final calculation and how many were initially found.*

Station G30

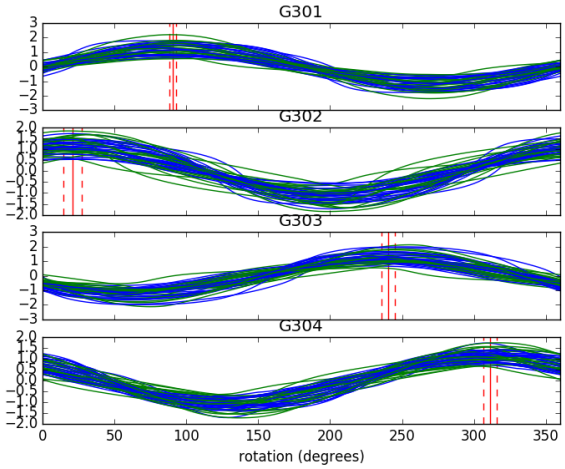

Figure 104: *Orientation curves for station G30. The lines indicate the maximum cross-correlation coefficient (with the surface accelerometer) as a function of counterclockwise rotation of the geophone. Blue lines are for the radial components, green lines for the transverse components. The vertical red lines indicate the average rotation +/- one standard deviation.*

Code	Channel 1	Channel 2	Data used	Standard deviation
G301	180.7°	90.7°	32/46	2.4°
G302	110.5°	20.5°	45/46	6.5°
G303	330.3°	240.3°	33/46	4.8°
G304	41.3°	311.3°	35/46	4.8°

Table 31: *This table shows the channel orientations of the geophones in station in degrees clockwise from north. The standard deviation refers to the orientations calculated from the individual events used. Data used shows how many traces were used for the final calculation and how many were initially found.*

Station G31

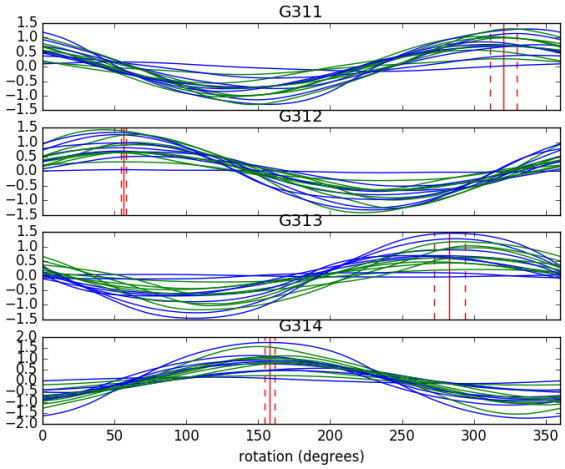

Figure 105: *Orientation curves for station G31. The lines indicate the maximum cross-correlation coefficient (with the surface accelerometer) as a function of counterclockwise rotation of the geophone. Blue lines are for the radial components, green lines for the transverse components. The vertical red lines indicate the average rotation +/- one standard deviation.*

Code	Channel 1	Channel 2	Data used	Standard deviation
G311	50.5°	320.5°	15/16	9.1°
G312	146.4°	56.4°	13/16	1.9°
G313	13.0°	283.0°	15/16	10.8°
G314	248.0°	158.0°	14/16	3.4°

Table 32: *This table shows the channel orientations of the geophones in station in degrees clockwise from north. The standard deviation refers to the orientations calculated from the individual events used. Data used shows how many traces were used for the final calculation and how many were initially found.*

Station G32

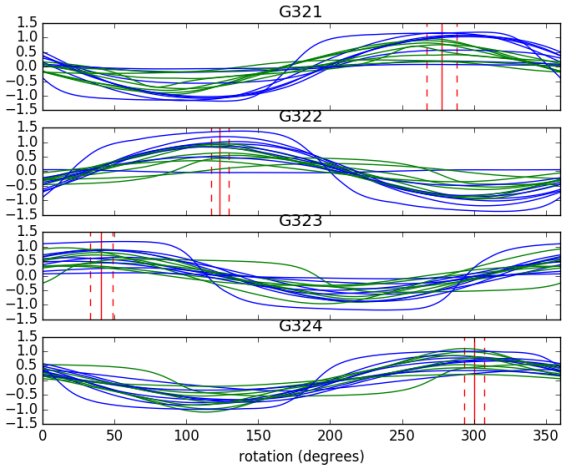

Figure 106: *Orientation curves for station G32. The lines indicate the maximum cross-correlation coefficient (with the surface accelerometer) as a function of counterclockwise rotation of the geophone. Blue lines are for the radial components, green lines for the transverse components. The vertical red lines indicate the average rotation +/- one standard deviation.*

Code	Channel 1	Channel 2	Data used	Standard deviation
G321	213.3°	123.3°	13/16	6.0°
G322	130.8°	40.8°	9/16	7.9°
G323	30.2°	300.2°	13/16	7.0°
G324	7.6°	277.6°	14/16	10.3°

Table 33: *This table shows the channel orientations of the geophones in station in degrees clockwise from north. The standard deviation refers to the orientations calculated from the individual events used. Data used shows how many traces were used for the final calculation and how many were initially found.*

Station G33

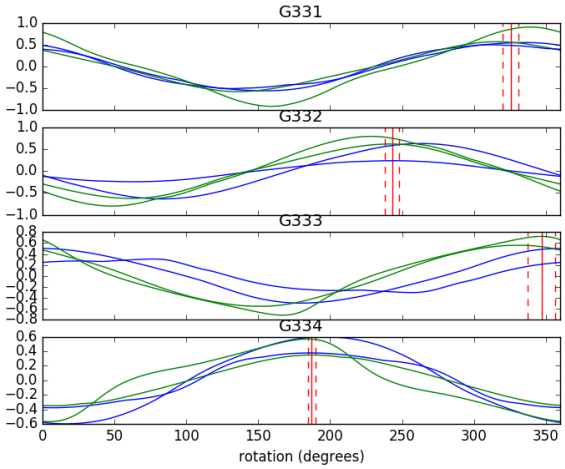

Figure 107: *Orientation curves for station G33. The lines indicate the maximum cross-correlation coefficient (with the surface accelerometer) as a function of counterclockwise rotation of the geophone. Blue lines are for the radial components, green lines for the transverse components. The vertical red lines indicate the average rotation +/- one standard deviation.*

Code	Channel 1	Channel 2	Data used	Standard deviation
G331	55.5°	325.5°	2/4	5.5°
G332	333.0°	243.0°	2/4	5.0°
G333	77.0°	347.0°	3/4	9.4°
G334	277.2°	187.2°	3/4	2.7°

Table 34: *This table shows the channel orientations of the geophones in station in degrees clockwise from north. The standard deviation refers to the orientations calculated from the individual events used. Data used shows how many traces were used for the final calculation and how many were initially found.*

Station G34

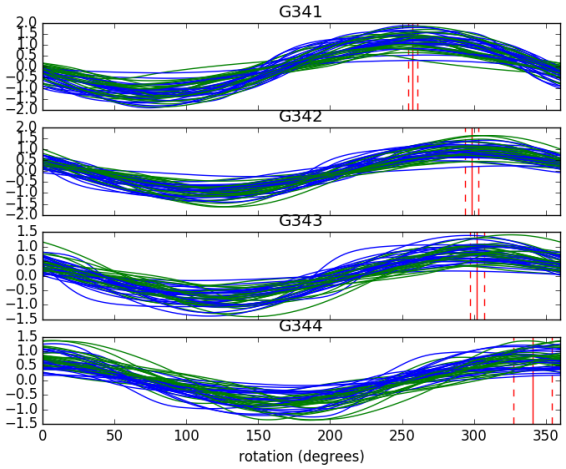

Figure 108: *Orientation curves for station G34. The lines indicate the maximum cross-correlation coefficient (with the surface accelerometer) as a function of counterclockwise rotation of the geophone. Blue lines are for the radial components, green lines for the transverse components. The vertical red lines indicate the average rotation +/- one standard deviation.*

Code	Channel 1	Channel 2	Data used	Standard deviation
G341	347.3°	257.3°	36/48	3.2°
G342	28.6°	298.6°	37/48	4.5°
G343	32.1°	302.1°	33/48	5.0°
G344	70.2°	340.2°	35/48	13.2°

Table 35: *This table shows the channel orientations of the geophones in station in degrees clockwise from north. The standard deviation refers to the orientations calculated from the individual events used. Data used shows how many traces were used for the final calculation and how many were initially found.*

Station G36

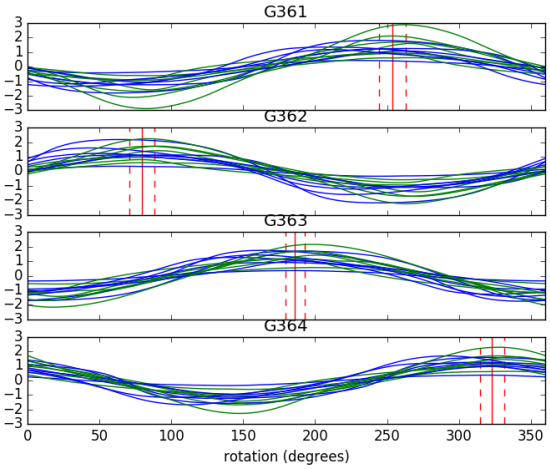

Figure 109: *Orientation curves for station G36. The lines indicate the maximum cross-correlation coefficient (with the surface accelerometer) as a function of counterclockwise rotation of the geophone. Blue lines are for the radial components, green lines for the transverse components. The vertical red lines indicate the average rotation +/- one standard deviation.*

Code	Channel 1	Channel 2	Data used	Standard deviation
G361	343.8°	253.8°	12/14	9.3°
G362	169.4°	79.4°	11/14	8.6°
G363	276.0°	186.0°	9/14	6.7°
G364	53.1°	323.1°	11/14	8.2°

Table 36: *This table shows the channel orientations of the geophones in station in degrees clockwise from north. The standard deviation refers to the orientations calculated from the individual events used. Data used shows how many traces were used for the final calculation and how many were initially found.*

Station G37

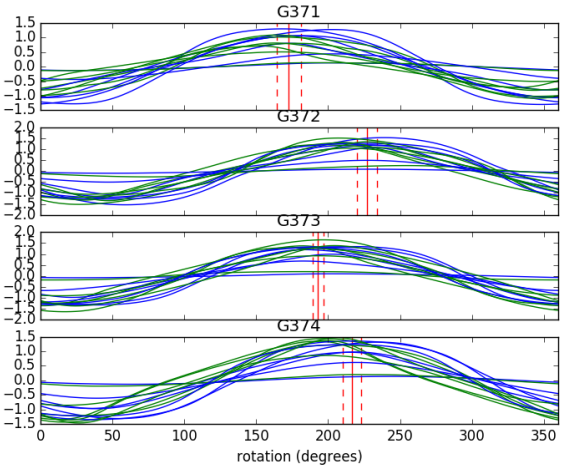

Figure 110: *Orientation curves for station G37. The lines indicate the maximum cross-correlation coefficient (with the surface accelerometer) as a function of counterclockwise rotation of the geophone. Blue lines are for the radial components, green lines for the transverse components. The vertical red lines indicate the average rotation +/- one standard deviation.*

Code	Channel 1	Channel 2	Data used	Standard deviation
G371	262.7°	172.7°	10/14	8.4°
G372	317.1°	227.1°	10/14	7.1°
G373	283.0°	193.0°	12/14	3.7°
G374	306.6°	216.6°	7/14	6.4°

Table 37: *This table shows the channel orientations of the geophones in station in degrees clockwise from north. The standard deviation refers to the orientations calculated from the individual events used. Data used shows how many traces were used for the final calculation and how many were initially found.*

Station G38

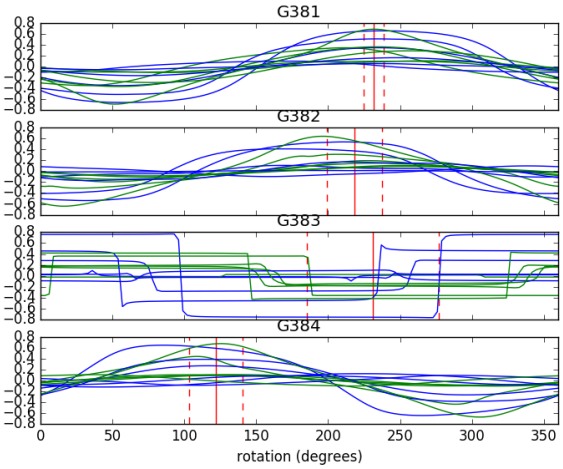

Figure 111: *Orientation curves for station G38. The lines indicate the maximum cross-correlation coefficient (with the surface accelerometer) as a function of counterclockwise rotation of the geophone. Blue lines are for the radial components, green lines for the transverse components. The vertical red lines indicate the average rotation +/- one standard deviation.*

Code	Channel 1	Channel 2	Data used	Standard deviation
G381	321.8°	231.8°	9/12	7.0°
G382	308.3°	218.3°	9/12	19.3°
G383	321.1°	231.1°	7/12	45.6°
G384	211.9°	121.9°	9/12	18.6°

Table 38: *This table shows the channel orientations of the geophones in station in degrees clockwise from north. The standard deviation refers to the orientations calculated from the individual events used. Data used shows how many traces were used for the final calculation and how many were initially found.*

NOTE: No data for events with $M_L > 1.5$ were available for this station, therefore the magnitude threshold was lowered to 1.0. However, the quality of the data is very poor, so therefore this station was not used in the final result.

Station G39

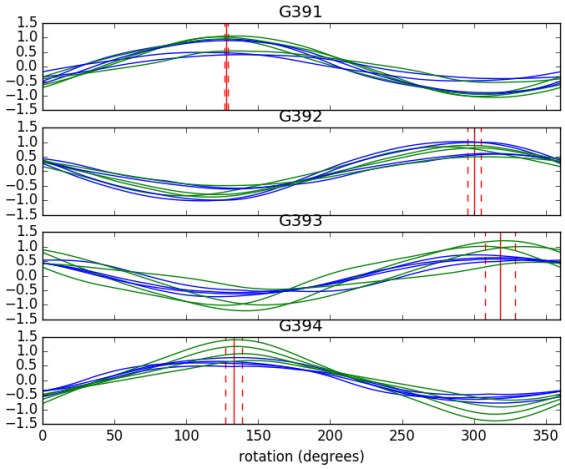

Figure 112: *Orientation curves for station G39. The lines indicate the maximum cross-correlation coefficient (with the surface accelerometer) as a function of counterclockwise rotation of the geophone. Blue lines are for the radial components, green lines for the transverse components. The vertical red lines indicate the average rotation +/- one standard deviation.*

Code	Channel 1	Channel 2	Data used	Standard deviation
G391	217.8°	127.8°	6/8	1.0°
G392	30.1°	300.1°	6/8	4.7°
G393	48.2°	318.2°	7/8	10.4°
G394	222.9°	132.9°	5/8	5.9°

Table 39: *This table shows the channel orientations of the geophones in station in degrees clockwise from north. The standard deviation refers to the orientations calculated from the individual events used. Data used shows how many traces were used for the final calculation and how many were initially found.*

Station G40

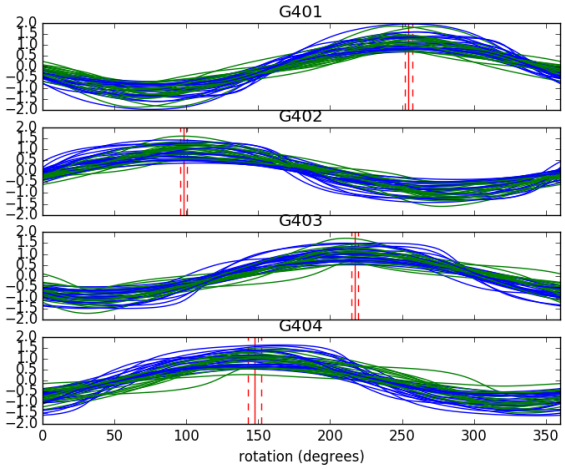

Figure 113: *Orientation curves for station G40. The lines indicate the maximum cross-correlation coefficient (with the surface accelerometer) as a function of counterclockwise rotation of the geophone. Blue lines are for the radial components, green lines for the transverse components. The vertical red lines indicate the average rotation +/- one standard deviation.*

Code	Channel 1	Channel 2	Data used	Standard deviation
G401	344.5°	254.5°	29/40	2.7°
G402	188.4°	98.4°	27/40	2.4°
G403	307.3°	217.3°	31/40	2.2°
G404	237.5°	147.5°	30/40	4.4°

Table 40: *This table shows the channel orientations of the geophones in station in degrees clockwise from north. The standard deviation refers to the orientations calculated from the individual events used. Data used shows how many traces were used for the final calculation and how many were initially found.*

Station G41

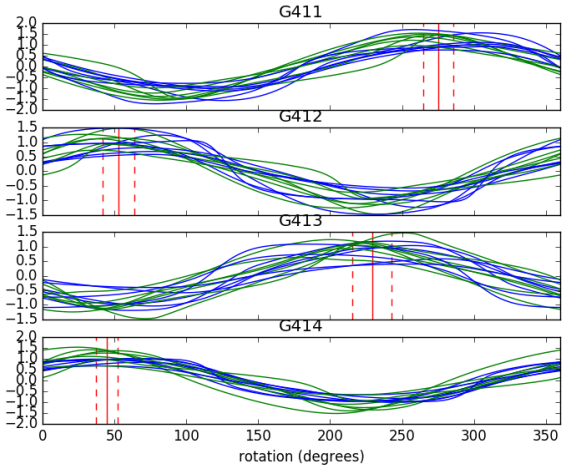

Figure 114: *Orientation curves for station G41. The lines indicate the maximum cross-correlation coefficient (with the surface accelerometer) as a function of counterclockwise rotation of the geophone. Blue lines are for the radial components, green lines for the transverse components. The vertical red lines indicate the average rotation +/- one standard deviation.*

Code	Channel 1	Channel 2	Data used	Standard deviation
G411	5.1°	275.1°	7/14	10.4°
G412	142.8°	52.8°	11/14	11.2°
G413	319.1°	229.1°	9/14	13.7°
G414	134.6°	44.6°	11/14	7.4°

Table 41: *This table shows the channel orientations of the geophones in station in degrees clockwise from north. The standard deviation refers to the orientations calculated from the individual events used. Data used shows how many traces were used for the final calculation and how many were initially found.*

Station G42

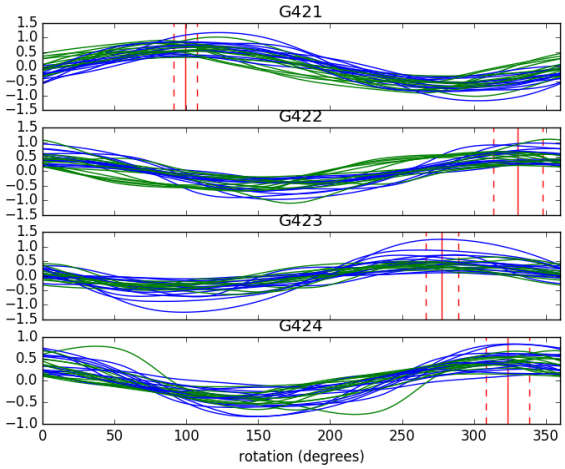

Figure 115: *Orientation curves for station G42. The lines indicate the maximum cross-correlation coefficient (with the surface accelerometer) as a function of counterclockwise rotation of the geophone. Blue lines are for the radial components, green lines for the transverse components. The vertical red lines indicate the average rotation +/- one standard deviation.*

Code	Channel 1	Channel 2	Data used	Standard deviation
G421	9.3°	279.3°	19/26	7.9°
G422	60.6°	330.6°	21/26	17.0°
G423	5.1°	275.1°	24/26	16.7°
G424	53.5°	323.5°	24/26	14.9°

Table 42: *This table shows the channel orientations of the geophones in station in degrees clockwise from north. The standard deviation refers to the orientations calculated from the individual events used. Data used shows how many traces were used for the final calculation and how many were initially found.*

NOTE: From the stacked cross-correlations of the transverse component in the seismic interferometry method, it appeared that the polarity of G421 was reversed. Therefore 180° were added manually to the orientation of this geophone.

Station G43

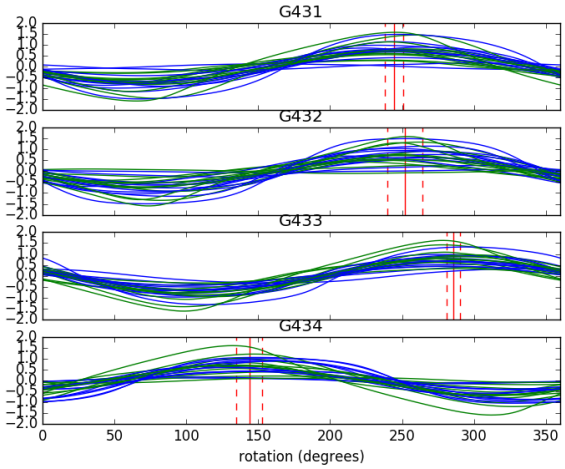

Figure 116: *Orientation curves for station G43. The lines indicate the maximum cross-correlation coefficient (with the surface accelerometer) as a function of counterclockwise rotation of the geophone. Blue lines are for the radial components, green lines for the transverse components. The vertical red lines indicate the average rotation +/- one standard deviation.*

Code	Channel 1	Channel 2	Data used	Standard deviation
G431	334.3°	244.3°	22/24	6.4°
G432	342.0°	252.0°	21/24	12.4°
G433	15.7°	285.7°	20/24	4.9°
G434	233.9°	143.9°	21/24	8.9°

Table 43: *This table shows the channel orientations of the geophones in station in degrees clockwise from north. The standard deviation refers to the orientations calculated from the individual events used. Data used shows how many traces were used for the final calculation and how many were initially found.*

Station G44

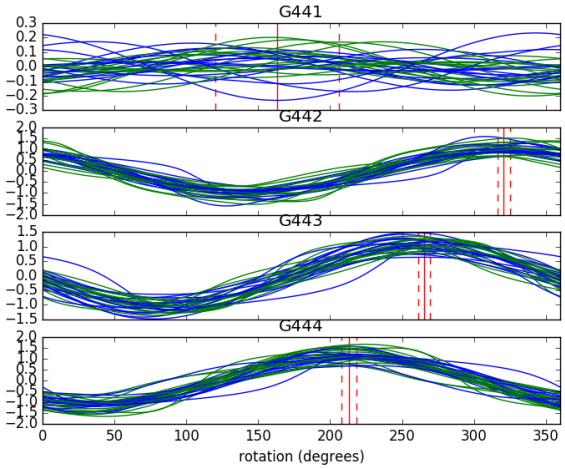

Figure 117: *Orientation curves for station G44. The lines indicate the maximum cross-correlation coefficient (with the surface accelerometer) as a function of counterclockwise rotation of the geophone. Blue lines are for the radial components, green lines for the transverse components. The vertical red lines indicate the average rotation +/- one standard deviation.*

Code	Channel 1	Channel 2	Data used	Standard deviation
G441	253.1°	163.1°	20/30	42.9°
G442	50.7°	320.7°	23/30	4.2°
G443	355.4°	265.4°	20/30	4.3°
G444	303.2°	213.2°	25/30	5.1°

Table 44: *This table shows the channel orientations of the geophones in station in degrees clockwise from north. The standard deviation refers to the orientations calculated from the individual events used. Data used shows how many traces were used for the final calculation and how many were initially found.*

Station G45

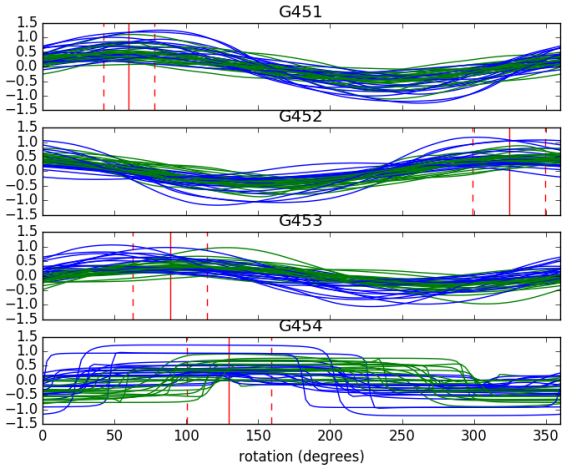

Figure 118: *Orientation curves for station G45. The lines indicate the maximum cross-correlation coefficient (with the surface accelerometer) as a function of counterclockwise rotation of the geophone. Blue lines are for the radial components, green lines for the transverse components. The vertical red lines indicate the average rotation +/- one standard deviation.*

Code	Channel 1	Channel 2	Data used	Standard deviation
G451	150.0°	60.0°	39/40	17.6°
G452	52.5°	322.5°	33/40	24.9°
G453	178.7°	88.7°	34/40	25.8°
G454	219.7°	129.7°	27/40	29.3°

Table 45: *This table shows the channel orientations of the geophones in station in degrees clockwise from north. The standard deviation refers to the orientations calculated from the individual events used. Data used shows how many traces were used for the final calculation and how many were initially found.*

Station G46

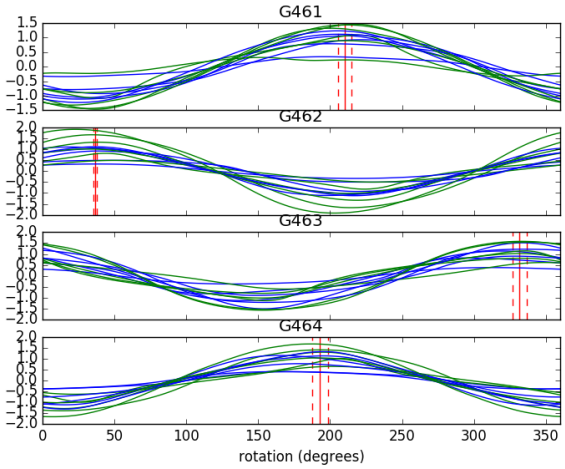

Figure 119: *Orientation curves for station G46. The lines indicate the maximum cross-correlation coefficient (with the surface accelerometer) as a function of counterclockwise rotation of the geophone. Blue lines are for the radial components, green lines for the transverse components. The vertical red lines indicate the average rotation +/- one standard deviation.*

Code	Channel 1	Channel 2	Data used	Standard deviation
G461	300.0°	210.0°	11/12	4.6°
G462	126.6°	36.6°	8/12	1.4°
G463	61.8°	331.8°	9/12	5.0°
G464	283.0°	193.0°	8/12	5.4°

Table 46: *This table shows the channel orientations of the geophones in station in degrees clockwise from north. The standard deviation refers to the orientations calculated from the individual events used. Data used shows how many traces were used for the final calculation and how many were initially found.*

Station G47

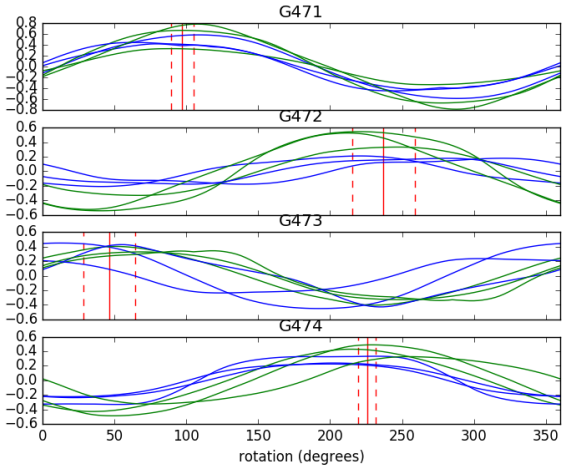

Figure 120: *Orientation curves for station G47. The lines indicate the maximum cross-correlation coefficient (with the surface accelerometer) as a function of counterclockwise rotation of the geophone. Blue lines are for the radial components, green lines for the transverse components. The vertical red lines indicate the average rotation +/- one standard deviation.*

Code	Channel 1	Channel 2	Data used	Standard deviation
G471	170.0°	80.0°	2/4	6.0°
G472	124.0°	34.0°	3/4	156.7°
G473	261.6°	171.6°	3/4	33.7°
G474	299.7°	209.7°	3/4	14.5°

Table 47: *This table shows the channel orientations of the geophones in station in degrees clockwise from north. The standard deviation refers to the orientations calculated from the individual events used. Data used shows how many traces were used for the final calculation and how many were initially found.*

Station G49

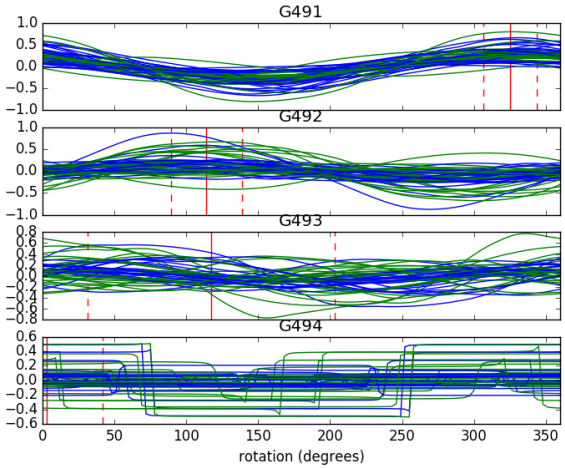

Figure 121: *Orientation curves for station G49. The lines indicate the maximum cross-correlation coefficient (with the surface accelerometer) as a function of counterclockwise rotation of the geophone. Blue lines are for the radial components, green lines for the transverse components. The vertical red lines indicate the average rotation +/- one standard deviation.*

Code	Channel 1	Channel 2	Data used	Standard deviation
G491	55.1°	325.1°	48/52	18.5°
G492	204.1°	114.1°	38/52	24.5°
G493	207.3°	117.3°	29/52	85.9°
G494	92.9°	2.9°	34/52	39.0°

Table 48: *This table shows the channel orientations of the geophones in station in degrees clockwise from north. The standard deviation refers to the orientations calculated from the individual events used. Data used shows how many traces were used for the final calculation and how many were initially found.*

Station G50

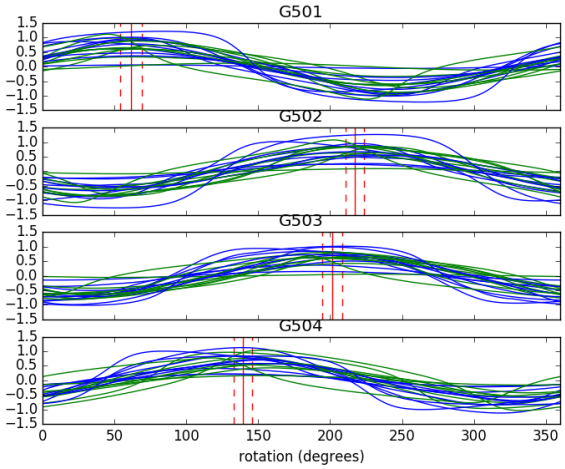

Figure 122: *Orientation curves for station G50. The lines indicate the maximum cross-correlation coefficient (with the surface accelerometer) as a function of counterclockwise rotation of the geophone. Blue lines are for the radial components, green lines for the transverse components. The vertical red lines indicate the average rotation +/- one standard deviation.*

Code	Channel 1	Channel 2	Data used	Standard deviation
G501	151.5°	61.5°	18/20	7.4°
G502	307.3°	217.3°	17/20	6.5°
G503	291.5°	201.5°	17/20	7.2°
G504	229.3°	139.3°	15/20	6.4°

Table 49: *This table shows the channel orientations of the geophones in station in degrees clockwise from north. The standard deviation refers to the orientations calculated from the individual events used. Data used shows how many traces were used for the final calculation and how many were initially found.*

Station G51

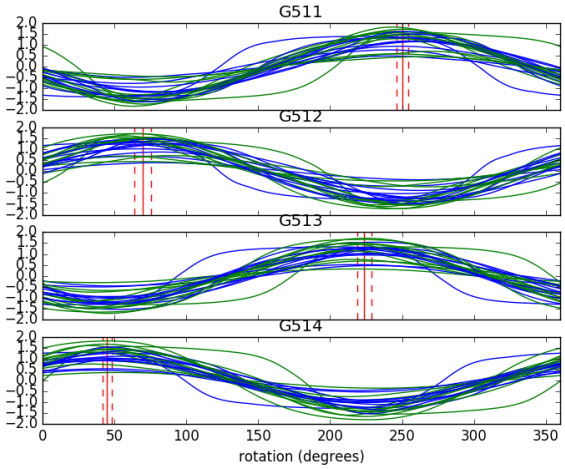

Figure 123: *Orientation curves for station G51. The lines indicate the maximum cross-correlation coefficient (with the surface accelerometer) as a function of counterclockwise rotation of the geophone. Blue lines are for the radial components, green lines for the transverse components. The vertical red lines indicate the average rotation +/- one standard deviation.*

Code	Channel 1	Channel 2	Data used	Standard deviation
G511	340.2°	250.2°	20/24	4.2°
G512	159.6°	69.6°	18/24	5.9°
G513	313.7°	223.7°	20/24	4.9°
G514	135.0°	45.0°	17/24	2.9°

Table 50: *This table shows the channel orientations of the geophones in station in degrees clockwise from north. The standard deviation refers to the orientations calculated from the individual events used. Data used shows how many traces were used for the final calculation and how many were initially found.*

Station G52

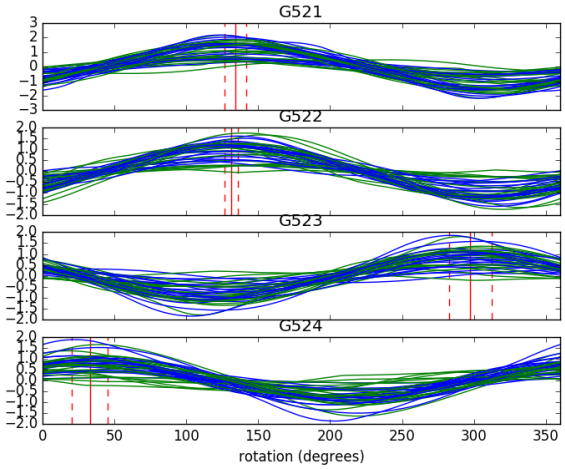

Figure 124: *Orientation curves for station G52. The lines indicate the maximum cross-correlation coefficient (with the surface accelerometer) as a function of counterclockwise rotation of the geophone. Blue lines are for the radial components, green lines for the transverse components. The vertical red lines indicate the average rotation +/- one standard deviation.*

Code	Channel 1	Channel 2	Data used	Standard deviation
G521	224.3°	134.3°	36/40	7.5°
G522	221.1°	131.1°	33/40	4.6°
G523	27.3°	297.3°	37/40	14.8°
G524	122.9°	32.9°	36/40	12.6°

Table 51: *This table shows the channel orientations of the geophones in station in degrees clockwise from north. The standard deviation refers to the orientations calculated from the individual events used. Data used shows how many traces were used for the final calculation and how many were initially found.*

Station G53

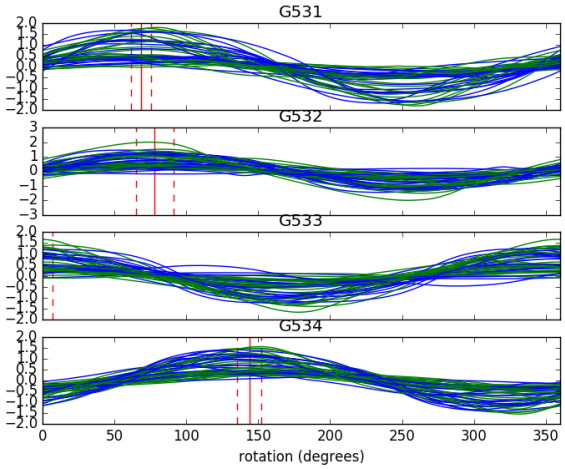

Figure 125: *Orientation curves for station G53. The lines indicate the maximum cross-correlation coefficient (with the surface accelerometer) as a function of counterclockwise rotation of the geophone. Blue lines are for the radial components, green lines for the transverse components. The vertical red lines indicate the average rotation +/- one standard deviation.*

Code	Channel 1	Channel 2	Data used	Standard deviation
G531	158.8°	68.8°	11/16	5.4°
G532	167.2°	77.2°	12/16	9.0°
G533	68.1°	338.1°	12/16	41.0°
G534	230.0°	140.0°	14/16	10.1°

Table 52: *This table shows the channel orientations of the geophones in station in degrees clockwise from north. The standard deviation refers to the orientations calculated from the individual events used. Data used shows how many traces were used for the final calculation and how many were initially found.*

Station G54

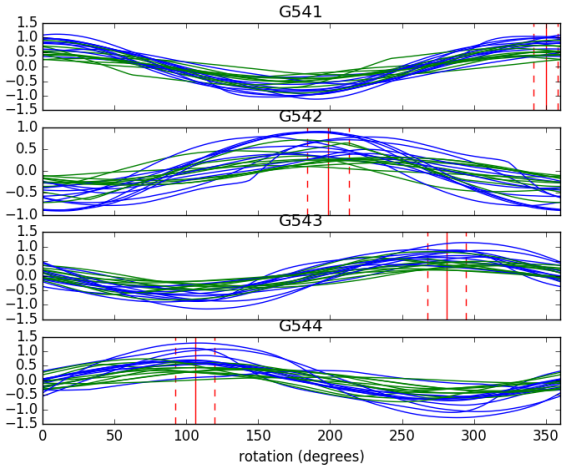

Figure 126: *Orientation curves for station G54. The lines indicate the maximum cross-correlation coefficient (with the surface accelerometer) as a function of counterclockwise rotation of the geophone. Blue lines are for the radial components, green lines for the transverse components. The vertical red lines indicate the average rotation +/- one standard deviation.*

Code	Channel 1	Channel 2	Data used	Standard deviation
G541	79.9°	349.9°	14/22	8.2°
G542	288.6°	198.6°	15/22	14.5°
G543	11.2°	281.2°	16/22	13.4°
G544	196.1°	106.1°	18/22	13.8°

Table 53: *This table shows the channel orientations of the geophones in station in degrees clockwise from north. The standard deviation refers to the orientations calculated from the individual events used. Data used shows how many traces were used for the final calculation and how many were initially found.*

Station G55

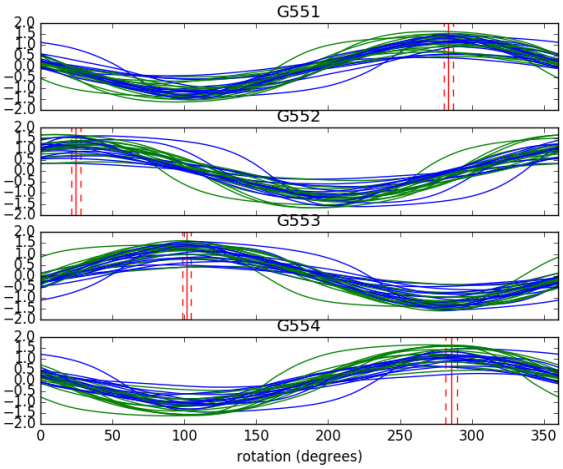

Figure 127: *Orientation curves for station G55. The lines indicate the maximum cross-correlation coefficient (with the surface accelerometer) as a function of counterclockwise rotation of the geophone. Blue lines are for the radial components, green lines for the transverse components. The vertical red lines indicate the average rotation +/- one standard deviation.*

Code	Channel 1	Channel 2	Data used	Standard deviation
G551	13.6°	283.6°	22/30	3.3°
G552	114.6°	24.6°	21/30	3.3°
G553	191.6°	101.6°	24/30	2.9°
G554	15.5°	285.5°	22/30	4.1°

Table 54: *This table shows the channel orientations of the geophones in station in degrees clockwise from north. The standard deviation refers to the orientations calculated from the individual events used. Data used shows how many traces were used for the final calculation and how many were initially found.*

Station G56

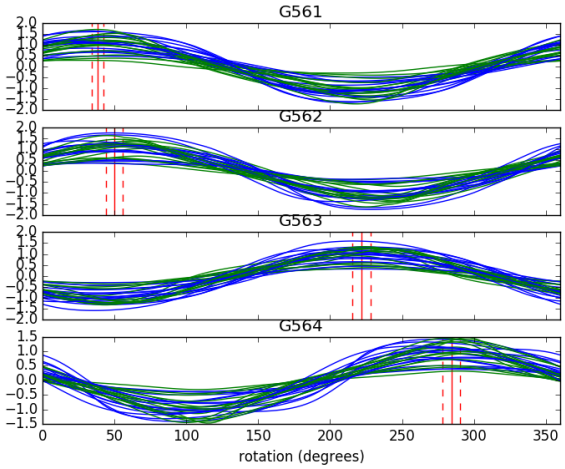

Figure 128: *Orientation curves for station G56. The lines indicate the maximum cross-correlation coefficient (with the surface accelerometer) as a function of counterclockwise rotation of the geophone. Blue lines are for the radial components, green lines for the transverse components. The vertical red lines indicate the average rotation +/- one standard deviation.*

Code	Channel 1	Channel 2	Data used	Standard deviation
G561	128.3°	38.3°	23/30	4.2°
G562	140.1°	50.1°	23/30	5.7°
G563	311.9°	221.9°	24/30	6.4°
G564	14.3°	284.3°	25/30	6.1°

Table 55: *This table shows the channel orientations of the geophones in station in degrees clockwise from north. The standard deviation refers to the orientations calculated from the individual events used. Data used shows how many traces were used for the final calculation and how many were initially found.*

Station G57

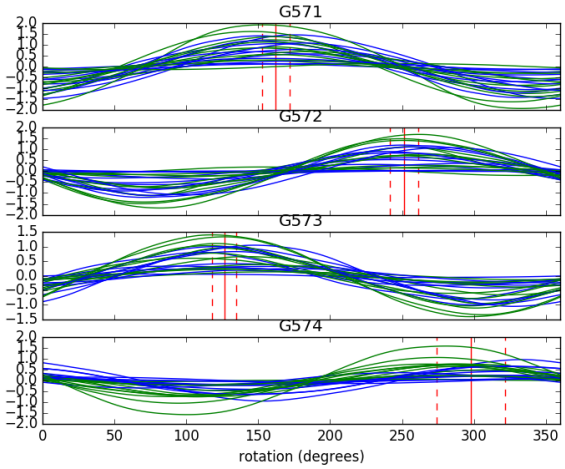

Figure 129: *Orientation curves for station G57. The lines indicate the maximum cross-correlation coefficient (with the surface accelerometer) as a function of counterclockwise rotation of the geophone. Blue lines are for the radial components, green lines for the transverse components. The vertical red lines indicate the average rotation +/- one standard deviation.*

Code	Channel 1	Channel 2	Data used	Standard deviation
G571	252.2°	162.2°	21/24	9.5°
G572	341.4°	251.4°	20/24	9.9°
G573	216.5°	126.5°	18/24	8.5°
G574	27.8°	297.8°	22/24	23.8°

Table 56: *This table shows the channel orientations of the geophones in station in degrees clockwise from north. The standard deviation refers to the orientations calculated from the individual events used. Data used shows how many traces were used for the final calculation and how many were initially found.*

Station G58

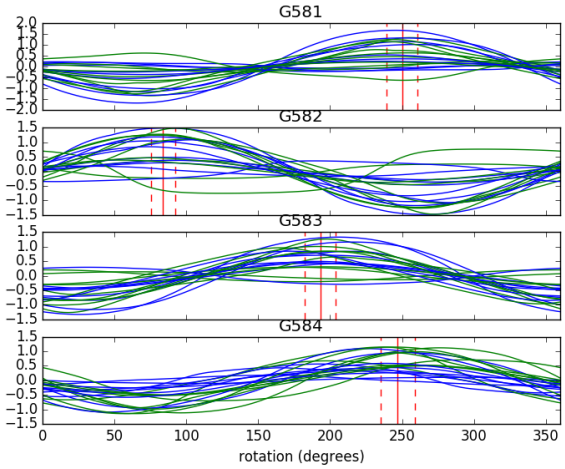

Figure 130: *Orientation curves for station G58. The lines indicate the maximum cross-correlation coefficient (with the surface accelerometer) as a function of counterclockwise rotation of the geophone. Blue lines are for the radial components, green lines for the transverse components. The vertical red lines indicate the average rotation +/- one standard deviation.*

Code	Channel 1	Channel 2	Data used	Standard deviation
G581	340.0°	250.0°	15/20	10.6°
G582	173.8°	83.8°	16/20	8.4°
G583	283.2°	193.2°	17/20	10.8°
G584	337.0°	247.0°	14/20	12.1°

Table 57: *This table shows the channel orientations of the geophones in station in degrees clockwise from north. The standard deviation refers to the orientations calculated from the individual events used. Data used shows how many traces were used for the final calculation and how many were initially found.*

Station G59

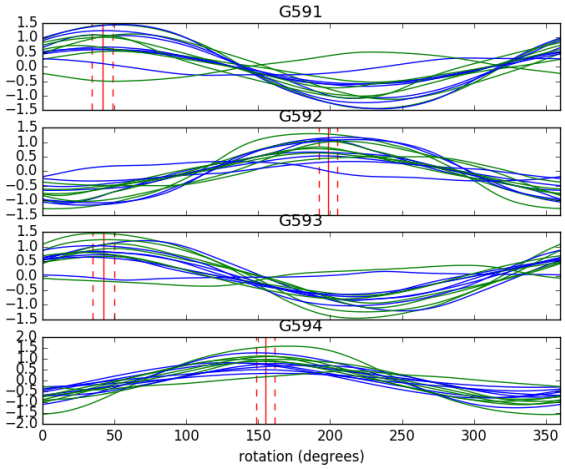

Figure 131: *Orientation curves for station G59. The lines indicate the maximum cross-correlation coefficient (with the surface accelerometer) as a function of counterclockwise rotation of the geophone. Blue lines are for the radial components, green lines for the transverse components. The vertical red lines indicate the average rotation +/- one standard deviation.*

Code	Channel 1	Channel 2	Data used	Standard deviation
G591	131.7°	41.7°	12/14	7.2°
G592	288.6°	198.6°	12/14	6.5°
G593	132.4°	42.4°	12/14	7.7°
G594	245.2°	155.2°	11/14	6.4°

Table 58: *This table shows the channel orientations of the geophones in station in degrees clockwise from north. The standard deviation refers to the orientations calculated from the individual events used. Data used shows how many traces were used for the final calculation and how many were initially found.*

Station G60

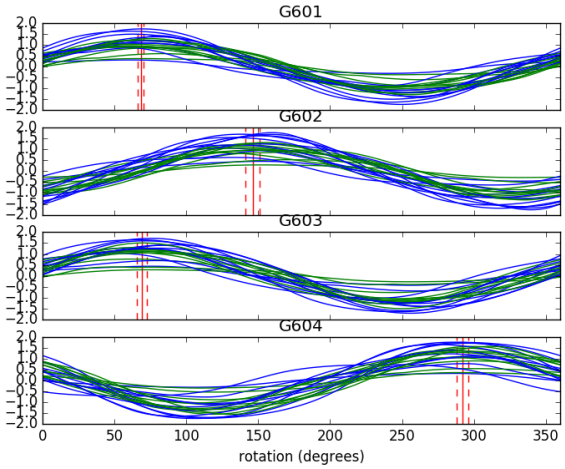

Figure 132: *Orientation curves for station G60. The lines indicate the maximum cross-correlation coefficient (with the surface accelerometer) as a function of counterclockwise rotation of the geophone. Blue lines are for the radial components, green lines for the transverse components. The vertical red lines indicate the average rotation +/- one standard deviation.*

Code	Channel 1	Channel 2	Data used	Standard deviation
G601	158.3°	68.3°	15/22	2.2°
G602	236.2°	146.2°	17/22	4.9°
G603	159.1°	69.1°	16/22	3.7°
G604	21.9°	291.9°	19/22	4.0°

Table 59: *This table shows the channel orientations of the geophones in station in degrees clockwise from north. The standard deviation refers to the orientations calculated from the individual events used. Data used shows how many traces were used for the final calculation and how many were initially found.*

Station G61

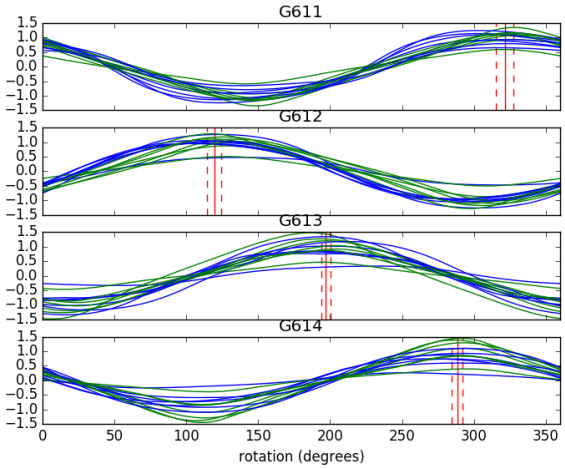

Figure 133: *Orientation curves for station G61. The lines indicate the maximum cross-correlation coefficient (with the surface accelerometer) as a function of counterclockwise rotation of the geophone. Blue lines are for the radial components, green lines for the transverse components. The vertical red lines indicate the average rotation +/- one standard deviation.*

Code	Channel 1	Channel 2	Data used	Standard deviation
G611	51.5°	321.5°	10/14	6.0°
G612	209.4°	119.4°	10/14	4.8°
G613	287.1°	197.1°	12/14	3.3°
G614	18.4°	288.4°	12/14	3.6°

Table 60: *This table shows the channel orientations of the geophones in station in degrees clockwise from north. The standard deviation refers to the orientations calculated from the individual events used. Data used shows how many traces were used for the final calculation and how many were initially found.*

Station G62

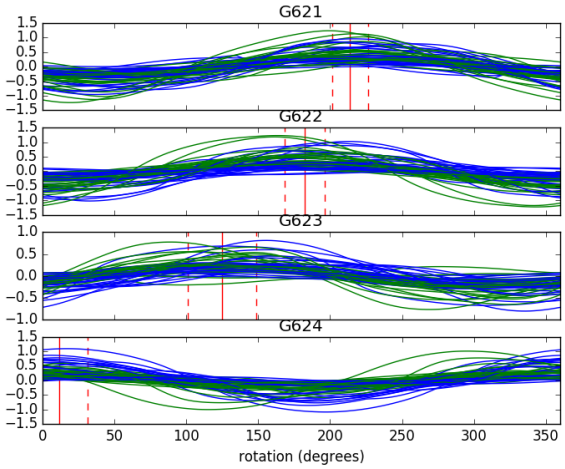

Figure 134: *Orientation curves for station G62. The lines indicate the maximum cross-correlation coefficient (with the surface accelerometer) as a function of counterclockwise rotation of the geophone. Blue lines are for the radial components, green lines for the transverse components. The vertical red lines indicate the average rotation +/- one standard deviation.*

Code	Channel 1	Channel 2	Data used	Standard deviation
G621	303.8°	213.8°	41/54	12.5°
G622	272.3°	182.3°	43/54	14.2°
G623	215.0°	125.0°	48/54	23.8°
G624	101.7°	11.7°	40/54	19.8°

Table 61: *This table shows the channel orientations of the geophones in station in degrees clockwise from north. The standard deviation refers to the orientations calculated from the individual events used. Data used shows how many traces were used for the final calculation and how many were initially found.*

Station G63

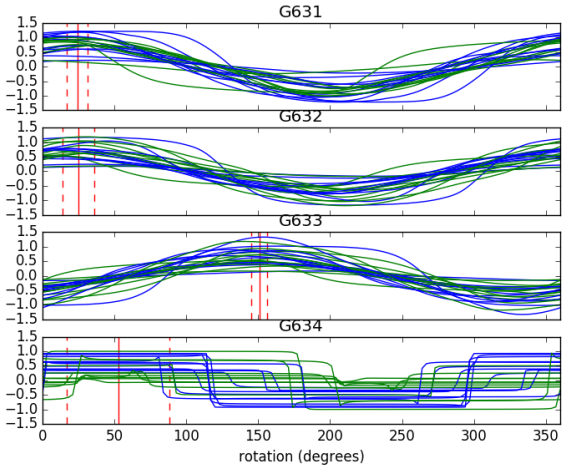

Figure 135: *Orientation curves for station G63. The lines indicate the maximum cross-correlation coefficient (with the surface accelerometer) as a function of counterclockwise rotation of the geophone. Blue lines are for the radial components, green lines for the transverse components. The vertical red lines indicate the average rotation +/- one standard deviation.*

Code	Channel 1	Channel 2	Data used	Standard deviation
G631	114.2°	24.2°	20/22	7.2°
G632	115.0°	25.0°	20/22	10.9°
G633	240.7°	150.7°	19/22	5.2°
G634	142.7°	52.7°	18/22	35.6°

Table 62: *This table shows the channel orientations of the geophones in station in degrees clockwise from north. The standard deviation refers to the orientations calculated from the individual events used. Data used shows how many traces were used for the final calculation and how many were initially found.*

Station G64

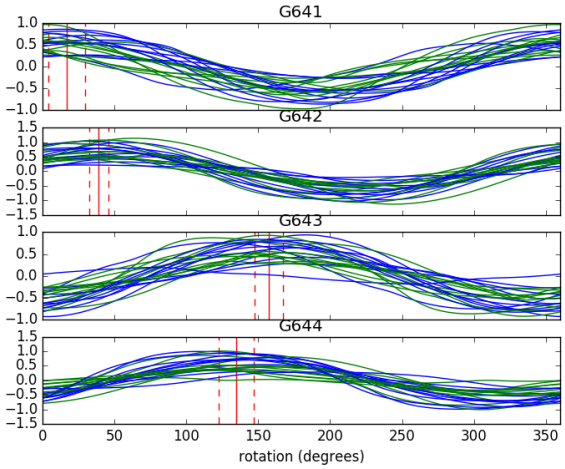

Figure 136: *Orientation curves for station G64. The lines indicate the maximum cross-correlation coefficient (with the surface accelerometer) as a function of counterclockwise rotation of the geophone. Blue lines are for the radial components, green lines for the transverse components. The vertical red lines indicate the average rotation +/- one standard deviation.*

Code	Channel 1	Channel 2	Data used	Standard deviation
G641	106.8°	16.8°	15/22	12.7°
G642	129.1°	39.1°	15/22	6.5°
G643	247.5°	157.5°	16/22	10.0°
G644	224.8°	134.8°	18/22	12.3°

Table 63: *This table shows the channel orientations of the geophones in station in degrees clockwise from north. The standard deviation refers to the orientations calculated from the individual events used. Data used shows how many traces were used for the final calculation and how many were initially found.*

Station G65

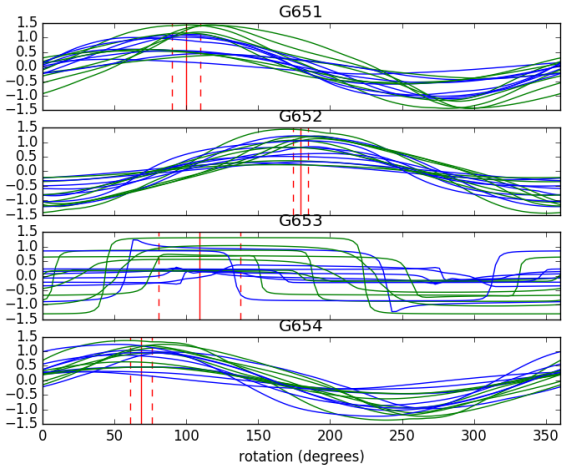

Figure 137: *Orientation curves for station G65. The lines indicate the maximum cross-correlation coefficient (with the surface accelerometer) as a function of counterclockwise rotation of the geophone. Blue lines are for the radial components, green lines for the transverse components. The vertical red lines indicate the average rotation +/- one standard deviation.*

Code	Channel 1	Channel 2	Data used	Standard deviation
G651	190.0°	100.0°	10/16	10.0°
G652	269.4°	179.4°	13/16	5.4°
G653	199.2°	109.2°	13/16	28.7°
G654	158.7°	68.7°	13/16	7.6°

Table 64: *This table shows the channel orientations of the geophones in station in degrees clockwise from north. The standard deviation refers to the orientations calculated from the individual events used. Data used shows how many traces were used for the final calculation and how many were initially found.*

Station G66

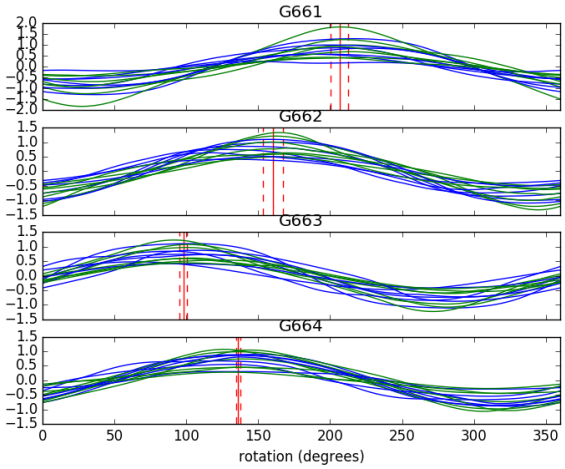

Figure 138: *Orientation curves for station G66. The lines indicate the maximum cross-correlation coefficient (with the surface accelerometer) as a function of counterclockwise rotation of the geophone. Blue lines are for the radial components, green lines for the transverse components. The vertical red lines indicate the average rotation +/- one standard deviation.*

Code	Channel 1	Channel 2	Data used	Standard deviation
G661	296.4°	206.4°	12/14	6.2°
G662	250.3°	160.3°	11/14	7.1°
G663	188.1°	98.1°	11/14	2.7°
G664	226.1°	136.1°	11/14	1.3°

Table 65: *This table shows the channel orientations of the geophones in station in degrees clockwise from north. The standard deviation refers to the orientations calculated from the individual events used. Data used shows how many traces were used for the final calculation and how many were initially found.*

Station G67

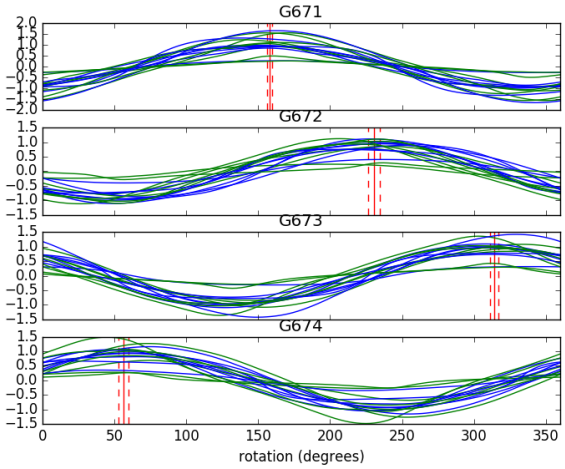

Figure 139: *Orientation curves for station G67. The lines indicate the maximum cross-correlation coefficient (with the surface accelerometer) as a function of counterclockwise rotation of the geophone. Blue lines are for the radial components, green lines for the transverse components. The vertical red lines indicate the average rotation +/- one standard deviation.*

Code	Channel 1	Channel 2	Data used	Standard deviation
G671	247.7°	157.7°	11/16	1.7°
G672	320.6°	230.6°	12/16	3.9°
G673	44.3°	314.3°	10/16	2.9°
G674	146.4°	56.4°	11/16	3.4°

Table 66: *This table shows the channel orientations of the geophones in station in degrees clockwise from north. The standard deviation refers to the orientations calculated from the individual events used. Data used shows how many traces were used for the final calculation and how many were initially found.*

Station G68

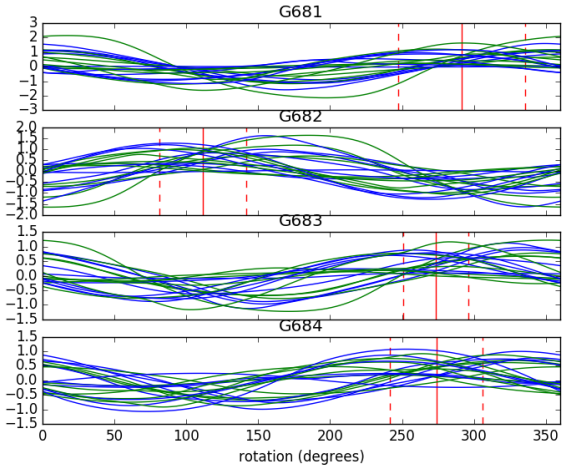

Figure 140: *Orientation curves for station G68. The lines indicate the maximum cross-correlation coefficient (with the surface accelerometer) as a function of counterclockwise rotation of the geophone. Blue lines are for the radial components, green lines for the transverse components. The vertical red lines indicate the average rotation +/- one standard deviation.*

Code	Channel 1	Channel 2	Data used	Standard deviation
G681	21.6°	291.6°	16/20	44.2°
G682	201.3°	111.3°	13/20	30.1°
G683	3.5°	273.5°	11/20	22.7°
G684	4.0°	274.0°	15/20	32.2°

Table 67: *This table shows the channel orientations of the geophones in station in degrees clockwise from north. The standard deviation refers to the orientations calculated from the individual events used. Data used shows how many traces were used for the final calculation and how many were initially found.*

Station G69

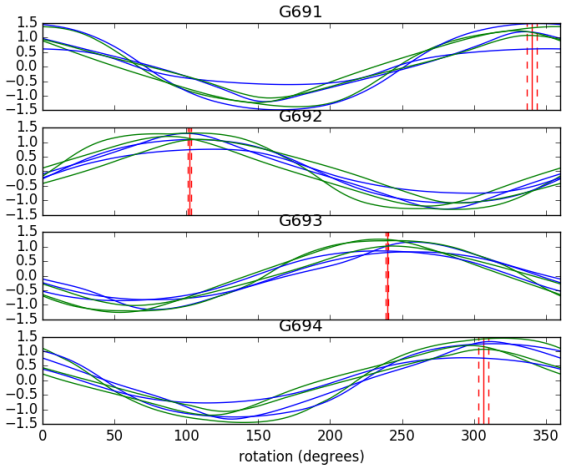

Figure 141: *Orientation curves for station G69. The lines indicate the maximum cross-correlation coefficient (with the surface accelerometer) as a function of counterclockwise rotation of the geophone. Blue lines are for the radial components, green lines for the transverse components. The vertical red lines indicate the average rotation +/- one standard deviation.*

Code	Channel 1	Channel 2	Data used	Standard deviation
G691	70.2°	340.2°	4/6	3.5°
G692	192.1°	102.1°	4/6	1.2°
G693	329.7°	239.7°	4/6	0.8°
G694	36.6°	306.6°	4/6	3.4°

Table 68: *This table shows the channel orientations of the geophones in station in degrees clockwise from north. The standard deviation refers to the orientations calculated from the individual events used. Data used shows how many traces were used for the final calculation and how many were initially found.*

C Event waveforms

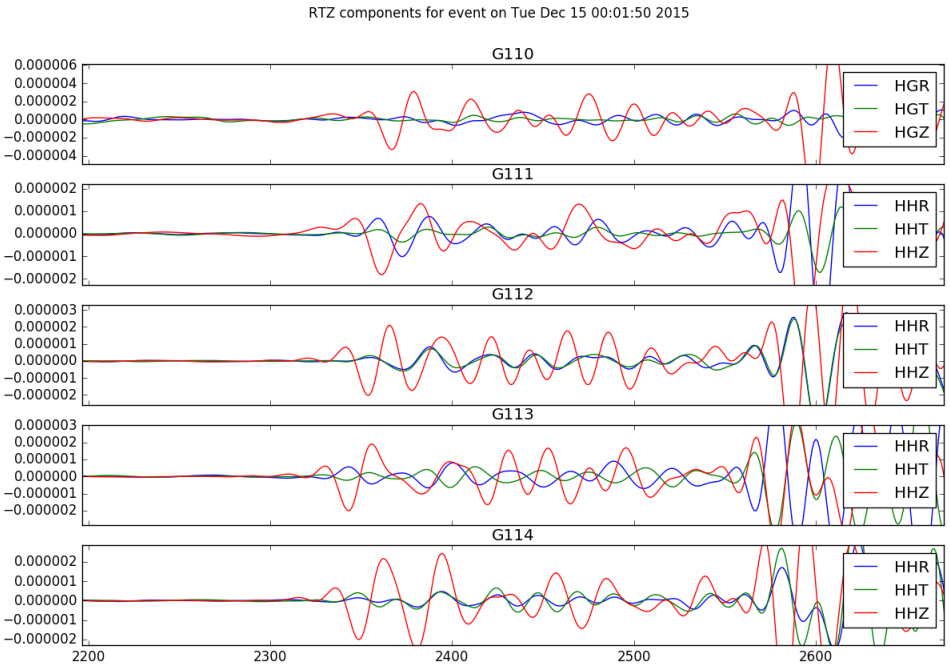

Figure 142: *Event waveforms for station G11. The names of geophones G113 and G114 should be switched.*

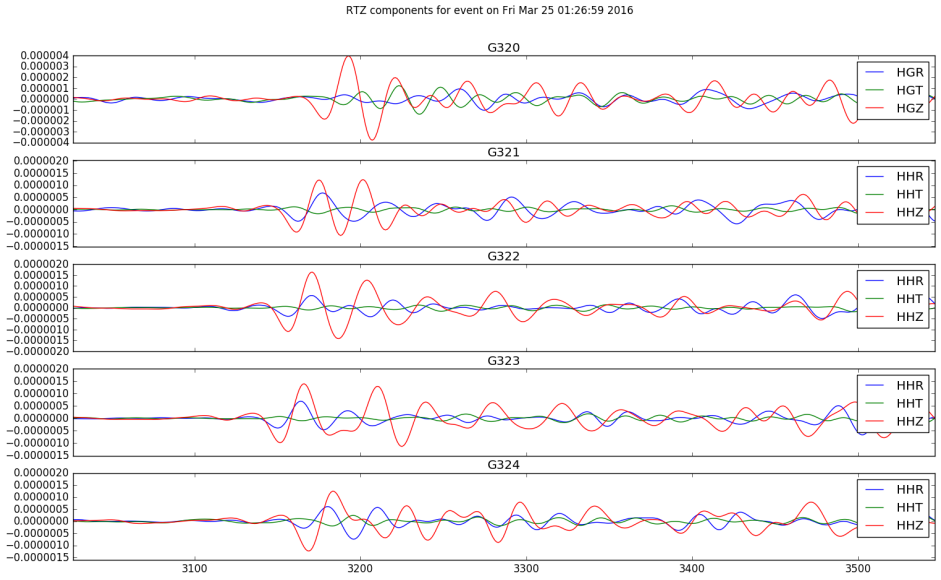

Figure 143: *Event waveforms for station G32. G324 should be G321 and the numbers in geophone codes G321 to G323 should be incremented by 1.*

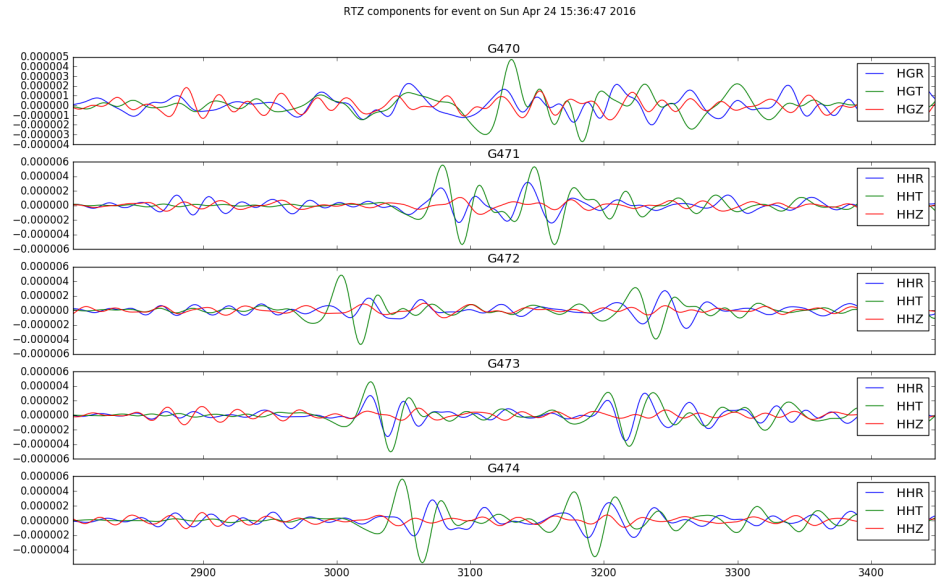

Figure 144: *Event waveforms for station G47. The names of geophones G472 and G474 should be switched.*